Synthesis, photophysical characterization and applications of N-heterocyclic based multibranched donor-acceptor derivatives

By

HASIM FAYIZ P.N.

10CC15A39006

A thesis submitted to the
Academy of Scientific and Innovative Research
for the award of the degree of
DOCTOR OF PHILOSOPHY
in
SCIENCE

Under the supervision of

Dr. V. KARUNAKARAN

CSIR-National Institute for Interdisciplinary Science and Technology (CSIR-NIIST), Thiruvananthapuram – 695 019

Academy of Scientific and Innovative Research
AcSIR Headquarters, CSIR-HRDC campus
Sector 19, Kamla Nehru Nagar,
Ghaziabad, U.P. – 201 002, India

January 2023

सी एस आई आर– राष्ट्रीय अंतर्विषयी विज्ञान तथा प्रौद्योगिकी संस्थान

वैज्ञानिक तथा औद्योगिक अनुसंधान परिषद्
फोटो साइंस और फोटोनिक्स अनुभाग, रसायन विज्ञान तथा प्रौद्योगिकी प्रभाग
इंडस्टिरयल इस्टेट-डाक घर, तिरुवनंतपुरम, भारत 695 019

CSIR–NATIONAL INSTITUTE FOR INTERDISCIPLINARY SCIENCE & TECHNOLOGY

Council of Scientific and Industrial Research
Photosciences and Photonic Section, Chemical Sciences and Technology Division
Industrial Estate P.O., Thiruvananthapuram, INDIA 695 019

डॉ. वी. करुणाकरण
प्रधान वैज्ञानिक

Dr. V. Karunakaran
Principal Scientist

January 6th, 2023
Thiruvananthapuram

CERTIFICATE

This is to certify that the work incorporated in this Ph.D. thesis entitled, **"Synthesis, photophysical characterization and applications of N-heterocyclic based multibranched donor-acceptor derivatives"**, submitted by *Mr. Hasim Fayiz P.N.,* to the Academy of Scientific and Innovative Research (AcSIR) in fulfillment of the requirements for the award of the Degree of *Doctor of Philosophy in Sciences*, embodies original research work carried out by the student. We further certify that this work has not been submitted to any other University or Institution in part or full for the award of any degree or diploma. Research materials obtained from other sources and used in this research work has been duly acknowledged in the thesis. Images, illustrations, figures, tables etc., used in the thesis from other sources, have also been duly cited and acknowledged.

Hasim Fayiz P.N.

Dr. V. Karunakaran

(Thesis Supervisor)

Tel: +91-471-2515240; Fax: +91-471-2491712; E-mail: k.venugopal@niist.res.in **website:http://www.niist.res.in**

STATEMENTS OF ACADEMIC INTEGRITY

I, Hasim Fayiz P.N., a Ph.D. student of the Academy of Scientific and Innovative Research (AcSIR) with Registration No. 10CC15A39006 hereby undertake that, the thesis entitled **"Synthesis, photophysical characterization and applications of N-heterocyclic based multibranched donor-acceptor derivatives"** has been prepared by me and that the document reports original work carried out by me and is free of any plagiarism in compliance with the UGC Regulations on *"Promotion of Academic Integrity and Prevention of Plagiarism in Higher Educational Institutions (2018)"* and the CSIR Guidelines for "*Ethics in Research and in Governance (2020)".*

Hasim Fayiz P.N.
January 6th, 2023
Thiruvananthapuram

It is hereby certified that the work done by the student, under my supervision, is plagiarism–free in accordance with the UGC Regulations on *"Promotion of Academic Integrity and Prevention of Plagiarism in Higher Educational Institutions (2018)"* and the CSIR Guidelines for "*Ethics in Research and in Governance (2020)".*

Dr. V. Karunakaran
January 6th, 2023
Thiruvananthapuram

DECLARATION

I, Hasim Fayiz P.N., bearing AcSIR Registration No. 10CC15A39006 declare: that my thesis entitled, **"Synthesis, photophysical characterization and applications of N-heterocyclic based multibranched donor-acceptor derivatives"** is plagiarism free in accordance with the UGC Regulations on *"Promotion of Academic Integrity and Prevention of Plagiarism in Higher Educational Institutions (2018)"* and the CSIR Guidelines for "*Ethics in Research and in Governance (2020)".*

I would be solely held responsible if any plagiarised content in my thesis is detected, which is violative of the UGC regulations 2018.

Hasim Fayiz P.N.
January 6th, 2023
Thiruvananthapuram

ACKNOWLEDGEMENTS

I have great pleasure in expressing my deep sense of gratitude to Dr. V. Karunakaran, my thesis supervisor, for suggesting the research problem and for his constant guidance, support, motivation and encouragement, leading to the successful completion of this work.

I thank Dr. C. Anandharamakrishnan, Director of the CSIR–National Institute for Interdisciplinary Science and Technology (CSIR–NIIST), Thiruvananthapuram, for providing the necessary facilities for carrying out this work.

My sincere thanks to

- *Dr. K. N. Narayanan Unni, Dr. Vijayakumar C. Nair and Dr. Ravi Shankar L, Doctoral Advisory Committee (DAC) members for their valuable comments and suggestions to improve the quality of my work.*
- *Dr. C. H. Suresh, Dr. Luxmi Varma, and Dr. Mangalam S. Nair, former AcSIR co-ordinators.*
- *Dr. K. R. Gopidas, Dr. Biswapriya Deb, Dr. Joshy Joseph, Dr. K. Yoosuf, Dr. Praveen V. K, Dr. Suraj Soman, Dr. Ishita Neogi and Dr. Adarsh Asok scientists of the Photosciences and Photonics Section, Chemical Sciences and Technology Division (CSTD) for their help and support.*
- *Mr. Robert Phillip and Kiran J. S. for general help and Mrs. Saumini Mathew and Mr. Saran for NMR analysis and Mrs. Viji, and Ms. Athira for HRMS data.*
- *Dr. K.N. Narayanan Unni, Mr Vipin C.K and Ms. Anjali Sajeev for their valuable helps and support in fabrication of OLEDs.*
- *Dr. Chinju Govind, Dr. Guruprasad M. S., Dr. Sumitha Paul, Mrs. Tessy T. D., Mrs. Megha Paul, Ms. Ranimol Mathew, Ms. Afeefah. N. and Ms. Amrutha Surendran present and former group members for their support and help.*
- *M. Sc. project students Mrs. Sareena., Ms. Dhrishya, Ms. Nandana S.K for their hard work.*
- *All my teachers and friends for their care and support.*
- *My parents and family members for their endless caring, love and support.*
- *UGC-CSIR for fellowship.*

Hasim Fayiz P.N.

TABLE OF CONTENTS

List of Abbreviations

Å	Angstrom
A	Acceptor
ACQ	Aggregation caused quenching
AgCl	Silver chloride
AIDF	Aggregation induced delayed fluorescence
AIE	Aggregation induced emission
AIEE	Aggregation induced enhanced emission
AIEgen	Aggregation induced emission luminogens
Al	Aluminium
Alq_3	Tris (8-hydroxyquinoline) aluminum
℃	Degree Celsius
CaF_2	Calcium fluoride
CHX	Cyclohexane
$CHCl_3$	Chloroform
CS	Charge separated state
CT	Charge transfer
CV	Cyclic voltammogram
D	Donor
D-A	Donor-acceptor
DADS	Decay associated difference spectra
DCM	Dichloromethane
EL	Electroluminescence
eV	Electron volt
E_{ox}	Oxidation potential
EQE	External quantum efficiency
EPR	Electron paramagnetic resonance
ESA	Excited state absorption
et al.	Et allii/alia
fs	Femtosecond
fsTAS	Femtosecond time−resolved transient absorption spectra
GSB	Ground state bleach

h	Hour
HLCT	Hybridized local and charge transfer
H_2O	Water
HOMO	Highest occupied molecular orbital
Hz	Hertz
I	Current
IC	Internal conversion
ICT	Intramolecular charge transfer state
IQE	Internal quantum efficiency
IR	Infrared
IRF	Instrument response function
ISC	Intersystem crossing
iSF	Intramolecular singlet fission
ITO	Indium tin oxide
K	Kelvin
l	Path length
LUMO	Lowest unoccupied molecular orbital
LiF	Lithium fluoride
M	Molar
MCL	Mechanochromic luminescence
MeOH	Methanol
MHz	Mega Hertz
mJ	Milli Joule
mm	Millimeter
mM	Millimolar
MO	Molecular orbital
mW	Milliwatt
n	Refractive index
Na	Sodium
nsTAS	Nanosecond transient absorption spectra
nJ	Nano Joule
nm	Nanometer
NMR	Nuclear magnetic resonance

OLEDs	Organic light emitting diodes
OD	Optical density
PEDOT:PPS	Poly(3,4-ethylenedioxythiophene)polystyrene sulfonate
PET	Photoinduced electron transfer
ppm	parts per million
ps	Picosecond
QY	Quantum yield
RIM	Restricted intramolecular motion
RIR	Restricted intramolecular rotation
RIV	Restricted intramolecular vibration
rt	Room temperature
S	Singlet
SADS	Species associated difference spectra
SE	Stimulated emission
SF	Singlet fission
SSA	Singlet singlet annihilation
STA	Singlet triplet annihilation
SQ	Shockley and Queisser
SVD	Singular value decomposition
T	Triplet
T	Time
TADF	Thermally activated delayed fluorescence
TAS	Transient absorption spectra
TCSPC	Time Correlated Single Photon Counting
THF	Tetrahydrofuran
TICT	Twisted intramolecular charge transfer
TPBi	2,2’,2”-(1,3,5-Benzinetriyl)-tris(1-phenyl-1-H-benzimidazole)
TPE	Tetraphenylethene
TPA	Triphenylamine
TPP	Tetraphenylpyrazine
TOPAS	Travelling optical parametric amplification system
TTA	Triplet-Triplet annihilation
UV	Ultraviolet

V	Volt
VC	Vibrational cooling
Vr	Vibrational relaxation
W	Watt
ΔA	Change in absorbance
ΔE	Band gap
λ	Wavelength
μM	Micromolar
τ	Lifetime
ε	Molar extinction coefficient
Φ	Efficiency

PREFACE

Organic N-heterocyclic based donor-acceptor derivatives have drawn great attention due to their various potential applications in organic light emitting diodes,[1] sensors,[2] lasers[3] and biomedical applications.[4] The precise tuning of donor-acceptor interactions allows the modification of their electron affinities and their ionization potentials, giving rise to new functional material with tunable band gaps and, consequently, having very different electronic and optical properties. In this regard, developing organic π conjugated molecules with donor-acceptor or donor-π-acceptor structures based on N-heterocyclic molecules is fascinating due to their unique optical and electronic properties. It is well known that optical and electronic properties of donor-acceptor systems are dependent on excited state dynamics involving intramolecular charge transfer state (ICT). Therefore, the photophysical properties such as the emission, fluorescent quantum yield, fluorescence lifetime, and phosphorescent emission of organic π-conjugated chromophores highly depend on the ICT state of chromophores. It is possible to tune the nature of the ICT state by manipulating the molecular structure of donor-acceptor systems, introducing different substituents, changing the reduction and oxidation potential of acceptor and donor, respectively, changing the length of bridges, and changing the geometry of chromophores.

The N-heterocyclic based donor-acceptor derivatives are considered important molecular architectures in the field of organic electronics, such as organic light emitting diodes (OLEDs) due to the possibilities through simple chemical modification in molecular structure, low power consumption efficiency, and ease of fabrication in a cost-effective manner. These derivatives are also considered aggregation induced emission luminogens (AIEgen); therefore, these molecules exhibit excellent solid emission properties, increasing device performance. The stimuli responsive materials based on N-heterocyclic compounds are well known due to the presence of noncovalent interactions such as π-π stacking, C-H-π interaction, halogen-π interaction hydrophobic forces, and hydrogen bonding interactions. Therefore, the introduction of minor alterations in the molecular structure will result in significant differences in their stimuli-responsive properties, such as mechanochromic and sensing properties.

Here, we present synthesis and applications of N-heterocyclic based multibranched donor-acceptor derivatives with different molecular architecture. Their photophysical properties in ground and excited states are characterized by using steady state and time resolved spectroscopy which provide further insight to the development of more advanced functional molecules.

An overview of organic π-conjugated molecules is provided in chapter 1based on their design strategy and properties, such as aggregation-induced emission, mechanochromism, electroluminescence and discussed their application in the field of optoelectronic devices such as organic light emitting diodes (OLEDs).

In Chapter 2, here to understand the effect of molecular geometry and strength of donors on the photophysical properties and ultrafast excited state relaxation pathways, multibranched tetraphenylpyrazine covalently linked with morpholine (weak donor and planar, **TPP-4MOP**) and phenoxazine (strong donor and twisted, **TPP-4PHO**) derivatives were synthesized and their steady state and time-resolved photophysical properties were investigated. **TPP-4MOP** showed feeble emission (~0.03) due to the weak donor by the delocalization of electron density supported by theoretical optimization. The **TPP-4PHO** exhibited strong emission (~0.18) comparatively in non-polar solvent, toluene. Whereas the emission spectra of **TPP-4PHO** in polar solvent, THF showed large Stokes shift (~9691cm^{-1}) with low fluorescence quantum yield (~0.01) due to the formation of twisted intramolecular charge transfer state (TICT). Aggregation studies of **TPP-4PHO** in THF and water mixture, reflect the elimination of TICT state by the restriction of intramolecular torsion in the aggregates leading to an increase (12 fold) of blue shifted fluorescence. The femtosecond and nanosecond transient absorption spectra of **TPP-4PHO** revealed the existence of partial TICT and TICT states in the THF leading to the triplet state. Whereas in the case of **TPP-4MOP**, the transient absorption spectra showed the formation of triplet state from the local excited state without involvement of TICT state. These studies revealed that the excited state relaxation pathways of derivatives are controlled by polarity dependent torsional motion.

In Chapter 3, to understand the effect of substitution of electron withdrawing group (EWG) on the photophysical properties of N-heterocyclic based derivatives having D–π–A-π–D structure consisting of quinoxaline (acceptor unit) and tert-butyl carbazole (donor unit), **QXTC-CN** and **QXTC-F** were synthesized, in which the acceptor strength of quinoxaline is increased further by substitution of cyano group and fluoride. The photophysical properties of these derivatives are studied in solution and solid states by measuring steady state absorption and emission spectra in solvents of various polarities and exhibited the existence of intramolecular charge transfer state (ICT). The nanosecond transient absorption studies showed the formation of triplet state in non-polar solvent (Cyclohexane) and while charge separation occurs in polar solvent (THF). The aggregation induced emission studies showed that both the

derivatives regained their emission during the aggregation of molecules. Remarkably, the **QXTC-CN** and **QXTC-F** showed reversible solid-state emission in response to mechanical grinding. Upon the mechanical grinding, the **QXTC-CN** showed greenish yellow at 545 nm by red shift of 30 nm from original powder form emitting at 515 nm (green). After treatment of the ground samples with fuming DCM vapour, the greenish yellow emission return to original colour green. In the case of **QXTC-F**, the emission maxima of the powder form (465 nm) shifted to red at 485 nm upon grinding and returned to the original colour on fuming DCM vapours. The acid sensing properties of both derivatives are also studied by using tetrafluoroacetic acid (TFA) and triethylamine (TEA).

In Chapter 4, to understand the effect of donor units (multibranching) on the photophysical properties of N-heterocyclic based donor acceptor derivatives, we synthesized quinoxaline based derivatives by substituting one (**QX-1TC**) and three (**QX-3TC**) tert-butyl carbazole unit using the Buchwald–Hartwig amination coupling reaction**.** The photophysical properties of the both derivatives were investigated by using UV-Vis absorption and fluorescence spectroscopy, time correlated single photon counting (TCSPC) and cyclic voltammetry. The steady state absorption and emission spectra showed the presence of intramolecular charge transfer (ICT) transitions. With the increase of solvent polarity, there is no significant change in absorption maxima but the emission maxima of compounds are shifted to red region about ~100 nm, which indicates that intramolecular charge transfer characteristics of the excited state of quinoxaline carbazole derivatives. The nanosecond transient absorption studies showed the triplet formation in a nanosecond time scale with lifetime 3.68 μs and confirmed with oxygen atmosphere where the peaks are quenched. We fabricated the OLED devices using these derivatives. Device 1, in which **QX-1TC** is used as the emitting layer, exhibited an emission peak at 480 nm and full width half maximum (FWHM) of 72 nm with a turn-on voltage of 9V, corresponding to CIE coordinates of 0.14, 0.28. Similarly, device 2, in which **QX-3TC** is used as an emitting layer, exhibited an emission peak at 488 nm FWHM of 76 nm, corresponding to CIE coordinates of 0.16, 0.39 with a turn-on voltage of 10V.

References

1. (a) Yu, L.; Wu, Z.; Xie, G.; Zeng, W.; Ma, D.; Yang, C., Molecular design to regulate the photophysical properties of multifunctional TADF emitters towards high-performance TADF-based OLEDs with EQEs up to 22.4% and small efficiency roll-offs. *Chem. Sci.* **2018,***9* (5), 1385-1391;(b) Yu, L.; Wu, Z.; Xie, G.; Zhong, C.; Zhu, Z.; Ma, D.; Yang, C., An efficient exciton harvest route for high-performance OLEDs based on aggregation-induced delayed fluorescence. *ChemComm* **2018,***54* (11), 1379-1382;(c) Feng, H.-T.; Zheng, X.; Gu, X.; Chen, M.; Lam, J. W. Y.; Huang, X.; Tang, B. Z., White-Light Emission of a Binary Light-Harvesting Platform Based on an Amphiphilic Organic Cage. *Chem. Mater.* **2018,***30* (4), 1285-1290.

2. (a) Han, M.; Chen, M.; Ebendorff-Heidepriem, H.; Fang, C.; Qin, A.; Zhang, H.; Tang, B. Z.; Tang, Y.; Ruan, Y., An optical fibre sensor for remotely detecting water traces in organic solvents. *RSC Adv.* **2016,***6* (85), 82186-82190;(b) Hu, F.; Xu, S.; Liu, B., Photosensitizers with Aggregation-Induced Emission: Materials and Biomedical Applications. *Adv. Mater.* **2018,***30* (45), 1801350;(c) Hu, W.; He, T.; Zhao, H.; Tao, H.; Chen, R.; Jin, L.; Li, J.; Fan, Q.; Huang, W.; Baev, A.; Prasad, P. N., Stimuli-Responsive Reversible Switching of Intersystem Crossing in Pure Organic Material for Smart Photodynamic Therapy. *Angew. Chem. Int. Ed. Engl.* **2019,***58* (32), 11105-11111.

3. (a) Kuehne, A. J. C.; Gather, M. C., Organic Lasers: Recent Developments on Materials, Device Geometries, and Fabrication Techniques. *Chem. Rev.* **2016,***116 21*, 12823-12864;(b) Jiang, Y.; Liu, Y.-Y.; Liu, X.; Lin, H.; Gao, K.; Lai, W.-Y.; Huang, W., Organic solid-state lasers: a materials view and future development. *Chem. Soc. Rev.* **2020,***49* (16), 5885-5944.

4. (a) Cao, S.; Shao, J.; Wu, H.; Song, S.; De Martino, M. T.; Pijpers, I. A. B.; Friedrich, H.; Abdelmohsen, L. K. E. A.; Williams, D. S.; van Hest, J. C. M., Photoactivated nanomotors via aggregation induced emission for enhanced phototherapy. *Nat. Commun.* **2021,***12* (1), 2077;(b) Cai, X.; Liu, B., Aggregation-Induced Emission: Recent Advances in Materials and Biomedical Applications. *Angew. Chem. Int. Ed. Engl.* **2020,***59* (25), 9868-9886;(c) Kue, C. S.; Ng, S. Y.; Voon, S. H.; Kamkaew, A.; Chung, L. Y.; Kiew, L. V.; Lee, H. B., Recent strategies to improve boron dipyrromethene (BODIPY) for photodynamic cancer therapy: an updated review. *J. Photochem. Photobiol. A* **2018,***17* (11), 1691-1708.

Chapter 1

An overview of aggregation induced emission (AIE), mechanochromic luminescence (MCL) and electroluminescence (EL) properties of organic π-conjugated derivatives

1.1 Abstract

The usage of N-heterocyclic compounds such as pyridine, pyrazine, triazine, quinoxaline, imidazole, oxadiazole, carbazole, phenoxazine and phenothiazine as building blocks has become increasingly important for the design of N-heterocyclic multibranched donor-acceptor derivatives. These derivatives act as photofunctional material applications including organic light emitting diodes (OLED) devices, photovoltaic devices and fluorescent sensors. The photophysical characterization of N-heterocyclic multibranched donor acceptor derivatives will provide further insight into the development of more advanced functional molecules. This chapter deals with a brief discussion of design principle of π-conjugated donor-acceptor derivatives*, mechanism of aggregation induced emission (AIE), mechanochromic luminescence (MCL), and electroluminescence (EL) properties and application of* π-conjugated donor-acceptor derivatives *in the field of optoelectronic devices such as OLEDs.*

1.2 Organic π-Conjugated Derivatives

The discovery of electrical conductivity in polyacetylene upon iodine vapor doping by Alan Heeger, Alan MacDiarmid, and Hideki Shirakawa led the Nobel Prize for chemistry in 2000, but also significantly contributed to the growth of the field of π-conjugated organic materials.[1] Following this, a number of the novel π-conjugated molecules have been discovered in the ensuing years, and their optical and electronic properties have been extensively studied.[2] In comparison to traditional inorganic-based

electronic materials, such as silicon, π-conjugated organic materials present considerable advantages such as low cost, structural tunability, and mechanical flexibility.[3] Synthesis of silicon-based materials requires high temperature (~500°C), but π-conjugated organic materials can be readily synthesized through organic transformations like palladium catalyzed reactions, which makes synthesis easier and reduces the cost.[4] The findings also show that organic π-conjugated molecules can act as semiconductors and have demonstrated a wide range of optical absorption, charge mobility, and charge storage. This discovery made organic π-conjugated molecules useful for organic photonic and electronic devices, such as organic light-emitting diodes (OLEDs), organic field-effect transistors (OFETs), and organic photovoltaics (OPVs).[5-11]The development of the π-conjugated donor-acceptor derivatives is gaining substantial attention because of their strong intramolecular charge-transfer effects. Small or multibranched donor-acceptor derivatives have the advantage of being tunable, as there have been several donors, such as phenoxazine, acridine phenothiazine, carbazole, and acceptors, such as pyridine, triazine, benzothiadiazole, pyrazine, quinoxaline reported in the literature, which could be combined to improve the properties optoelectronic materials and functional materials.

1.2.1 Designing of Donor-Acceptor (D-A) Organic π-Conjugated Derivatives

The design principle of effective D-A and D-π-A systems is based on molecular orbital (MO) theory, as the intramolecular orbital mixing between the donor and acceptor units lowers the energy level of the lowest unoccupied molecular orbital (LUMO) and raises that of the highest occupied molecular orbitals (HOMO), thereby narrowing the HOMO-LUMO energy gap (ΔE) of the new molecule. The reduction of the HOMO-LUMO

energy gap facilitates the excitation of electron from the HOMO to higher energy levels. This in turn facilitates broader solar absorption and improves the charge-transfer in organic semiconductors, which is beneficial for the development of organic optoelectronic martials. Numerous research groups have been motivated by this feature of D-A systems to work on the "bandgap engineering" of organic materials in an attempt to improve their optoelectronic properties. **Figure 1.1** illustrates how design strategy to generate the donor-acceptor (D-A) or donor-π-acceptor (D-π-A) derivatives by using various coupling reaction.

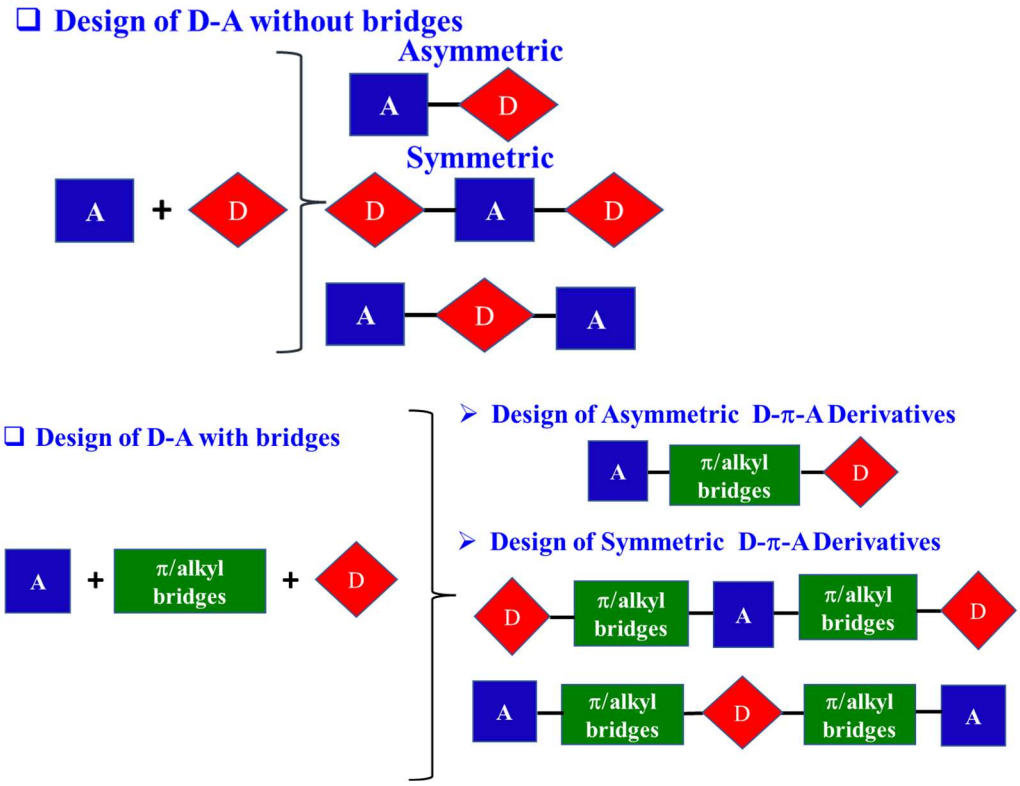

Figure 1.1 General design strategy of donor-acceptor (D-A) or donor-π-acceptor (D-π-A) derivatives.

Current research on the development of one-branched, two-branched or multibranched organic π conjugated donor-acceptor molecular architecture has become scientific interest in the field of development of functional materials with properties such

as aggregation induced emission (AIE), mechanochromic luminescent (MCL) and electroluminescent (EL). In this contest, the N- heterocycles based donors and acceptors are considered as attractive candidates for designing of D-A or D-π-A organic π-conjugated molecules because of easy modification of the structure of N-heterocycle, good stability, tunability, well defined HOMO-LUMO energy band gap, and low cost of production.

The organic π-conjugated molecules undergo different photophysical processes upon absorption of light. According to the Jablonski diagram (**Figure 1.2**), upon absorption of near-ultraviolet or visible light by a molecule, an electronic excitation occurs, which means that an electron gets excited from the ground state S_0 to the vibrational levels of higher singlet excited states such as S_1 or S_2 within the time scale of order10^{-15} s.

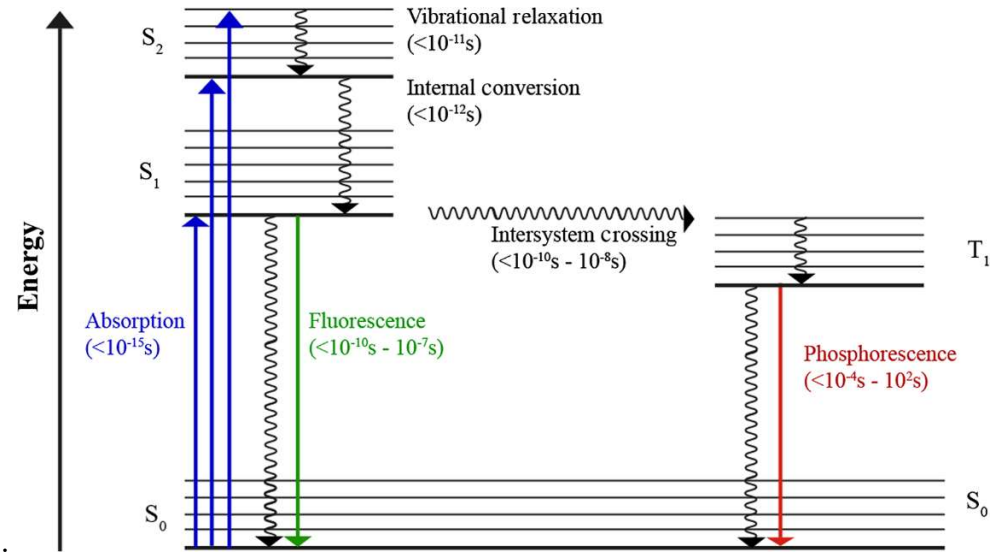

Figure 1.2 Jablonski diagram representing the different photophysical relaxation processes.

A molecule can relax to ground state by either radiative transition or non-radiative transition after the absorption of an incident photon. As a molecule gains energy through light absorption (excitation), it is in a state of non-equilibrium, and the energy is eventually dissipated, resulting in a return to the lowest vibrational level of the excited electronic state.

This primary way of relaxation process is known as vibrational relaxation, a non-radiative process taking place in a picosecond timescale of order 10^{-12} to 10^{-11} s, where the excess vibrational energy is lost either within molecules or through inelastic collisions with the solvent molecules. After internal conversion, the vibrational state immediately relaxes to its lowest vibrational level of S_1 state. As the energy gap between the two electronic states increases, the rate of internal conversion decreases. It is expected that the internal conversion of the closely spaced higher-lying singlet states (S_3 to S_2, S_2 to S_1, etc.) will proceed rapidly between 10^{-11} and 10^{-9} s.

Fluorescence is the radiative transition between two electronic states of the same spin multiplicity with the order of 10^{-9} and 10^{-7} s, shown by the green arrows in **Figure 1.2.** Based on Kasha's rule, the fluorescence typically occurs from the lowest vibrational level of the first electronic excited singlet state to the singlet ground state (S_1 to S_0). This energy loss prior to fluorescence is the physical origin of the famous Kasha's Rule which states that: "luminescence (fluorescence or phosphorescence) only occurs with appreciable yield from the lowest excited state of a given multiplicity".[5] It is also responsible for the Stokes shift; where the fluorescence occurs at a longer wavelength than the absorption.

An alternative transition to fluorescence and internal conversion is intersystem crossing from the S_1 to the T_1 state, one of slowest form of relaxation with the order of 10^{-8} and 10^{-3} s. This transition is in principle forbidden due to conservation of spin angular momentum; however, spin-orbit coupling between the spin angular momentum and the orbital angular momentum makes it weakly allowed. Intersystem crossing is in competition with the other S_1 depopulation transitions (internal conversion and fluorescence) and is too slow to be relevant for the majority of purely organic molecules.

One method of increasing the intersystem crossing rate is the incorporation of heavy atoms into the molecule, which increases the spin-orbit coupling strength. After intersystem crossing, the molecule will immediately undergo vibrational relaxation to the ground vibrational level of T_1. The emission of photons from the $T_1 \rightarrow S_0$ transition is known as phosphorescence. Similarly, to the intersystem crossing; phosphorescence is in principle a forbidden transition but is weakly allowed through spin-orbit coupling. A consequence of being a forbidden transition is that the phosphorescence rate constant is very low and therefore phosphorescence occurs on a much longer timescale than fluorescence, with typical phosphorescence lifetimes being in the 10^{-6} to 10 s range.

1.3 N-Heterocycle Based Donor-Acceptor Derivatives

Organic N-heterocyclic based donor-acceptor derivatives have drawn great attention due to their various potential applications in organic light emitting diodes,[12-14] sensors,[15-17] lasers[18-19] and biomedical applications.[20-22] The precise tuning of donor-acceptor interactions allows the modification of their electron affinities and their ionization potentials, giving rise to new functional material with tunable band gaps and, consequently, having very different electronic and optical properties. In this regard, developing organic π conjugated molecules with donor-acceptor or donor-π-acceptor structures based on N-heterocyclic molecules is fascinating due to their unique optical and electronic properties. It is well known that optical and electronic properties of donor-acceptor systems are dependent on excited state dynamics involving intramolecular charge transfer state (ICT). Therefore, the photophysical properties such as the emission, fluorescent quantum yield, fluorescence lifetime, and phosphorescent emission of organic π-conjugated chromophores highly depend on the ICT state of chromophores. It is possible to tune the nature of the ICT

state by manipulating the molecular structure of donor-acceptor systems, introducing different substituents, changing the reduction and oxidation potential of acceptor and donor, respectively, changing the length of bridges, and changing the geometry of chromophores.

The N-heterocyclic based donor-acceptor derivatives are considered important molecular architectures in the field of organic electronics, such as organic light emitting diodes (OLEDs) due to the possibilities through simple chemical modification in molecular structure, low power consumption efficiency, and ease of fabrication in a cost-effective manner. These derivatives are also considered aggregation induced emission luminogens (AIEgen); therefore, these molecules exhibit excellent solid emission properties, increasing device performance. The stimuli responsive materials based on N-heterocyclic compounds are well known due to the presence of noncovalent interactions such as π-π stacking, C-H-π interaction, halogen-π interaction hydrophobic forces, and hydrogen bonding interactions. Therefore, the introduction of minor alterations in the molecular structure will result in significant differences in their stimuli-responsive properties, such as mechanochromic and sensing properties.

This broad possibility to control the properties of the N- heterocycle derived organic materials by combining different organic π-conjugated building blocks make these materials attractive candidates for optoelectronic applications and smart materials such as mechanoresponsive materials. Here we focus on the aggregation induced emission (AIE), mechanochromic luminescence (MCL) and electroluminescence (EL) of N-heterocycle based D-A or D-π-A organic π-conjugated molecules and their applications in the area of OLED and stimuli responsive materials.

1.4 Aggregation Induced Emission (AIE) of Organic π-Conjugated Derivatives

One of the thorniest problems of conventional luminophores, perylene, fluorescein, porphyrins, naphthalene diimides, with planar and strong intermolecular interactions, generally show excellent emission in solution but weakened or even quenched emission in the solid or aggregated state. This quenching effect is known as aggregation-caused quenching (ACQ). [23] **Figure 1.3** (left panel) shows the aggregation caused quenching effect of perylene. Consequently, this concentration quenching effect is an obstacle to the practical application of organic fluorescent materials as they are often used in solids or aggregates, where the emission is often quenched.

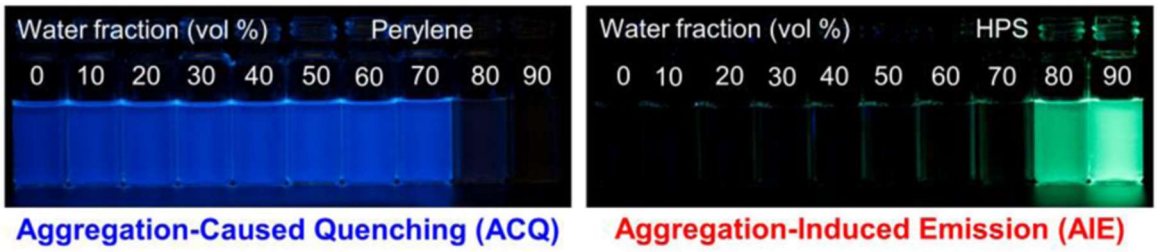

Figure 1.3 Photographs of perylene (left) and hexaphenylsilole (HPS) solutions (right) with different poor solvent fractions taken under ultraviolet (UV) light irradiation. The Figure is copied from ref 26.

In 2001, Ben zhong et al [24] reported new type of luminogens which are highly emissive in aggregation state as compared with solution state where the aggregation in constructive role not in destructive role. The investigation was based 1- methyl hexaphenyl silole (**Figure 1.4**) derivative which possess freely rotating five phenyl rotors twisted out the centre core silole stator. The molecule will be non-emissive due to free rotation of five phenyl group which will automatically increases the non-radiative decay of excitons. But the free rotation of phenyl groups will be get arrested during aggregation leading to open radiative decay path and close the non-radiative decay path. This will boost up the emission

efficiency of silole derivative turning it from a weak luminophore into strong emitter. **Figure 1.3**, right panel, clearly demonstrate the aggregation induced emission of HPS in THF water mixture.

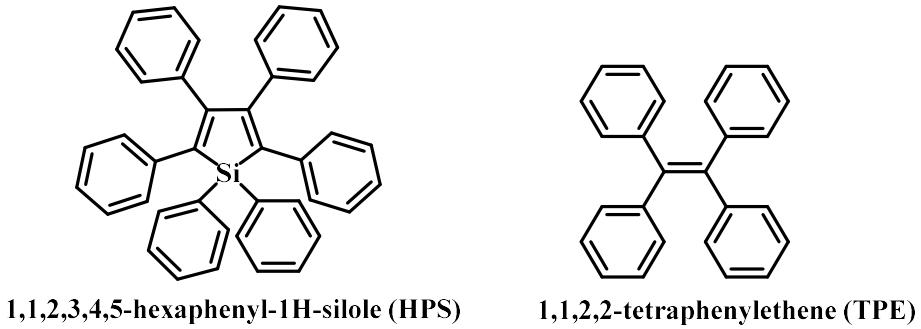

Figure 1.4 Molecular structure of **HPS** and **TPE**.

It can observe that the HPS is non-emissive in pure THF solvent but on increasing water fraction up to 90% the molecules get aggregated and become emissive. This phenomenon is called aggregation induced emission (AIE) which is exactly opposite to ACQ phenomenon. The inspiring phenomenon is practically helpful since it can alleviate the notorious ACQ effect of emitters, paving an alternative avenue to prepare efficient OLEDs. The integration of delayed fluorescence into AIEgens is anticipated to generate robust aggregate-state emitters with improved exciton utilization. Indeed, the newly emerged aggregation-induced delayed fluorescence (AIDF) luminogens have exhibited impressive EL properties and may bring about a new breakthrough for OLEDs.[25]

1.4.1 Mechanism of AIE Property

The understanding of mechanism for the novel AIE phenomenon is very much important because it may definitely guide us to draw a clear picture on the light emission processes and help us to develop new AIE systems and technological innovations. After

the AIE concept was proposed in 2001, researchers have made persistent effort to clarify and unify their working mechanisms and to derive structural design strategies for creating new AIEgens. Several probable mechanisms are introduced to explain AIE phenomenon such as conformational planarization, J-aggregate formation, E/Z isomerization, twisted intramolecular charge transfer (TICT), and ESIPT etc. But they are not applicable to all the reported AIE system because these are not fully supported by the experimental data. Actually, AIE process is associated with three main hypotheses, that is, restriction of intramolecular rotation (RIR), restriction of intramolecular vibration (RIV), and restriction of intramolecular motion (RIM).[26]

The RIR mechanism is proposed on the basis of well-studied AIE systems such as hexaphenylsilole (HPS)[27-28] and tetraphenylethene (TPE)[29-30] as shown in the **Figure 1.4**. The propeller-like luminogenic molecules possess peripheral rotors, such as phenyl rings which can undergo active intramolecular rotational/twisting motions against the stator in solution state (top panel, **Figure 1.5**). Such dynamic rotations will annihilate the excited states in a non-radiative fashion in solution while in aggregated state the intramolecular rotations are restricted due to physical constraint, which blocks the non-radiative path and activates the radiative decay.

A series of experiments have been conducted to modulate the intramolecular rotations externally and internally for verifying this mechanism, whether, it is true or not. The external control experiments involve observing the changes in luminescence properties of HPS system in different environment such as increasing solvent viscosity, decreasing solution temperature, and pressurizing solid film. It has been found that the emission of HPS was significantly high at viscous solvent, at lower temperature, and under higher

pressure, which confirms that the RIR process is indeed a cause for the AIE effect of HPS[27, 31-32]

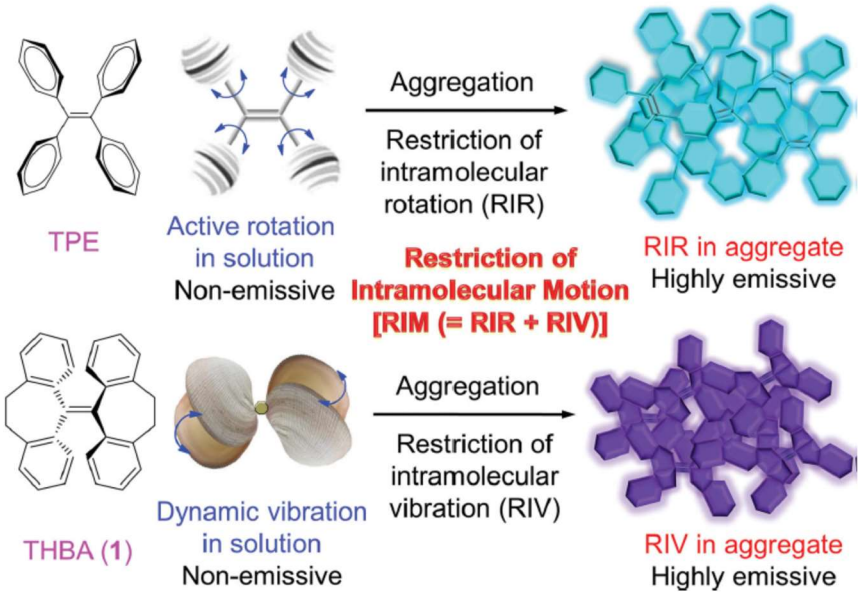

Figure 1.5 Working mechanism of propeller-shaped luminogen of tetraphenylethene (TPE) (top panel) and shell-like luminogen of 10,10′,11,11′-tetrahydro-5,5′-bidibenzo[*a* , *d*][7]annulenylidene (THBA) (bottom panel). The Figure is copied from ref 26.

The internal control experiments, also support RIR mechanism, includes restriction of intramolecular motion of aromatic rings by introducing sterically bulky groups and cross-locking with tethering units leading to enhanced emission intensity of AIEgens.[33-34] Some AIE systems without rotatable units have been reported, such as THBA (10,10′,11,11′-tetrahydro-5,5′-bidibenzo[*a,d*][7]annulenylidenene (bottom panel, **Figure 1.5**) cannot be fully interpreted by the RIR mechanism.[35] The THBA molecule adopts anti-conformation, composed of two flexible parts, in each of which two phenyl rings are connected by a bendable flexure. The phenyl rings of non-coplanar flexible parts of THBA can dynamically bend or vibrate in the solution state, which serves as a relaxation pathway for its excited states to non-radiatively decay. The intramolecular vibration of THBA is in some sense like the breathing movement of a clam or scallop, as illustrated by the cartoon

shown in the lower panel of **Figure 1.5**. The THBA become emissive in the aggregate state due to the restriction of intramolecular vibration (RIV) of its bendable vibrators.

Now it become clear that the RIR and restriction of intramolecular vibrations (RIV) are the main causes for the AIE phenomena observed in the propeller-shaped and shell-like luminogen systems, respectively. In a RIM system, the RIR and RIV mechanisms can work independently or together, but all follow one trend: any intramolecular motion can consume energy and enhance non-radiative decay rates of molecules, whereas blocking the non-radiative pathways via structural restriction will relax excitons through radiative channels to lead to the AIE effect. Finally, restriction of intramolecular motion has been recognized as the general working mechanism of AIE.[26, 36-37]

1.4.2 Hydrocarbon Based AIE System as Acceptor Core

Pure hydrocarbon systems are simpler systems and exhibiting excellent chemical, electro, photophysical properties and used for building blocks for the construction of functional AIEgens. Tetraphenylethylene (TPE) is best-known hydrocarbon AIEgen and has been extensively used for mechanistic studies, AIE macromolecules construction as well as the ACQ-to-AIE transformation.

The hexaphenylbenzene, (HPB, **Figure 1.6**), in which the benzene are decorated with six phenyl rings, shows an aggregation induced enhanced emission (AIEE) character in solid state. The fluorescence of HPB in solution is weak but detectable its emission is intensified by 12-fold at fw = 80 vol %, in THF/ water mixture. In the aggregate state, the RIR effect comes into play due to many intra- and intermolecular C−H···π interactions aid in rigidifying the molecules, stabilizing the packing, hindering phenyl ring motions, and

thus enhance the emission. A series of HPB derivatives have been synthesized with AIE/AEE properties.[38]

The 9,10-Di((E)-styryl)anthracene (DSA, **Figure 1.6**) is, generated by decorating the both sides of an anthracene core with styryl moieties practically non-fluorescent when it is dissolved in THF but showed fluorescent enhancement in aggregated state.[39] The examination on its crystal structure gives us a deep insight into its AIE mechanism:, the orthogonal styryl arms prevent the anthracene cores from forming π–π stacking which could decrease the emission. A large number of different C–H···π interactions rigidify the highly twisted conformation and restrain the free rotation of the styryl arms, rendering an activated RIR process which is responsible for the 127-fold emission enhancement in the crystal state.

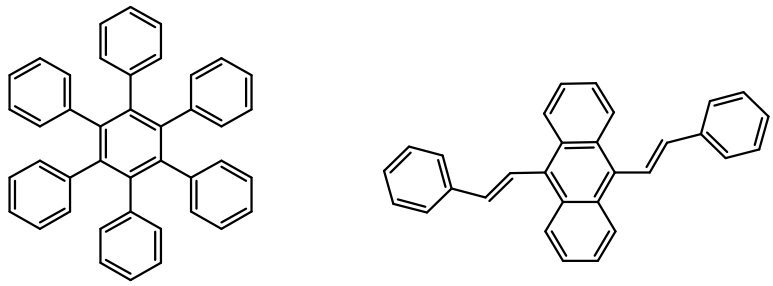

Figure 1.6 Molecular structure of HPS and DSA, hydrocarbon based AIE system as acceptor core.

1.4.3 Heterocyclic Based AIE System as Acceptor Core

Replacing the silicon atom in HPS with group- 14, 15, or 16 elements have resulted in a diverse array of AIEgens. For example, germoles with the 1,1-positions of the germanium-bridged pentacyclic cores substituted by methyl groups and phenyl groups, have very low emission in THF, but 21 to 32-fold emission enhancement in the aggregate state are observed (**Figure 1.7**).[40] Stannoles, a tin atom in the cyclopentadiene core, with AIE features have also been reported.[41] However, stannoles are slightly less emissive

compared to their silole and germole counterparts in the aggregate state. Stannole derivatives exhibited a 7 to 11 fold emission enhancement. The general reduction in emission intensity of the stannoles has been attributed to the heavy-atom effect of the tin atom.

The propeller-shaped pyrrole derivatives with multiple aryl substituents (**Figure1.7**) show typical AIE activity [42-43]. As the water fraction is increased in its THF/water mixtures, pronounced emission enhancement could be observed.

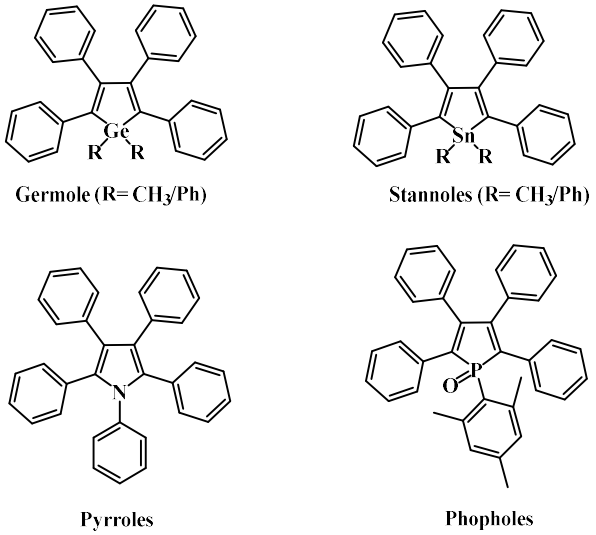

Figure 1.7 Molecular structures of AIE active cores such as germole, stannole, pyrrole and phophole.

Phosphole oxide derivatives containing multiple phenyl groups show typical AIE phenomenon, and observed that when phosphole oxide (**Figure 1.7**) was dissolved in good solvent, e.g., THF, the fluorescence is almost negligible, but in the crystalline state, it strongly luminesces with a greenish yellow light with a Φ_F as high as 91.0%.[44] The photophysics of these all AIEgens are often analogous to their silole counterparts whose AIE activity can primarily be explained be interpreted by the principle of RIR that is

rotations of the phenyl rings on the centre cores quickly relax the excited state via non-radiative channels while in aggregation state the activation of RIR and the lack of intermolecular π-π stacking interaction give rise to the enhanced emission.

1.4.4 AIE Cores in Donor-Acceptor π-Conjugated Systems

The AIE core structures can be divided based on the electron withdrawing/donating abilities of the AIE core structure into three categories: (a) neutral AIE core, (b) donor AIE core and (c) acceptor AIE cores, as shown in **Figure 1.8**.[45] If AIE cores incorporated with donor-acceptor frame work, then entire system will be AIE active and good emissive in solid state. Some general design strategy to incorporate AIE cores in donor-acceptor architecture are given in **Figure 1.9**.

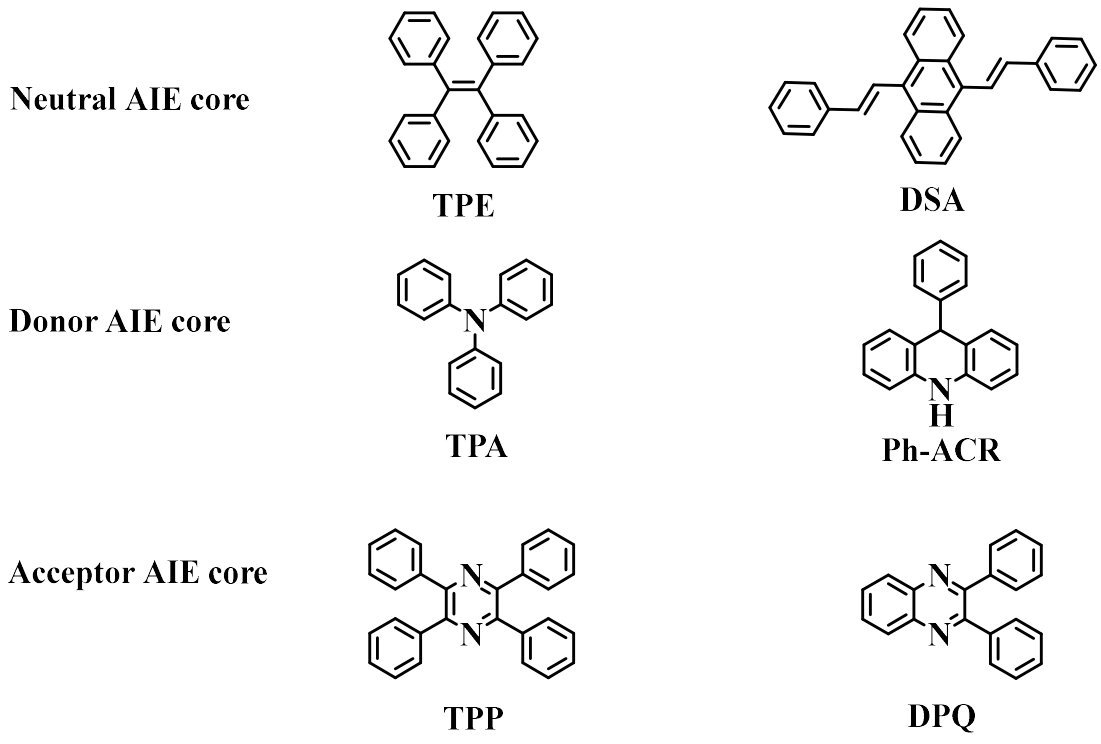

Figure 1.8 Examples for neutral AIE core, donor AIE core and acceptor AIE core.

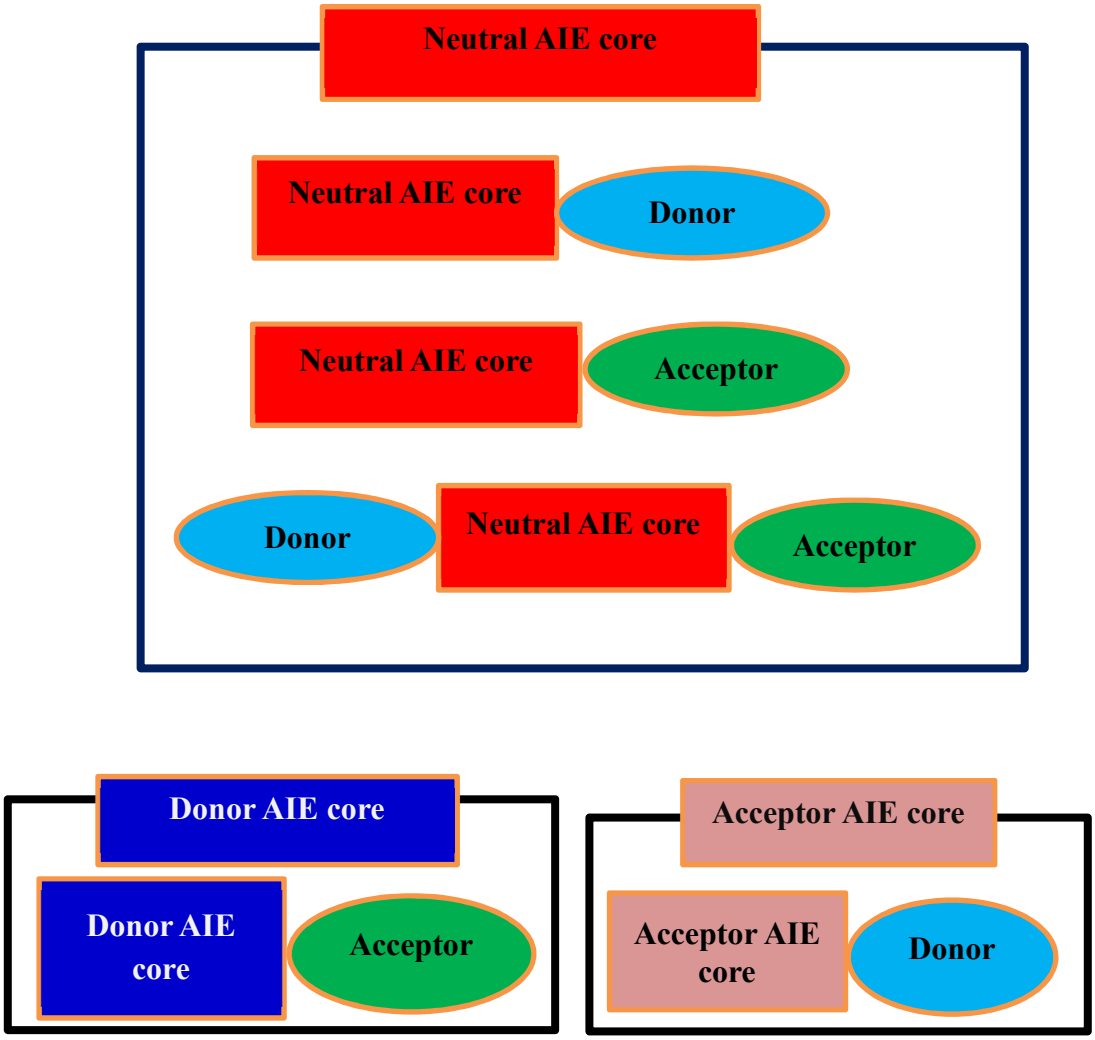

Figure 1.9 Design strategy of neutral AIE core, donor AIE core and acceptor AIE core in donor-acceptor architecture.

1.4.4.1 Donor-Acceptor π-Conjugated Derivatives Using Neutral AIE core

Generally, adding more donors and acceptors to an AIE central core leads to the development of new AIE-active molecules with tunable emission. Zhang et al reported tetraphenylethylene derivatives (1-5) as shown in **Figure 1.10**, having donor- neutral AIE-acceptor architecture, which contain electron-accepting (dicyanomethane) and electron-donating (methoxy) groups, and investigated as AIE-active molecules with a tunable emission colour and their emission maxima are redshifted in ascending order (603, 628, and 645 nm). The reason for such red-shifts is an increase in intramolecular interactions

between electron donors and electron acceptors with increase of methoxy group. It also plays an important role in determining the emission range of a molecule where the donor and acceptor moieties are positioned. As an example, changing the position of the dicyanomethylene group of 4 (para-) to meta (5)- will result in a blue of emission max at 595 nm, resulting from the weakened conjugation.[46]

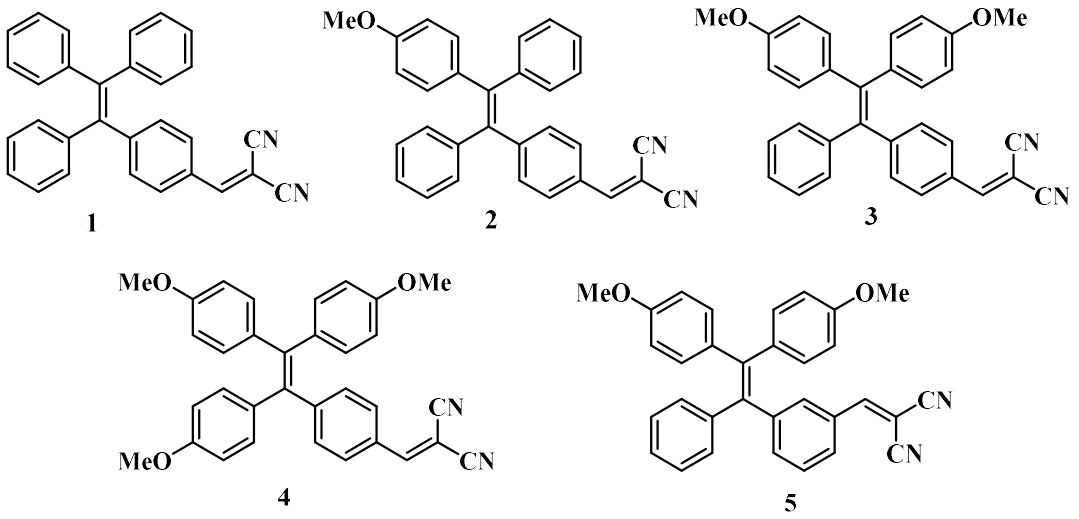

Figure 1.10 Molecular structures of TPE based donor-acceptor derivatives (1-5) in which TPE is used neutral as AIE core.

1.4.4.2 Donor-Acceptor π-Conjugated Derivatives Using Donor AIE core

Michiaki Ogawa et al. demonstrated a new strategy based on the simple combination of an electron-accepting core and electron-donating amino moieties. The derivatives, triphenylamine benzothiadiazole (**6a-6d**), triphenylamine benzoselenodiazole (**7**), and triphenylamine quinoxaline (**8**), are synthesised using triphenylamines as donor AIE core (**Figure 1.11**). As result of aggregation, the solvation-induced non-radiative deactivation is limited, leading to recovery and enhancement of the emission. In 90% water, 6a, 6b, 6c, and 6d provide red/orange light emissions at 610, 647, 622, and 588 nm

respectively, with fluorescence quantum yield of 0.80, 0.15, 0.28, 0.44, and 0.54, which can be applied to biological imaging in a useful optical window.[47]

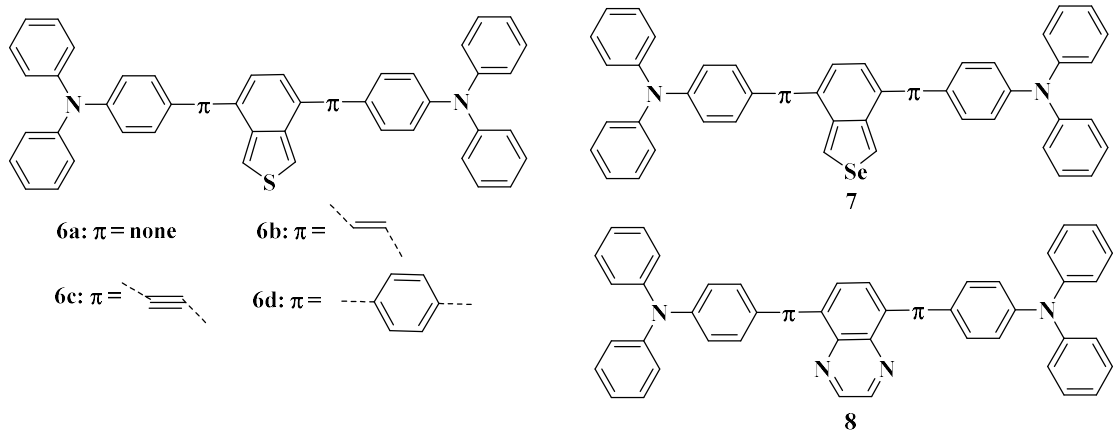

Figure 1.11 Molecular structures of donor-acceptor derivatives based on benzothiadiazole (**6a-6d**), benzoselenodiazole (**7**) and quinoxaline (**8**), in which TPA is used as donor AIE core.

Similarly, Wenhan Xu synthesized series of donor-acceptor based AIEgens with widely tunable emissions covering the whole visible region extending to the NIR area in which TPA used as donor AIE core (**Figure 1.12**). These TPA-thiophene building block-based AIEgens (**9- 14**)can be facilely prepared using straightforward synthetic protocols, and their intrinsic aggregation-induced emission nature enables high fluorescence quantum yields up to 40.79%. They have been successfully utilized for cell imaging, showing excellent image contrast to the cell background and higher photostability. Additionally, the high brightness and homology of these AIEgens endow them with excellent performance for visualizing cell fusion. Notably, upon exposure to white light irradiation, one of these presented AIEgens, **11**, displays high ROS generation efficiency, enabling its effective application for photodynamic ablation of cancer cells. Using these systems, one can adjust emission colours widely and with high brightness, allowing for the exploration of organic fluorophores with AIE features for preclinical research as well as clinical treatment.[48]

.

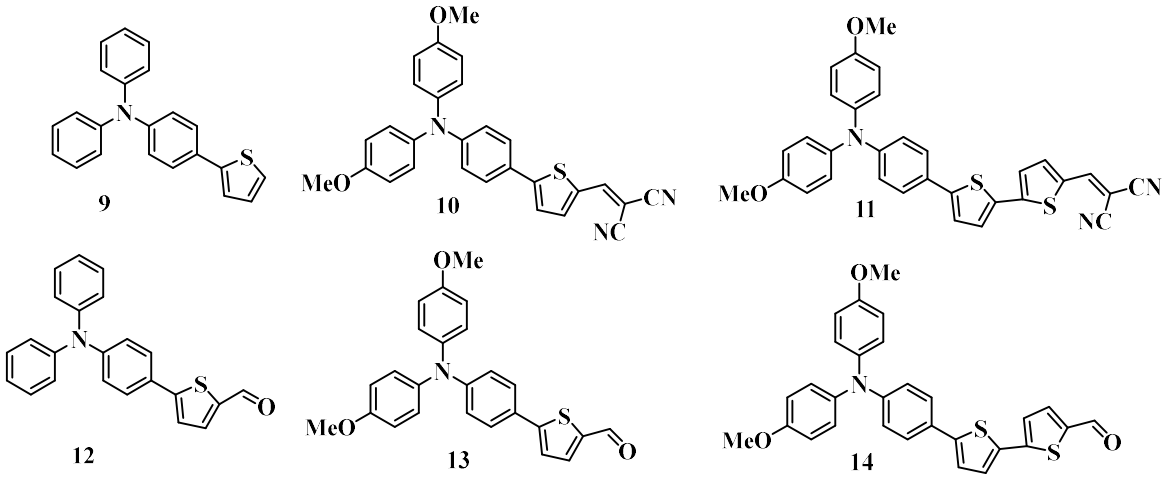

Figure 1.12 Molecular structures of TPA-thiophene donor-acceptor derivatives in which TPA is used as donor AIE core.

1.4.4.3 Donor-Acceptor π-Conjugated Derivatives Using Acceptor AIE Core

In 2014, Benzong tang reported new kind of AIEgen based on tetraphenylpyrazine (TPP), which could be readily prepared under mild reaction conditions. Following this many TPP based AIEgens are developed for this different application such as OLED. For example, TPP-based deep-blue AIEgens of TPP-Cz (**15**) and TPP-PhCz (**17**) with a line-shaped structure and TPP-2Cz (**16**) and TPP-2PhCz (**18**) with an X-shaped pattern were designed and prepared, in which TPP as used as acceptor AIE core (**Figure 1.13**). These derivatives exhibited enhanced emission from solution to aggregate with the non-radiative decay channel blocked and exhibited tenfold higher radiative decay rates from solution to film. Therefore, these TPP-based AIE luminogens (AIEgens) are used in nondoped OLEDs as emitting layers exhibited good performance due to the valuable emission they produce in their film states. Among these, the TPP-Cz-based device exhibited the best performance with external quantum efficiency of 1.49% and an ideal current efficiency roll-off of 3.3%

at unchanged CIE coordinates of (0.16, 0.11). According to these results, TPP showed a great deal of potential as a deep-blue AIE core for optoelectronic devices.[49]

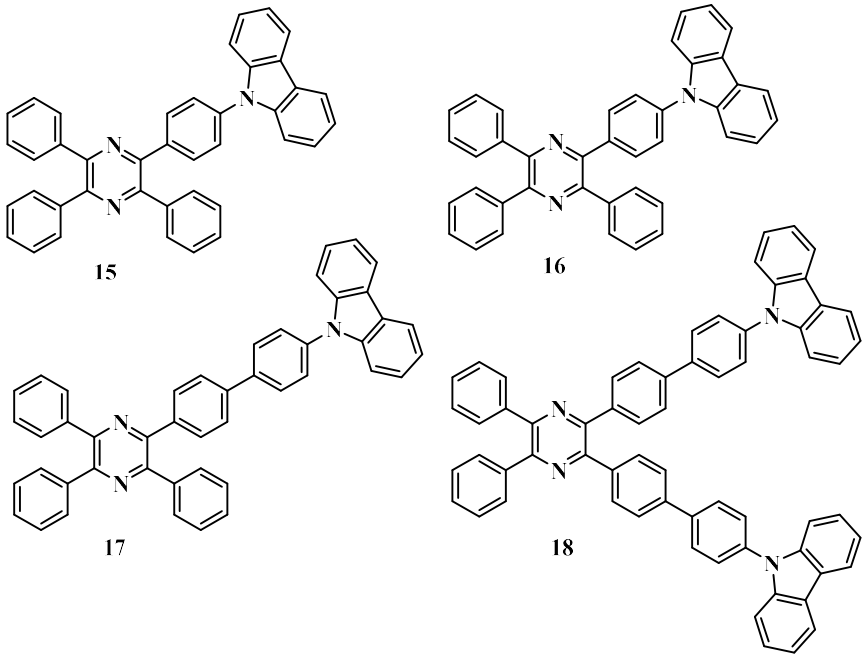

Figure 1.13 Molecular structures of TPP-carbazole donor acceptor derivatives in which TPP is used as acceptor AIE core.

Similarly, Tang et al. developed a new AIEgen of TPP-mCP (**19**) as shown in **Figure 1.14** by integrating a typical AIE moiety of tetraphenylpyrazine (TPP) with a conventional host of 1,3-di(9H-carbazol-9-yl) benzene (mCP, **20**) which is considered as effective strategies to generate AIE-active hosts which will facilitate more efficient charge transfer from the highly emissive hosts to the guest molecules. As a result, the performance of TPP-mCP-hosted OLEDs showed much higher electroluminescent performance than those with mCP. This strategy will enlighten researchers on the design and synthesis of more efficient AIE-active hosts from conventional ACQ ones.[50]

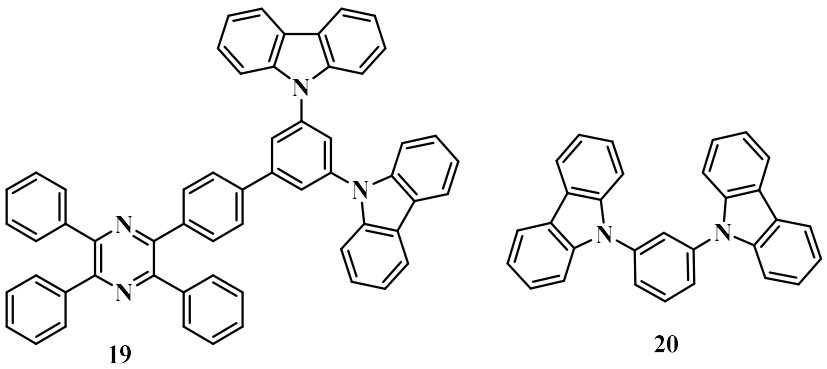

19 20

Figure 1.14 Molecular structure of TPP- carbazole donor acceptor derivative (**19**) in which TPP is used as acceptor AIE core and molecular structure of mCP (**20**).

1.5 Electroluminescence (EL) of Organic π-Conjugated Derivatives

1.5.1 Electroluminescent Materials

Electroluminescence (EL) is an optical phenomenon and electrical phenomenon in which a material emits light in response to an electric current passed through. Electroluminescence is the result of radiative recombination of electrons and holes in a material (usually a semiconductor) (**Figure 1.15b**). The excited electrons release their energy as photons – light. Through electroluminescence innovation, the possibility for conversion of electrical energy directly into light energy came into picture. Recently, blue, red, and green emitting thin film electroluminescent materials have been developed that offer the potential for long life and full color electroluminescent displays.

In either case, the EL material must be enclosed between two electrodes and at least one electrode must be transparent to allow the escape of the produced light. Glass coated with indium oxide or tin oxide is commonly used as the front (transparent) electrode while the back electrode is or is coated with reflective metal. Charge carriers bearing opposite sign [holes (+) and electrons (-)] recombine to emit luminescent light. It is essential to transport electrons to the higher energy level within the crystal lattice for production of

light. This detaches them from lattice of the crystal. The emitted light wavelength is governed by the defect level energy difference in agreement with the equation E= hv. These light emitting materials are used as emitting layer in OLED devices.

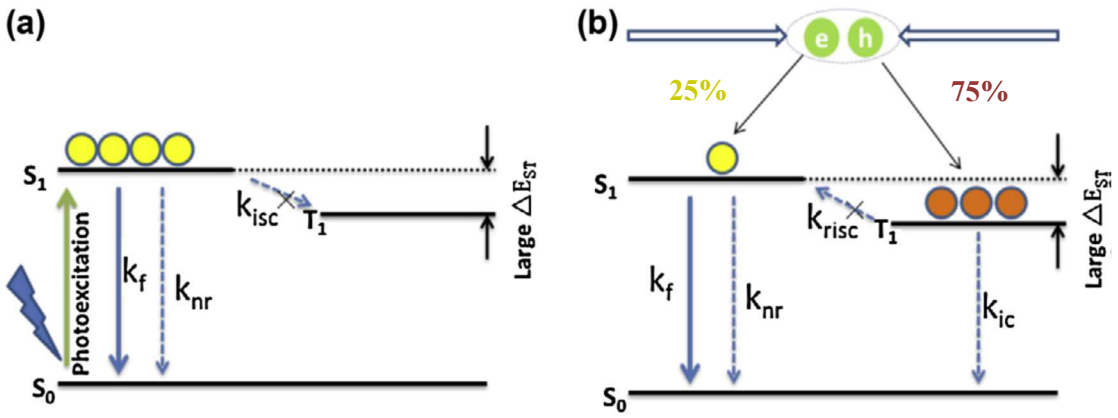

Figure 1.15 Dynamics processes of photoexcited molecules (a) Dynamic of exciton formed by charge recombination of electron and hole in the emissive layer of OLED (b).

1.5.2 Organic Emitters and OLEDs

Light-emitting materials have helped to drive technological advancements around the world, especially organic light emitting diodes (OLED) which are widely used in flat-panel displays. With the discovery of the first practical OLED in 1987 by W Tang et al, OLED technology has generated huge interest from both academics and industrialists due to its advantages such as ease of preparation, low driving voltage, low cost, safe application and fast response. The technology has already been widely adopted in mobile devices, such as phones, watches, cameras, and other devices, and is expected to become the dominant technology for lightening and flat-panel displays in the future. Scientific attention has been drawn to organic light-emitting diodes (OLEDs) because of their promise as future flat-panel displays and lighting sources. Organic light-emitting diodes are also referred to organic electroluminescent (organic EL) diodes, in which the emissive electroluminescent

layer is a film of organic material that emits light in response to an electric current. OLEDs offer excellent picture quality - bright, saturated colours, infinite contrast, and fast response time. Also, OLEDs can be made into lighting - which is thin, efficient, and free of harmful metals.

An OLED's primary operating concept is that hole and electrons are injected into the emissive layer (EML) of the OLED to produce light. Tang and VanSlyke built the first practical OLED in 1987, which used tris (8-hydroxyquinoline) aluminum (Alq3) as the emitting layer, sandwiched between a transparent anode and a metallic cathode.[51-52] If high efficiency is to be achieved using such a layer, it must have a high luminescence yield as well as good hole/electron transport properties. Finding a single molecule that possesses all these properties is extremely rare. As a result, the introduction of two or more layers, such as an electron or hole transport layer (ETL or HTL), and an electron or hole injection layer (ELI or HIL), will provide OLEDs with the required functionality.[53] Therefore, modern OLED devices use many more layers to improve efficiency and durability, but their basic functionality remains the same (**Figure 1.16**). Such an effective scheme has tremendous applications in display and lighting, which have drawn considerable attention from both basic and commercial researchers.

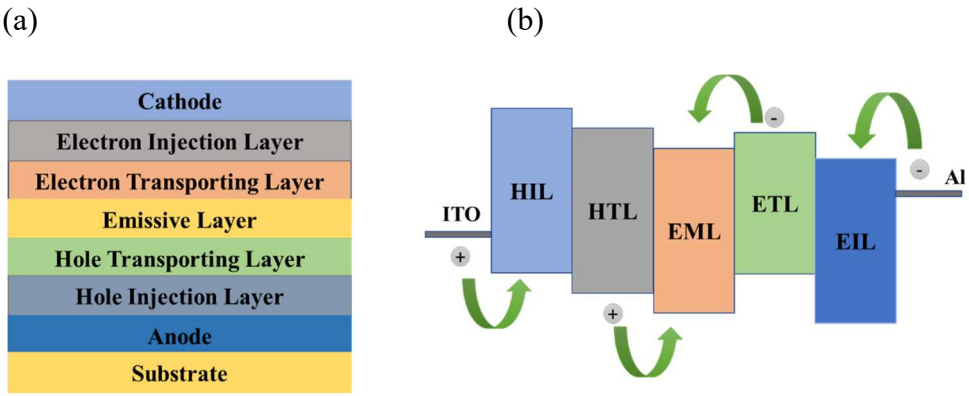

Figure 1.16 Device structure of OLED (a) and schematic representation of electron flow in OLED (b).

For OLEDs, materials and structures must be carefully designed, such as materials with suitable HOMO and LUMO levels, minimizing losses between layers and a balanced charge injection/recombination system. OLEDs use a transparent conducting anode such as indium tin oxide (ITO) which exhibits good electrical conductivity and optical transparency with a high work function. Typical cathode materials for OLEDs include metals with low work functions, such as Al, Ag, and Au. Most commonly, Al is used since it is much more stable under ambient conditions and much cheaper than Ag or Au. Lithium fluoride (LiF) deposited between Al and organic layers is used as a buffer layer to lower the injection barrier and improve electron injection efficiency. Electrons from the cathode are injected into LUMO level of the adjacent organic layer, while holes from the anode are injected into HOMO level. For proper hole injection, the HOMO of the HTL should lie near the work function of the anode and the EML. Similarly, for ease of electron injection, the LUMO level of ETL should lie close to the cathode work function and the EML, while its low-lying HOMO level can prevent escaped holes from reaching the cathode. The electron flow in OLED devices is shown in **Figure 1.16**. EML is located in the middle of the device, where the charges are recombined. To simplify device structure, it is desirable to use a non-doped single material EML. However, this approach has many challenges. Rather, appropriate host matrices are common in the process to improve recombination efficiency, as they often possess better transport properties than emitters alone, as well as increasing the charge balance and preventing the concentration of excitons from quenching.

The emitters of OLEDs are categorized into different groups based on the mechanism by which they operate **Figure 1.17** . The spin statistics suggest that singlet and triple excitons will be generated at a ratio of 1:3 upon electric excitation **Figure 1.16b**.

However typical fluorescent emitters can only employ singlet excitons to emit fluorescence, hence their maximal IQE is 25% in principle, with 75% triplet excitons dissipated in the form of heat. Given that out-coupling efficiency is typically less than 20%, the fluorescent OLED's maximum EQE is only 5%, significantly below expectation. To improve the efficiency of OLED devices, nonemissive triplet excitons should be explored for lightening. As a result, numerous processes have been proposed, as well as related emitters that have been built and used in OLEDs.[9, 54]

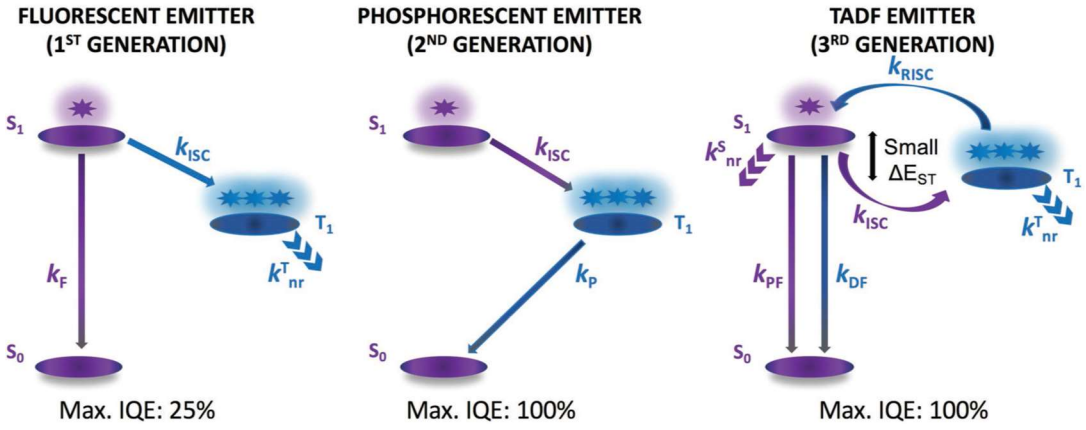

Figure 1.17 Different emitters for OLEDs and their exciton dynamic process. The Figure is copied from ref 54.

Phosphorescent materials, as the second-generation emitters, can utilize both singlets and triplets for phosphorescence to reach 100% IQE, with the mechanism of spin–orbit coupling. The phosphorescent materials have already made great commercial success, especially for the green and red emitters, however phosphorescent emitters contain some intrinsic disadvantages, like high cost and low stability. In order to develop both highly efficient and cost-effective OLED materials, several other strategies have been reported, among which thermally activated delayed fluorescence (TADF), triplet–triplet annihilation (TTA), and hybridized local and charge transfer (HLCT) are the most applied methods.[54]

1.5.3 N-Heterocycle Based Donor-Acceptor Derivatives for OLEDs

N-heterocyclic based donor-acceptor derivatives can be used for the development of high performance OLED devices. For example, The 1,4-diazatriphenylene (ATP) derivatives (**Figure 1.18**) were synthesized with various peripheral donor units and characterized as thermally activated delayed fluorescence (TADF) emitters[5]. The influence of the donor substituent on the electronic and photophysical properties of the materials was investigated by theoretical calculations and experimental spectroscopic measurements. These ATP-based molecules with donor–acceptor–donor (D–A–D) structures can reduce the singlet–triplet energy gap (0.04–0.26 eV) upon chemical modification of the ATP core, and thus exhibit obvious TADF characteristics in solution and doped thin films. These materials were used for fabrication and obtained the external electroluminescence quantum efficiencies above 12% and 8% for green- and sky-blue-emitting devices, respectively.[55]

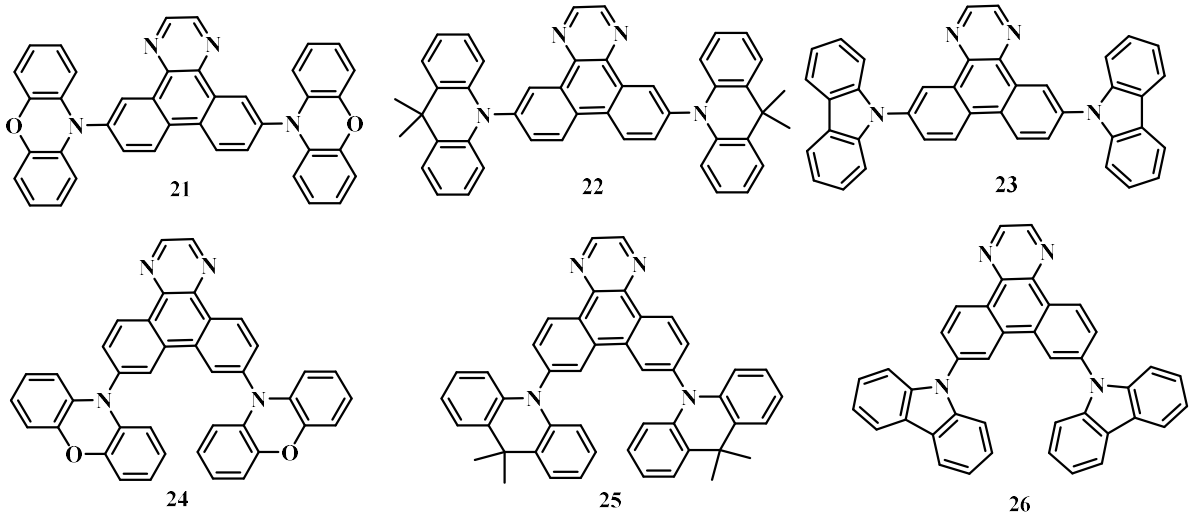

Figure 1.18 Molecular structures of donor-acceptor derivatives based on 1,4-diazatriphenylene (ATP) acceptor core, used for OLED device.

Shi-Jian Su et. al reported TADF materials having D-π- A molecular structure as shown in **Figure 1.19**, in which dicyano-pyrazine as an acceptor and t-butyl carbazole and dimethyl acridine as donors and the effects of k_F, k_{ISC}, k_{IC} and k_{RISC} on τ_{TADF} governing were investigated. It is observed that when TADF materials with short τ_{TADF} are employed in OLEDs, more suppressed efficiency roll-off at practical relevant brightness. OLEDs containing dimethyl acridine derivatives (**28**) as the emitting guest achieved orange-red TADF-OLEDs with an emission peak at 590 nm and the best EQEs of 12.4%, 9.9%, 5.1% at practical luminance of 100/ 1000/10000 cd m^{-2}.[56]

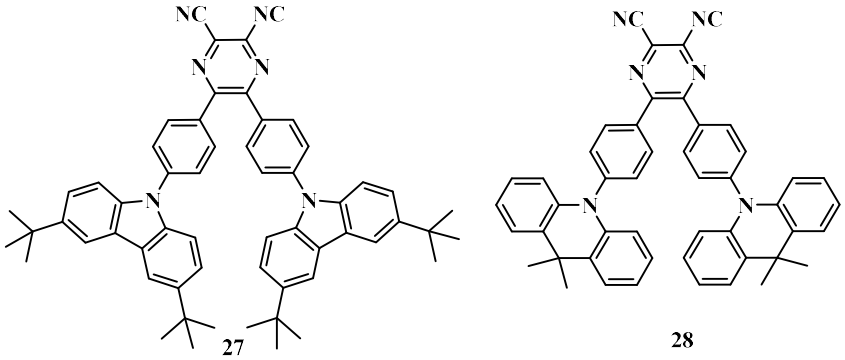

Figure 1.19 Molecular structures of dicyano-pyrazine derivatives having D-π-A structure for OLED application.

AIE active N-heterocyclic based donor-acceptor derivatives can be used for the development of non-doped OLED materials with high efficiency in the solid state.[57-58] For example, Yinghao Li, et al synthesized efficient red emitters consisting of TPE, benzo-2,1,3-thiadiazole, phenanthro[9,10-d]imidazole and triphenylamine moieties (**Figure 1.20**) show aggregation-induced emission (AIE) properties and emit strong red fluorescence in the aggregated state and carefully investigated the structure– property relationship.

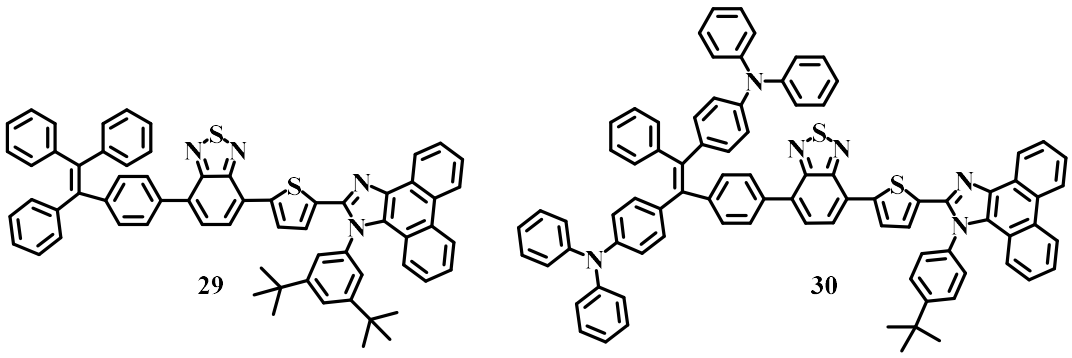

Figure 1.20 Molecular structures of benzothiazole based donor-acceptor derivatives for OLED application.

These derivatives exhibited strong red emissions in solid films also and perform well as light-emitting layers in nondoped red OLEDs with electroluminescence at 650 nm ($CIE_{x,y}$ = 0.665, 0.334) and a high luminance and an external quantum efficiency of up to 6277 cd m^{-2} and 2.17%, respectively.[59]

Han Zhang, et al reported six molecule based phenanthroimidazole derivatives (**31** to **36**) by introducing an aggregation-induced emission (AIE) moiety (tetraphenylethene,TPE) and a cyano group (CN) to the HLCT-typed core, phenanthroimidazole (PI), six luminescent compounds with different conjugation patterns at the C_2 and N_1 substituent positions were obtained (**Figure 1.21**) , and their excited states were regulated effectively. The non-doped OLED based on phenanthroimidazole derivatives exhibited excellent performance with a maximum luminance, current efficiency, and external quantum efficiency of up to 31070 cd m^{-2}, 18.46 cd A^{-1}, and 7.16%, respectively, and a very small efficiency roll-off of 4.0% at 1000 cd m^{-2} luminance.[60]

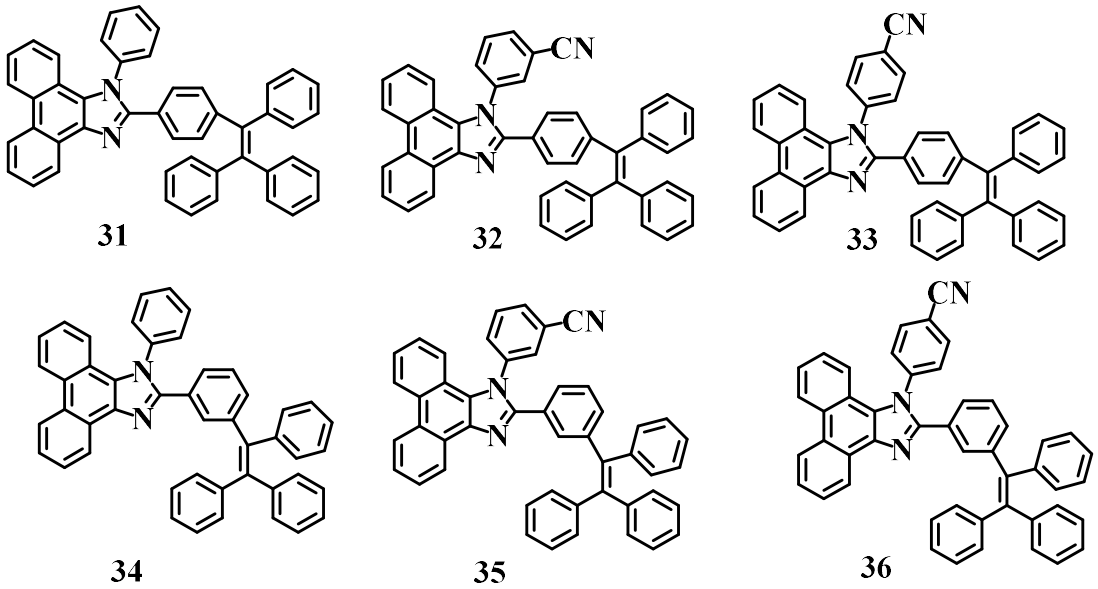

Figure 1.21 Molecular structures of phenanthroimidazole based donor-acceptor derivatives for OLEDs.

1.6 Mechanoresponsive Organic π-Conjugated Derivatives

1.6.1 Mechanochromism

Mechanochromic fluorescent material (also known as piezochromic materials) is a special class of 'smart' material that can change its colour or emission based on external stimulations such as grinding, compression and mechanical forces. Because organic solid emission properties are highly governed by molecular arrangements, and therefore external stimuli affecting molecular packing properties may have a tunable effect on solid-state emissions.[61-62] Mechanochromic behavior can be induced either by chemical or physical structural modification. However, physical structural change has been found to be more straight forward than chemical structural change to achieve highly efficient and reversible solid state fluorescence. In mechanosensors and optoelectronic devises as well as in security inks, mechanochromic fluorescent materials are widely used.[62]

Intermolecular interactions such as π-π interaction, C-H…π, C-H…N interactions and hydrogen bonding play an important for mechanochromic materials. It means that when a material is mechanically ground or subjected to hydrostatic pressure, intermolecular interactions can change, which will result in colour change or emission changes.

Therefore, it can be concluded that mechanochromic responses are caused by physical structural changes in molecules and are influenced primarily by their conformation, their molecular packing modes, and their intermolecular interactions. Further modulation of MFC properties can be achieved by changing their molecular configurations, such as incorporation of heteroatoms, heavy atoms, or halogen atoms, alkyl or aryl moieties, utilization of a DA framework, which result in distinct intermolecular interactions.[63]

1.6.2 N-Heterocyclic Based Mechanochromic Materials

Here are some examples of N-heterocycle derivatives that are used as mechanochromic materials. Zhang et al reported, in 2011, piezochromic behaviors of an organic small-molecule system based on 3(5)-(9-anthryl)pyrazole based derivative (**Figure 1.22**) and this study demonstrates the important role of π-π interactions in piezochromism. It is found that that these derivatives showed quite different emission-colour changes when ground in mortars or on quartz substrates by pestle: **37** changed from blue to green, and **38** changed from green to blue. It was also observed that, after heating 1b and 2b at 90 °C and 110 °C for 5 min, respectively, and allowing them to cool to room temperature, they regained their original emission colours which indicate the reversibility of piezochromic phenomenon. The photophysical and PXRD studies of pristine and ground samples showed the switching of emission colour upon griding due to phase changes and variation p-stacking of anthracene rings.[61]

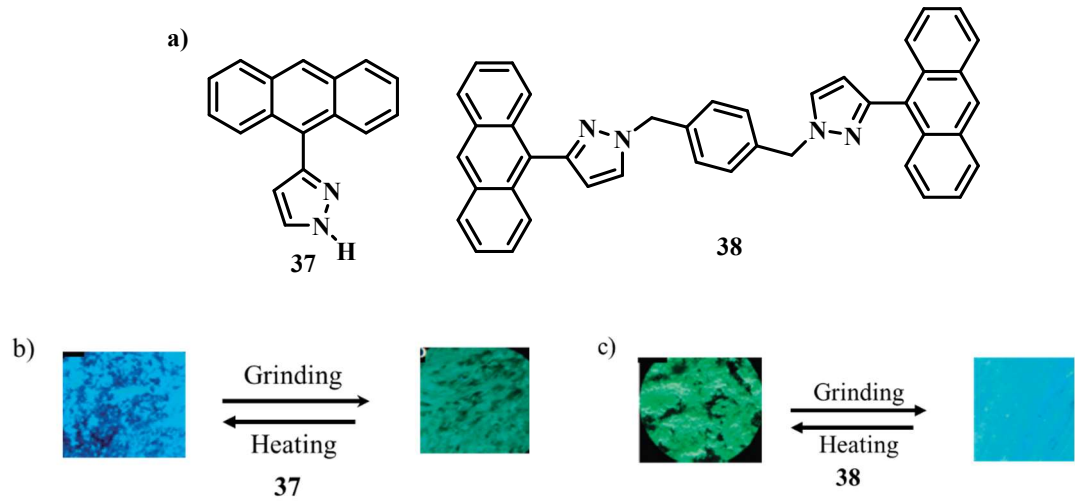

Figure 1.22 Molecular structures of 3(5)-(9-anthryl)pyrazole and its derivative (a); colour changes of **37** and **38** during griding and heating (b) and (c).

Similarly, Wang et al synthesized and studied benzothiazole derivative (**Figure 1.23**), **39,** with multistimuli-responsive properties. The **39** exhibited mechanochromism in such way that the orange coloured powder, obtained by vacuum sublimation or recrystallization, changed into yellow coloured powder with green emission after griding with a pestle or spatula.[62]

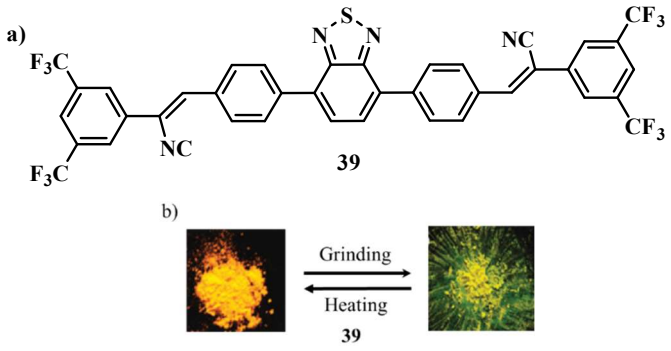

Figure 1.23 Molecular structure of benzothiazole derivative (a); colour changes during griding and heating (b).

Wang et al, in 2019, synthesized a series of mechanochromic materials composed of benzothiadiazole and phenoxazine with D-A-D and D-A-A architecture (**Figure 1.24**).

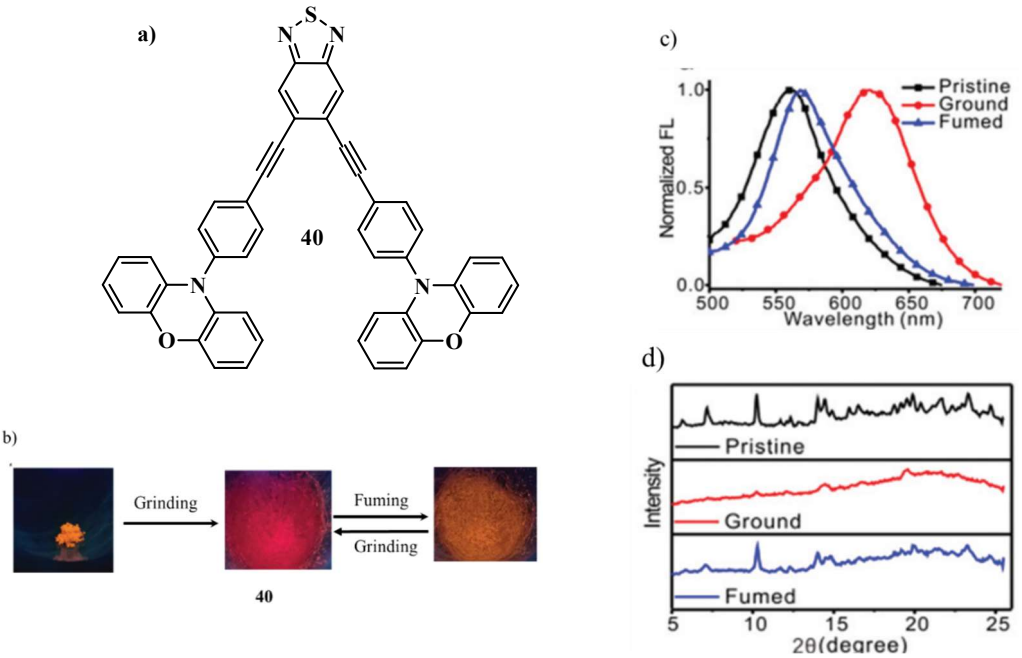

Figure 1.24 Molecular structure of benzothiazole derivative, **40**; Emission changes of **40** during griding and fuming; Emission spectra (c) and PXRD (d) of pristine, ground and fumed sample of **40**.

Among these N-phenoxazinyl based derivatives showed effective mechanochromic behaviour with colour change from orange to red (from 563 nm to 621 nm) upon grinding and red to orange after fuming ground sample.[64]

Khan et al developed different donor-acceptor architectures based phenanthroimidazole derivatives and studied the role of mode of attachment and position mode of different donors such as tetraphenylethylene (TPE) and phenothiazine in mechanochromic (**Figure 1.25**). Some of the derivatives are synthesized by utilizing an aggregation induced emission (AIE) fluorophores like TPE to achieve efficient mechanofluorochromic (MFC) materials. This work involves a comprehensive study of the MFC properties, AIE photophysical and electronic properties of the PI derivatives based on donor position, donor-acceptor strength, and conformation change with addition of spacers.[63]

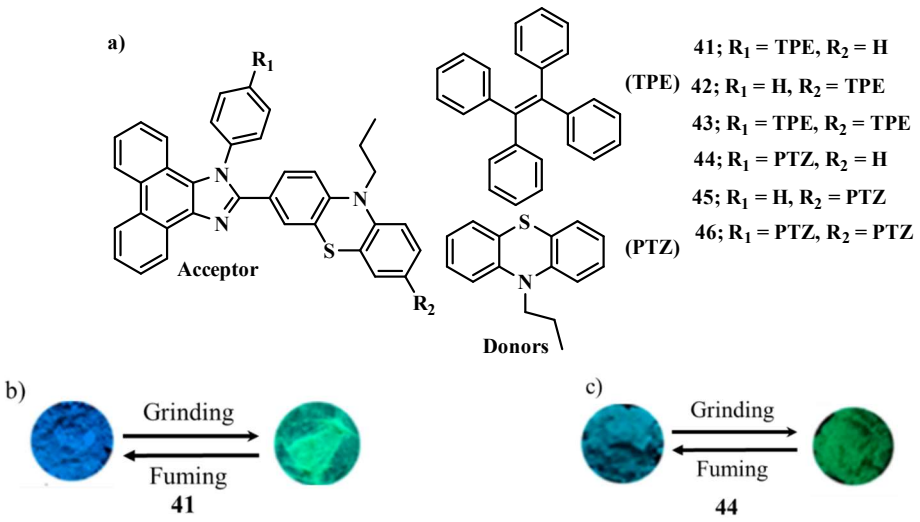

Figure 1.25 Molecular structures of phenanthroimidazole derivative and emission colour change of **41** and **44** during griding and fuming.

The pyrenoimidazoles derivatives **47** and **48** (**Figure 1.26**) exhibit reversible mechanochromic behavior with a color contrast between blue and green. The solid state absorption, emission and powder XRD studies reveal that the transformation of the twisted crystalline state to the planar amorphous state is the main cause of mechanochromism in the pyrenoimidazoles derivatives.[65]

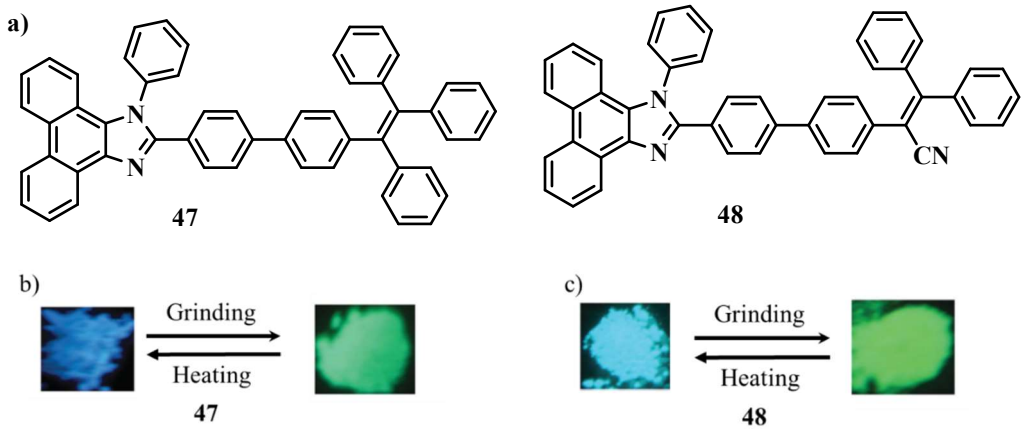

Figure 1.26 Molecular structures of pyrenoimidazoles derivatives derivative and their respective colour changes of **47** and **48** during griding and heating.

1.7 Objectives of the Thesis

The broad possibility to control the properties of the N-heterocyclic based organic π conjugated molecules by combining different π-conjugated building blocks, changing the donor and acceptor strength, changing the planarity or length of bridges between donor and acceptor, and tuning orbital interactions, making these materials attractive candidates for optoelectronic applications and smart materials such as mechano- responsive materials. The focus of this thesis is the synthesis, photophysical characterization and application of N-heterocyclic based multibranched donor-acceptor derivatives by changing the donor strength, or by changing the acceptor strength and by increasing the number of donors using steady state and time resolved spectroscopy such as femtosecond pump-probe spectroscopy and nanosecond transient laser flash photolysis spectroscopy. In **Chapter 2**, we synthesized tetraphenylpyrazine based multibranched donor-acceptor systems exhibiting aggregation induced emission properties and studied the excited states properties (singlet and triplet) using time resolved transient absorption techniques such as nanosecond transient absorption spectroscopy and femtosecond transient absorption spectroscopy. In **Chapter 3**, the effect of the electron withdrawing groups such as cyanide (CN) and fluoride (F) on photophysical properties of N-heterocycle based multibranched donor acceptor derivatives is investigated. For this, we selected quinoxaline as an acceptor moiety substituted with CN and F on quinoxaline ring and tert-butyl carbazole as donor moiety. We also studied the effect of substitution of CN and F on mechanoresponsive and acid sensing properties in solid state. In **chapter 4**, the effect of increasing the number of donor units on the photophysical properties of N-heterocycle based multibranched donor acceptor derivatives is studied. For this purpose, quinoxaline is used as acceptor and substituted with mono and tri tert-butyl carbazole as donor. Further, we studied the electroluminescent properties of these quinoxaline-tertbutyl carbazole derivatives by fabricating OLED devices.

1.8 References

1. Shirakawa, H.; Louis, E. J.; MacDiarmid, A. G.; Chiang, C. K.; Heeger, A. J., Synthesis of Electrically Conducting Organic Polymers: Halogen Derivatives of Polyacetylene, (Ch). *J. Chem. Soc., Chem. Commun.* **1977**, 578-580.

2. Bredas, J. L.; Silbey, R.; Boudreaux, D. S.; Chance, R. R., Chain-Length Dependence of Electronic and Electrochemical Properties of Conjugated Systems: Polyacetylene, Polyphenylene, Polythiophene, and Polypyrrole. *J. Am. Chem. Soc.* **1983**, *105*, 6555-6559.

3. Ostroverkhova, O., Organic Optoelectronic Materials: Mechanisms and Applications. *Chem. Rev.* **2016**, *116*, 13279-13412.

4. Meng, D., et al., High-Performance Solution-Processed Non-Fullerene Organic Solar Cells Based on Selenophene-Containing Perylene Bisimide Acceptor. *J. Am. Chem. Soc.* **2016**, *138*, 375-380.

5. Chen, H.; Zhang, W.; Li, M.; He, G.; Guo, X., Interface Engineering in Organic Field-Effect Transistors: Principles, Applications, and Perspectives. *Chem. Rev.* **2020**, *120*, 2879-2949.

6. Yuvaraja, S.; Nawaz, A.; Liu, Q.; Dubal, D.; Surya, S. G.; Salama, K. N.; Sonar, P., Organic Field-Effect Transistor-Based Flexible Sensors. *Chem. Soc. Rev.* **2020**, *49*, 3423-3460.

7. Zhang, Q.; Tsang, D.; Kuwabara, H.; Hatae, Y.; Li, B.; Takahashi, T.; Lee, S. Y.; Yasuda, T.; Adachi, C., Nearly 100% Internal Quantum Efficiency in Undoped Electroluminescent Devices Employing Pure Organic Emitters. *Adv. Mater.* **2015**, *27*, 2096-2100.

8. Hong, G.; Gan, X.; Leonhardt, C.; Zhang, Z.; Seibert, J.; Busch, J. M.; Bräse, S., A Brief History of Oleds—Emitter Development and Industry Milestones. *Adv. Mater.* **2021**, *33*, 2005630.

9. Wei, Q.; Fei, N.; Islam, A.; Lei, T.; Hong, L.; Peng, R.; Fan, X.; Chen, L.; Gao, P.; Ge, Z., Small-Molecule Emitters with High Quantum Efficiency: Mechanisms, Structures, and Applications in Oled Devices. *Adv. Opt. Mater.* **2018**, *6*, 1800512.

10. Shockley, W.; Queisser, H. J., Detailed Balance Limit of Efficiency of P-N Junction Solar Cells. *J. Appl. Phys.* **1961**, *32*, 510-519.

11. Rao, A.; Chow, P. C. Y.; Gélinas, S.; Schlenker, C. W.; Li, C.-Z.; Yip, H.-L.; Jen, A. K. Y.; Ginger, D. S.; Friend, R. H., The Role of Spin in the Kinetic Control of Recombination in Organic Photovoltaics. *Nature* **2013**, *500*, 435-439.

12. Yu, L.; Wu, Z.; Xie, G.; Zeng, W.; Ma, D.; Yang, C., Molecular Design to Regulate the Photophysical Properties of Multifunctional Tadf Emitters Towards High-Performance Tadf-Based Oleds with Eqes up to 22.4% and Small Efficiency Roll-Offs. *Chem. Sci.* **2018**, *9*, 1385-1391.

13. Yu, L.; Wu, Z.; Xie, G.; Zhong, C.; Zhu, Z.; Ma, D.; Yang, C., An Efficient Exciton Harvest Route for High-Performance Oleds Based on Aggregation-Induced Delayed Fluorescence. *ChemComm* **2018**, *54*, 1379-1382.

14. Feng, H.-T.; Zheng, X.; Gu, X.; Chen, M.; Lam, J. W. Y.; Huang, X.; Tang, B. Z., White-Light Emission of a Binary Light-Harvesting Platform Based on an Amphiphilic Organic Cage. *Chem. Mater.* **2018**, *30*, 1285-1290.

15. Han, M.; Chen, M.; Ebendorff-Heidepriem, H.; Fang, C.; Qin, A.; Zhang, H.; Tang, B. Z.; Tang, Y.; Ruan, Y., An Optical Fibre Sensor for Remotely Detecting Water Traces in Organic Solvents. *RSC Adv.* **2016**, *6*, 82186-82190.

16. Hu, F.; Xu, S.; Liu, B., Photosensitizers with Aggregation-Induced Emission: Materials and Biomedical Applications. *Adv. Mater.* **2018**, *30*, 1801350.

17. Hu, W., et al., Stimuli-Responsive Reversible Switching of Intersystem Crossing in Pure Organic Material for Smart Photodynamic Therapy. *Angew. Chem. Int. Ed. Engl.* **2019**, *58*, 11105-11111.

18. Kuehne, A. J. C.; Gather, M. C., Organic Lasers: Recent Developments on Materials, Device Geometries, and Fabrication Techniques. *Chem. Rev.* **2016**, *116 21*, 12823-12864.

19. Jiang, Y.; Liu, Y.-Y.; Liu, X.; Lin, H.; Gao, K.; Lai, W.-Y.; Huang, W., Organic Solid-State Lasers: A Materials View and Future Development. *Chem. Soc. Rev.* **2020**, *49*, 5885-5944.

20. Cao, S.; Shao, J.; Wu, H.; Song, S.; De Martino, M. T.; Pijpers, I. A. B.; Friedrich, H.; Abdelmohsen, L. K. E. A.; Williams, D. S.; van Hest, J. C. M., Photoactivated Nanomotors Via Aggregation Induced Emission for Enhanced Phototherapy. *Nat. Commun.* **2021**, *12*, 2077.

21. Cai, X.; Liu, B., Aggregation-Induced Emission: Recent Advances in Materials and Biomedical Applications. *Angew. Chem. Int. Ed. Engl.* **2020**, *59*, 9868-9886.

22. Kue, C. S.; Ng, S. Y.; Voon, S. H.; Kamkaew, A.; Chung, L. Y.; Kiew, L. V.; Lee, H. B., Recent Strategies to Improve Boron Dipyrromethene (Bodipy) for Photodynamic Cancer Therapy: An Updated Review. *J. Photochem. Photobiol. A* **2018**, *17*, 1691-1708.

23. Watson, W. F.; Livingston, R., Concentration Quenching of Fluorescence in Chlorophyll Solutions. *Nature* **1948**, *162*, 452-453.

24. Luo, J., et al., Aggregation-Induced Emission of 1-Methyl-1,2,3,4,5-Pentaphenylsilole. *ChemComm* **2001**, 1740-1741.

25. Bryce, M. R., Aggregation-Induced Delayed Fluorescence (Aidf) Materials: A New Break-through for Nondoped Oleds. *Science China Chemistry* **2017**, *60*, 1561-1562.

26. Mei, J.; Leung, N. L. C.; Kwok, R. T. K.; Lam, J. W. Y.; Tang, B. Z., Aggregation-Induced Emission: Together We Shine, United We Soar! *Chem. Rev.* **2015**, *115*, 11718-11940.

27. Chen, J.; Law, C. C. W.; Lam, J. W. Y.; Dong, Y.; Lo, S. M. F.; Williams, I. D.; Zhu, D.; Tang, B. Z., Synthesis, Light Emission, Nanoaggregation, and Restricted Intramolecular Rotation of 1,1-Substituted 2,3,4,5-Tetraphenylsiloles. *Chemistry of Materials* **2003**, *15*, 1535-1546.

28. Fan, X.; Sun, J.; Wang, F.; Chu, Z.; Wang, P.; Dong, Y.; Hu, R.; Tang, B. Z.; Zou, D., Photoluminescence and Electroluminescence of Hexaphenylsilole Are Enhanced by Pressurization in the Solid State. *Chem. Commun.* **2008**, 2989-2991.

29. Zhao, Z.; Lam, J. W. Y.; Tang, B. Z., Tetraphenylethene: A Versatile Aie Building Block for the Construction of Efficient Luminescent Materials for Organic Light-Emitting Diodes. *J. Mater. Chem.* **2012**, *22*, 23726-23740.

30. Wang, X.; Hu, J.; Zhang, G.; Liu, S., Highly Selective Fluorogenic Multianalyte Biosensors Constructed Via Enzyme-Catalyzed Coupling and Aggregation-Induced Emission. *J. Am. Chem. Soc.* **2014**, *136*, 9890-9893.

31. Li, S.; Wang, Q.; Qian, Y.; Wang, S.; Li, Y.; Yang, G., Understanding the Pressure-Induced Emission Enhancement for Triple Fluorescent Compound with Excited-State Intramolecular Proton Transfer. *J. Phys. Chem. A* **2007**, *111*, 11793-11800.

32. Fan, X.; Sun, J.; Wang, F.; Chu, Z.; Wang, P.; Dong, Y.; Hu, R.; Tang, B. Z.; Zou, D., Photoluminescence and Electroluminescence of Hexaphenylsilole Are Enhanced by Pressurization in the Solid State. *ChemComm* **2008**, 2989-2991.

33. Peng, Q.; Yi, Y.; Shuai, Z.; Shao, J., Toward Quantitative Prediction of Molecular Fluorescence Quantum Efficiency: Role of Duschinsky Rotation. *J. Am. Chem. Soc.* **2007**, *129*, 9333-9339.

34. Peng, Q.; Yi, Y.; Shuai, Z.; Shao, J., Excited State Radiationless Decay Process with Duschinsky Rotation Effect: Formalism and Implementation. *Chem. Phy.* **2007**, *126*, 114302.

35. Luo, J.; Song, K.; Gu, F. l.; Miao, Q., Switching of Non-Helical Overcrowded Tetrabenzoheptafulvalene Derivatives. *Chem. Sci.* **2011**, *2*, 2029-2034.

36. Mei, J.; Hong, Y.; Lam, J. W. Y.; Qin, A.; Tang, Y.; Tang, B. Z., Aggregation-Induced Emission: The Whole Is More Brilliant Than the Parts. **2014**, *26*, 5429-5479.

37. Feng, G.; Kwok, R. T. K.; Tang, B. Z.; Liu, B., Functionality and Versatility of Aggregation-Induced Emission Luminogens. *Appl. Phy. Rev.* **2017**, *4*, 021307.

38. Hu, R.; Lam, J. W. Y.; Liu, Y.; Zhang, X.; Tang, B. Z., Aggregation-Induced Emission of Tetraphenylethene–Hexaphenylbenzene Adducts: Effects of Twisting Amplitude and Steric Hindrance on Light Emission of Nonplanar Fluorogens. *Chem. Eur. J* **2013**, *19*, 5617-5624.

39. He, J.; Xu, B.; Chen, F.; Xia, H.; Li, K.; Ye, L.; Tian, W., Aggregation-Induced Emission in the Crystals of 9,10-Distyrylanthracene Derivatives: The Essential Role of Restricted Intramolecular Torsion. *J. Phys. Chem. C* **2009**, *113*, 9892-9899.

40. L. Mullin, J.; Tracy, H.; R. Ford, J.; R. Keenan, S.; Fridman, F., *Characteristics of Aggregation Induced Emission in 1,1dimethyl2,3,4,5-Tetraphenyl and 1,1,2,3,4,5-Hexaphenyl Siloles and Germoles*, 2007; Vol. 17, p 201-213.

41. Tracy, H. J.; Mullin, J. L.; Klooster, W. T.; Martin, J. A.; Haug, J.; Wallace, S.; Rudloe, I.; Watts, K., Enhanced Photoluminescence from Group 14 Metalloles in Aggregated and Solid Solutions. *Inorg. Chem.* **2005**, *44*, 2003-2011.

42. Feng, X.; Tong, B.; Shen, J.; Shi, J.; Han, T.; Chen, L.; Zhi, J.; Lu, P.; Ma, Y.; Dong, Y., Aggregation-Induced Emission Enhancement of Aryl-Substituted Pyrrole Derivatives. *J. Phys. Chem. B* **2010**, *114*, 16731-16736.

43. Lai, C.-T.; Hong, J.-L., Aggregation-Induced Emission in Tetraphenylthiophene-Derived Organic Molecules and Vinyl Polymer. *J. Phys. Chem. B* **2010**, *114*, 10302-10310.

44. Fukazawa, A.; Ichihashi, Y.; Yamaguchi, S., Intense Fluorescence of 1-Aryl-2,3,4,5-Tetraphenylphosphole Oxides in the Crystalline State. *New J. Chem.* **2010**, *34*, 1537-1540.

45. Xu, S.; Duan, Y.; Liu, B., Precise Molecular Design for High-Performance Luminogens with Aggregation-Induced Emission. *Adv. Mater.* **2020**, *32*, 1903530.

46. Gu, X.; Yao, J.; Zhang, G.; Zhang, C.; Yan, Y.; Zhao, Y.; Zhang, D., New Electron-Donor/Acceptor-Substituted Tetraphenylethylenes: Aggregation-Induced Emission with Tunable Emission Color and Optical-Waveguide Behavior. *Chem Asian J.* **2013**, *8*, 2362-2369.

47. Ishi-i, T.; Ikeda, K.; Kichise, Y.; Ogawa, M., Red-Light-Emitting System Based on Aggregation of Donor–Acceptor Derivatives in Polar Aqueous Media. *Chem. Asian J.* **2012**, *7*, 1553-1557.

48. Xu, W.; Lee, M. M. S.; Zhang, Z.; Sung, H. H. Y.; Williams, I. D.; Kwok, R. T. K.; Lam, J. W. Y.; Wang, D.; Tang, B. Z., Facile Synthesis of Aiegens with Wide Color Tunability for Cellular Imaging and Therapy. *Chem. Sci.* **2019**, *10*, 3494-3501.

49. Pan, L.; Wu, H.; Liu, J.; Xue, K.; Luo, W.; Chen, P.; Wang, Z.; Qin, A.; Tang, B. Z., Tetraphenylpyrazine Based Aie Luminogens: Unique Excited State Decay and Its Application in Deep-Blue Light-Emitting Diodes. *Adv. Opt. Mater.* **2019**, *7*, 1801673.

50. Guo, J., et al., Tetraphenylpyrazine Decorated 1,3-Di(9h-Carbazol-9-Yl)Benzene (Mcp): A New Aie-Active Host with Enhanced Performance of Organic Light-Emitting Diodes. *J. Mater. Chem. C* **2019**, *7*.

51. History of Oleds. In *Oled Displays and Lighting*, 2016; pp 1-11.

52. Tang, C. W.; VanSlyke, S. A., Organic Electroluminescent Diodes. *Appl. Phys. Lett.* **1987**, *51*, 913-915.

53. Bizzarri, C.; Spuling, E.; Knoll, D. M.; Volz, D.; Bräse, S., Sustainable Metal Complexes for Organic Light-Emitting Diodes (Oleds). *Coord. Chem. Rev.* **2018**, *373*, 49-82.

54. Wong, M. Y.; Zysman-Colman, E., Purely Organic Thermally Activated Delayed Fluorescence Materials for Organic Light-Emitting Diodes. *Adv. Mater.* **2017**, *29*, 1605444.

55. Takahashi, T.; Shizu, K.; Yasuda, T.; Togashi, K.; Adachi, C., Donor-Acceptor-Structured 1,4-Diazatriphenylene Derivatives Exhibiting Thermally Activated Delayed Fluorescence: Design and Synthesis, Photophysical Properties and Oled Characteristics. *Sci. Technol. Adv. Mater.* **2014**, *15*, 034202.

56. Cai, X.; Li, X.; Xie, G.; He, Z.; Gao, K.; Liu, K.; Chen, D.; Cao, Y.; Su, S.-J., "Rate-Limited Effect" of Reverse Intersystem Crossing Process: The Key for Tuning Thermally Activated Delayed Fluorescence Lifetime and Efficiency Roll-Off of Organic Light Emitting Diodes. *Chem. Sci.* **2016**, *7*, 4264-4275.

57. Li, J.; Shan, T.; Yao, M.; Gao, Y.; Han, X.; Yang, B.; Lu, P., The Effect of Different Binding Sites on the Optical and Electronic Properties of Tetraphenylethylene-Substituted Thiophene Isomers. *J. Mater. Chem. C* **2017**, *5*, 2552-2558.

58. Lo, D.; Chang, C.-H.; Krucaite, G.; Volyniuk, D.; Grazulevicius, J. V.; Grigalevicius, S., Sky-Blue Aggregation-Induced Emission Molecules for Non-Doped Organic Light-Emitting Diodes. *J. Mater. Chem. C* **2017**, *5*, 6054-6060.

59. Li, Y. H.; Wang, W. G.; Zhuang, Z. Y.; Wang, Z. M.; Lin, G. W.; Shen, P. C.; Chen, S. M.; Zhao, Z. J.; Tang, B. Z., Efficient Red Aiegens Based on Tetraphenylethene: Synthesis, Structure, Photoluminescence and Electroluminescence. *J. Mater. Chem. C* **2018**, *6*, 5900-5907.

60. Zhang, H.; Zeng, J. J.; Luo, W. W.; Wu, H. Z.; Zeng, C.; Zhang, K. X.; Feng, W. Q.; Wang, Z. M.; Zhao, Z. J.; Tang, B. Z., Synergistic Tuning of the Optical and Electrical Performance of Aiegens with a Hybridized Local and Charge-Transfer Excited State. *J. Mater. Chem. C* **2019**, *7*, 6359-6368.

61. Zhang, Z.; Yao, D.; Zhou, T.; Zhang, H.; Wang, Y., Reversible Piezo- and Photochromic Behaviors Accompanied by Emission Color Switching of Two Anthracene-Containing Organic Molecules. *ChemComm* **2011**, *47*, 7782-7784.

62. Chi, Z.; Zhang, X.; Xu, B.; Zhou, X.; Ma, C.; Zhang, Y.; Liu, S.; Xu, J., Recent Advances in Organic Mechanofluorochromic Materials. *Chem. Soc. Rev.* **2012**, *41*, 3878-3896.

63. Khan, F.; Ekbote, A.; Mobin, S. M.; Misra, R., Mechanochromism and Aggregation-Induced Emission in Phenanthroimidazole Derivatives: Role of Positional Change of Different Donors in a Multichromophoric Assembly. *J. Org. Chem.* **2021**, *86*, 1560-1574.

64. Wang, Z.; Peng, Z.; Huang, K.; Lu, P.; Wang, Y., Butterfly-Shaped Π-Extended Benzothiadiazoles as Promising Emitting Materials for White Oleds. *J. Mater. Chem. C* **2019**, *7*, 6706-6713.

65. Jadhav, T.; Dhokale, B.; Mobin, S. M.; Misra, R., Aggregation Induced Emission and Mechanochromism in Pyrenoimidazoles. *J. Mater. Chem. C* **2015**, *3*, 9981-9988.

Chapter 2

Molecular torsion controls the excited state relaxation pathways of multibranched tetraphenylpyrazines: Effect of molecular geometry and strength of donors

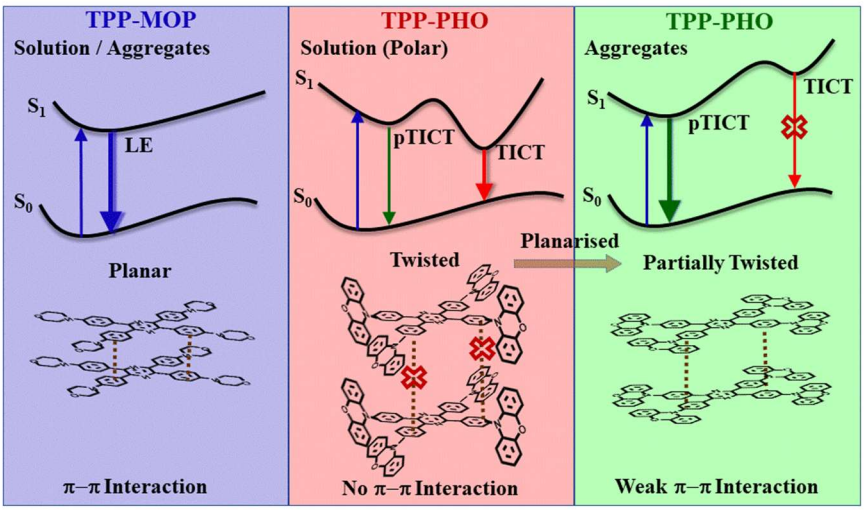

2.1 Abstract

Here to understand the effect of molecular geometry and strength of donors on the photophysical properties and ultrafast excited state relaxation pathways, multibranched tetraphenylpyrazine covalently linked with morpholine (weak donor and planar, ***TPP-4MOP****) and phenoxazine (strong donor and twisted,* ***TPP-4PHO****) derivatives were synthesized and their steady state and time-resolved photophysical properties were investigated.* ***TPP-4MOP*** *showed feeble emission (~0.03) and* ***TPP-4PHO*** *exhibited strong emission (~0.18) comparatively in non-polar solvent, toluene. Whereas the emission spectra of* ***TPP-4PHO*** *in polar solvent, THF showed large Stokes shift (~9691cm^{-1}) with low fluorescence quantum yield (~0.01) due to the formation of twisted intramolecular charge transfer state (TICT). Aggregation studies of* ***TPP-4PHO*** *in THF and water mixture reflect the elimination of TICT state by the restriction of intramolecular torsion in the aggregates leading to an increase (12 fold) of blue shifted fluorescence. The femtosecond*

and nanosecond transient absorption and picosecond time-resolved emission spectra of ***TPP-4PHO*** *revealed the existence of partial TICT and TICT states in the THF leading to the triplet state. Whereas in the case of* ***TPP-4MOP****, the transient absorption spectra showed the formation of triplet state from the local excited state without involvement of TICT state. These studies revealed that the excited state relaxation pathways of derivatives are controlled by polarity dependent torsional motion.*

2.2 Introduction

The enrichment of efficient fluorescence materials having donor-acceptor organic chromophores is important for their various potential applications including organic light emitting diodes[1-3], sensors,[4-5] lasers[6-8] and biomedical applications.[9-12] Compared to simple donor-acceptor (D-A) systems, multibranched organic derivatives having donor-acceptor architectures of D_3−A or D_4−A have attracted great interest[13-15] due to their better photophysical properties compared to their monomer units. However, their excited state relaxation dynamics are not well understood due to their complexity of their delocalization of excitation[16-17]. Indeed, their photophysical properties significantly depend on the various factors including electronic nature of the donor and acceptor, planarity of the bridge, and nature of ground and excited states.[16-22]

Here we selected the central moiety of pyrazine with four peripheral phenyl groups, acting as an acceptor and considered as a potential aggregation-induced emission (AIE) core[23-26] among the AIE luminogens.[27-29] Based on the geometry of the donor, the tetraphenylpyrazine (TPP) derivatives could lead to either planar or twisted conformation exhibiting the aggregation caused fluorescence quenching by π−π interaction or aggregation induced fluorescence enhancement by restriction of intramolecular torsion respectively, during the aggregation or in the solid state.[24, 30-31] To shed more light on the intramolecular torsion, especially to understand the twisted intramolecular charge transfer

(TICT) dynamics controlling the fluorescence behavior, many theoretical[32-34] and experimental[35-43] studies of the various donor-acceptor systems have been carried out.[44] Nevertheless, excited state relaxation dynamics of multibranched donor-acceptor derivatives have not been investigated in detail.[45-48] These studies would help to understand the inherent nature of (de)localization of excitation of these derivatives to improve the efficiency when applied to the optoelectronic devices.[49-52]

Here we investigated the steady-state and excited state dynamics of TPP derivatives by substituting the electron donor of morpholine (weak and planar, **TPP-4MOP**) and phenoxazine (strong and twisted, **TPP-4PHO**) in non-polar (toluene) and polar (THF) solvents to understand the effect of intramolecular torsion on the photophysical properties. The molecular structures of TPP derivatives are shown in **Figure 2.1**. It is found that **TPP-4MOP** showed weak fluorescence in both solvents (~0.03), whereas **TPP-4PHO** exhibited strong emission in toluene (~0.18) and reduced to ~0.01 in THF due to the occurrence of TICT. Femtosecond transient absorption spectra supported the occurrence of TICT in **TPP-4PHO** in THF and excited state relaxation pathways of both the derivatives are characterized.

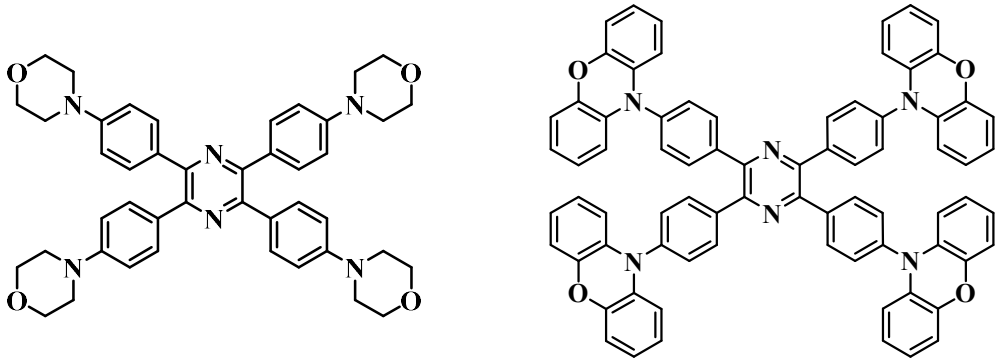

TPP-4MOP **TPP-4PHO**

Figure 2.1 Molecular structure of **TPP-4MOP** and **TPP-4PHO**.

2.3 Results and Discussion

2.3.1 Synthesis

The chemical structures and synthetic scheme of the intermediates and desired TPP derivatives are shown in the **Scheme 2.1**. The TPP derivatives were synthesized from the intermediate of 2,3,5,6-tetrakis(4-bromophenyl) pyrazine by coupling with corresponding donors (morpholine and phenoxazine) using the palladium catalyzed Buchwald−Hartwig reaction method.[1, 53] The chemical structure of **TPP-4MOP** and **TPP-4PHO** was characterized by ^{1}H and ^{13}C NMR and MALDI-TOF or HRMS and spectral data are provided in the Supporting Information.

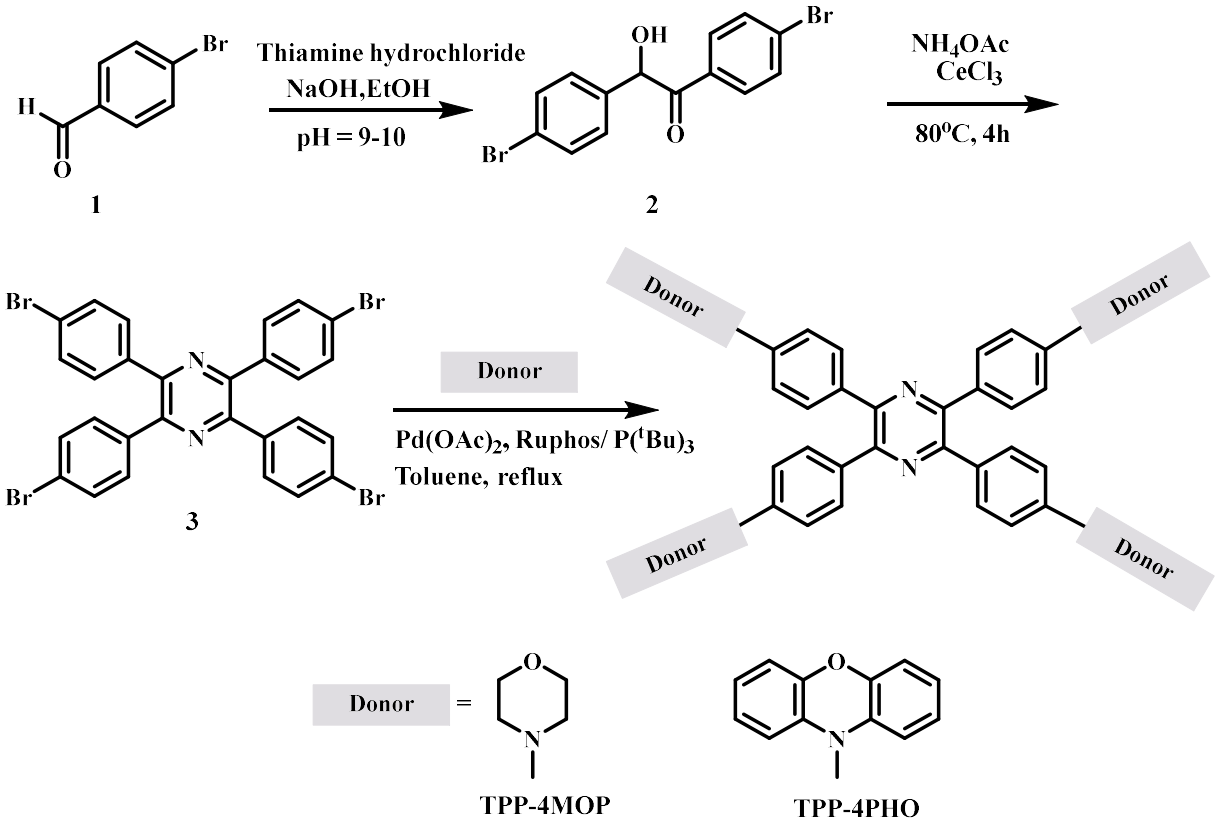

Scheme 2.1 Synthesis scheme of TPP derivatives.

2.3.2 Steady State Photophysical Characterization

The absorption and emission spectra of TPP derivatives were measured in toluene and THF (**Figure 2.2**). **TPP-4MOP** showed two absorption maxima at ~318 and 385 nm. The absorption spectra of **TPP-4PHO** exhibiting a strong absorption maximum at ~326 nm and weak band at ~395 nm could be due to the $\pi-\pi^*$ and intramolecular charge transfer (ICT) transitions of the derivative respectively.[24] The molar extinction coefficient (ε) of **TPP-4MOP** and **TPP-4PHO** is calculated to be 37,912 $M^{-1}cm^{-1}$ and 4,728 $M^{-1}cm^{-1}$, respectively. The lower value of ε of **TPP-4PHO** indicates that the **TPP-4PHO** possess more twisted conformation than **TPP-4MOP**, which is also supported by theoretical optimization. The absorption and emission spectra of **TPP-4MOP** did not show any significant changes with increase of solvent polarity from toluene to THF. In the case of **TPP-4PHO**, though no major changes in the absorption spectra upon changing the polarity of the solvent, there is a significant shift of the emission maximum to red region (640 nm) in THF supporting the occurrence of TICT. This is consistent with more electron donating ability of phenoxazine (E°_{ox} (V) = 0.23)[54] compared to morpholine (E°_{ox} (V) = 0.86).[55] Further to evaluate the variation of the dipole moment between the ground and excited states, the Lippert-Mataga equation[56-57] was used.

$$\upsilon_a - \upsilon_f = \frac{2(\mu_e-\mu_g)^2}{hca^3}\left[\frac{\varepsilon-1}{2\varepsilon+1} - \frac{n^2-1}{2n^2+1}\right] \quad (1)$$

Where μ_e and μ_g are the dipole moments of the molecule in the excited and ground states, respectively, a is the effective radius of Onsager's cavity, and ε and n are the static dielectric constant and the refractive index of the solvent respectively. Lippert-Mataga plot (**Figure 2.2 (d**)) of **TPP-4PHO** using solvent polarity function and Stokes shift provided the change in the excited state dipole moment which is found to be around 9.84 D and consistent with theoretical value (9.90 D) attained by the optimization.

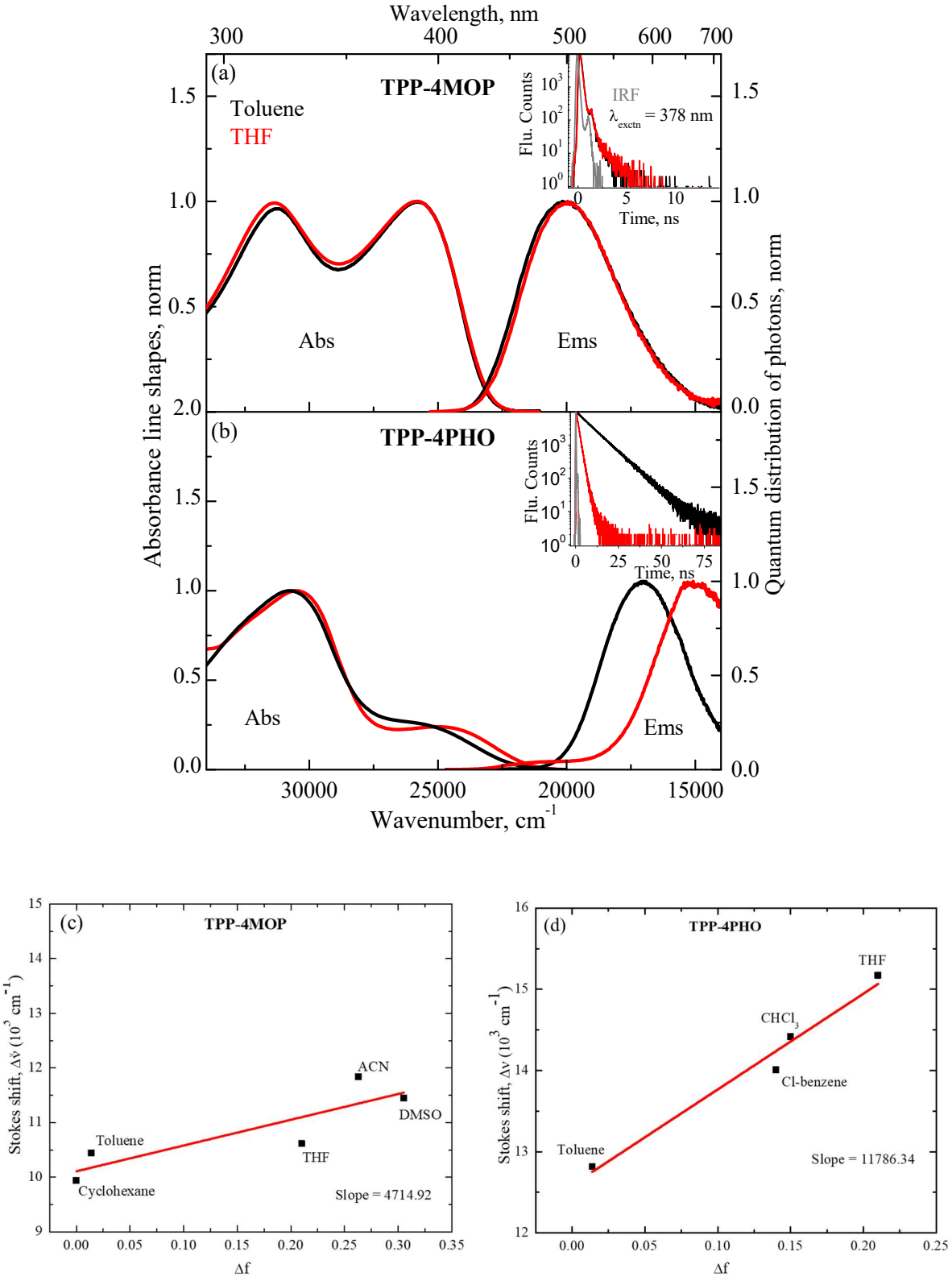

Figure 2.2 Steady state absorption and emission spectra of **TPP-4MOP** (a) and **TPP-4PHO** (b) in toluene and THF at room temperature. The insets show the fluorescence decay profile obtained upon excitation at 378 nm. Lippert- Mataga plot for **TPP-4MOP** (c) and **TPP-4PHO** (d).

Table 1 Absorption and fluorescence maxima, quantum yield and lifetime of TPP derivatives.

Compounds	Solvent	Absorption max, nm (λ_{max})	Fluorescence max, nm (λ_{max})	Stokes shift, cm^{-1}	Fluorescence quantum yield[a] (Φ_f)	Fluorescence lifetime[b], ns (τ)	Radiative constant, 10^7 s^{-1} (K_r)	Non-Radiative Constant, 10^9 s^{-1} (K_{nr})
TPP-4MOP	Toluene	318, 385	478	4966	0.03	0.134	22.38	7.23
	THF	318, 385	480	5141	0.03	0.136	22.05	7.13
TPP-4PHO	Toluene	326, 400	563	7554	0.18	8.91	2.02	0.09
	THF	326, 395	640	9691	0.01	0.133 (4.79%) 1.35 (95.21%)	1.06	1.05

[a]Fluorescence quantum yield in toluene and THF obtained upon excitation at 385 nm. [b] Fluorescence lifetime was obtained upon excitation at 378 nm.

The relative fluorescence quantum yield and lifetime of TPP derivatives were measured in toluene and THF. Though there is no significant changes in the fluorescence quantum yield of **TPP-4MOP** (0.03) upon increasing the polarity of the solvent, there is a decrease of fluorescence quantum yield of **TPP-4PHO** from 0.18 (toluene) to 0.01(THF) suggesting the involvement of non-radiative decay pathway in the polar solvent. The fluorescence quantum yield in the solid-state was found to be 0.04 and 0.12 for **TPP-4MOP** and **TPP-4PHO** respectively and matching with the values obtained in the non-polar solvent of toluene.The fluorescence lifetime of **TPP-4MOP** (0.13 ns) did not change significantly upon increasing the polarity of solvent, however in the case of **TPP-4PHO**, a decrease of lifetime was observed in THF (0.13 and 1.35 ns) compared to that of in toluene (8.91 ns), (Inset of **Figure 2.2a** and **2.2b**).The radiative and non-radiative rate constants of TPP derivatives are calculated from their fluorescent lifetime and quantum yield using the following equations.[58]

$$k_r = \frac{\Phi}{\tau_f} \tag{2}$$

$$k_{nr} = \frac{1}{\tau_f} - k_r \tag{3}$$

Upon increasing the polarity of the solvent, an increase of non-radiative constant was observed in **TPP-4PHO**. Thus, the large Stokes shift, decrease of fluorescence quantum yield and lifetime could be due to the occurrence of the non-radiative conformational changes leading to the TICT as observed in other derivatives. [36, 59]

2.3.3 Electrochemical Characterization

The electrochemical properties of **TPP-4MOP** and **TPP-4PHO** in dichloromethane (DCM) were characterized using cyclic voltammetry (CV) with conventional three electrodes system (**Figure 2.3**). The reversible oxidation waves at +0.34 and +0.80 V and quasi-reversible reduction wave at −1.25 V were observed

for **TPP-4MOP**. The reversible oxidation and quasi-reversible reduction wave of **TPP-4PHO** were observed at +0.38 and −1.25 V respectively (**Table 2.2**).

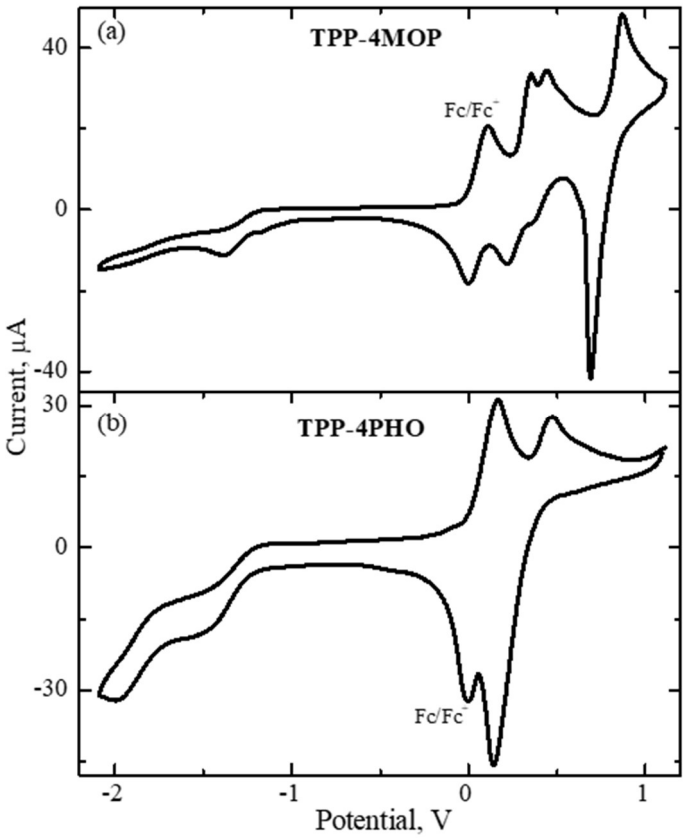

Figure 2.3 Cyclic voltammogram of **TPP-4MOP** (a) and **TPP-4PHO** (b) in deaerated DCM solutions. The internal standard, ferrocene (Fc) was used to set 0 V in the cyclic voltammograms. (Scan rate = 0.50 mV/s).

Table 2.2. Electrochemical data of **TPP-4MOP** and **TPP-4PHO**

	E_{ox}, V	E_{red}, V	HOMO[a], eV	LUMO[b], eV
TPP-4MOP	+0.34, +0.80	-1.25	-5.20	-3.15
TPP-4PHO	+0.38	-1.25	-4.78	-3.15

[a] Calculated by $E_{HOMO} = -(E_{ox} + 4.78 – E_{ox}(Fc))$. [b] Calculated by $E_{LUMO} = -(E_{red} + 4.78 – E_{ox}(Fc))$.

The highest occupied molecular orbital (HOMO) and lowest unoccupied molecular orbital (LUMO) energy levels of **TPP-4MOP** and **TPP-4PHO** were calculated using the oxidation potential and the optical band gap energies, E_g. The

values of HOMO (LUMO) were found to be –5.20 (–3.15) and –4.78 (–3.15) eV for **TPP-4MOP** and **TPP-4PHO** respectively.

The thermodynamic feasibility of photo-induced charge separation of TPP derivatives are examined by calculating the Gibbs free energy change (ΔG_{CS}) using Rehm-Weller equation as follows.[60]

$$\Delta G_{CS} = [\, E_{ox} - E_{red}] - E_{00} + \Delta G_S \quad (4)$$

$$\Delta G_S = \frac{e^2}{4\pi\varepsilon_S\varepsilon_0 R_{CC}} - \frac{e^2}{8\pi\varepsilon_0}\left(\frac{1}{R_D} + \frac{1}{R_A}\right)\left(\frac{1}{\varepsilon_{REF}} - \frac{1}{\varepsilon_S}\right) \quad (5)$$

Where ΔG_S is the static Coulombic energy as defined by equation (5), e is the electronic charge, E_{ox} and E_{red} are the oxidation and reduction potentials of the donor and acceptor moieties, respectively, and E_{00} denotes approximated energy level with the cross point of normalized absorption and emission spectra at singlet excited state, ε_S is static dielectric constant of the solvent, R_{CC} is center-to-center distance between the MOP, PHO (electron donor unit) and pyrazine (electron acceptor unit) determined by DFT optimization of the geometry, R_D and R_A are the radius of the electron donor and acceptor respectively, ε_{REF} is the static dielectric constant of the solvent used for the electrochemical studies, and ε_0 is the permittivity of free space.

The ΔG_{CS} of the **TPP-4MOP** and **TPP-4PHO** in THF was found to be –0.98 eV and –1.24 eV respectively and the negative value of the ΔG_{CS} represents the feasibility of the intramolecualr charge separation thermodynamically. The more negative value of ΔG_{CS} of the **TPP-4PHO** is consistent with the decrease of fluorescence quantum yield and the more electron donating capability of phenoxazine compared to morpholine, leading to the intramolecular charge transfer state. It is to be noted that Rehm−Weller equation will be appropriate for individual or weakly coupled or well separated donor-acceptor derivatives rather than the multibranched donor-acceptor derivatives.

Table 2.3. Thermodynamic characteristics of TPP derivatives**.**

TPP Derivatives	Solvent	E_{00}[a], eV	ΔG_{CS}[b], eV
TPP-4MOP	Toluene	2.90	1.21
	THF	2.90	-0.98
TPP-4PHO	Toluene	2.65	0.12
	THF	2.65	-1.24

[a] Calculated from the cross point of normalized absorption and emission spectra at singlet excited state. Calculate using Rehm−Weller equation.

2.3.4 Theoretical Calculations

Theoretical optimizations were carried out to understand the conformational structures of the TPP derivatives. The results of energy gap between HOMO and LUMO, ground state and excited state dipole moments, S_1 and T_1 vertical excitation energies are provided in the **Table 2.4**. **Figure 2.4** shows that the electron density of **TPP-4MOP** is delocalised on entire molecule in HOMO and LUMO. Whereas in the case of **TPP-4PHO**, the electron density is well confined on phenoxazine and pyrazine moieties in the HOMO and in LUMO respectively. Such a difference of observation could be due to the stronger electron donating capability of phenoxazine compared to morpholine. It is also found that the **TPP-4PHO** showed high torsional angle of 76.8° between the phenoxazine moieties and phenyl bridges compared to that of **TPP-4MOP** (5.6°). This further supports the formation of TICT in **TPP-4PHO** compared to **TPP-4MOP**.

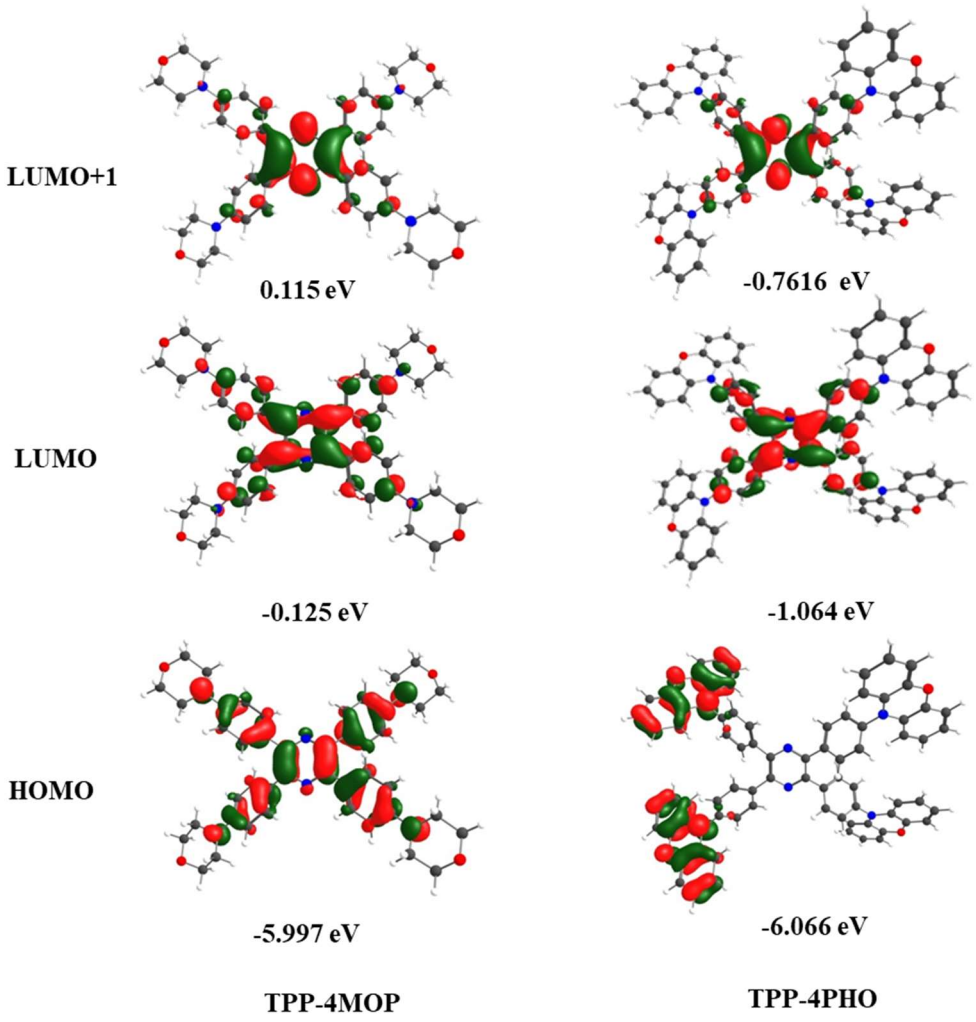

Figure 2.4 Molecular orbitals of TPP derivatives with the corresponding energy levels.

Table 2.4 Results of CAM B3LYP/6-31G(d) calculations for TPP derivatives in gaseous medium.

Compound	λ_{max} (nm)[a]	f_{os}[b]	Major Transitions (weight)	μ_g[c],D	μ_e[d],D	E_{S1vert} (eV)	E_{T1vert} (eV)	$E_{HOMO-LUMO}$ (eV)	ΔE_{ST}
TPP-4MOP	271.22	1.07	HOMO-2→LUMO (100%)	0.23	0.33	3.71	1.85	5.87	1.86
	330.40	0.77	HOMO→LUMO+1 (100%)						
	334.08	0.69	HOMO→LUMO (100%)						

TPP-4PHO	360.32	0.57	HOMO-3→LUMO (9%) HOMO-1→LUMO+2 (49%) HOMO→LUMO+1 (19%) HOMO-1→LUMO (23%)	0.24	9.90	3.41	2.00	5.00	1.41

[a]λ_{max} value obtained from the simulated absorption spectrum. [b]Oscillatory strength. [c]ground state dipole moment.[d] excited state dipole moment.

2.3.5 Effect of Aggregation

In order to examine the effect of aggregation induced emission enhancement in these derivatives, the emission spectra of **TPP-4MOP** and **TPP-4PHO** in THF upon increasing the volume fraction of water (f_w) were measured. The plot of I/I_0 vs the f_w in THF shown in **Figure 2.5** exhibits the enhancement of fluorescence of TPP derivatives with increase of f_w. The fluorescence enhancement of about 12 times for **TPP-4PHO** in 90% of f_w was observed compared to that of in neat THF, whereas **TPP-4MOP** in 90% of f_w showed very feeble increase (~1.6 times) of fluorescence intensity.

The increase of fluorescence intensity along with shifting of the maximum towards the blue region, especially in the case of **TPP-4PHO**, is attributed to the formation of nanoaggregates with size ranges from 100 to 550 nm (f_w = 90%) confirmed by DLS experiments (**Figure 2.6b**). The high fluorescence in the nanoaggregates could be due to the restriction of intramolecular torsion by eliminating the non-radiative TICT state leading to increase of the radiative decay from the intramolecular charge transfer state having partially twisted (pTICT) in nature in **TPP-4PHO**. The observation of low fluorescence enhancement in the **TPP-4MOP** could be due to the π–π interaction in the aggregates as they are inherently planar in nature compared to **TPP-4PHO**. The fluorescent decay profile of TPP derivatives in THF-Water mixture (f_w = 90%) was measured, exhibiting long-lived fluorescent component (~13.75 ns) due to the formation of nanoaggregates (Inset of **Figure 2.5**).

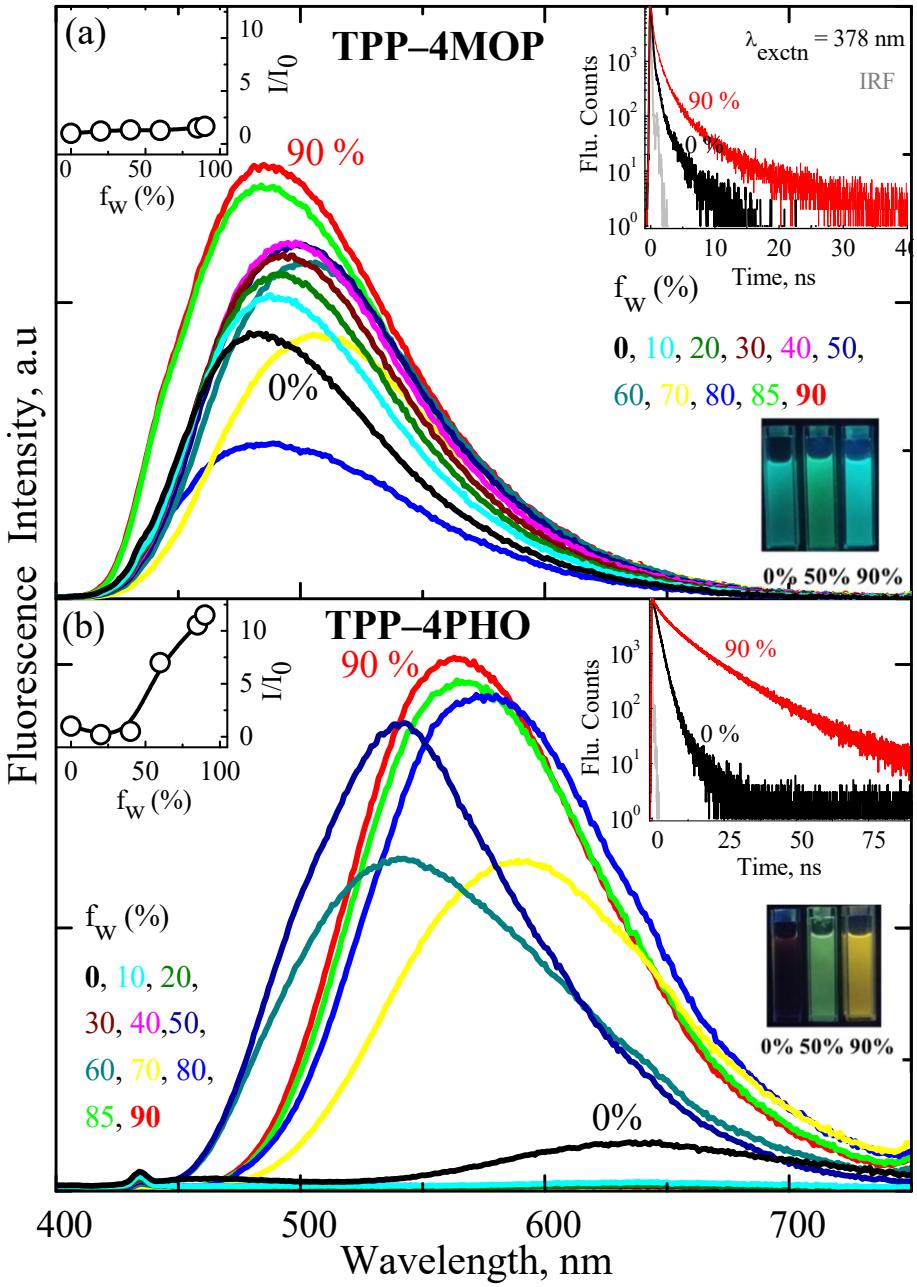

Figure 2.5 Fluorescence spectra of (a) **TPP-4MOP** and **TPP-4PHO** in THF/water mixtures with various volume water fractions (f_w) upon excitation at 385 nm. Left side insets show the plot of I/I_0 vs f_w. Right side insets show the fluorescent decay profiles in the f_w of 0 and 90% obtained upon excitation at 378 nm.

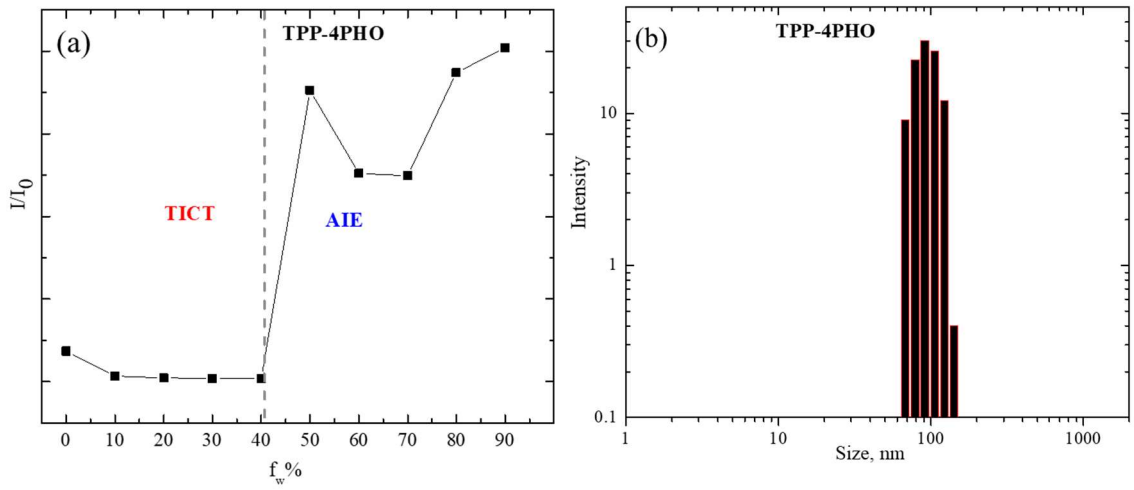

Figure 2.6 Size distribution of of nanoaggregates of **TPP-4PHO** (b) in THF-Water mixture of f_w = 90%, obtained by DLS measurements.

2.3.6 Time-Resolved Photophysical Characterizations

The femtosecond pump-probe spectroscopy is used to investigate the ultrafast components involved in the excited state relaxation pathway of **TPP-4MOP** and **TPP-4PHO** in non-polar (toluene) and polar (THF) solvents upon excitation at 385 nm. The **Figure 2.7a** and **2.7b** show the femtosecond transient absorption spectra of **TPP-4MOP** in toluene.

At early time scale (300 fs), it showed a positive broad excited state absorption at ~530 nm along with negative absorption at ~385 nm corresponding to ground state bleach. With increase of delay time of 13 ps, there was a formation of peak at ~430 nm and shoulder at ~620 nm. Further, increase of delay time to ~1.5 ns, though the overall spectral intensity was decreased, absorption maximum at 530 nm was disappeared completely and the absorption maxima at ~430 and 620 nm were persisted. These spectral features are matching with the transient absorption spectra obtained upon nanosecond laser excitation (**Figure 2.9a**). The femtosecond transient absorption spectra of **TPP-4MOP** obtained in THF is similar to that of in the toluene (**Figure 2.7c** and **2.7d**).

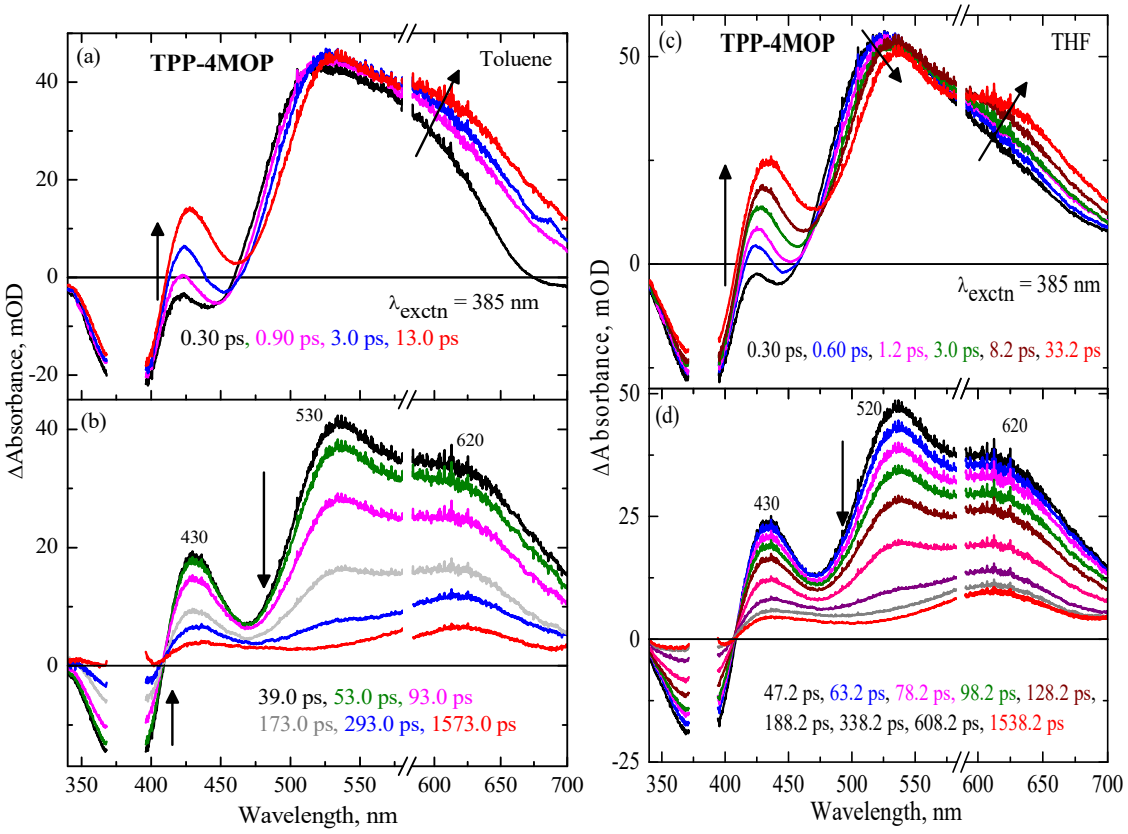

Figure 2.7 Femtosecond transient absorption spectra of **TPP-4MOP** in toluene (a and b) and THF (c and d) obtained upon excitation at 385 nm at different delay times.

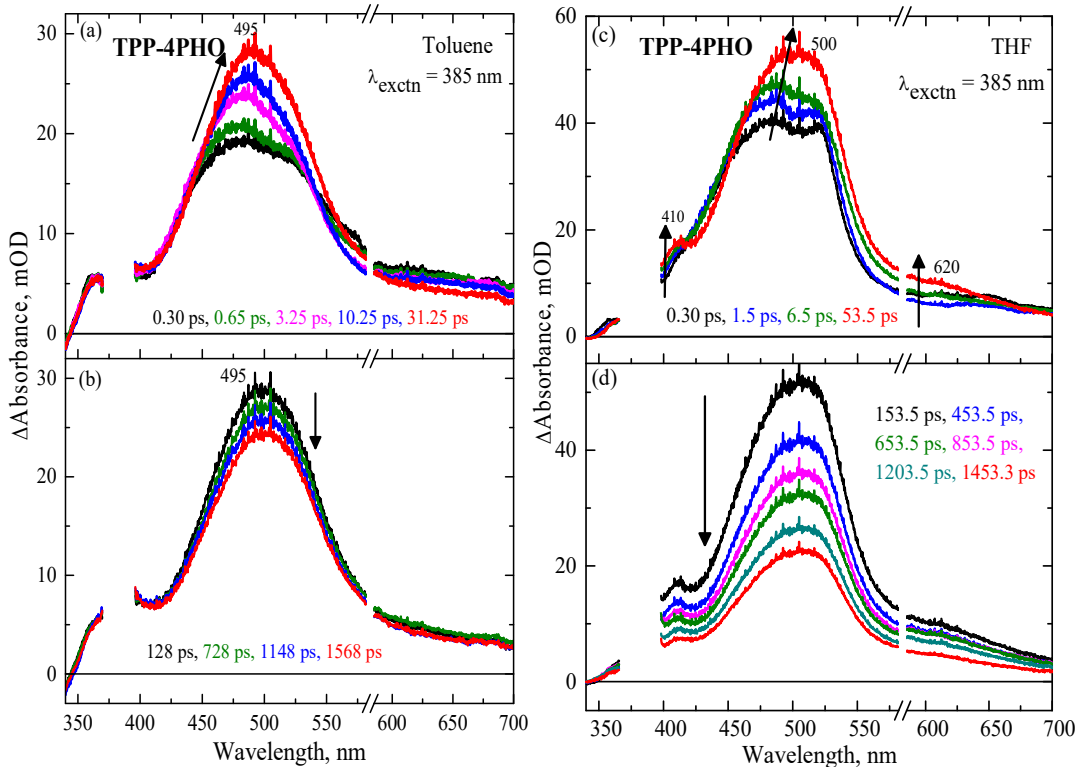

Figure 2.8 Femtosecond transient absorption spectra of **TPP-4PHO** in toluene (a and b) and THF (c and d) obtained upon excitation at 385 nm at different delay times.

The femtosecond transient absorption spectra of **TPP-4PHO** in toluene are shown in **Figure 2.8a** and **2.8b**. At early time scale of 350 fs, it exhibited a broad transient absorption maximum at ~495 nm. With increase of delay time until ~31.25 ps, there was an increase of intensity of absorption at ~ 495 nm. Further increase of delay time to ~1.5 ns, the intensity of absorption was reduced feebly. Whereas in the case of THF, femtosecond transient absorption spectra of **TPP-4PHO** showed broad absorption at ~487 nm at early time scales (**Figure 2.8c**). With increase of delay time at ~53 ps, there is an increase of intensity along with shifting of maximum to ~500 nm. Interestingly a formation of peak at ~ 410 nm and a broad shoulder at ~620 nm with weak in intensity was observed during this time scale. Further increase of delay time to ~1.5 ns (**Figure 2.8d**), an overall decrease of absorption intensity is observed. When compared to the toluene, the excited state relaxation dynamics of **TPP-4PHO** are faster in THF.

To obtain the complete dynamics of long-lived components (viz., triplet state and radical ions) observed in the femtosecond transient absorption spectra, the nanosecond transient absorption spectra of TPP derivatives were measured in toluene and THF upon excitation at 355 nm. **Figure 2.9a** shows the nanosecond transient absorption spectra of **TPP-4MOP** in toluene under Ar atmosphere obtained at different delay times exhibiting the two absorption bands at around 460 and 630 nm along with bleach bands at around 320 and 380 nm corresponding to the ground state (S_0) absorption maxima. The intensity of the transient absorption spectra was decreased with increase of delay time. As in toluene, transient absorption spectral pattern was similarly observed in the THF (**Figure 2.9b**). The transient absorption spectra were also measured under oxygen atmosphere and quenching of dynamics were observed (**Figure 2.9c** and inset of **Figure 2.9b**) in both the solvents.

The nanosecond transient absorption spectra of **TPP-4PHO** (**Figure 2.10a**) in toluene under Ar atmosphere upon excitation at 355 nm showed a broad absorption maximum at 520 nm with shoulder at ~460 and 370 nm along with bleach band at 330 nm corresponding to the ground state (S_0) absorption maximum. With increase of delay time to 2.5 μs, a decrease of shoulder at ~ 460 nm and persistent of absorption at ~540 and 370 nm were observed. The transient absorption spectra were also measured in oxygen atmosphere exhibiting the quenching of dynamics (**Figure 2.10c**). The nanosecond transient absorption spectra of **TPP-4PHO** (**Figure 2.10b**) in THF showed similar behaviour to that of toluene.

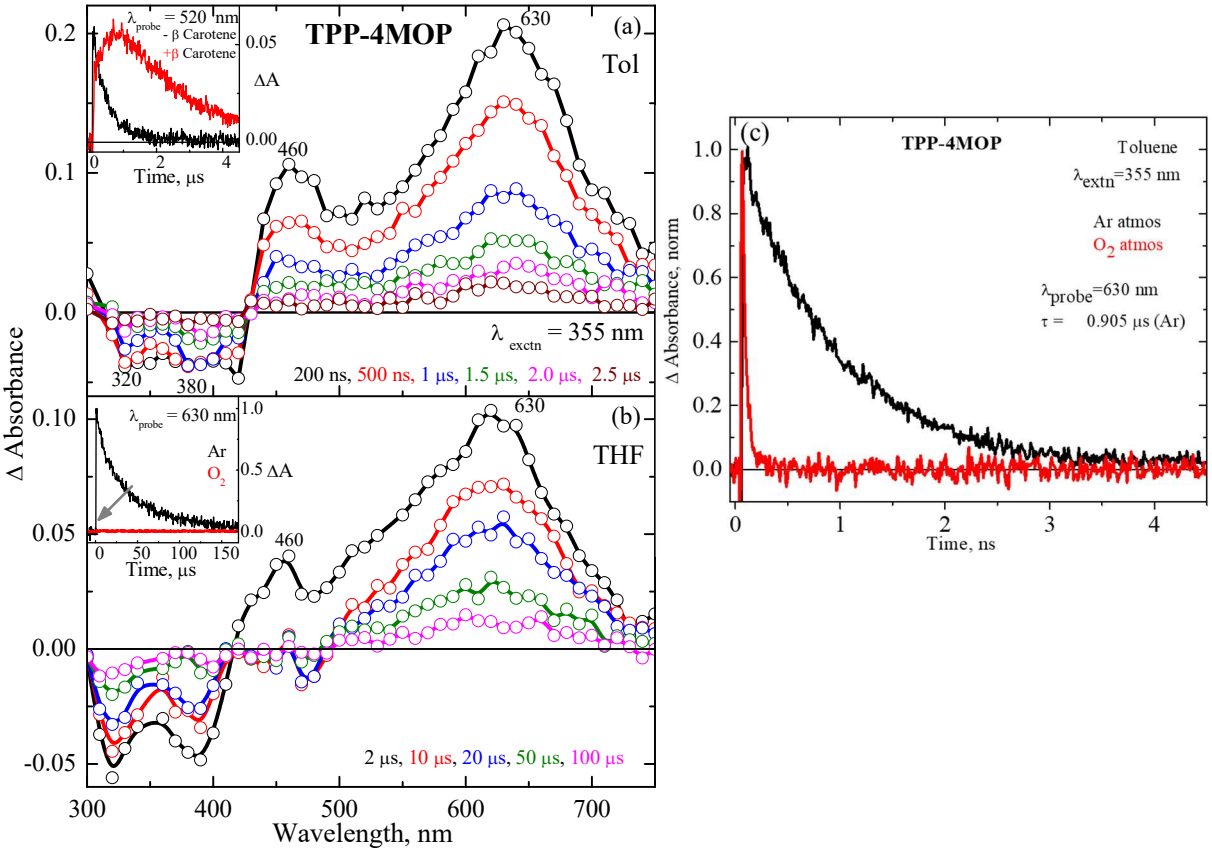

Figure 2.9 Nanosecond transient absorption spectra of **TPP-4MOP** in argon saturated toluene (a) and THF (b) obtained upon exciting at 355 nm. The inset a shows the growth profile of ^{3}(β-carotene)* formed in the mixture of **TPP-4MOP** and β-carotene at 520 nm revealing the triplet−triplet energy transfer from **TPP-4MOP** to β-carotene. The Figure 2.9c and inset b shows the kinetic decay at 630 nm measured in argon and oxygen saturated solvents.

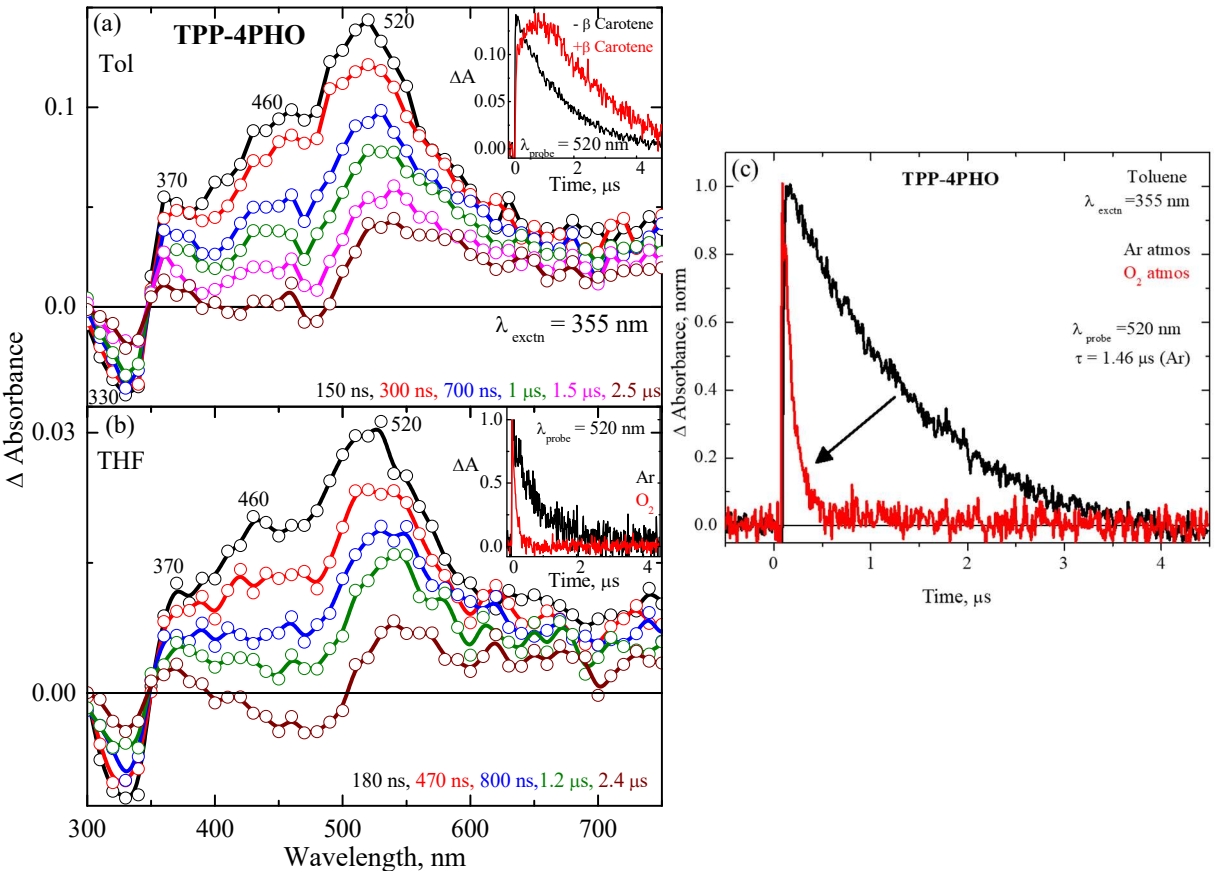

Figure 2.10 Nanosecond transient absorption spectra of **TPP-4PHO** in argon saturated toluene (a) and THF (b) obtained upon exciting at 355 nm. The inset a shows the growth profile of ^{3}(β-carotene)* formed in the mixture of **TPP-4PHO** and β-carotene at 520 nm revealing the triplet−triplet energy transfer from **TPP-4PHO** to β-carotene. The Figure 2.10c and inset b shows the kinetic decay at 520 nm measured in argon and oxygen saturated solvents**2.3.7**

Analysis of Time-Resolved Data: The femtosecond transient absorption spectra obtained in the format of a three-dimensional data set (wavelength, time, and change in absorbance) was analysed using the global analysis program GLOTARAN[61] with a sequential model. Global analysis of the transient absorption data provides optimally three or four time constants to completely define the excited state relaxation dynamics of TPP derivatives. The resulting time constants are given in **Table 2.5** and the corresponding decay associated difference spectra are provided in **Figure 2.11.**

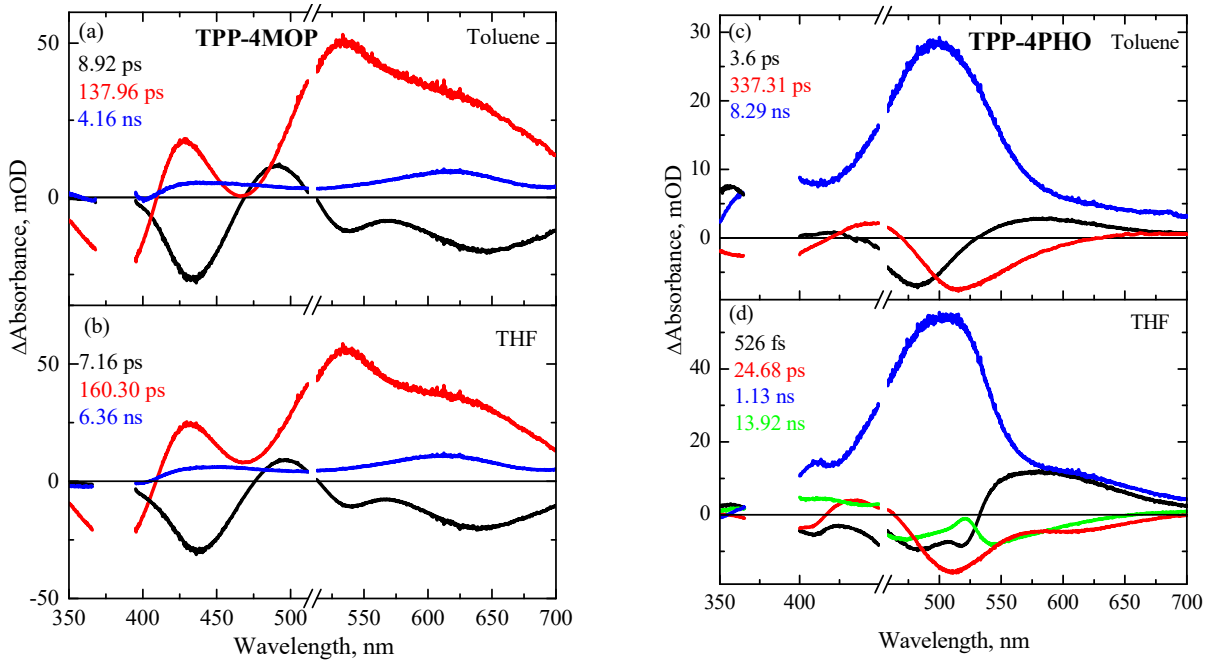

Figure 2.11 Decay associated differential spectra of **TPP** derivatives in toluene (a and c) and THF (b and d).

The global analysis of femtosecond transient absorption spectra of **TPP-4MOP** in toluene (THF) resulted three time constants of τ_1 = 8.92 (7.16) ps, τ_2 = ~137.96 (160.30) ps and τ_3 = 4.16 (6.36) ns (**Table 2.5)**. The DADS of time constant of 8.92 (7.16) ps for **TPP-4MOP** in toluene (THF) showed negative amplitude with maxima at around 430,530 and 620 nm consistent with FTAS representing the formation of component after the laser excitation. The fastest component of τ_1, 8.92 ps is attributed to the decay time constant of hot singlet state to vibrationally relaxed local excited state of S_1. The second time constant of ~137.96 ps is consistent with the fluorescence lifetime of **TPP-MOP** obtained by TCSPC, hence it could be due to the fluorescence lifetime of vibrationally relaxed local excited state of S_1. The third time constant might be due to the formation of triplet state through intersystem crossing [*vide infra*]. This is supported by the fact that the transient absorption spectra at 1.5 ns and decay associated spectra of this time constant are exactly matching with the nanosecond transient absorption spectra. (It is to be noted that the longest time constant would have erroneousness, since the measurable maximum delay time in our spectrometer is ~1.7 ns). The features of the transient

absorption spectra and decay associated spectra in THF are appeared to be same compared to those of toluene, hence it is proposed to follow the similar excited state relaxation pathways in THF as in toluene. It is to be noted that the longer time constants such as 4.16 and 6.36 ns obtained by the global analysis would be imprecision, since the translational delay stage in our spectrometer can reach 1.7 ns maximum limiting the capability of measuring the transient absorption spectra until 1.7 ns.

Table2.5 Time constants for TPP derivatives in toluene and THF obtained from fsTAS.

.

TPP derivatives	Toluene	THF
TPP-4MOP	$\tau_1 = 8.92 \pm 0.5$ ps $\tau_2 = 137.96 \pm 3$ ps $\tau_3 = 4.16 \pm 1$ ns	$\tau_1 = 7.16 \pm 0.4$ ps $\tau_2 = 160.30 \pm 4$ ps $\tau_3 = 6.36 \pm 1$ ns
TPP-4PHO	$\tau_1 = 3.60 \pm 0.3$ ps $\tau_2 = 337.3 \pm 5$ ps $\tau_3 = 8.29 \pm 1$ ns	$\tau_1 = 526 \pm 100$ fs $\tau_2 = 24.68 \pm 1$ ps $\tau_3 = 1.13 \pm 0.3$ ns $\tau_4 = 13.92 \pm 2$ ns

In order to confirm the formation of the triplet state, the nanosecond transient absorption spectra were measured with triplet sensitizer, β-carotene. The quenching of the dynamics at 460 and 630 nm and simultaneous growth of the peak at 520 nm due to the formation of the triplet state of β -carotene were observed (inset 2.9a). Thus, the transient absorption maxima at 460 and 630 nm having similar time constants, are assigned to triplet-triplet state absorption. The decay profile of the triplet absorption at 630 nm in argon saturated solution is fitted with monoexponential and time constant was found to be ~0.90 and 34.07 μs for toluene and THF respectively (**Figure 2.10c** and inset **2.10b**). The triplet state quantum

yield was also determined using β-carotene as standard and found to be around 74% ±10 and 84% ±10 in toluene and THF respectively.

In the case of **TPP-4PHO** in THF, there is a clear change in the spectral evolution in femtosecond transient absorption spectra (**Figure 2.8c** and **2.8d**) compared to that of toluene and spectral analysis resulted four (τ_1 = 526 fs, τ_2 = 24.68 ps, and τ_3 = 1.13 ns and τ_4 = 13.92 ns) time constants, which are described as follows. The fastest time constant of ~526 fs is attributed to the relaxation of hot singlet state to intramolecular charge transfer state with partially twisted in nature, pTICT. Generally, the appearance of large Stokes shift (9691cm^{-1}) and broad fluorescence spectra in polar solvent, compared to the nonpolar solvents reflect that derivatives undergo a significant structural change upon photoexcitation in polar solvents[36]. Since the **TPP-4PHO** has an inherent property of twisting supported by the theoretical optimization and has the various degree of freedom to rotate in polar solvent, ICT state would have partially twisted in nature , pTICT.[59] The time constant of τ_2 = 24.68 ps is due to the decay time constant of pTICT state leading to the completely twisted intramolecular charge transfer state, TICT. The occurrence of the pTICT and TICT are further confirmed by the time-resolved emission spectra of **TPP-4PHO** in THF exhibiting the evolution of shifting of emission maximum from 600 to 640 nm corresponding to pTICT and TICT respectively during the delay time of 50 to 500 ps. Indeed fluorescence lifetimes probed at 640 nm obtained from TCSPC exhibiting two components of 133 ps (4.79%) and 1.35 ns (95.21%) attributed to fluorescence lifetime of pTICT and TICT state respectively. Further the formation of TICT state leading to the charge separated species is confirmed by the nanosecond transient absorption spectra. For example the transient absorption maxima at 370 nm quenched in the presence of oxygen, could be due to the pyrazine radical anion and consistent with the literature.[62] The absorption peak at 540 nm having longer time constant (2.86 μs), not quenched by the presence of oxygen, is assigned to radical cation of phenoxazine, consistent with the previous reports.[63-64] The time

constant of τ_4 ~ 13.92 ns which is beyond our experimental capability, might be due to formation of triplet state by charge recombination[64-66] and needs further investigation. The nanosecond transient absorption maximum appeared at 520 nm having time constant of 1.46 (1.29) μs in toluene (THF) (**Figure 2.10c** and inset of **Figure 2.10b**) is attributed to triplet state absorption, which is confirmed by sensitization experiment with the triplet sensitizer, β-carotene (Inset of **Figure 2.10a**) and consistent with literature. The triplet state quantum yield was also determined using standard β-carotene and found to be 41 ± 10 % and 28 ± 10% in toluene and THF respectively.

The global analysis of femtosecond transient absorption spectra of **TPP-4PHO** in toluene resulted three (τ_1 = 3.60 ps, τ_2 = 337.3 ps and τ_3 = 8.29 ns) time constants. As no significant evolution of new peaks and change in the dynamics were observed for the **TPP-4PHO** in toluene, the same excited state relaxation pathways as mentioned in THF is proposed without involvement of TICT.

Overall, upon substitution of phenoxazine compared to morpholine in the tetraphenylpyrazines, there is an increase of molecular torsion leading to the formation of non-radiative TICT state. This is supported by the experimental observations of the large Stokes shift, decrease of fluorescence quantum yield and lifetime and also by the femtosecond and nanosecond transient absorption and picosecond time-resolved emission spectra in polar solvent. This TICT state is overcome in the aggregates by the restriction of intramolecular torsion. Thus, based on the spectral features and analysis of the dynamics from the femtosecond and nanosecond transient absorption and time-resolved emission spectra, excited state relaxation pathways of **TPP-4MOP** and **TPP-4PHO** in both solvents are proposed in the **Scheme 2.2**.

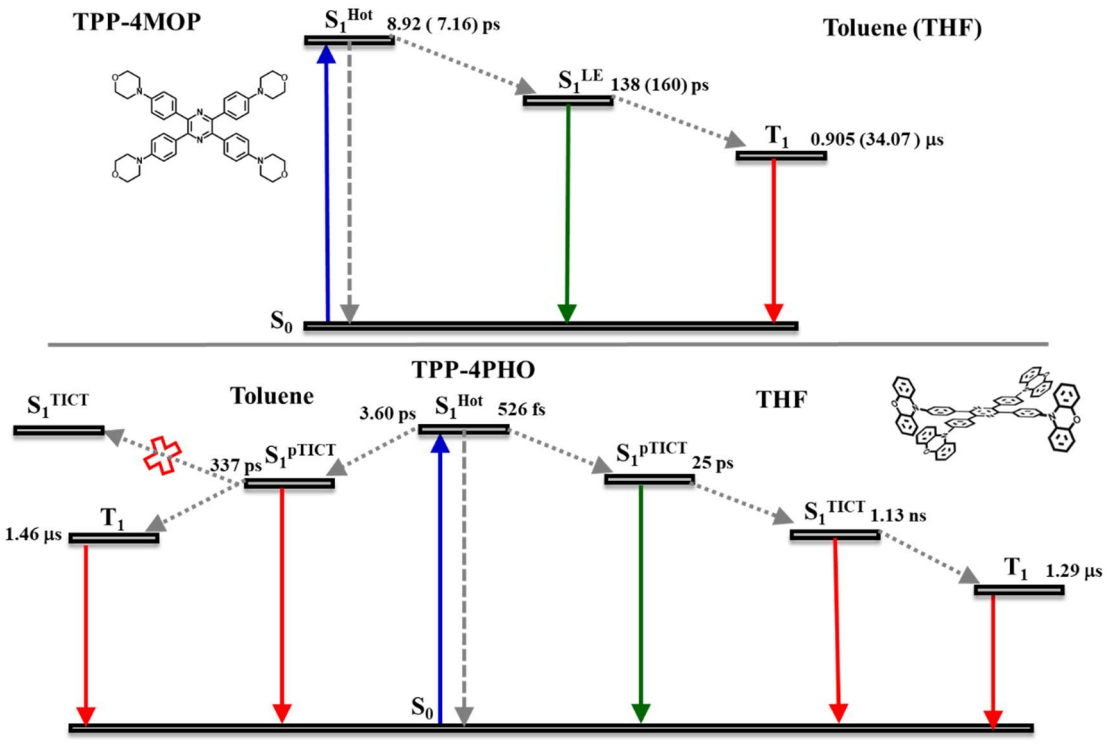

Scheme 2.2 Proposed excited state relaxation dynamics of **TPP-4MOP** and **TPP-4PHO**.

2.4 Conclusion

Stationary and excited state relaxation dynamics of **TPP-4MOP** and **TPP-4PHO** were systematically investigated in toluene and THF to understand the photophysical properties of multibranched donor-acceptor derivatives. It is found that **TPP-4MOP** in toluene exhibited low fluorescence quantum yield compared to **TPP-4PHO** having strong electron donor of phenoxazine. AIE effect of **TPP-4PHO** and **TPP-4MOP** could be due to restriction of conformational changes in aggregated state and due to their twisted structure which will eliminate π-π stacking in during aggregation. In addition these two factors, restriction of formation of TICT state also responsible for AIE effect of **TPP-4PHO**. Femtosecond and nanosecond transient absorption spectra are used to investigate the excited dynamics of TPP derivatives in toluene and THF and revealed that the occurrence of TICT dynamics in the **TPP-4PHO**.

2.5 Experimental Section

2.5.1 General Details: The reagents and materials were purchased from Sigma–Aldrich and TCI. ^{1}H and ^{13}C NMR spectra were recorded using a Bruker AMX spectrometer at 500 and 125 MHz respectively using tetramethylsilane (TMS) as an internal standard. High resolution mass spectra were recorded using Thermo Scientific Exactive–LCMS by electron spray ionization method. The matrix assisted laser desorption ionization time–of–flight (MALDI–TOF) mass spectra were recorded using Bruker Autoflex speed instrument.

2.5.2 Steady State Measurements: Steady state absorption spectra and fluorescence spectra were recorded using UV–Visible absorption spectrophotometer (Shimadzu, UV–2600) and a fluorescence spectrometer (FluoroLog–3, Horiba, equipped with a 450 W Xenon arc lamp) at ambient temperature, respectively. The fluorescence quantum yields of compounds were determined in various solvents by the relative method employing quinine sulphate as a reference (Φ_R = 0.54) by adjusting same absorbance at the excitation wavelength. The following equation was used for calculating relative fluorescence quantum yield

$$\Phi_S = \frac{Abs_R}{Abs_S} \times \frac{Area_S}{Area_R} \times \frac{\eta_S^2}{\eta_R^2} \times \Phi_R \quad (1)$$

where subscripts R and S refer to the reference and sample, respectively. Abs, Area and η are the absorbance at the excitation wavelength, area under the fluorescence spectrum and refractive index of the solvent, respectively.

2.5.3 Electrochemical Measurements: Electrochemical measurements were carried in N_2-purged dichloromethane by using CHI-660 voltametric analyzer with three electrode cell assemblies. Tetrabutylammonium hexafluorophosphate, N-Bu_4PF_6, was used as the supporting electrolyte. The conventional three-electrode configuration consists of a

platinum wire as a counter electrode, glassy carbon as a working electrode and $Ag/AgNO_3$ couple as a reference electrode and ferrocenium/ ferrocene (Fc^+/Fc) redox couple was used as the internal standard. Cyclic voltammograms were obtained at a scan rate of 100 mV s^{-1}.

2.5.4 Theoretical Calculations: Theoretical calculations were carried out using Density Functional Theory (DFT) and Time Dependent DFT (TDDFT) with the B3LYP functional and the 6-31G (d) basis set. The ground state geometry was optimized using Gaussian 09.[67] The same optimized ground state geometry was used to calculate S_1 and T_1 vertical excitation energy. All states were calculated using DFT except the S_1 state, for which the TDDFT was employed.

2.5.5 Time Correlated Single Photon Counting (TCSPC): Fluorescence lifetimes were measured by using a picosecond single photon counting system (Horiba, DeltaFlex). The samples were excited by employing 378 nm LED as excitation sources and detected using picosecond photon detection module (PPD-850). The fluorescence time constants are obtained by deconvoluting with the LED profiles. The decay of the fluorescence intensity (I) with time (t) was fitted either by a mono or double-exponential function

$$I = A_1 e^{-\frac{t}{\tau_1}} \quad (2)$$

$$I = A_1 e^{-\frac{t}{\tau_1}} + A_2 e^{-\frac{t}{\tau_2}} \quad (3)$$

where t_1 and t_2 are the lifetimes of different species, and A_1 and A_2 are their respective amplitudes.

2.5.6 Nanosecond Transient Absorption Spectra: Nanosecond transient absorption spectra were obtained by exciting the samples with the third harmonic of fundamental light (1064 nm) from an Quanta Ray Nd: YAG laser (wavelength, 355 nm, ~10 ns) and using an

Applied Photophysics model LKS 60 laser kinetics spectrometer. The probing light source was a 150 W Xenon arc lamp. The light of the probe transmitted through a 1 cm quartz cuvette was dispersed by a monochromator and detected by a photomultiplier tube coupled to a digital oscilloscope (Agilent Infiniium DSO8064A, 600 MHz, 4 $GSas^{-1}$). The analyzing and laser beams were fixed at right angles to each other. The power of each laser pulse was monitored using a fast silicon photodiode.

2.5.7 Quantification of Triplet State Properties of TPP derivatives

A Quanta Ray Nd:YAG laser was used as the laser (laser energy was 64 mJ at 355 nm) and laser beam and analysing beam were fixed at right angles. In order to measure the triplet quantum yields of TPP derivatives using $Ru(bpy)_3^{2+}$, we measured the energy transfer to β carotene with a previously described method.[68] This experiment used optically matched $Ru(bpy)_3^{2+}$ and TPP derivatives mixed with a β carotene solution of known volume. The transient absorbance (ΔA) of the β carotene triplet, formed by the energy transfer from $Ru(bpy)_3^{2+}$ or the TPP derivatives triplet, was monitored at 520 nm. Comparison of plateau absorbance following the completion of sensitized triplet formation, properly corrected for the decay of the donor triplets in competition with energy transfer to β carotene, enabled us to estimate Φ_T of TPP derivatives based on equation.[68]

$$\Phi_T{}^S = \Phi_T{}^R \frac{\Delta A^S}{\Delta A^R} \frac{k_{obs}^S}{k_{obs}^S - k_0^S} \frac{k_{obs}^R - k_0^R}{k_{obs}^R} \quad (4)$$

where superscripts 'S' and 'R' designate the different TPP derivatives and $Ru(bpy)_3^{2+}$, respectively, k_{obs}, is the pseudo-first-order rate constant for the growth of the β carotene triplet and k_0 is the rate constant for the decay of the donor triplets, in the absence of β carotene observed in solutions containing $Ru(bpy)_3^{2+}$ or TPP derivatives at the same optical density (OD) as those used for sensitization. As a result of negligible triplet yield, direct

excitation of β carotene did not result in any significant triplet formation under these conditions. For $Ru(bpy)_3^{2}$+ in methanol, the triplet quantum yield was assumed to be one. This method yields reliable data and is consistent with the assumption that energy transfer to β carotene is 100% efficient.

2.5.8 Femtosecond Transient Absorption Measurements: The seed laser is the Ti:sapphire laser (MaiTai HP, Spectra Physics, USA) having a center wavelength of 800 nm with a pulse width of <100 fs and a repetition rate of 80 MHz. The amplified laser was divided into two and the beam with high energy was used for exciting the compounds (385 nm) using TOPAS (prime, light conversion). The other portion (200 mW) of the amplified beam was focused on a CaF_2 plate (1 mm) to obtain a white light continuum (340− 1000 nm) that further divided into two beams (reference and sample probe beams). The sample (0.4 mm thickness) was refreshed by spinning at a constant speed. After passing through the sample, the white light continuum was focused into an optical fiber (100 μm) attached to the imaging spectrometer. The spectrophotometer setup is ExciPro, CDP Systems Corp, Russia. The transient absorption spectra were recorded at a magic angle (54.7°) by averaging about 2000 excitation pulses for each delay time. All the transient absorption spectra are corrected for chirp of the white light by estimating the time zero with the coherent artifact found in the solvent. The laser fluence used for all the transient absorption measurements is ~3 $\mu J/cm^2$. The IRF of the ultrafast spectrometer is found to be about ≤120 fs. The stability of the sample is checked by recording the absorption spectra of the sample (before and after the measurements) and observed to have no substantial differences in the absorption spectra. The absorbance of solutions of TPP derivatives was ~0.7 OD for femtosecond transient absorption measurements.

2.5.9 Synthesis and Characterisation Details of TPP derivatives:

Synthesis of 1,2-bis(4-bromophenyl)-2-hydroxyethanone (2): Thiamine hydrochloride (2.0 mmol) was dissolved in 1mL of water in a 100 mL round bottom flask followed by adding 6.5 mL of EtOH and the solution was cooled down to 0°C and the mixture of solution was stirred well. The pH of solution (9-10) was adjusted by adding 8% cold NaOH aqueous solution. Then, 4-bromo benzaldehyde **1** (8 mmol) was added very slowly to the above mixture. The solution mixture was heated at 60°C for 12 h. The reaction mixture was extracted using dichloromethane solvent. The organic layer was washed thoroughly with water and dried over anhydrous sodium sulphate. The excess solvent was removed under reduced pressure and the crude product was further purified by column chromatography using silica (100-200 mesh) as the stationary phase and EtOAc/Hexane mixture (10:90) as the eluting solvent. Yield 28%; White solid. ^{1}H NMR (500 MHz, $CDCl_3$): δ 7.75-7.73 (d, 2H), 7.56-7.55 (d, 2H), 7.47-7.45 (d, 2H), 7.19-7.18 (d, 2H), 5.86-5.85 (d, 1H), 4.49-4.48 (d, 1H) ppm; ^{13}C NMR (125 MHz, $CDCl_3$): δ 197.63, 137.61, 132.42, 132.21, 131.93, 130.47, 129.56, 129.36, 122.99, 75.53 ppm.

Synthesis of 2,3,5,6-tetrakis(4-bromophenyl)pyrazine (3): The mixture of 1,2-bis(4-bromophenyl)-2-hydroxyethanone (1.35 mmol) and NH_4OAc (6.4 mmol), $CeCl_3.7H_2O$ (0.13 mmol) and ethanol (6 ml) were kept over 4 h under refluxing condition . The mixture was cooled down to room temperature. The reaction mixture was then extracted with dichloromethane. The organic layer was washed thoroughly with water and dried over anhydrous sodium sulphate. The excess solvent was removed under reduced pressure and the crude product was further purified by column chromatography using silica gel (100-200 mesh) as the stationary phase and EtOAc/Hexane mixture (5:95) as the eluting solvent. Yield: 48%; White solid. ^{1}H NMR (500 MHz, $CDCl_3$): δ 7.48 (s,16H) ppm; ^{13}C NMR (125 MHz, $CDCl_3$): δ 147.39, 136.68, 131.75, 131.33, 123.69 ppm; HRMS: (ESI+): m/z calcd for $C_{28}H_{16}{}^{81}Br_3{}^{79}BrN_2H_{17}$: 700.8047$[M]^+$; found: 700.8094.

TPP-4MOP: The compound was synthesized by using solvent free Buchwald-Hartwig reaction according the reported procedure.[69] The intermediate **3** (1.05 mmol), morpholine (4.2 mmol), palladium acetate (0.04 mmol), 2-dicyclohexylphosphino-2′,6′-diisopropoxybiphenyl (RuPhos, 0.08 mmol), and powdered sodium tert-butoxide (4.4 mmol) were added in to a screw cap vial. The reaction vial was transferred to a preheated oil bath (110 °C). After 24 h, the reaction mixture was cooled and dissolved in CH_2Cl_2/H_2O mixture (1:1). The organic phase was separated, the solvent was evaporated and the product was isolated by chromatography using a silica gel (100-200 mesh) as the stationary phase and 2% Methanol: CH_2Cl_2 as the mobile phase. The compound is further purified with HPLC chromatography. Yield, 65%; Yellow solid.^{1}H NMR (500 MHz, $CDCl_3$): δ 7.62-7.61 (d, 8H), 6.85-6.83 (d, 8H), 3.87-3.85 (t, 16H), 3.21-3.19 (t, 16H) ppm; ^{13}C NMR (125 MHz, $CDCl_3$): δ 151.02, 146.26, 130.68, 130.31, 114.77, 66.85, 48.75 ppm; HRMS (ESI+): m/z calcd for $C_{44}H_{48}N_6O_4$: 724.3737 $[M+H]^+$; found: 725.3816.

TPP-4PHO: The intermediate **3** (1.4 mmol), phenoxazine (7 mmol), palladium acetate (0.05 mmol), mmol), tri(tert-butyl)phosphine (0.11 mmol) and potassium carbonate (4.2 mmol) were dissolved in dry toluene (40 ml) and refluxed at 120°C for 24 h under argon atmosphere. On completion of the reaction, the reaction mixture was cooled to room temperature and dissolved in CH_2Cl_2/H_2O mixture (1:1). The organic phase was separated and the solvent was removed under reduced pressure. The product was purified by column chromatography using a silica gel (100-200 mesh) as the stationary phase and 2% Methanol: CH_2Cl_2 as the eluting solvent. Yield, 69%; Yellow solid. ^{1}H NMR (500 MHz, $CDCl_3$): δ 7.94-7.92 (d, 8H), 7.41-7.39 (d, 8H), 6.71-6.69 (d, 8H), 6.66-6.63 (t, 8H), 6.57-6.54 (t, 8H), 6.00-5.98 (d, 8H) ppm; ^{13}C NMR (125 MHz, $CDCl_3$): δ 147.69, 142.95, 138.86, 137.06, 132.94, 131.59, 129.92, 122.36, 120.60, 114.59, 112.12 ppm; MALDI-TOF: m/z calcd for $C_{76}H_{48}N_6O_4$: 1108.3737 $[M+H]^+$; found: 1109.3817.

2.6 References

1. Yu, L.; Wu, Z.; Xie, G.; Zeng, W.; Ma, D.; Yang, C., Molecular Design to Regulate the Photophysical Properties of Multifunctional Tadf Emitters Towards High-Performance Tadf-Based Oleds with Eqes up to 22.4% and Small Efficiency Roll-Offs. *Chem. Sci.* **2018**, *9*, 1385-1391.

2. Baldo, M. A.; O'Brien, D. F.; You, Y.; Shoustikov, A.; Sibley, S.; Thompson, M. E.; Forrest, S. R., Highly Efficient Phosphorescent Emission from Organic Electroluminescent Devices. *Nature* **1998**, *395*, 151-154.

3. Feng, H.-T.; Zheng, X.; Gu, X.; Chen, M.; Lam, J. W. Y.; Huang, X.; Tang, B. Z., White-Light Emission of a Binary Light-Harvesting Platform Based on an Amphiphilic Organic Cage. *Chem. Mater.* **2018**, *30*, 1285-1290.

4. Hu, F.; Xu, S.; Liu, B., Photosensitizers with Aggregation-Induced Emission: Materials and Biomedical Applications. *Adv. Mater.* **2018**, *30*, 1801350.

5. Hu, W., et al., Stimuli-Responsive Reversible Switching of Intersystem Crossing in Pure Organic Material for Smart Photodynamic Therapy. *Angew. Chem. Int. Ed. Engl.* **2019**, *58*, 11105-11111.

6. Kuehne, A. J. C.; Gather, M. C., Organic Lasers: Recent Developments on Materials, Device Geometries, and Fabrication Techniques. *Chem. Rev.* **2016**, *116 21*, 12823-12864.

7. Okada, D.; Azzini, S.; Nishioka, H.; Ichimura, A.; Tsuji, H.; Nakamura, E.; Sasaki, F.; Genet, C.; Ebbesen, T. W.; Yamamoto, Y., Π-Electronic Co-Crystal Microcavities with Selective Vibronic-Mode Light Amplification: Toward Förster Resonance Energy Transfer Lasing. *Nano Lett.* **2018**, *18*, 4396-4402.

8. Jiang, Y.; Liu, Y.-Y.; Liu, X.; Lin, H.; Gao, K.; Lai, W.-Y.; Huang, W., Organic Solid-State Lasers: A Materials View and Future Development. *Chem. Soc. Rev.* **2020**, *49*, 5885-5944.

9. Dolmans, D. E. J. G. J.; Fukumura, D.; Jain, R. K., Photodynamic Therapy for Cancer. *Nat. Rev. Cancer.* **2003**, *3*, 380-387.

10. Cao, S.; Shao, J.; Wu, H.; Song, S.; De Martino, M. T.; Pijpers, I. A. B.; Friedrich, H.; Abdelmohsen, L. K. E. A.; Williams, D. S.; van Hest, J. C. M., Photoactivated Nanomotors Via Aggregation Induced Emission for Enhanced Phototherapy. *Nat. Commun.* **2021**, *12*, 2077.

11. Cai, X.; Liu, B., Aggregation-Induced Emission: Recent Advances in Materials and Biomedical Applications. *Angew. Chem. Int. Ed. Engl.* **2020**, *59*, 9868-9886.

12. Kue, C. S.; Ng, S. Y.; Voon, S. H.; Kamkaew, A.; Chung, L. Y.; Kiew, L. V.; Lee, H. B., Recent Strategies to Improve Boron Dipyrromethene (Bodipy) for Photodynamic Cancer Therapy: An Updated Review. *J. Photochem. Photobiol. A* **2018**, *17*, 1691-1708.

13. Huang, W.; Wang, H.; Sun, L.; Li, B.; Su, J.; Tian, H., Propeller-Like D–Π–a Architectures: Bright Solid Emitters with Aiee Activity and Large Two-Photon Absorption. *J. Mater. Chem. C* **2014**, *2*, 6843-6849.

14. Hu, R.; Leung, N. L. C.; Tang, B. Z., Aie Macromolecules: Syntheses, Structures and Functionalities. *Chem. Soc. Rev.* **2014**, *43*, 4494-4562.

15. Barman, D.; Narang, K.; Parui, R.; Zehra, N.; Khatun, M. N.; Adil, L. R.; Iyer, P. K., Review on Recent Trends and Prospects in Π-Conjugated Luminescent Aggregates for Biomedical Applications. *Aggreg.* **2022**, 172.

16. Dereka, B.; Rosspeintner, A.; Stężycki, R.; Ruckebusch, C.; Gryko, D. T.; Vauthey, E., Excited-State Symmetry Breaking in a Quadrupolar Molecule Visualized in Time and Space. *J. Phys. Chem. Lett.* **2017**, *8*, 6029-6034.

17. Vauthey, E., Watching Excited-State Symmetry Breaking in Multibranched Push–Pull Molecules. *J. Phys. Chem. Lett.* **2022**, *13*, 2064-2071.

18. Ghosh, R.; Palit, D. K., Effect of Donor–Acceptor Coupling on Tict Dynamics in the Excited States of Two Dimethylamine Substituted Chalcones. *J. Phys. Chem. A* **2015**, *119*, 11128-11137.

19. Wells, K. A.; Palmer, J. R.; Yarnell, J. E.; Garakyaraghi, S.; Pemberton, B. C.; Favale, J. M.; Valchar, M. K.; Chakraborty, A.; Castellano, F. N., Understanding the Influence of Geometric and Electronic Structure on the Excited State Dynamical and Photoredox Properties of Perinone Chromophores. *Phys. Chem. Chem. Phys.* **2021**, *23*, 24200-24210.

20. Paul, S.; Govind, C.; Karunakaran, V., Planarity and Length of the Bridge Control Rate and Efficiency of Intramolecular Singlet Fission in Pentacene Dimers. *J. Phys. Chem. B* **2021**, *125*, 231-239.

21. Kong, J.; Zhang, W.; Shao, J.-Y.; Huo, D.; Niu, X.; Wan, Y.; Song, D.; Zhong, Y.-W.; Xia, A., Bridge-Length- and Solvent-Dependent Charge Separation and Recombination Processes in Donor–Bridge–Acceptor Molecules. *J. Phys. Chem. B* **2021**, *125*, 13279-13290.

22. Kong, J.; Zhang, W.; Li, G.; Huo, D.; Guo, Y.; Niu, X.; Wan, Y.; Tang, B.; Xia, A., Excited-State Symmetry-Breaking Charge Separation Dynamics in Multibranched Perylene Diimide Molecules. *J. Phys. Chem. Lett.* **2020**, *11*, 10329-10339.

23. Guo, J., et al., Tetraphenylpyrazine Decorated 1,3-Di(9h-Carbazol-9-Yl)Benzene (Mcp): A New Aie-Active Host with Enhanced Performance in Organic Light-Emitting Diodes. *J. Mater. Chem. C* **2019**, *7*, 11160-11166.

24. Pan, L.; Wu, H.; Liu, J.; Xue, K.; Luo, W.; Chen, P.; Wang, Z.; Qin, A.; Tang, B. Z., Tetraphenylpyrazine Based Aie Luminogens: Unique Excited State Decay and Its Application in Deep-Blue Light-Emitting Diodes. *Adv. Opt. Mater.* **2019**, *7*, 1801673.

25. Chen, M., et al., Malonitrile-Functionalized Tetraphenylpyrazine: Aggregation-Induced Emission, Ratiometric Detection of Hydrogen Sulfide, and Mechanochromism. *Adv. Funct. Mater.* **2018**, *28*, 1704689.

26. Chen, M., et al., Tetraphenylpyrazine-Based Aiegens: Facile Preparation and Tunable Light Emission. *Chem. Sci.* **2015**, *6*, 1932-1937.

27. Feng, G.; Kwok, R. T. K.; Tang, B. Z.; Liu, B., Functionality and Versatility of Aggregation-Induced Emission Luminogens. *Appl. Phys. Rev.* **2017**, *4*, 021307.

28. He, Z.; Ke, C.; Tang, B. Z., Journey of Aggregation-Induced Emission Research. *ACS Omega* **2018**, *3*, 3267-3277.

29. Mei, J.; Leung, N. L. C.; Kwok, R. T. K.; Lam, J. W. Y.; Tang, B. Z., Aggregation-Induced Emission: Together We Shine, United We Soar! *Chem. Rev.* **2015**, *115*, 11718-11940.

30. Wu, H., et al., Novel Strategy for Constructing High Efficiency Oled Emitters with Excited State Quinone-Conformation Induced Planarization Process. *Adv. Opt. Mater* **2019**, *7*, 1900283.

31. Chen, M.; Nie, H.; Song, B.; Li, L.; Sun, J. Z.; Qin, A.; Tang, B. Z., Triphenylamine-Functionalized Tetraphenylpyrazine: Facile Preparation and Multifaceted Functionalities. *J. Mater. Chem. C* **2016**, *4*, 2901-2908.

32. Parusel, A. B. J.; Köhler, G.; Grimme, S., Density Functional Study of Excited Charge Transfer State Formation in 4-(N,N-Dimethylamino)Benzonitrile. *J. Phys. Chem. A* **1998**, *102*, 6297-6306.

33. Tsai, H.-H. G.; Sun, H.-L. S.; Tan, C.-J., Td-Dft Study of the Excited-State Potential Energy Surfaces of 2-(2′-Hydroxyphenyl)Benzimidazole and Its Amino Derivatives. *J. Phys. Chem. A* **2010**, *114*, 4065-4079.

34. El-Zohry, A. M.; Orabi, E. A.; Karlsson, M.; Zietz, B., Twisted Intramolecular Charge Transfer (Tict) Controlled by Dimerization: An Overlooked Piece of the Tict Puzzle. *J. Phys. Chem. A* **2021**, *125*, 2885-2894.

35. Li, G.; Magana, D.; Dyer, R. B., Direct Observation and Control of Ultrafast Photoinduced Twisted Intramolecular Charge Transfer (Tict) in Triphenyl-Methane Dyes. *J. Phys. Chem. B* **2012**, *116*, 12590-12596.

36. Peckus, D.; Matulaitis, T.; Franckevičius, M.; Mimaitė, V.; Tamulevičius, T.; Simokaitienė, J. r.; Volyniuk, D.; Gulbinas, V.; Tamulevičius, S.; Gražulevičius, J. V., Twisted Intramolecular Charge Transfer States in Trinary Star-Shaped Triphenylamine-Based Compounds. *J. Phys. Chem. A* **2018**, *122*, 3218-3226.

37. Liu, S.; Zhou, X.; Zhang, H.; Ou, H.; Lam, J. W. Y.; Liu, Y.; Shi, L.; Ding, D.; Tang, B. Z., Molecular Motion in Aggregates: Manipulating Tict for Boosting Photothermal Theranostics. *J. Am. Chem. Soc.* **2019**, *141*, 5359-5368.

38. Peng, Q.; Yang, L.; Li, Y.; Zhang, Y.; Li, T.; Qin, Y.; Song, Y.; Hou, H.; Li, K., Aggregation/Viscosity-Induced Emission and Third-Order Nonlinear Optical Signal Inversion in a Tict System. *J. Phys. Chem. B* **2020**, *124*, 22684-22691.

39. Alarcos, N.; Cohen, B.; Ziółek, M.; Douhal, A., Photochemistry and Photophysics in Silica-Based Materials: Ultrafast and Single Molecule Spectroscopy Observation. *Chem. Rev.* **2017**, *117*, 13639-13720.

40. Kuang, Z.; He, G.; Song, H.; Wang, X.; Hu, Z.; Sun, H.; Wan, Y.; Guo, Q.; Xia, A., Conformational Relaxation and Thermally Activated Delayed Fluorescence in

Anthraquinone-Based Intramolecular Charge-Transfer Compound. *J. Phys. Chem. C* **2018**, *122*, 3727-3737.

41. Choi, J.; Ahn, D.-S.; Oang, K. Y.; Cho, D. W.; Ihee, H., Charge Transfer-Induced Torsional Dynamics in the Excited State of 2,6-Bis(Diphenylamino)Anthraquinone. *J. Phys. Chem. C* **2017**, *121*, 24317-24323.

42. Ghosh, R.; Palit, D. K., Effect of Donor–Acceptor Coupling on Tict Dynamics in the Excited States of Two Dimethylamine Substituted Chalcones. *J. Phys. Chem. A* **2015**, *119*, 11128-11137.

43. Grabowski, Z. R.; Rotkiewicz, K.; Rettig, W., Structural Changes Accompanying Intramolecular Electron Transfer: Focus on Twisted Intramolecular Charge-Transfer States and Structures. *Chem. Rev.* **2003**, *103*, 3899-4032.

44. Sasaki, S.; Drummen, G. P. C.; Konishi, G.-i., Recent Advances in Twisted Intramolecular Charge Transfer (Tict) Fluorescence and Related Phenomena in Materials Chemistry. *J. Mater. Chem. C* **2016**, *4*, 2731-2743.

45. Kong, J.; Zhang, W.; Li, G.; Huo, D.; Guo, Y.; Niu, X.; Wan, Y.; Tang, B.; Xia, A., Excited-State Symmetry-Breaking Charge Separation Dynamics in Multibranched Perylene Diimide Molecules. *J. Phys. Chem. Lett.* **2020**, *11*, 10329-10339.

46. Liu, C.; Tang, K.-C.; Zhang, H.; Pan, H.-A.; Hua, J.; Li, B.; Chou, P.-T., Studies of Excited-State Properties of Multibranched Triarylamine End-Capped Triazines. *J. Phys. Chem. A* **2012**, *116*, 12339-12348.

47. Makarov, N. S.; Mukhopadhyay, S.; Yesudas, K.; Brédas, J.-L.; Perry, J. W.; Pron, A.; Kivala, M.; Müllen, K., Impact of Electronic Coupling, Symmetry, and Planarization on One- and Two-Photon Properties of Triarylamines with One, Two, or Three Diarylboryl Acceptors. *J. Phys. Chem. A* **2012**, *116*, 3781-3793.

48. Ramakrishna, G.; Goodson, T., Excited-State Deactivation of Branched Two-Photon Absorbing Chromophores: A Femtosecond Transient Absorption Investigation. *J. Phys. Chem. A* **2007**, *111*, 993-1000.

49. Athanasopoulos, S.; Alfonso Hernandez, L.; Beljonne, D.; Fernandez-Alberti, S.; Tretiak, S., Ultrafast Non-Förster Intramolecular Donor–Acceptor Excitation Energy Transfer. *J. Phys. Chem. Lett.* **2017**, *8*, 1688-1694.

50. Nelson, T.; Fernandez-Alberti, S.; Roitberg, A. E.; Tretiak, S., Electronic Delocalization, Vibrational Dynamics, and Energy Transfer in Organic Chromophores. *J. Phys. Chem. Lett.* **2017**, *8*, 3020-3031.

51. Duvanel, G.; Grilj, J.; Vauthey, E., Ultrafast Long-Distance Excitation Energy Transport in Donor–Bridge–Acceptor Systems. *J. Phys. Chem. A* **2013**, *117*, 918-928.

52. Tautz, R., et al., Charge Photogeneration in Donor–Acceptor Conjugated Materials: Influence of Excess Excitation Energy and Chain Length. *J. Am. Chem. Soc.* **2013**, *135*, 4282-4290.

53. Topchiy, M. A.; Asachenko, A. F.; Nechaev, M. S., Solvent-Free Buchwald–Hartwig Reaction of Aryl and Heteroaryl Halides with Secondary Amines. *Eur. J. Org. Chem.* **2014**, *2014*, 3319-3322.

54. Xiao, X.; Pang, J.; Sukhanov, A. A.; Hou, Y.; Zhao, J.; Li, M.-D.; Voronkova, V. K., The Effect of One-Atom Substitution on the Photophysical Properties and Electron Spin Polarization: Intersystem Crossing of Compact Orthogonal Perylene/Phenoxazine Electron Donor/Acceptor Dyad. *J. Chem. Phys.* **2020**, *153*, 184312.

55. Zhang, X.-F.; Wang, J., Morpholine-Phthalocyanine (Donor–Acceptor) Construct: Photoinduced Intramolecular Electron Transfer and Triplet Formation from Its Charge Separation State. *J. Phys. Chem. A* **2011**, *115*, 8597-8603.

56. Lippert, E., Dipolmoment Und Elektronenstruktur Von Angeregten Molekülen. *Z. Naturforsch. A* **1955**, *10*, 541-545.

57. Noboru, M.; Yozo, K.; Masao, K., Solvent Effects Upon Fluorescence Spectra and the Dipolemoments of Excited Molecules. *Bull. Chem. Soc. Jpn.* **1956**, *29*, 465-470.

58. Bin, C.; Zhang, H.; Luo, W.; Nie, H.; Hu, R.; Qin, A.; Zhao, Z.; Tang, B. Z., Oxidation-Enhanced Emission: Exploring Novel Aiegens from Thieno[3,2-B]Thiophene S,S-Dioxide. *J. Mater. Chem. C* **2017**, *5*, 960-968.

59. Xu, B.; Zhang, J.; Fang, H.; Ma, S.; Chen, Q.; Sun, H.; Im, C.; Tian, W., Aggregation Induced Enhanced Emission of Conjugated Dendrimers with a Large Intrinsic Two-Photon Absorption Cross-Section. *Polymer Chemistry* **2014**, *5*, 479-488.

60. Zhang, X.; Elmali, A.; Duan, R.; Liu, Q.; Ji, W.; Zhao, J.; Li, C.; Karatay, A., Charge Separation, Recombination and Intersystem Crossing of Directly Connected Perylenemonoimide–Carbazole Electron Donor/Acceptor Dyads. *Phys. Chem. Chem. Phys.* **2020**, *22*, 6376-6390.

61. Snellenburg, J. J.; Laptenok, S. P.; Seger, R.; Mullen, K. M.; Stokkum, I. H. M. v., Glotaran: A Java-Based Graphical User Interface for the R Package Timp. *J. Stat. Softw.* **2012**, *49*, 1-22.

62. Hay, R.; Pomery, P., Reactions of Pyrazine Radical Anions in Solution:I. Study of the Kinetics of the Dimerization of Pyrazine Radical Anions. *Aust. J. Chem.* **1971**, *24*, 2287-2292.

63. Akasaka, T., et al., Synthesis and Photoinduced Electron-Transfer Reactions in a La2@Ih-C80–Phenoxazine Conjugate. *ChemPlusChem* **2017**, *82*, 1067-1072.

64. Dong, Y.; Elmali, A.; Zhao, J.; Dick, B.; Karatay, A., Long-Lived Triplet Excited State Accessed with Spin–Orbit Charge Transfer Intersystem Crossing in Red Light-

Absorbing Phenoxazine-Styryl Bodipy Electron Donor/Acceptor Dyads. *ChemPhysChem* **2020**, *21*, 1388-1401.

65. Chen, K.; Zhao, J.; Li, X.; Gurzadyan, G. G., Anthracene–Naphthalenediimide Compact Electron Donor/Acceptor Dyads: Electronic Coupling, Electron Transfer, and Intersystem Crossing. *J. Phys. Chem. A.* **2019**, *123*, 2503-2516.

66. Imran, M.; Zhang, X.; Wang, Z.; Chen, X.; Zhao, J.; Barbon, A.; Voronkova, V. K., Electron Spin Dynamics in Excited State Photochemistry: Recent Development in the Study of Intersystem Crossing and Charge Transfer in Organic Compounds. *Phys. Chem. Chem. Phys.* **2021**, *23*, 15835-15868.

67. Frisch, M. J., et al. *Gaussian 16 Rev. C.01*, Wallingford, CT, 2016.

68. Adarsh, N.; Avirah, R. R.; Ramaiah, D., Tuning Photosensitized Singlet Oxygen Generation Efficiency of Novel Aza-Bodipy Dyes. *Org. Lett.* **2010**, *12*, 5720-5723.

69. Topchiy, M. A.; Asachenko, A. F.; Nechaev, M. S., Solvent-Free Buchwald–Hartwig Reaction of Aryl and Heteroaryl Halides with Secondary Amines. *Eur. J. Org. Chem.* **2014**, *2014*, 3319-3322.

Chapter 3

Synthesis and characterization of photophysical and mechanochromic properties quinoxaline-t-butyl carbazole derivatives: Effect of CN and F substitution

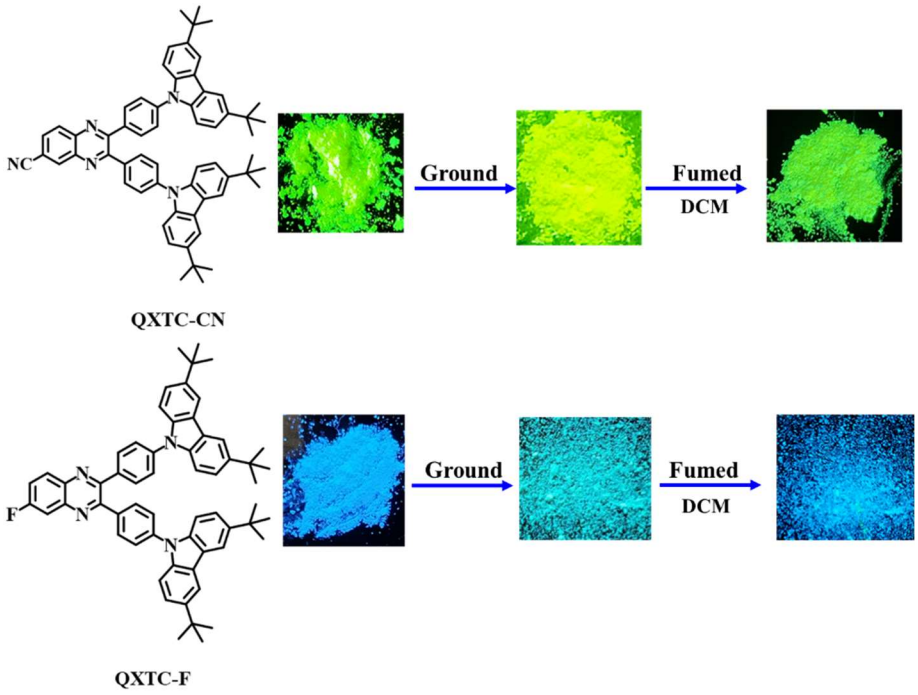

3.1 Abstract

*This work involves the investigation of effect of electron withdrawing groups on photophysical properties of two mechanochromic fluorophores with D–π–A-π–D structure, namely **QXTC-CN** and **QXTC-F**, based on quinoxaline as the acceptor unit and tertbutyl carbazole as the donor unit. For this, the acceptor strength of quinoxaline is tuned with the substitution of electron withdrawing groups such as cyano group (CN) and fluoride (F). Photophysical properties of these derivatives were studied in solution, aggregation state and solid state by measuring steady state absorption and emission spectroscopy and time resolved spectroscopy such as time correlated single photon counting (TCSPC) and nanosecond transient absorption spectroscopy (nsTAS). The electrochemical properties are analysed by cyclic voltammetry (CV). The steady state absorption and emission studies show that the*

presence of intramolecular charge transfer state (ICT). The nsTAS showed that the formation of triplet state in nonpolar solvent and occurrence of charge separation in polar solvent indicating the formation of radical anion of quinoxaline and radical cation of t-butyl carbazole. The aggregation induced emission studies showed that the fluorophores could emit in both solution and amorphous state. Both fluorophores, susceptible to external stimuli, including mechanical force (mechanochromism) and acid. Remarkably, the ***QXTC-CN*** *and* ***QXTC-F*** *showed reversible solid-state emission in response to mechanical stimuli and found that both molecules are sensitive to acid (TFA).*

3.2 Introduction

Mechanochromic or piezochromic materials are class of stimuli responsive materials which show switchable fluorescent properties by perturbing the molecular packing or conformation and non-covalent interactions with external mechanical stimuli such as pressing, crushing, grinding or rubbing in the solid state and become great interest in functional material research for the past two decades.[1-3] [4]Therefore, materials exhibiting mechanochromism have drawn increasing attention owing to their wide range of applications in rewritable materials, mechanosensors, security ink, optical electronic devices.[2,] [4-11]However, traditional fluorophores do not perform well in mechanofluorochromic material, as their non-emissivity in the solid state due to aggregation-caused quenching (ACQ).[12] Since traditional organic fluorophores usually contain planar aromatic cores, which promote π-π stacking during aggregating, so the ACQ effect is common and widely accepted. In 2001, the Tang group designed a family of molecule that was emissive in the solid state or when the molecules are aggregated and termed this phenomenon aggregation-induced emission (AIE), in contradiction with ACQ, and it is a powerful approach to handle the challenge of ACQ to use AIE luminogens (AIEgen).[13-14] AIE-active compounds exhibited intense solid-state emission due to the restriction of intramolecular motions and the prevention of intermolecular stacking.[15-16]

In aggregated state, AIEgens generally display twisted structures, strong emission and weak intermolecular π-π interaction between the molecules. In this way, fluorophores that exhibit aggregate-induced emission properties are well suited to stimuli-responsive applications, such as mechanochromism. Previous studies also indicated that specific C-H ⋯ N, C-H⋯O and C-H ⋯π contacts aid in locking and rigidifying the propeller-like conformations or twisted conformation of molecules, which effectively inhibit their intramolecular rotations and result in dramatic enhancements in their gas emission properties in both the crystalline state and aggregated state.[17] The properties of mechanochromic fluorophores are influenced by molecular packing, molecular conformation and different type intermolecular interactions generated in the molecules.[18-21] Besides these, the optical properties of D-π-A type mechanochromic fluorophores also depend on the intramolecular charge transfer (ICT) state.

The structure tuning with cyano groups and fluoride substitution play an important role in the molecular arrangement through the non-covalent bonds and affects the optoelectronic properties of D-A systems. It is worth to note that one CN group is close in its electron accepting properties to two fluorine atoms being close one to another. Therefore, it is crucial to introduce multiple adjustable interactions for the design of ideal mechanochromic materials. These interactions should be strong enough to maintain the orientation and arrangement of the fluorophores but mutable to external mechanical forces.

For example, W. Z Yuan et al. studied synergetic effects of intramolecular interactions and twisted conformations while designing mechanochromic fluorescent materials in 2013.[22]

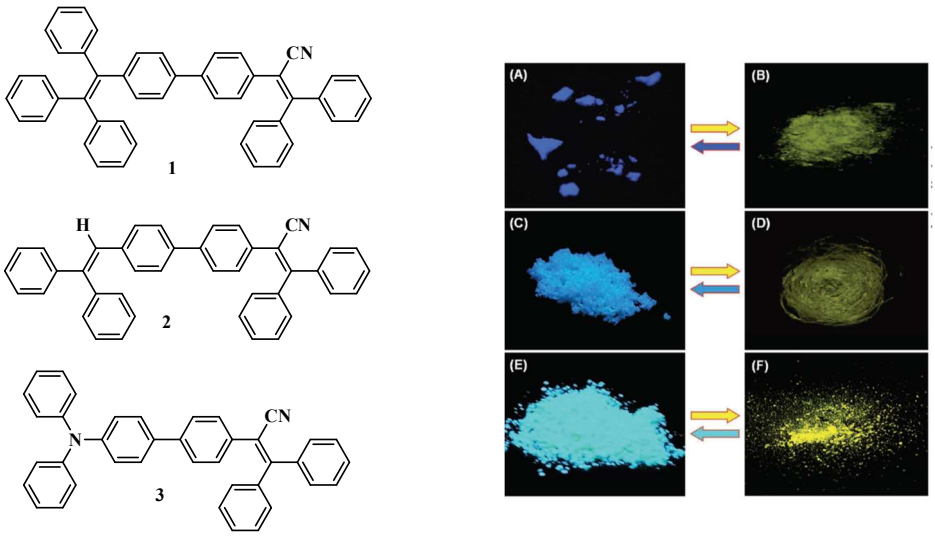

Figure 3.1 Molecular structures of mechanochromic materials based on triphenylacrylonitrile (**1**, **2** and **3**); Photograph powder samples (left) and ground samples (right) of respective molecules

To achieve this, they prepared a cyano-containing triphenylacrylonitrile (TPAN) decorated with TPE and triphenylamine, which also exhibited AIE properties. The C-H···N interaction is known to occur between cyano groups. and aromatic hydrogen atoms. The single crystal structure of these molecules showed their twisted conformation and different intramolecular interaction. Finally they confirmed that these properties can be attributed to planarizing the twisted conformations and destroying the multiple noncovalent interactions such as C-H···N, C-H···O and C-H···π intermolecular interactions upon mechanical stimulation.[23] Chen et al. also reported two constitutional isomers based on tetraphenylethene (TPE) as a AIE core tailored with cyanobenzene units. These target luminogens show obvious AIE characteristics. In addition, mechanochromic studies show that the fluorescence of the two luminogens can switch between blue and blue-green emissions, while the blue-green emission could spontaneously return to the initial blue colour within 10 min, demonstrating self-reversible mechanochromism.[24]

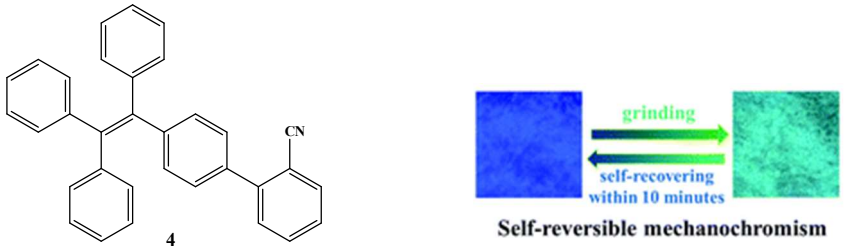

Figure 3.2 Molecular structure of tetraphenylethene-cyanobenzene derivatives (**4**); Photograph of powder samples and ground samples of respective molecules.

Recently, a few halogen substituted organic p conjugated derivatives have also found to be reported for mechanochromic behaviour. For example, Feng-Zho et al[25] reported four halogen substituted benzothiadiazole exhibiting mechanochromic fluorescent characteristics. Upon treating the mechanical forces stimulus, the orange emission of solid samples of **5** and **6** changed to red emission (593 nm) and initial orange emission is restored after treatment of the ground sample with fuming dichloromethane (DCM). While the solid sample of **7** and **8** changed its green colour to yellow green colour upon grinding with a pestle in an agate mortar. Further, after treatment with DCM, the original green colour is reverted. The powder X-ray diffraction (XRD) pattern were also studied for understanding the mechanism of mechanochromic behaviour of different form of solid samples of each halogenated benzothiadiazole derivatives. The unground samples of **5-8** showed sharp and intense peaks, which represented their crystalline nature. While the ground sample showed lack of sharp diffraction peaks, representing the amorphous nature of ground samples. When the ground sample was exposed to DCM, the sharp diffraction peaks were reappeared, indicative of the recovery of crystalline nature. The experiment evidence demonstrated that transition between crystalline to amorphous state is responsible for mechanochromic fluorescence behaviour of compounds **5-8**.[25]

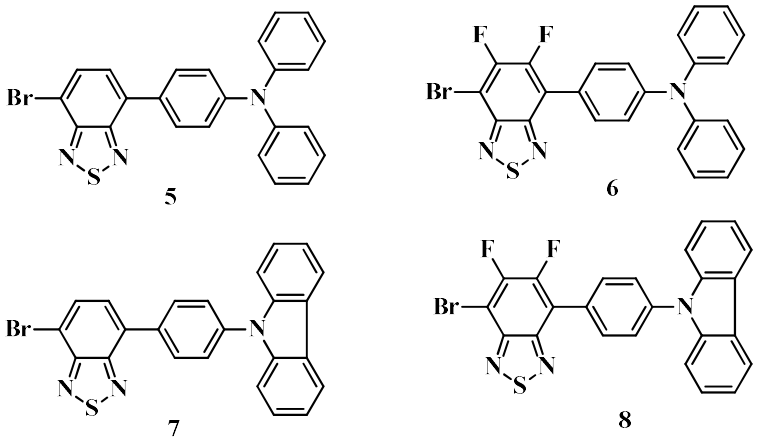

Figure 3.3 Molecular structures of tetraphenylethene-cyanobenzene derivatives (**5**-**8**);.

It is reported that N-heterocyclic based donor-π acceptor compounds have also been found to exhibit mechanochromic behaviour due to presence of multiple adjustable interactions, flexible and nonplanar or twisted molecular structure. The general feature of donor-acceptor or donor-π-acceptor compounds is the presence of intramolecular charge transfer (ICT). The ICT properties of D-π-A compounds and therefore their luminescent properties can be readily tuned by facile modifications of the D, A or π-spacer moiety, which facilitates the development of ML materials with diverse response behaviours.[26-27] These attractive properties of D-π-A compounds provide a broad prospect for achieving good mechanochromic fluorophores materials based on this type of system.[28-29]

For example, Ling Zang et al synthesised three donor-acceptor (D-A) containing cruciform luminophores, named **9**, **10** and **11**, with twisted molecular conformation have been synthesized (**Figure 3.4)**. The D-A type cross-conjugated compounds showed unique intramolecular charge transfer (ICT) properties. Interestingly, they showed substituent-dependent aggregation-induced emission (AIE) and mechanofluorochromic (MFC) behaviour. The mechanochromic colour changes are shown in **Figure 3.4**.

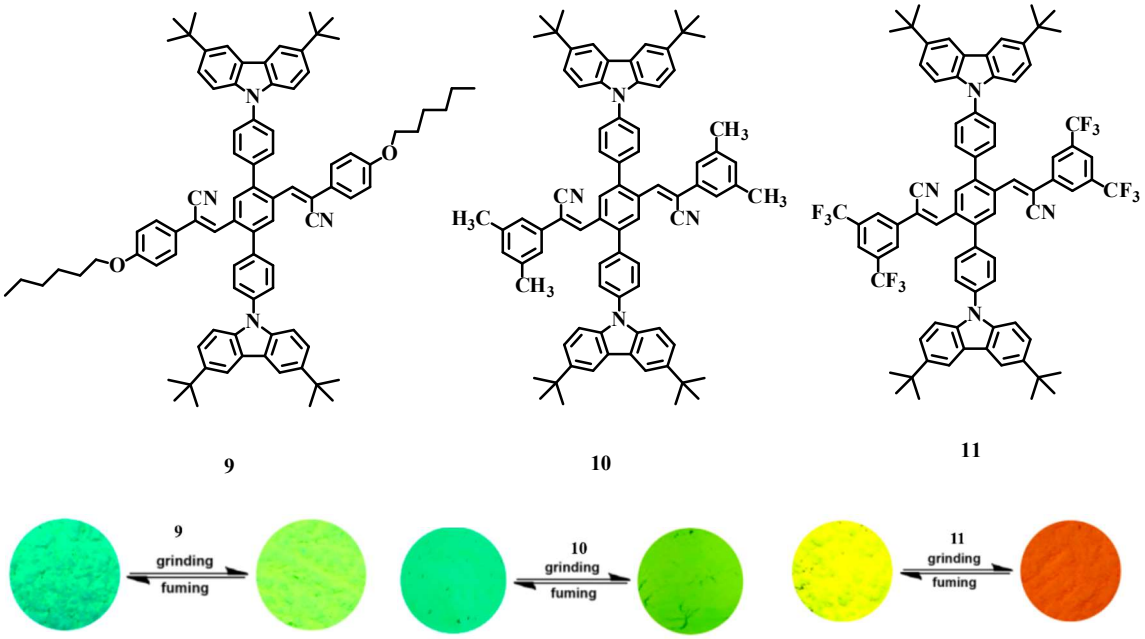

Figure 3.4 Molecular structurse of t-butyl carbazole- acrylonitrile derivatives (**9**, **10** and **11**); Photograph of powder samples and ground samples of respective molecules

Quinoxaline is an N-heterocyclic compound, which as excellent electron withdrawing group and it can be act as an acceptor in donor-acceptor systems. Meanwhile the quinoxaline unit also advantageous to construction of donor-acceptor type molecules, which is emerged as significative class of optical application in some areas such as display and fluorescent sensors.

Rao et al designed and synthesized stimuli-responsive quinoxaline based D-A-D molecules by integrating diphenylquinoxaline (acceptor) with two aromatic chromophores, pyrene/anthracene (donor) (**Figure 3.5)**. These highly pre-twisted molecules are emissive in both solution and solid state. The twisted conjugated skeleton of molecules due to steric hindrance and intramolecular C-H···N and C-H···π hydrogen bonds, is responsible for their aggregation induced emission. The pyrene derivative (**12**) showed reversible mechanofluorochromic behaviour and changing the emission colour from bluish green to yellow reversibly upon grinding and heating.

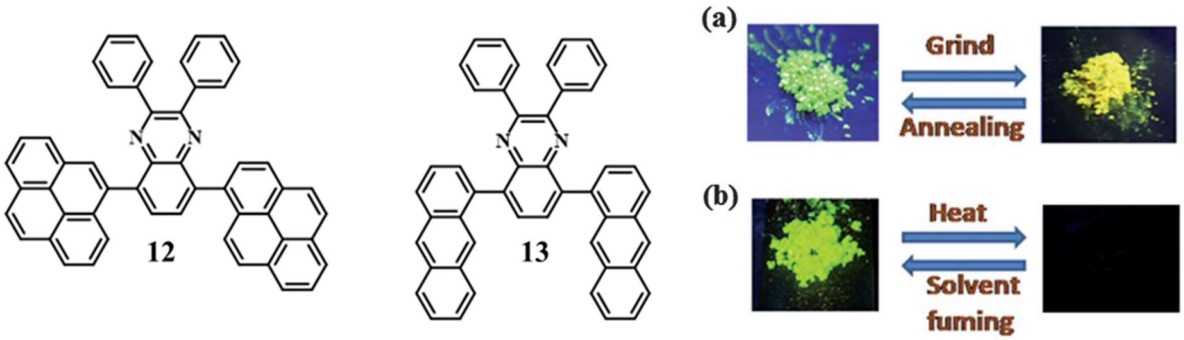

Figure 3.5 Chemical structure of quinoxaline-pyrene/anthracene derivatives (**12** and **13**); Photograph of powder and ground samples in various solid phase under UV light (365 nm).

On other hand, the anthracene derivative (**13**) exhibited thermochromism upon heating and solvent fuming processes. The mechanochromism of pyrene derivative is due to structural order to disorder phase transition while the thermochromism of anthracene derivatives is attributed to transformation of molecular packing from a two dimensional erringbone to one dimensional poorly ordered J-type molecular arrangements.[30]

The Ekbote et al investigated the mechanochromic properties of two quinoxaline derivatives having a donor (D) and acceptor (A) type (D-A-D) structure and effectively synthesized by incorporating well-known AIE active fluorophores, tetraphenylethylene (TPE) (**Figure 3.6**). The TPE substituted acenenaphene-quinoxaline (**14**) displayed reversible emission colour change from bluish green to green and TPE substituted phenanthrene quinoxaline (**15**) showed a colour change from green to yellow in response to a mechanical stimuli. Based on powder XRD studies, the observed mechanochromic properties of TPE-based quinoxaline derivatives is attributed to morphological change from crystalline to amorphous.[31]

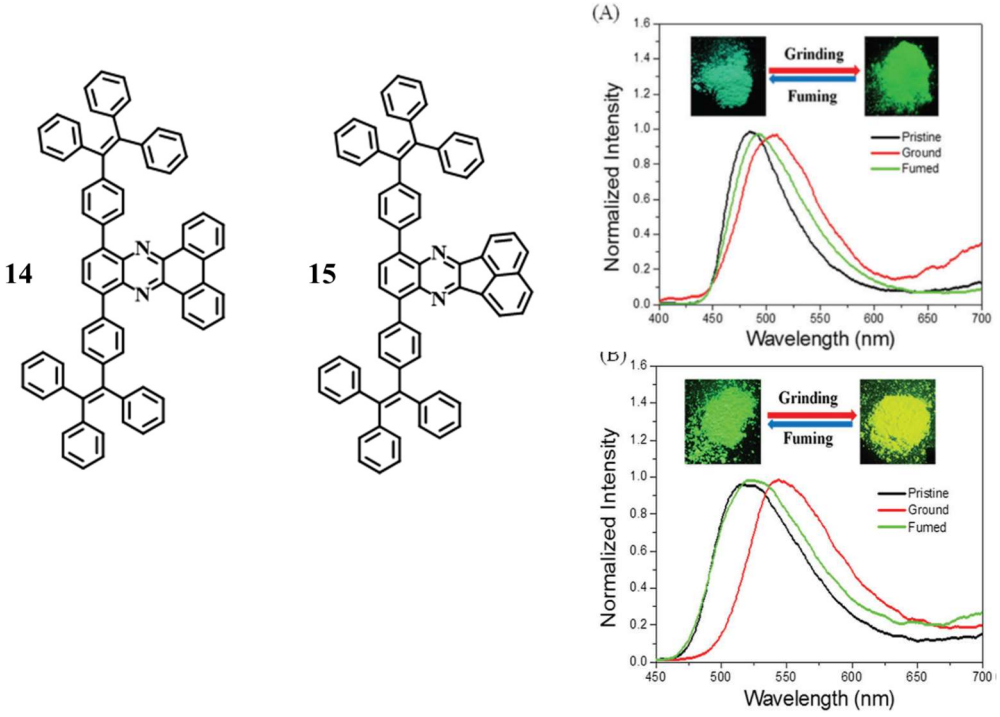

Figure 3.6 Chemical structure of TPE substituted acenaphthene- quinoxaline and phenanthrene-quinoxaline (**14** and **15**); Emission spectra of acenaphthene- quinoxaline, **14** (A) and phenanthrene-quinoxaline, **15** (B) as pristine, ground and fumed solid sample; Photographs taken under 365 nm UV illumination

In this work, we present synthesis and photophysical characterisation of new D- π-A-π-D type quinoxaline derivatives, **QXTC-CN** and **QXTC-F**, that show solid-state fluorescence and reversible mechanoresponsive behaviour. The structure of **QXTC-CN** and **QXTC-F** were confirmed by using ^{1}H NMR and ^{13}C NMR spectroscopy, as well as HRMS analysis. As a result of grinding the **QXTC-CN** and **QXTC-F**, a change in fluorescence colour occurs, which can be restored to its original colour when heated or exposed to solvent vapours. The transformation from crystalline to amorphous solid-state packing is responsible for the change in emission. Through experiments using TFA vapor, it was demonstrated that **QXTC-CN** and **QXTC-F** can sense acid vapours. In the solid-state, their emissions were quenched by TFA vapour, however, they were regained after exposure to TEA.

3.3 Results and Discussion

3.3.1 Synthesis of Quinoxaline Derivatives

The two quinoxaline derivatives were readily synthesized according to procedure shown in **Scheme 3.1**. The intermediate products were synthesized by using Buchwald-Hartwig coupling reaction and final step consist of a condensation reaction. The products **QXTC-CN** and **QXTC-F** were isolated in 76% and 84% yield, respectively. The target molecules are purified by column chromatography and the structural characterisation is carried out by ^{1}H NMR, ^{13}C NMR and MALDI-TOF spectroscopy. The compound showed good solubility in cyclohexane, toluene, dichloromethane (DCM), chloroform ($CHCl_3$), tetrahydrofuran (THF), N,N-dimethylformamide (DMF) and showed poor solubility in ethanol, acetonitrile and ethanol.

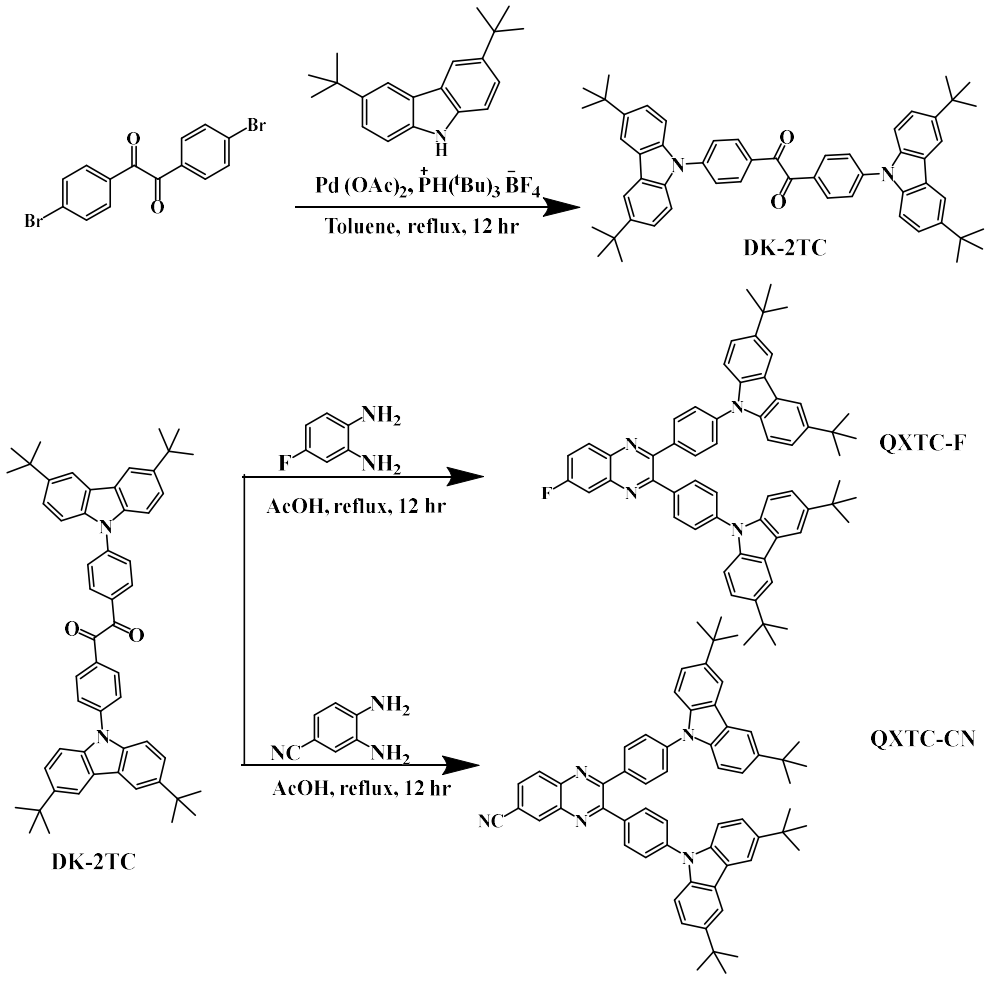

Scheme 3.1 Synthesis scheme of **QXTC-CN** and **QXTC-F**.

3.3.2 Photophysical Characterization in Solution

UV-Visible absorption and fluorescence spectra have been used to characterize the photophysical properties of **QXTC-CN** and **QXTC-F** at room temperature in different solvents. **Figures 3.7** and **Figure 3.8** display the UV-Visible absorption spectra and emission spectra of two quinoxaline derivatives in solvents of various polarities. The Table 1 summarizes the photophysical parameters in different solvents of two quinoxaline derivatives. It is found that the molar extinction coefficient (ε) for **QXTC-CN** (26,998 cm^{-1}) is two times less than that of **QXTC-F** (57,875 cm^{-1})**.** The higher extinction coefficient of **QXTC-F** reflects its enhanced electronic coupling between acceptor moiety quinoxaline and donor moiety tert-butyl carbazole

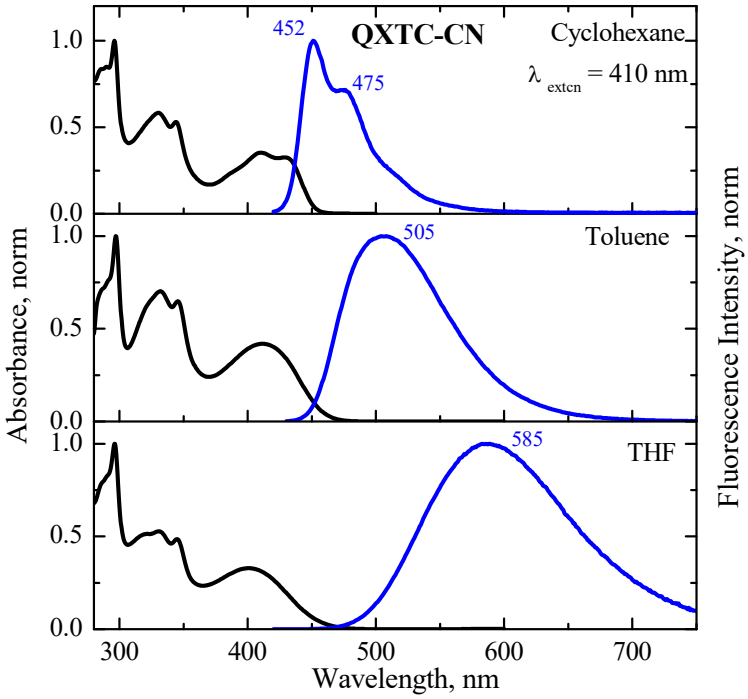

Figure 3.7 Steady state absorption and emission spectra of **QXTC-CN** in different solvents, obtained upon excitation at 410 nm.

The absorption bands between 280 nm and 350 nm in higher energy region of absorption spectra, corresponds to absorption of the carbazole (280 nm) and quinoxaline (330 nm). But the lowest energy transition of both derivatives between 350 and 450 nm, could be

attributed to intramolecular charge transfer (ICT) transition from donor to acceptor unit. The ICT band of **QXTC-CN** (~410 nm) is more red shifted than **QXTC-F** (~380 nm), which also indicating that CN group exert more inductive effect on quinoxaline acceptor core, while fluorine exert less only. With increasing solvent polarity, emission spectra display a redshift, unlike absorption spectra in which no significant changes observed. It gives evidence that the dipole moment in the excited state is higher than ground state, along with the charge transfer characteristics of the S_1 state.

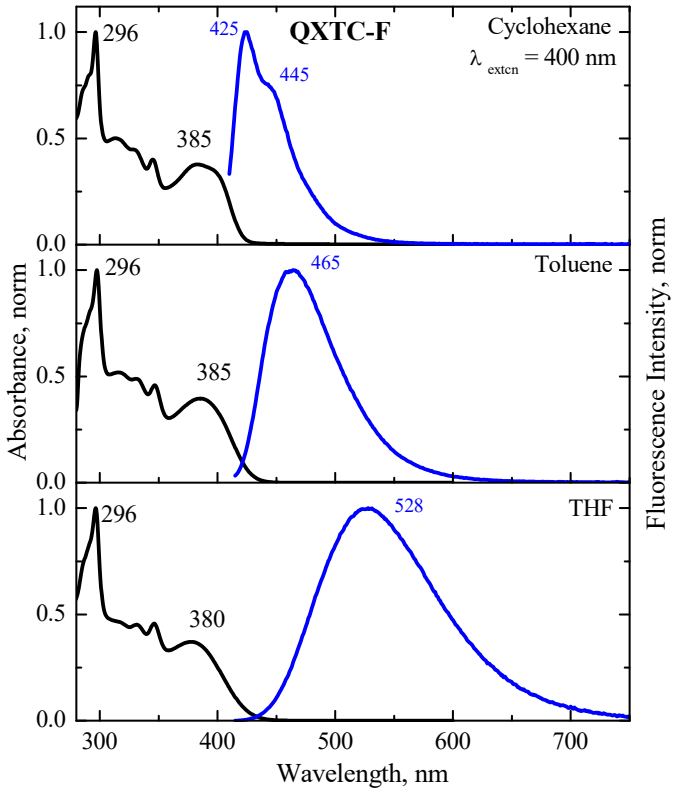

Figure 3.8 Steady state absorption and emission spectra of **QXTC-F** in different solvents, obtained upon excitation at 410 nm.

It is noted that the emission maxima of two molecules in toluene are at 505 and 465 nm for **QXTC-CN** and **QXTC-F** , respectively. Here the redshift of **QXTC-CN** in toluene was greater (505 nm) than that of **QXTC-F** (465 nm), which can be due to more the electron-withdrawal effect produced by the CN than F. (**Figure 3.7** and **Figure 3.8**). The Stokes shift

of two derivatives is increased from ~2000 cm^{-1} to ~7500 cm^{-1} with increasing solvent polarity. The relative fluorescence quantum yield and lifetime of quinoxaline derivatives were measured in cyclohexane, toluene and THF. The substitution of electron withdrawing groups also influenced the fluorescence lifetime (τ), radiative decay constant (k_r) and fluorescence quantum yield (FLQY) both derivatives. For comparison, there is a decrease of fluorescence quantum yield of **QXTC-CN** from 0.24 (Cyclohexane) to 0.06 (THF) while in the case of **QXTC-F,** it is from 0.18 (Cyclohexane) to 0.17 (THF), in which no significant differences observed. It may due to more twisted conformation **QXTC-CN**, which will lead the formation of more, stabilized and polarized charge separated state (CS) in excited state. Due to stabilization of CS state of **QXTC-CN** in more polar solvent (THF), the rate of charge recombination of CS will be lower therefore the **QXTC-CN** exhibited higher τ value and lower k_r in THF.

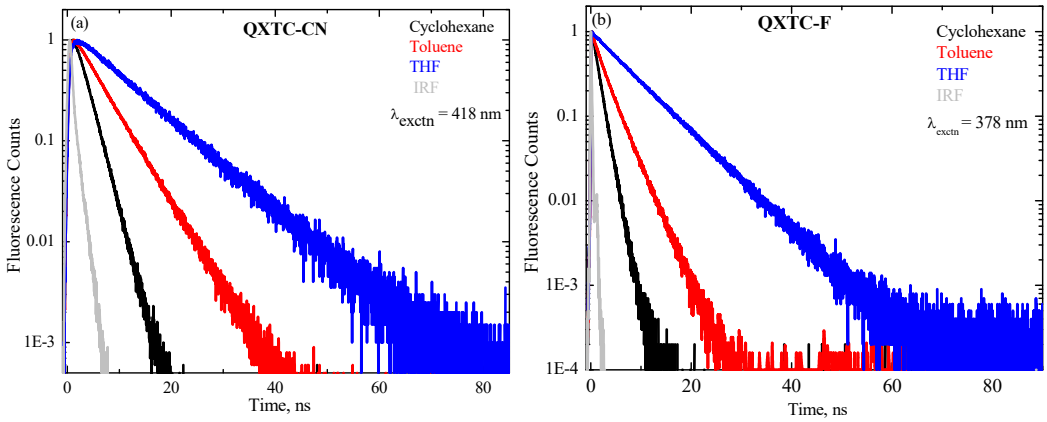

Figure 3.9 Fluorescent decay profile of **QXTC-CN** (a) and **QXTC-F** (b).

While in the case of **QXTC-F**, the rate of charge recombination of charge separated state will be faster due to more overlapping of HOMO and LUMO of **QXTC-F** in which inductive effect of fluoride is not much with respect to CN, and therefore **QXTC-F** exhibited lower τ values and higher k_r than **QXTC-CN** in both nonpolar and polar solvent. The fluorescence lifetime values, radiative decay constants and nonradiative decay constants for both derivatives are provided in Table **3.1**.

Table 3.1: Photophysical properties of **QXTC-CN** and **QXTC-F**

Compound	Solvents	Absorption max, (nm)	Fluorescence max, (nm)	Stokes shift, (cm^{-1})	Φ_{PL}	τ (ns)	k_r (10^7 s^{-1})	k_{nr} (10^7 s^{-1})
	Cyclohexane	296, 410, 430	452, 475	2203	0.24	2.16	11.1	35.18
QXTC-CN	Toluene	296, 410	505	4588	0.23	4.95	4.64	15.55
	THF	296, 400	585	7905	0.06	9.52	0.63	9.87
	Cyclohexane	296, 385, 395	425, 445	2844	0.18	1.20	15.0	68.33
QXTC-F	Toluene	296, 385	465	4469	0.24	2.77	8.66	27.43
	THF	296, 380	528	7376	0.17	7.40	2.29	11. 21

3.3.3 Determination of Energy Level of Singlet State (S_1) and Triplet State (T_1)

To determine effect of CN and F substitution on the energy level of singlet and triplet state of **QXTC-CN** and **QXTC-F**, low temperature fluorescence spectra and phosphorescence spectra of both derivatives were measured in toluene glass matrix at 77K, as shown in **Figure 3.10** and calculated the singlet-triplet energy gap (ΔE_{ST}). In room temperature, the quinoxaline derivatives showed broad and unstructured emission spectra upon excitation. At low temperature (77K), the emission spectra is blue shifted with emission max at 454 (**QXTC-F**) and 480 nm (**QXTC-CN)** revealing that the emission from locally excited state (^{1}LE). From the onset of low temperature emission spectra (**Figure 3.10c** and **3.10d**), the energy level of S_1 state can be calculated to be 2.95 (**QXTC-F**) and 2.82 eV (**QXTC-CN)**. The broad and unstructured phosphorescence spectra indicates that the radiative decay mainly from charge transfer state (^{3}CT) with emission maximum peak of 530 (**QXTC-F**) and 542 nm (**QXTC-CN**).

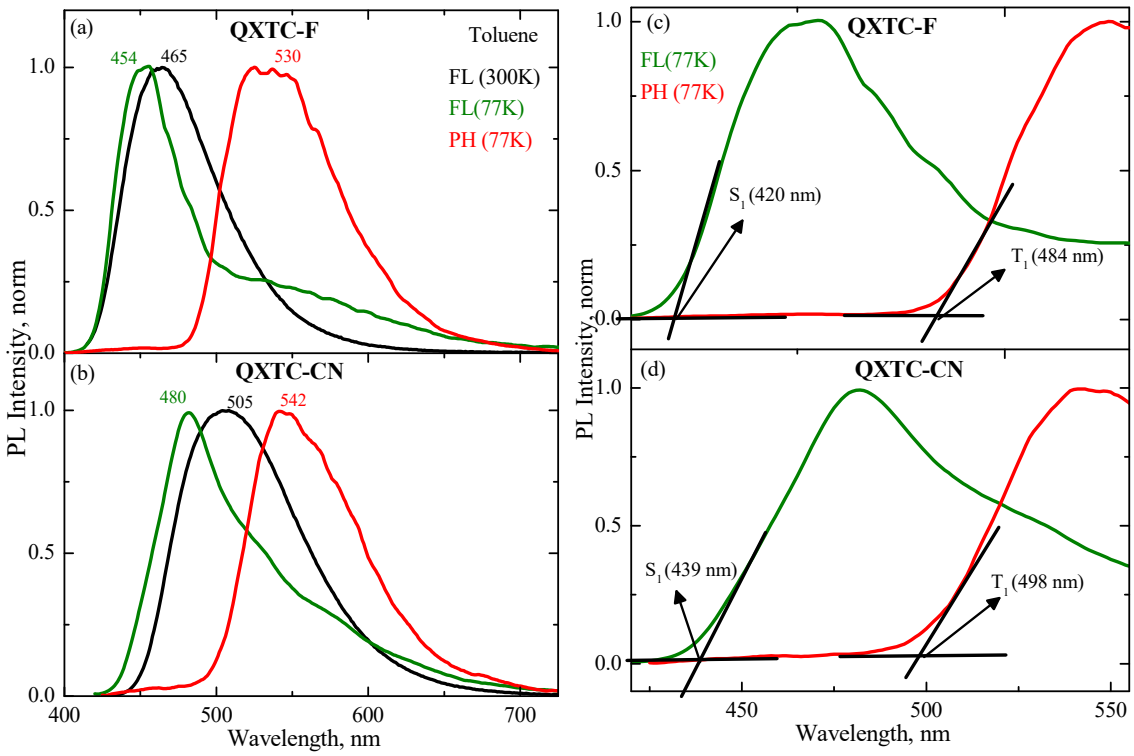

Figure 3.10 Steady state room temperature fluorescence emission (black) and low temperature fluorescence emission (77K, green) spectra and phosphorescence emission of **QXTC- F** (a) and **QXTC-CN** (b) in toluene. Calculation of ΔE_{ST} (c) and (d).

Table 3.2. Energy of level of singlet and triplet state of **QXTC-CN** and **QXTC-F**.

Quinoxaline derivatives	E $(S_1)_{onset}$ (nm)	E $(T_1)_{onset}$ (nm)	E $(S_1)_{onset}$ (eV)	E $(T_1)_{onset}$ (eV)	ΔE_{ST} (eV)
QXTC-F	420	484	2.95	2.56	0.39
QXTC-CN	439	498	2.82	2.48	0.34

Consequently, the energy level of T_1 state can be calculated to be 2.95 (**QXTC-F**) and 2.82 eV (**QXTC-CN)** from the onset of phosphorescence spectra. From the values of singlet and triplet state, the ΔE_{ST} values for F and CN substituted quinoxaline derived donor-acceptor systems are determined to be 0.39 eV for **QXTC-F** and 0.34 eV for **QXTC-CN**. The energy level of singlet state and triplet state and ΔE_{ST} are provided in **Table 3.2**. Interestingly, the

more inductive effect of CN effected the energy level of singlet state and triplet state and ΔE_{ST} value of **QXTC-CN** in which singlet state, triplet energy and ΔE_{ST} are comparatively is lower than **QXTC-F**. This could be due to the more localization of LUMO of quinoxaline acceptor unit which can reduce overlap between HOMO and LUMO, and therefore attaining low value of ΔE_{ST} with respect to **QXTC-F**.

3.3.4 Nanosecond Transient Absorption Studies

Nanosecond laser flash photolysis spectrophotometer is used to understand the formation of long lived components in excited states like triplet state and radical anion and cation. Nanosecond transient absorption spectra of **QXTC-CN** and **QXTC-F** were measured at different delay times in cyclohexane and THF upon laser excitation at 355 nm. The transient absorption spectra of **QXTC-CN** in nonpolar solvent (cyclohexane) showed three absorption maxima at 370, 460, and 730 nm as shown in **Figure 3.11**. The negative change in absorbance, the bleach at around 330 and 410 nm is due to the ground state absorption of the compound. The transient absorption bands are attributed due to triplet excited state of respective derivative and is confirmed by the experiment under aerated condition where peaks are quenched (**Figure 3.11b**). It is found that the triplet dynamics in cyclohexane showed mono exponential relaxation processes with the lifetime of 1.67 μs. While in the case of polar solvent (THF), the nanosecond transient absorption spectra of **QXTC-CN**, having completely different spectral pattern compared to spectra obtained in cyclohexane and showed a broad absorption maximum at 490 nm and weak absorption maximum at 780 nm (**Figure 3.12**). The peak at 780 nm could be due to formation of carbazole radical cation and 490 nm could be due to quinoxaline radical anion, suggesting that formation charge transfer state, with the lifetime of 1.89 μs. The transient absorption spectra were also measured in oxygen atmosphere exhibiting the quenching of dynamics (**Figure 3.13b**).

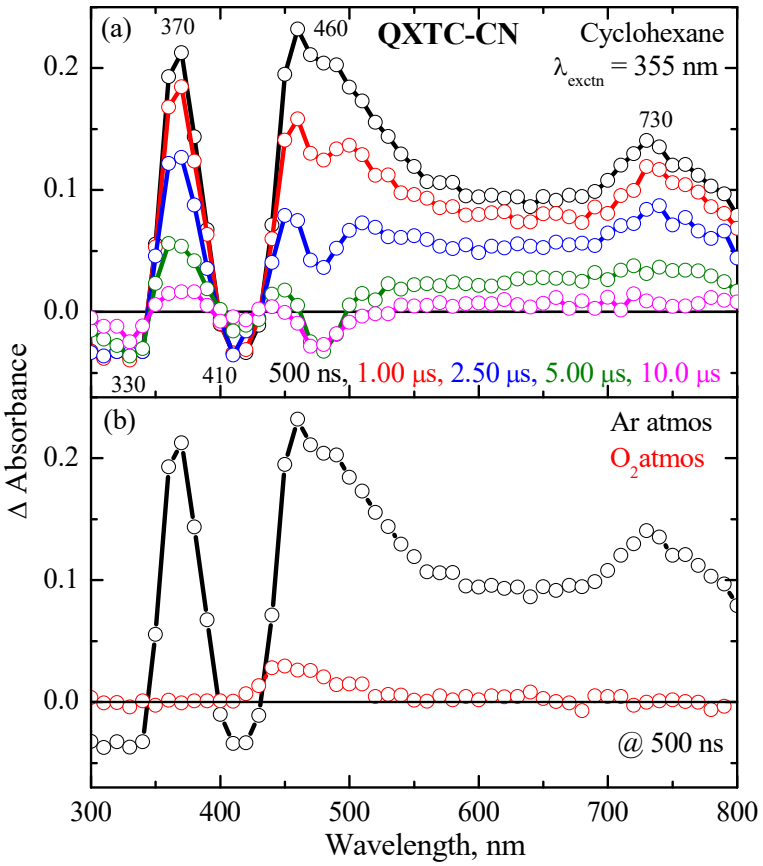

Figure 3.11 Transient absorption spectra of **QXTC-CN** in cyclohexane obtained upon excitation at 355 nm in inert atmosphere (a); a comparison of transient absorption spectra of **QXTC-CN** in argon and oxygen purged solution (b).

Figure 3.14 shows the nanosecond transient absorption spectra of **QXTC-F** in cyclohexane under inert atmosphere obtained at different delay times exhibiting the two absorption bands at around 360 and 430 and 700 nm along with bleach bands at around 330 nm corresponding to the ground state (S_0) absorption maxima. The intensity of the transient absorption spectra was decreased with increase of delay time. The transient absorption spectra were also measured under oxygen atmosphere and quenching of dynamics were showed in **Figure 3.16b**. The quenching dynamics with oxygen suggesting that the bands in transient absorption could be due to triplet absorption of **QXTC-F**.

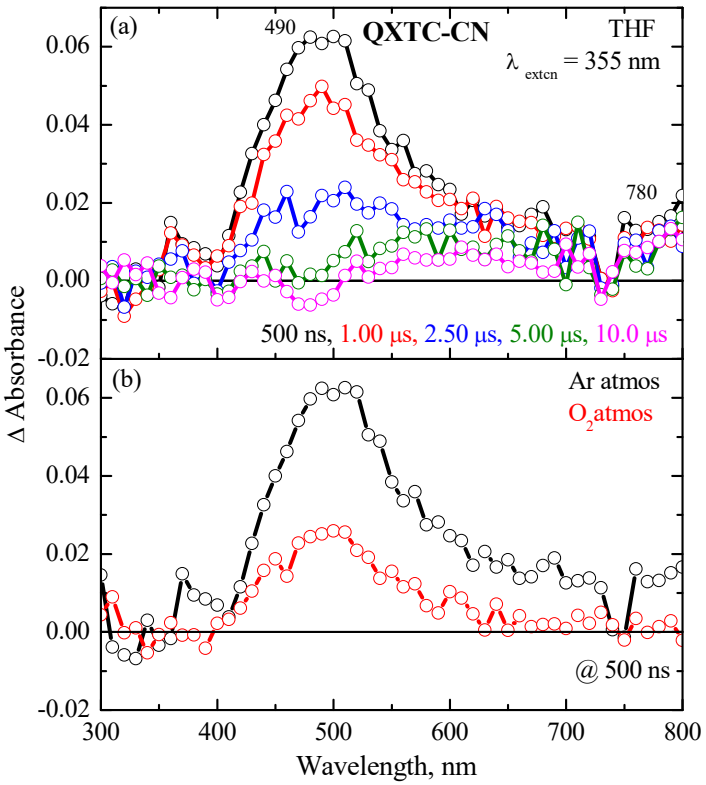

Figure 3.12 Transient absorption spectra of **QXTC-CN** in THF obtained upon excitation at 355 nm in inert atmosphere (a); a comparison of transient absorption spectra of **QXTC-CN** in argon and oxygen purged solution (b).

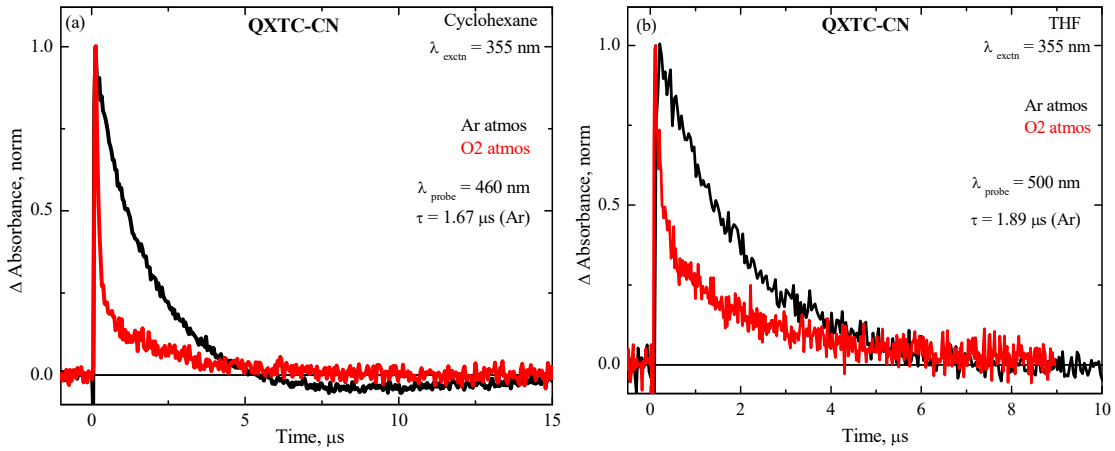

Figure 3.13 (a) Kinetic decay of **QXTC-CN** in cyclohexane (a) probed at 460 nm and THF (b) probed at 500 nm, obtained upon excitation at 355 nm in argon and oxygen purged solution.

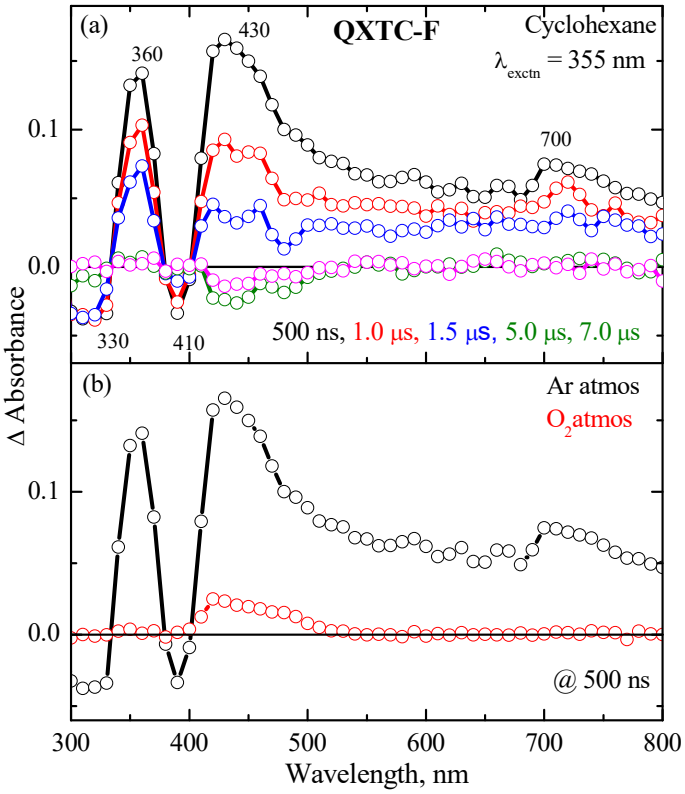

Figure 3.14 Transient absorption spectra of **QXTC-F** in cyclohexane, obtained upon excitation at 355 nm in inert atmosphere; a comparison of transient absorption spectra of **QXTC-CN** in argon and oxygen purged solution

It is also noticed that the excited state absorption maximum of **QXTC-F** are more blue shifted compared with excited state absorption maximum of **QXTC-CN**, which supports that the triplet state of **QXTC-CN** is more stabilized than triple state of **QXTC-F**. The lifetime of triple state of **QXTC-F** is found to be 0.84 μs, less than that of **QXTC-CN** (1.64 μs) (**Figure 3.16a**). The nanosecond transient absorption spectra of **QXTC-F** (**Figure 3.15**) in THF showed that broad absorption maximum at 430 and 490 nm and weak absorption maximum at 770 nm which could be due to formation of radical anion of quinoxaline and radical cation of t-butyl carbazole as observed in transient absorption spectra of **QXTC-CN** suggesting that formation of charge separated state (CS). The decay time constant of CS is found to be 1.48 μs (**Figure 3.16b**). Therefore, the nanosecond transient absorption studies of both derivatives provides an insight to their excited state relaxation dynamic after excitation.

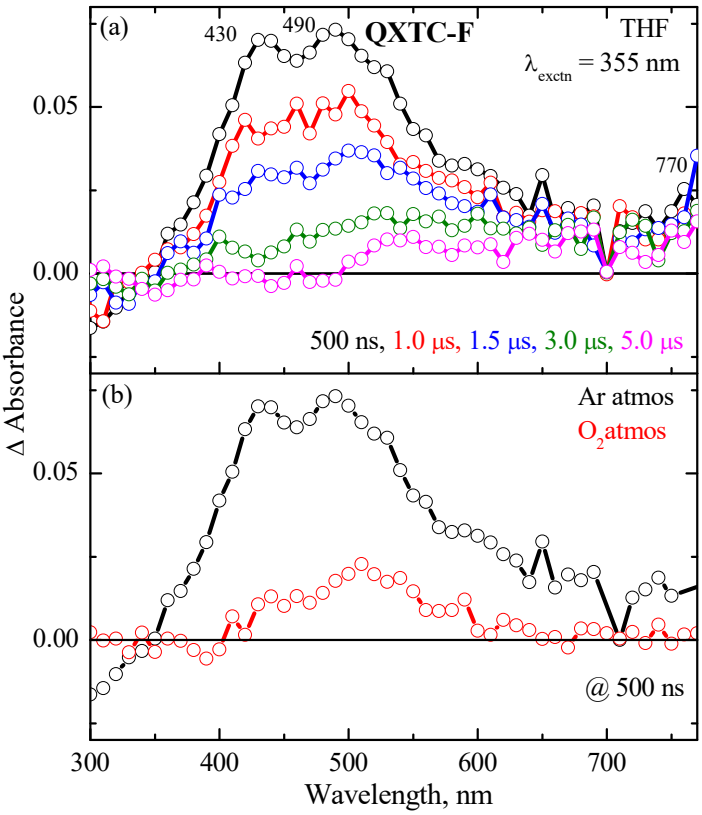

Figure 3.15 Transient absorption spectra of **QXTC-F** in THF respectively, obtained upon excitation at 355 nm in inert atmosphere.

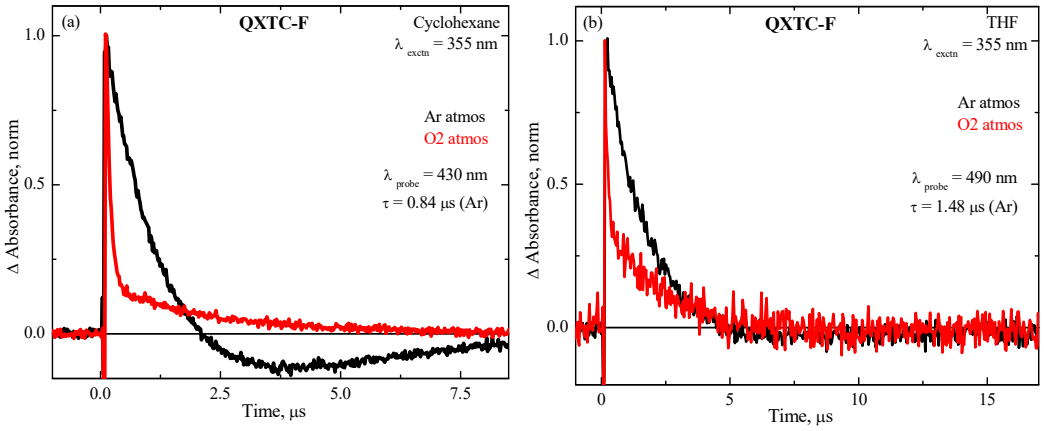

Figure 3.16 Kinetic decay of **QXTC-F** in cyclohexane (a) probed at 430 nm and THF (b) probe at 490 nm, obtained upon excitation at 355 nm in argon and oxygen purged solution.

3.3.5 Electrochemical Characterization

A cyclic voltametric analysis was performed to determine the electrochemical properties and ascertain the energy levels of the luminophores. The experiment was performed in dichloromethane (DCM) with tetrabutylammonium hexafluorophosphate (TBAPF6) as a supporting electrolyte. The cyclic voltammograms of **QXTC-CN** and **QXTC-F** is showed in the **Figure 3.17**. The energy levels of the highest occupied molecular orbital (HOMO) were calculated on the basis of the onset oxidation (E onset).

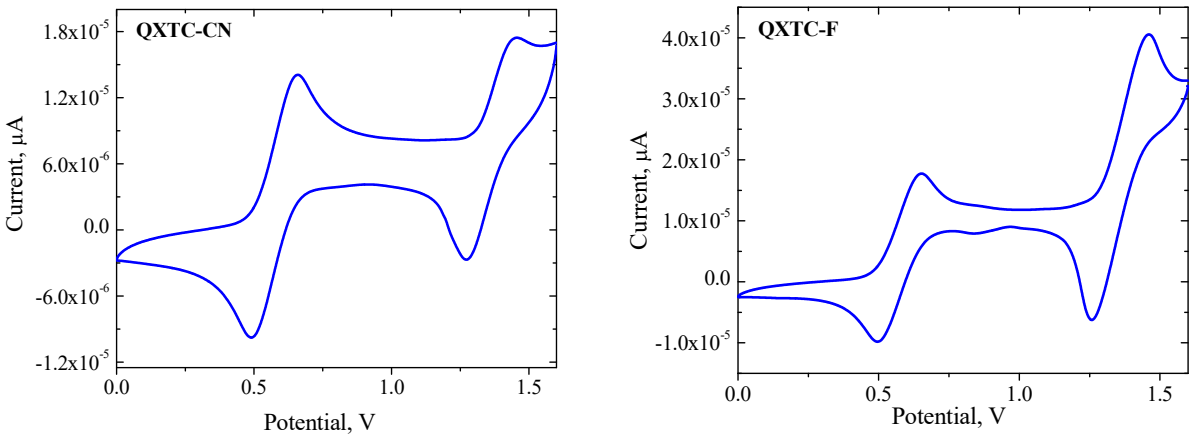

Figure 3.17 Cyclic voltammogram of **QXTC-CN** and **QXTC-F**

Table 3.3 Electrochemical data of **QXTC-CN** and **QXTC-F**

Compound	E_{oxd} (V)	E_{HOMO} (eV)	E_{LUMO} (eV)	E_g (opt) (eV)
QXTC-CN	1.36	-6.16	-3.49	2.66
QXTC-F	1.35	-6.15	-3.26	2.89

The oxidation potentials of **QXTC-CN** and **QXTC-F** were calculated to be 1.36 V and 1.35 V. Therefore, HOMO energy level of **QXTC-CN** and **QXTC-F** was calculated to be -6.16 and -6.15 eV, respectively, based on oxidation potential. At the same time, their bandgaps (E_g) estimated from the onset of absorption spectra in solutions are 2.66 and 2.89 eV,

respectively. From which the LUMO energy levels of **QXTC-CN** and **QXTC-F** were determined to be -3.49 and -3.20 eV, respectively. The data are provided in **Table 3.3.** The oxidation potential of both compounds is similar. It means that the substitution with cyano group and fluoride did not change the energy of HOMO value of both molecules (-6.16 eV and -6.15 eV, respectively). However, the energy of LUMO of **QXTC-CN** is lower (-3.49 eV) than **QXTC-F** (-3.26). The results implies that cyano group induces more electron withdrawing effect on quinoxaline acceptor core than fluorine substitution which will lead more localization of LUMO and thus less overlapping between HOMO and LUMO occurs in **QXTC-CN**. Therefore, comparing with **QXTC-F**, **QXTC-CN** showed more red shifted ICT absorption due to the lowering LUMO energy as well as more stabilized charge transfer state in excited state due to more separation of HOMO-LUMO molecular orbital.

3.3.6 Aggregation Studies

Figure 3.18a and **Figure 3.18b** display the fluorescence emission spectra of **QXTC-CN** and **QXTC-F**, respectively**,** in THF/water upon increasing the volume fraction of water (f_w) were measured to determine whether they exhibit AIE activity. The solute did not aggregate when water was added in small amounts. But it was observed that emission was relatively weaker and red shifted as polarity of THF-Water mixture is increased, which was mainly due to solvation of ICT state, as shown in **Figure 3.19a** and **3.19b**. The increase of fluorescence intensity along with shifting of the maximum towards the blue region in the both cases, is attributed to the formation of nanoaggregates with size ranges from 100 to 550 nm (f_w = 90%) confirmed by DLS experiments (**Figure 3.19c** and **3.19d**).

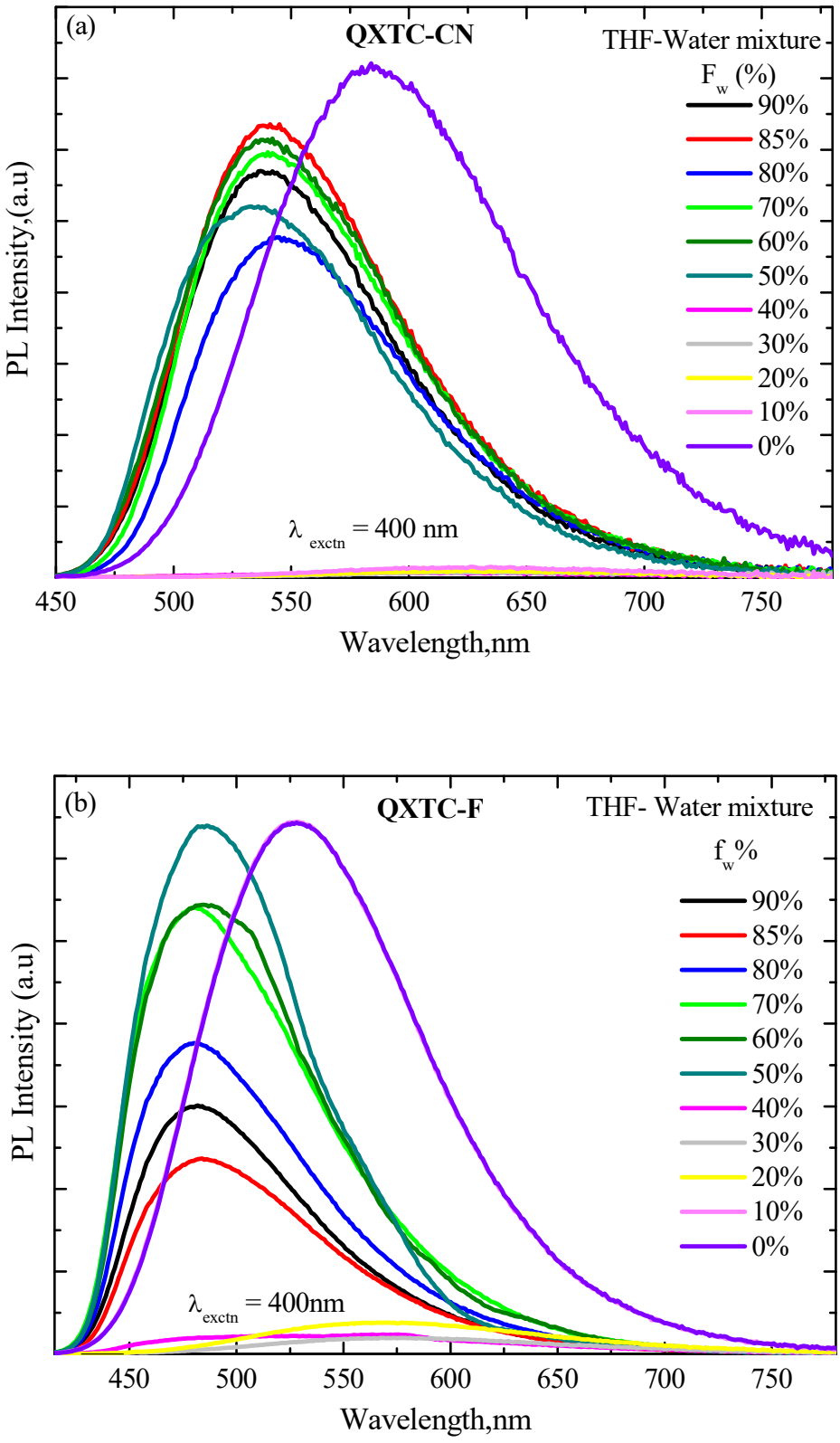

Figure 3.18 Emission spectra of **QXTC-CN** (a) and **QXTC-F**(b) in different THF -Water mixture.

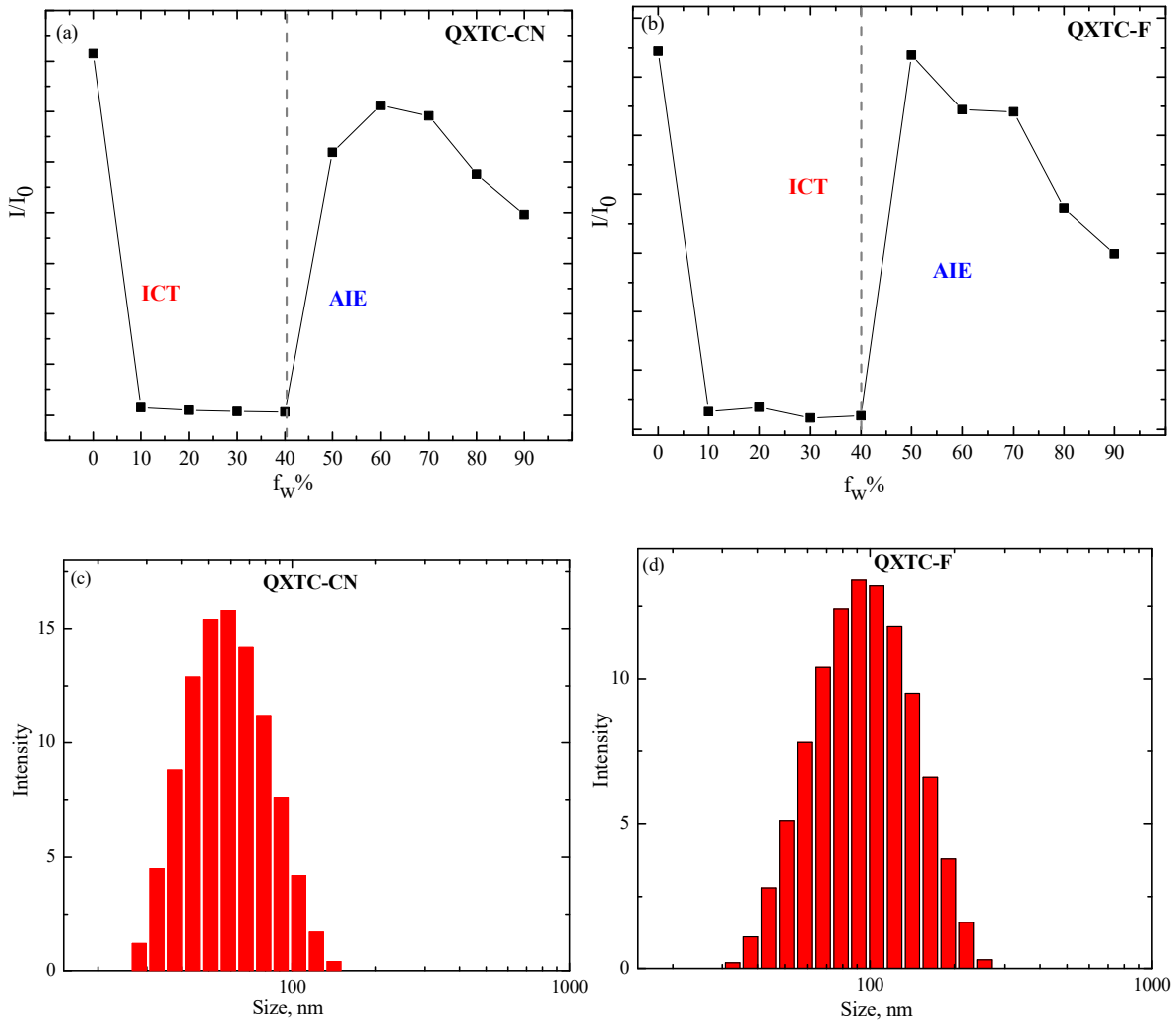

Figure 3.19 The plot of emission intensity of **QXTC-CN** (a) and **QXTC-F**(b) vs % of water fraction (f_w). The size distribution of nanoaggregates of **QXTC-CN** (c) and **QXTC-F**(d) in THF-Water mixture of f_w = 90%, obtained by DLS measurements.

The emission is recovered during the formation of nanoaggregates due to the restriction of intramolecular motion (RIM) in aggregated state which will block nonradiative decay path and enables the exciton to decay through radiative decay path. This study reveals that these derivatives are emissive in both solution state and aggregation state.

3.3.6 Mechanochromic Properties in Solid State

QXTC-CN and **QXTC-F** are measured for their solid state emission in unground and ground form in order to confirm their mechanochromic luminescence (MCL) properties. **Figure 3.20** shows photographs of unground state, ground state, and fumed state, taken under illumination of 365 nm UV lamp. The green colour of unground sample is changed to yellow colour upon grinding in agate mortar with a pestle. The yellow colour of ground sample of **QXTC-CN** recovered to green upon exposure of DCM vapour. While in the case of **QXTC-F**, the colour change between cyan colour to blue colour. To further study the MCL properties in detail, the emission spectra of **QXTC-CN** and **QXTC-F** in various states were evaluated.

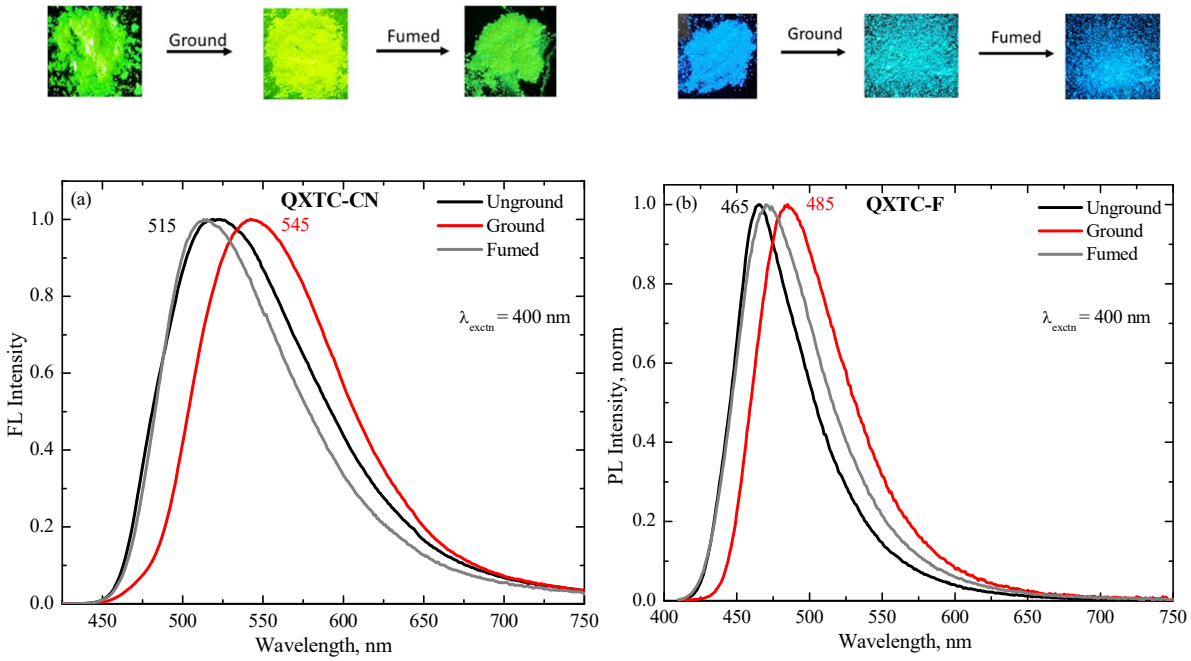

Figure 3.20 Emission spectra of **QXTC-CN** (a) and **QXTC-F** (b) as unground, ground and fumed solid samples and photograph taken under 365 nm UV illumination.

As clearly seen from **Figure 3.20**, **QXTC-CN** exhibited a green emission at 515 nm and after grinding the unground sample in an agate mortar with a pestle, an obvious visible yellow emission emerged at 545 nm with red shift of 30 nm. Upon treatment of the ground samples with fuming DCM vapour, the yellow luminescence reverted green luminescence. In

the case of **QXTC-F**, the emission maxima of powder sample, 465 nm red shifted to 485 nm with red shift of 20 nm upon grinding and recovered back to original colour on fuming DCM vapour.

To gain more insight into the MCL mechanism of **QXTC-CN** and **QX-TC-F**, their powder X-ray diffraction (PXRD) studies in various solid states were carried out. As depicted in **Figure 3.21**, the unground sample of **QXTC-CN** displayed sharp and intense diffraction peaks in the spectra, which suggested that the solid powders obtained by column chromatography possessed crystalline structures. In contrast, after grinding, its PXRD diffractogram showed very weak and broad diffraction signals, indicating the formation of an amorphous solid. These results confirmed that the different emission behaviours between the unground and ground sample should be attribute to mechanical grinding which effectively transformed the well-ordered crystalline structure to the amorphous phase. Upon exposure of the ground sample to DCM vapour, some sharp diffraction peaks appeared again, demonstrating the formation of crystalline phase structures instead of the amorphous solids. Thus, the MCL nature of **QXTC-CN** was caused by the disruption of the molecular packing. Similar observations were found in the **QXTC-F**.

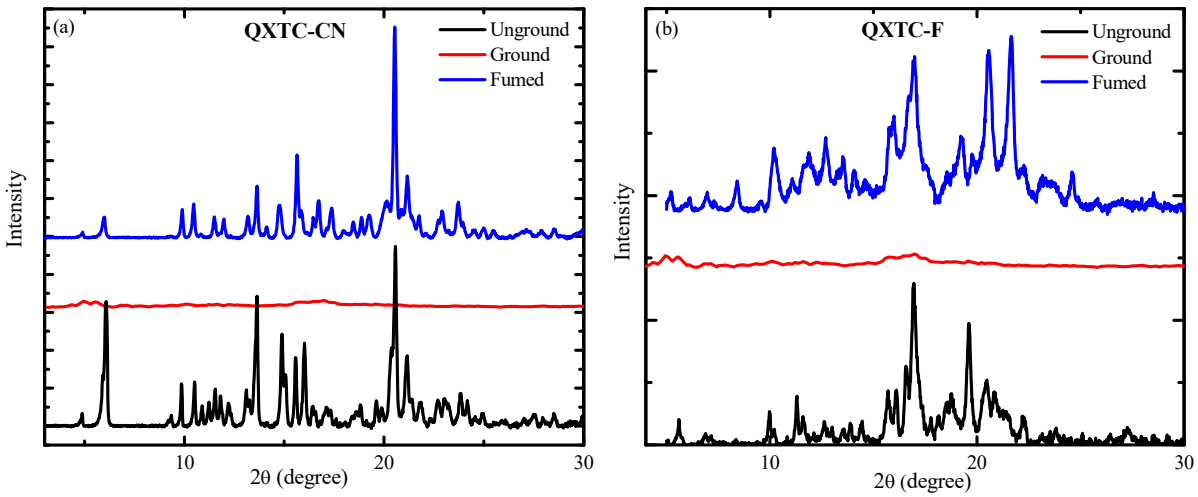

Figure 3.21 PXRD pattern of three solid form of **QXTC-CN** (a) and **QXTC-F** (b)

3.3.7 Acid Sensing Properties

The acid sensing properties of these **QXTC-CN** and **QXTC-F** were investigated with trifluoroacetic acid (TFA). The quinoxaline moiety has two nitrogen atoms in its which are sensitive to acid. It is found that the original colour of **QXTC-CN and QXTC-F** in toluene solution disappeared with addition of TFA. We checked the corresponding absorption spectrum also in which two new absorption peaks are appeared at 380 and 560 nm. This can be due to the protonation of the nitrogen atom of quinoxaline (**Figure 3.22)**.

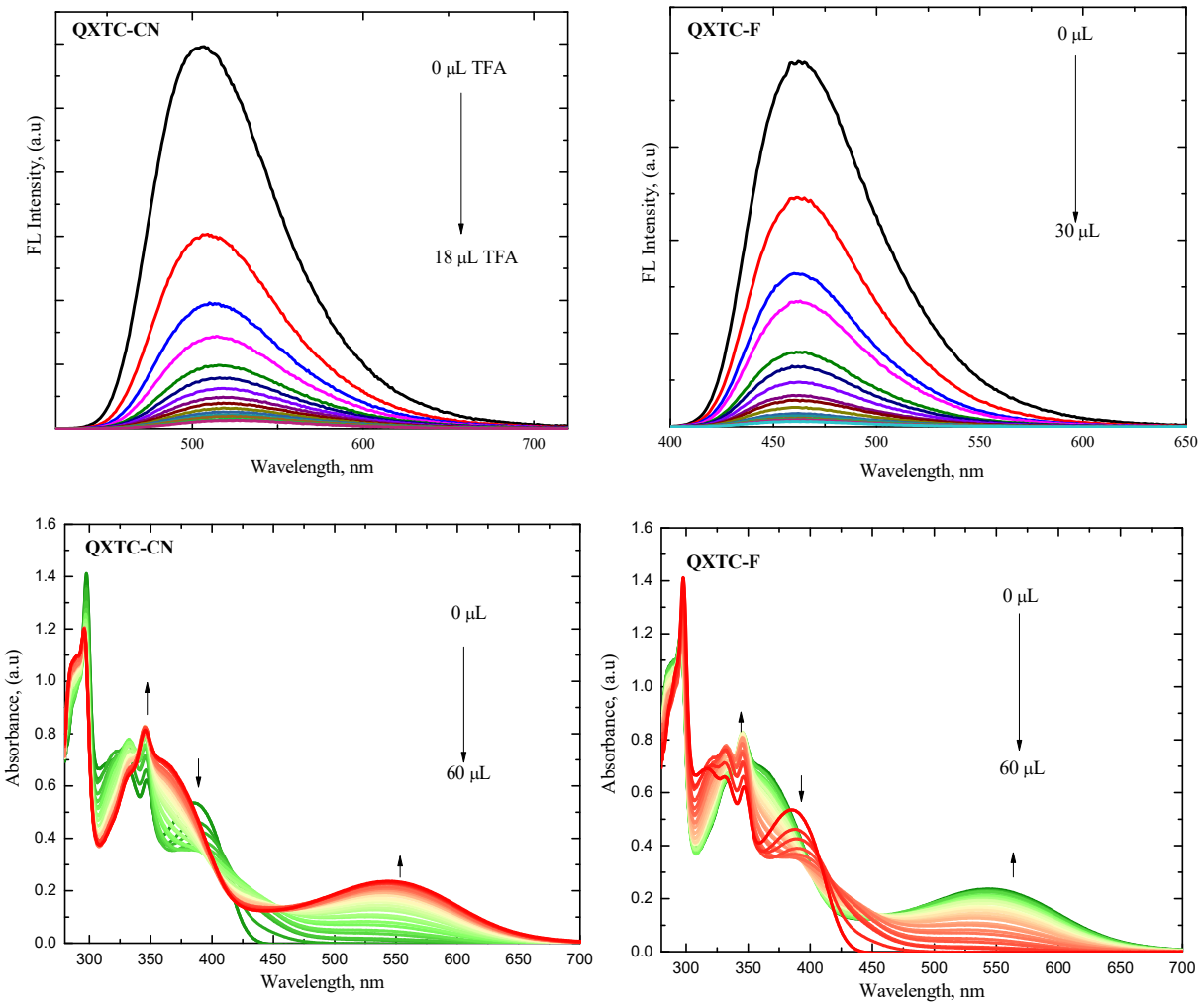

Figure3.22 Acid sensitive properties of **QXTC-CN** and **QXTC-F** towards trifluoroacetic acid (TFA); Emission and absorption spectral properties of **QXTC-CN** and **QXTC-F** in the presence of TFA.

We checked the acid sensitives of the powder samples of these quinoxaline derivatives toward the TFA vapour and the emission intensity changes was investigated using fluorescence spectroscopy (**Figure 3.23**). The green emission of powder of sample of **QXTC-CN** (528 nm) are regained upon treatment with triethyl amine (TEA) but the with red shift of emission maxima (550 nm). Similarly, the emission maximum of powder sample of **QXTC-F** (480 nm) is quenched during exposure of TFA but the emission intensity is regained in the presence of TEA but with the red shift of emission maxima (504 nm).

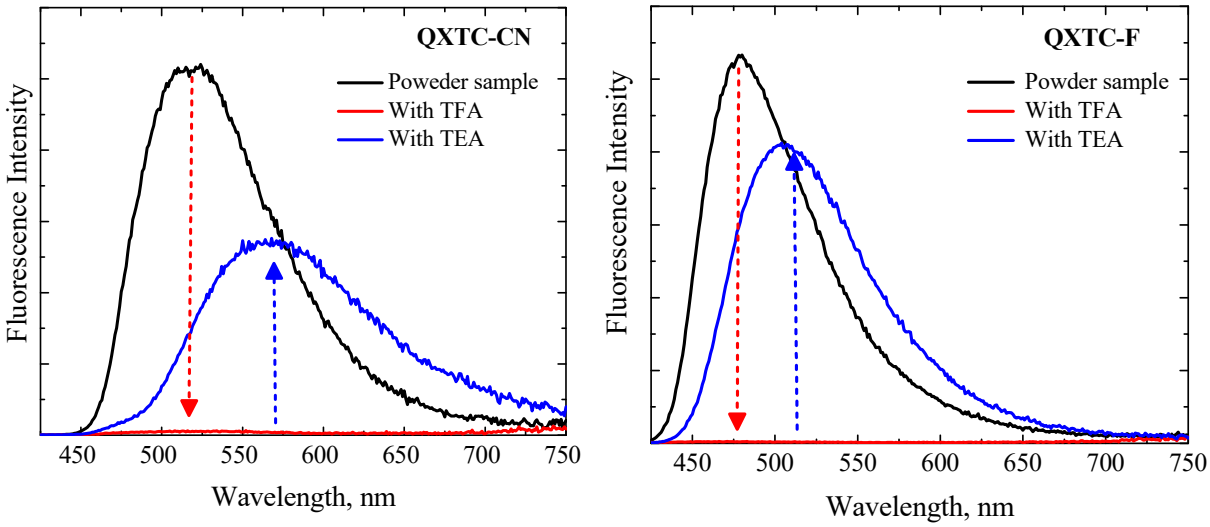

Figure 3.23 The emission properties of powder sample of (a) **QXTC-CN** and (b) **QXTC-F** in the presence of TFA and TEA.

The interactions of the compounds with TFA were further confirmed by ^{1}H NMR spectral analysis in the absence and presence of TFA. The comparison showed that quinoxaline protons were significantly shifted and the bridged phenyl ring are merged together on the addition of TFA (**Figure 3.24**). This implies that the protonation on the nitrogen atoms of the quinoxaline acceptor moiety leading to the decrease of electron density in the vicinity of these protons.

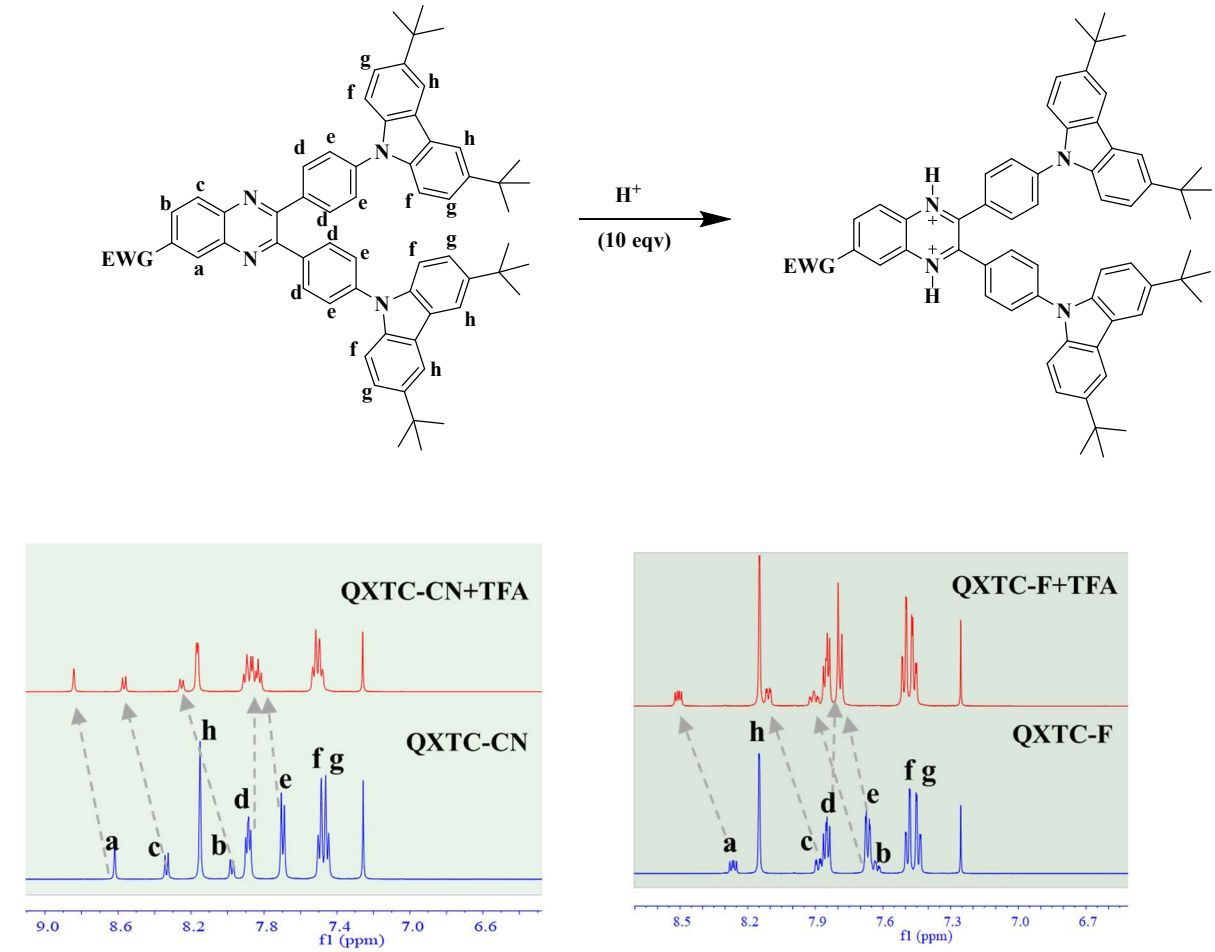

Figure 3.24 ^{1}H NMR Analysis of acid sensitive properties of **QXTC-CN** and **QXTC-F**.

3.4 Conclusion

In conclusion, we synthesized two D-π-A-π-D systems, namely **QXTC-CN** and **QXTC-F** based on quinoxaline (acceptor) and tert-butyl carbazole (donor) and explored the stimuli responsive properties of these derivatives towards the external stimuli such as mechanical grinding and acid vapour. The photophysical studies in different solvents revealed that the occurrence of intramolecular charge transfer (ICT) state. The **QXTC-CN** and **QXTC-F** exhibit strong solvatochromism in the emission when the increasing solvent polarity. The nanosecond transient absorption studies reveals that both derivatives shows triplet absorption in nonpolar solvent and formation of charge transfer state in polar solvent. The AIE properties of mechanochromic fluorophores **QXTC-CN** and **QXTC-F** were studied in THF-water

mixture and observed that they exhibited good emission in solution state and aggregated state of molecules. The functional group substitution such as cyano group and fluoride group play important to activate mechanochromic behaviour of quinoxaline-tert butyl carbazole derivatives. **QXTC-CN** shows a colour change from green to yellow and **QXTC-F** shows a colour change from blue to cyan. The mechanochromic behaviour was further studied using powder XRD suggesting that a morphological change from crystalline to amorphous was responsible for mechanochromism. Since the molecules containing quinoxaline as centre core, we studied the proton effect of these system. The fluorescence of **QXTC-CN** and **QXTC-F** was quenched significantly upon the addition of TFA. The emission of **QXTC-CN** and **QXTC-F** in the film was also quenched by TFA vapor due to the protonation of quinoxaline moiety. Our studies illustrate that how functional group such as cyanide and fluoride influence the stimuli responsive properties of organic chromophores. These results may help in the better design of stimuli responsive materials with precise control over the optical and electronic properties for advanced applications

3.5 Experimental Section

3.5.1 Materials and Methods

General Remarks: The chemicals, reagents and solvents for synthesis were used as received without further purification unless otherwise stated. ^{1}H-NMR and ^{13}C NMR spectra were recorded on a 500 MHz Bruker Advance II spectrometer using CDCl3 as solvent. The chemical shifts (δ) are reported in ppm nd referenced to $(CH_3)_4Si$ (TMS; δ = 0 ppm) for ^{1}H or residual $CHCl_3$ (δ = 77 ppm) for ^{13}C. Mass spectral analysis was performed by using a MALDI-TOF mass spectrophotometer system.

3.5.2 Absorption and Fluorescence Spectroscopy: Solution-state UV-vis absorption spectrum was recorded on a Shimadzu UV-2600 spectrophotometer at room temperature. Fluorescent emission spectra of the solution, powder and ground samples were recorded on a

HORIBA SPEX Fluorolog-3 spectrofluorometer FL-1039 equipped with a 450W Xenon arc lamp. The powder or ground samples were sandwiched between two quartz plates placed in optical path, and spectra were recorded in front face mode.

3.5.3 Fluorescence Lifetime: Time-resolved fluorescence spectra and lifetime decays were measured by using a picosecond single photon counting system (Horiba, DeltaFlex) employing 418 nm LED as excitation sources and Picosecond photon detection module (PPD-850) as a detector. The decay of the fluorescence intensity (I) with time (t) was fitted either by a mono or double-exponential function:

3.5.4 Cyclic Voltammetry: Cyclic voltammetry (CV) was performed on a CHI 604C voltammetric analyzer in DCM containing Bu_4NBF_4 (0.1 M) as a Platinum button and platinum plate were used as a working electrode and a counter electrode, respectively. All potentials were recorded versus Ag/Ag+ as a reference electrode (using ferrocene as internal standard). The scan rate was maintained at 100 mV/s.

3.5.5 Nanosecond Transient Absorption Spectra: Nanosecond transient absorption spectra were obtained by exciting the samples with the third harmonic of fundamental light (1064 nm) from an Quanta Ray Nd: YAG laser (wavelength, 355 nm, ~10 ns) and using an Applied Photophysics model LKS 60 laser kinetics spectrometer. The probing light source was a 150 W Xenon arc lamp. The light of the probe transmitted through a 1 cm quartz cuvette was dispersed by a monochromator and detected by a photomultiplier tube coupled to a digital oscilloscope (Agilent Infiniium DSO8064A, 600 MHz, 4 $GSas^{-1}$). The analyzing and laser beams were fixed at right angles to each other. The power of each laser pulse was monitored using a fast silicon photodiode.

3.5.6 Powder XRD Measurements: Powder X-ray diffraction (PXRD) patterns of the samples were recorded using the Cu Ka radiation (1.542 Å) on a Philips X'pert PROX-Ray Diffractometer

3.5.7 Synthesis and Characterisation:

Synthesis of **DK-2TC**: 4.4'- dibromobenzil (914mg, 2.48 mmol), tert-butyl carbazole (1.38g, 4.96 mmol), K_2CO_3 (1.79 g, 3.02 mmol), Pd $(OAc)_2$ (48.71 mg, 0.217 mmol), $PH(^tBu)_3$ BF_4 (226.54 mg, 0.781 mmol) were transferred into a 100ml round bottom flask under argon atmosphere. The degassed toluene (50ml) was then added and resultant mixture was refluxed and stirred at 120^{o}C for 12 hours. After cooling to room temperature, the solvent was removed under reduced pressure. The reaction mixture is treated with DCM and water and organic layer is collected and dried. The product is purified by using column chromatography with chloroform/hexane 50:50 as eluent and subsequently evaporated and dried under reduced pressure to afford solid yellow product. Yield, 72%.^{1}H NMR (500 MHz, $CDCl_3$): δ 8.29-8.27 (d, 4H), 8.13 (s, 4H), 7.82-7.80 (d, 4H), 7.49 (s, 8H), 1.47 (s, 36H) ppm; ^{13}C NMR (125 MHz, $CDCl_3$): δ 192.95, 144.58, 144.13, 138.22, 131.90, 130.46, 126.04, 124.21, 124.02 116.52, 109.40, 34.81, 31.95 ppm.

Synthesis of QXTC-CN: DK-TC and cyano group substituted diamine were dissolved in 50 ml acetic acid and refluxed for a 4hrs. The reaction mixture is cooled and treated with DCM and water and organic layer is collected and dried. The product is purified by using column chromatography with chloroform/hexane 30:70 as eluent. The final product is dried for the characterisation. Yellow in colour, Yield: 74%. ^{1}HNMR (500 MHz, $CDCl_3$): δ 8.62 (s, 1H), 8.34-8.33 (d, 1H), 8.15 (s, 4H), 7.99-7.97 (d, 1H), 7.90-7.87 (m, 4H), 7.71-7.69 (d, 4H), 7.50-7.45 (m, 8H), 1.47 (s, 36H) ppm; ^{13}C NMR (125 MHz, $CDCl_3$): δ 154.49,143.51, 139.94, 138.71, 136.06, 135.15, 131.52, 131.45, 131.01, 126.26, 123.87, 123.78, 116.41, 113.62, 109.24, 34.78, 32.00 ppm; MALDI-TOF: m/z calcd for $C_{61}H_{59}N_5$: 863.1780 $[M+H]^+$; found: 863.4510.

Synthesis of QXTC-F: **DK-2TC** and fluorine substituted diamine were dissolved in 50 ml acetic acid and refluxed for a 4 hrs. The reaction mixture is cooled and treated with DCM

and water and organic layer is collected and dried over anhydrous Na_2CO_3. The product is purified by using column chromatography with chloroform/hexane 30:70 as eluent. The final product is dried for the characterisation. Yellow in colour, Yield: 86%. ^{1}HNMR (500 MHz, $CDCl_3$): δ 8.28- 8.25 (m, 1H), 8.15 (s, 4H), 7.90-7.88 (m, 1H), 7.86-7.84 (m, 4H), 7.68-7.66 (m, 4H), 7.64-7.61 (m, 1H), 7.50-7.43 (m, 8H), 1.47 (s, 36H) ppm; ^{13}C NMR (125 MHz, $CDCl_3$): δ 153.38, 143.34, 143.31 139.36, 139.19, 138.84, 138.81, 136.92, 131.47, 131.39, 126.32, 123.83, 123.67, 116.35, 109.25, 34.78, 32.02 ppm; MALDI-TOF: m/z calcd for $C60H_{59}N_4F$: 856.1584 $[M+H]^+$; found: 856.4340.

3.6 References

1. Xu, J.; Chi, Z., *Mechanochromic Fluorescent Materials: Phenomena, Materials and Applications*; Royal Society of Chemistry, 2014.

2. Chi, Z.; Zhang, X.; Xu, B.; Zhou, X.; Ma, C.; Zhang, Y.; Liu, S.; Xu, J., Recent Advances in Organic Mechanofluorochromic Materials. *Chem. Soc. Rev.* **2012**, *41*, 3878-3896.

3. Ciardelli, F.; Ruggeri, G.; Pucci, A., Dye-Containing Polymers: Methods for Preparation of Mechanochromic Materials. *Chem. Soc. Rev.* **2013**, *42*, 857-870.

4. Xue, P.; Ding, J.; Wang, P.; Lu, R., Recent Progress in the Mechanochromism of Phosphorescent Organic Molecules and Metal Complexes. *J. Mater. Chem. C* **2016**, *4*, 6688-6706.

5. Zhang, Y.; Zhuang, G.; Ouyang, M.; Hu, B.; Song, Q.; Sun, J.; Zhang, C.; Gu, C.; Xu, Y.; Ma, Y., Mechanochromic and Thermochromic Fluorescent Properties Of cyanostilbene Derivatives. *Dyes Pigm.* **2013**, *98*, 486-492.

6. Kishimura, A.; Yamashita, T.; Yamaguchi, K.; Aida, T., Rewritable Phosphorescent Paper by the Control of Competing Kinetic and Thermodynamic Self-Assembling Events. *Nat. Mater.* **2005**, *4*, 546-549.

7. Dong, Y. Q.; Lam, J. W. Y.; Tang, B. Z., Mechanochromic Luminescence of Aggregation-Induced Emission Luminogens. *J. Phy. Chem. Lett.* **2015**, *6*, 3429-3436.

8. Xu, B., et al., Achieving Remarkable Mechanochromism and White-Light Emission with Thermally Activated Delayed Fluorescence through the Molecular Heredity Principle. *Chem. Sci.* **2016**, *7*, 2201-2206.

9. Wang, L.; Wang, K.; Zou, B.; Ye, K.; Zhang, H.; Wang, Y., Luminescent Chromism of Boron Diketonate Crystals: Distinct Responses to Different Stresses. *Advanced Materials* **2015**, *27*, 2918-2922.

10. Sagara, Y.; Kato, T., Mechanically Induced Luminescence Changes in Molecular Assemblies. *Nat. Chem.* **2009**, *1*, 605-610.

11. Mizoshita, N.; Tani, T.; Inagaki, S., Isothermally Reversible Fluorescence Switching of a Mechanochromic Perylene Bisimide Dye. *Advanced Materials* **2012**, *24*, 3350-3355.

12. v. Bünau, G., J. B. Birks: Photophysics of Aromatic Molecules. Wiley-Interscience, London 1970. 704 Seiten. Preis: 210s. *Berichte der Bunsengesellschaft für physikalische Chemie* **1970**, *74*, 1294-1295.

13. Luo, J., et al., Aggregation-Induced Emission of 1-Methyl-1,2,3,4,5-Pentaphenylsilole. *ChemComm* **2001**, 1740-1741.

14. G. R, S.; Pandey, M.; Chakravarthy, A. S. J., Review on New Horizons of Aggregation Induced Emission: From Design to Development. *Mater. Chem. Front.* **2021**, *5*, 1541-1584.

15. Zhao, J.; Chi, Z.; Zhang, Y.; Mao, Z.; Yang, Z.; Ubba, E.; Chi, Z., Recent Progress in the Mechanofluorochromism of Cyanoethylene Derivatives with Aggregation-Induced Emission. *Journal of Materials Chemistry C* **2018**, *6*, 6327-6353.

16. Mei, J.; Leung, N. L. C.; Kwok, R. T. K.; Lam, J. W. Y.; Tang, B. Z., Aggregation-Induced Emission: Together We Shine, United We Soar! *Chem. Rev.* **2015**, *115*, 11718-11940.

17. Yoon, S.-J.; Chung, J. W.; Gierschner, J.; Kim, K. S.; Choi, M.-G.; Kim, D.; Park, S. Y., Multistimuli Two-Color Luminescence Switching Via Different Slip-Stacking of Highly Fluorescent Molecular Sheets. *J. Am. Chem. Soc.* **2010**, *132*, 13675-13683.

18. Sasaki, S.; Suzuki, S.; Sameera, W. M. C.; Igawa, K.; Morokuma, K.; Konishi, G.-i., Highly Twisted N,N-Dialkylamines as a Design Strategy to Tune Simple Aromatic Hydrocarbons as Steric Environment-Sensitive Fluorophores. *J. Am. Chem. Soc.* **2016**, *138*, 8194-8206.

19. Zhang, H. Y.; Zhang, Z. L.; Ye, K. Q.; Zhang, J. Y.; Wang, Y., Organic Crystals with Tunable Emission Colors Based on a Single Organic Molecule and Different Molecular Packing Structures. *Advanced Materials* **2006**, *18*, 2369-2372.

20. Varghese, S.; Das, S., Role of Molecular Packing in Determining Solid-State Optical Properties of Π-Conjugated Materials. *The Journal of Physical Chemistry Letters* **2011**, *2*, 863-873.

21. Gong, Y.; Zhao, L.; Peng, Q.; Fan, D.; Yuan, W. Z.; Zhang, Y.; Tang, B. Z., Crystallization-Induced Dual Emission from Metal- and Heavy Atom-Free Aromatic Acids and Esters. *Chemical Science* **2015**, *6*, 4438-4444.

22. Yuan, W. Z., et al., Synergy between Twisted Conformation and Effective Intermolecular Interactions: Strategy for Efficient Mechanochromic Luminogens with High Contrast. *Advanced Materials* **2013**, *25*, 2837-2843.

23. Yuan, W. Z., et al., Synergy between Twisted Conformation and Effective Intermolecular Interactions: Strategy for Efficient Mechanochromic Luminogens with High Contrast. *Adv. Mater.* **2013**, *25*, 2837-2843.

24. Zhao, F.; Fan, C.; Chen, Z.; Liu, G.; Pu, S., Cyanobenzene-Containing Tetraphenylethene Derivatives with Aggregation-Induced Emission and Self-Recovering Mechanofluorochromic Characteristics. *RSC Adv.* **2017**, *7*, 43845-43848.

25. Zhu, Y.-y.; Xia, H.-y.; Yao, L.-f.; Huang, D.-p.; Song, J.-y.; He, H.-f.; Shen, L.; Zhao, F., High-Contrast Mechanochromic Benzothiadiazole Derivatives Based on a Triphenylamine or a Carbazole Unit. *RSC Adv.* **2019**, *9*, 7176-7180.

26. Zhang, Z.; Edkins, R. M.; Nitsch, J.; Fucke, K.; Steffen, A.; Longobardi, L. E.; Stephan, D. W.; Lambert, C.; Marder, T. B., Optical and Electronic Properties of Air-Stable Organoboron Compounds with Strongly Electron-Accepting Bis(Fluoromesityl)Boryl Groups. *Chemical Science* **2015**, *6*, 308-321.

27. Zhang, Z.; Edkins, R. M.; Nitsch, J.; Fucke, K.; Eichhorn, A.; Steffen, A.; Wang, Y.; Marder, T. B., D–Π–a Triarylboron Compounds with Tunable Push–Pull Character Achieved by Modification of Both the Donor and Acceptor Moieties. *Chemistry – A European Journal* **2015**, *21*, 177-190.

28. Yang, Y.; Tian, J.-j.; Wang, L.; Chen, Z.; Pu, S., D-Π-a Type Carbazole and Triphenylamine Derivatives with Different Π-Conjugated Units: Tunable Aggregation-Induced Emission (Aie) and Mechanofluorochromic Properties. *Journal of Photochemistry and Photobiology A: Chemistry* **2022**, *429*, 113905.

29. Zhou, Y.; Yang, Z.; Qiu, Z.; Tang, N.; Sun, D.; Liu, B.; Wu, X.; Ji, S.; Chen, W.-C.; Huo, Y., New Donor–Π–Acceptor Aiegens: Influence of Π Bridge on Luminescence Properties and Electroluminescence Application. *Journal of Photochemistry and Photobiology A: Chemistry* **2022**, *428*, 113891.

30. Rao M, R.; Liao, C.-W.; Su, W.-L.; Sun, S.-S., Quinoxaline Based D–a–D Molecules: High Contrast Reversible Solid-State Mechano- and Thermo-Responsive Fluorescent Materials. *J. Mater. Chem. C* **2013**, *1*, 5491-5501.

31. Ekbote, A.; Jadhav, T.; Misra, R., T-Shaped Donor–Acceptor–Donor Type Tetraphenylethylene Substituted Quinoxaline Derivatives: Aggregation-Induced Emission and Mechanochromism. *New. J. Chem.* **2017**, *41*, 9346-9353.

Chapter 4

Synthesis and photophysical characterization of quinoxaline derivatives for OLED application: Effect of mono and tri substitution of t-butyl carbazole

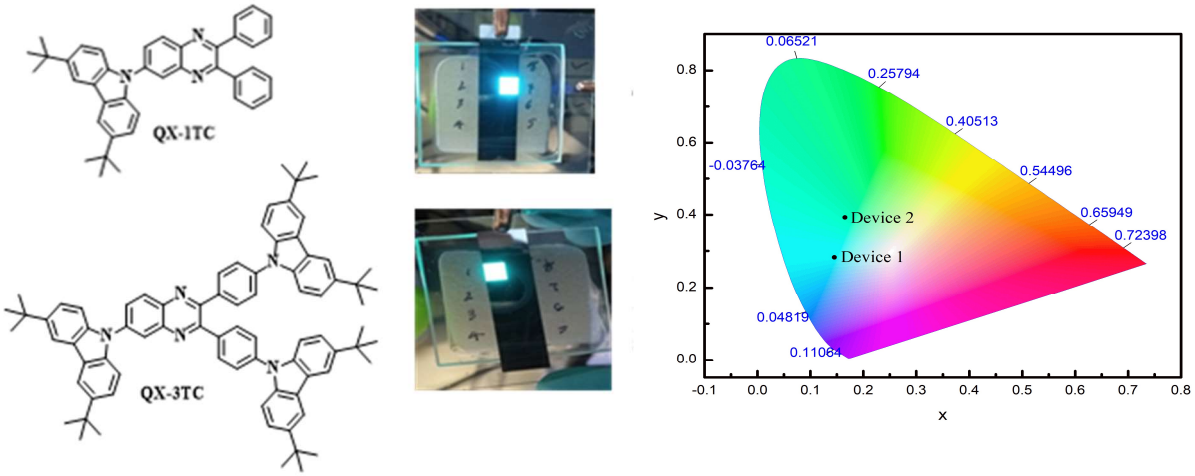

4.1 Abstract

Here, to understand the effect of increasing the number (multibranching) of donor units on acceptor, we have synthesized and studied the photophysical properties of quinoxaline-based donor-acceptor derivatives having t-butyl carbazole as donor and quinoxaline as acceptor, namely **QX-1TC** (one t-butyl carabzole) and **QX-3TC** (three t-butyl carbazole). The photophysical properties of the quinoxaline derivatives were investigated by using UV-Vis absorption and fluorescence spectroscopy, time-correlated single photon counting, and cyclic voltammetry. The steady-state absorption and emission spectra showed that the presence of intramolecular charge transfer transitions and emitting in the red region in polar solvents. The effect of multibranching on **QX-1TC** did not change the emission maximum, fluorescence lifetime, fluorescence quantum yield and energy of singlet and triplet state significantly (in **QX-3TC**). This can be due to localization of HOMO to one of the donor units of **QX-3TC**. The nanosecond transient absorption studies showed the formation of triplets in nonpolar solvent (cyclohexane) and occurrence of charge separation in polar solvent

(THF). Interestingly, aggregation-induced emission studies in THF-Water mixture showed that they are emissive in both solution and aggregated state representing good candidates for fabricating OLED devices. Device 1, in which **QX-1TC** is used as the emitting layer, exhibited an emission peak at 480 corresponding to CIE coordinates of 0.14 and 0.28 nm and full width half maximum of 72 nm with a turn-on voltage of 9V. Similarly, device 2, in which **QX-3TC** is used as an emitting layer, exhibited an emission peak at 488 nm FWHM of 76 nm, corresponding to CIE coordinates of 0.16, 0.39 with a turn-on voltage of 10V.

4.2 Introduction

Quinoxaline is a heterocyclic aromatic compound consisting of a benzene ring tethered to a pyrazine moiety.[1] In addition to their fascinating biological applications in the pharmaceutical industry, quinoxaline have been studied for application in optoelectronic devices and as photo-initiators. In recent years, there has been increasing interest in the use of this molecule and its derivatives as building blocks in order to build a variety of optoelectronic and photovoltaic compounds.[2-6] For examples, the materials based on quinoxaline derived donor-acceptor architectures are promising materials for fluorescence imaging,[7] fluorescence chemosensors,[8-9] electrochromic devices,[10-11] bulk heterojunction solar cells,[12-13] dye-sensitized solar cells,[14-15] organic thin-film transistors[16-17] and organic light-emitting diodes.[18-21] This is due to the fact that these materials have unique properties such as molar extinction coefficient and emission, flexibility in colour tuning and high mobility of charge carriers. [2] In donor-acceptor systems (D-A) or donor-π-acceptor systems (D-π-A), quinoxaline itself functions as an electron-acceptor unit (A), which is combined with different electron-donor units (D). The precise tuning of donor-acceptor interactions allows the modification of their electron affinities (EA), as well as their ionization potentials (IP), giving rise to semiconductors and electroluminophores with tunable band gaps and, consequently, having very different

electronic and optical properties. There are many design strategies which affect the photophysical and electronic properties of quinoxaline based donor-acceptor derivatives.

Ledwon et al investigated the optoelectronic properties of donor-acceptor-donor (D-A-D) and donor-π-bridge-acceptor-π-bridge-donor (D-π-A-π-D) systems based on a quinoxaline acceptor by changing the effective conjugation length (**Figure 4.1**). It is found that significant difference in electrochemical and photophysical properties. Here, quinoxaline-carbazole derivatives named as **1** and **2** correspond to the D-A-D type of molecules, while the **3** and **4** extended molecules correspond to more complicated D-π-A-π-D type of systems. The measured oxidation potential of the **3** and **4** compounds are significantly shifted to lower potentials comparing with the **1** and **2** species. It means that the extension of π-conjugation strongly affects the oxidation potential and the related IP energy in the sequence **1** > **2** >**3** > **4** in contrast to the reduction potentials and EA energies that are only weakly sensitive to the elongation of π-conjugation. At the same time the elongation of π-conjugation introduces only a negligible decrease of the reduction potential.[2]

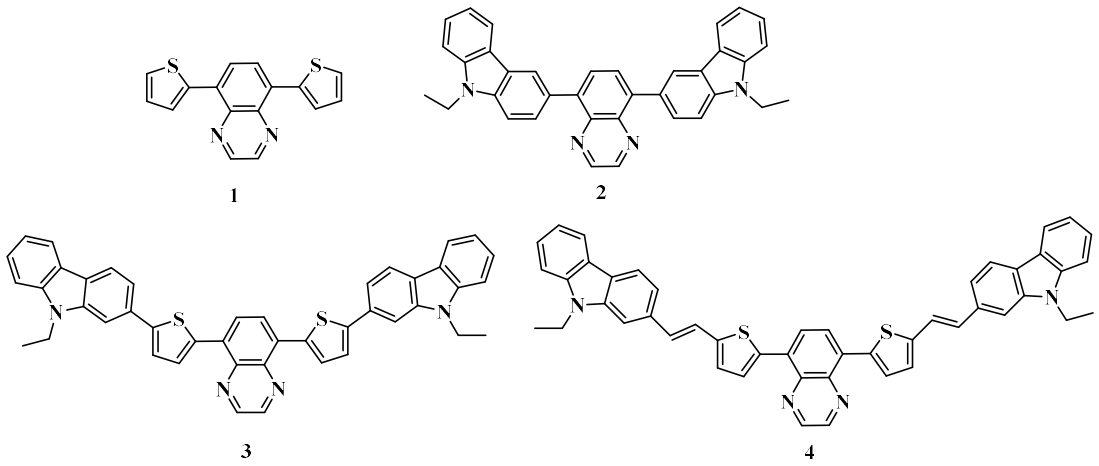

Figure 4.1 Molecular structures of quinoxaline- carbazole derivatives with D-A and D-π-A structure.

The results indicate that, in agreement with quantum-chemical calculations, the change of the optical and electrochemical properties is related mainly to a variation of the HOMO

energy while the effect on the LUMO energy is much weaker. The studied compounds were tested in OLEDs with an external quantum yield up to 4.5% for a deep red non-doped device with a maximum electroluminescence intensity observed at 662 nm.[2]

The nature of electron-donating amines are also responsible for the opto-electrochemical properties of D-A systems containing charge-transfer transitions. For example, the effect of nature of substituted donors on indolo-quinoxaline are studied by Kamble and his co-workers.[22] A series of donor–acceptor-based indolo-quinoxaline amine derivatives were synthesized with different donor amines as shown in Figure 4.2. The presence of ICT is proof that there is a D-A assembly in the dyes, and it is greatly influenced by the donating nature of the substituted amines. It was found that the nature of peripheral amines influenced these photophysical properties of molecules, such as charge transfer transitions (400 to 462 nm) and emission (491 to 600 nm). The variation in the strength of the peripheral amines in the derivatives also led to reduced band gap energies (1.56 to 2.21 eV) and comparable HOMO–LUMO levels with ambipolar materials reported previously.

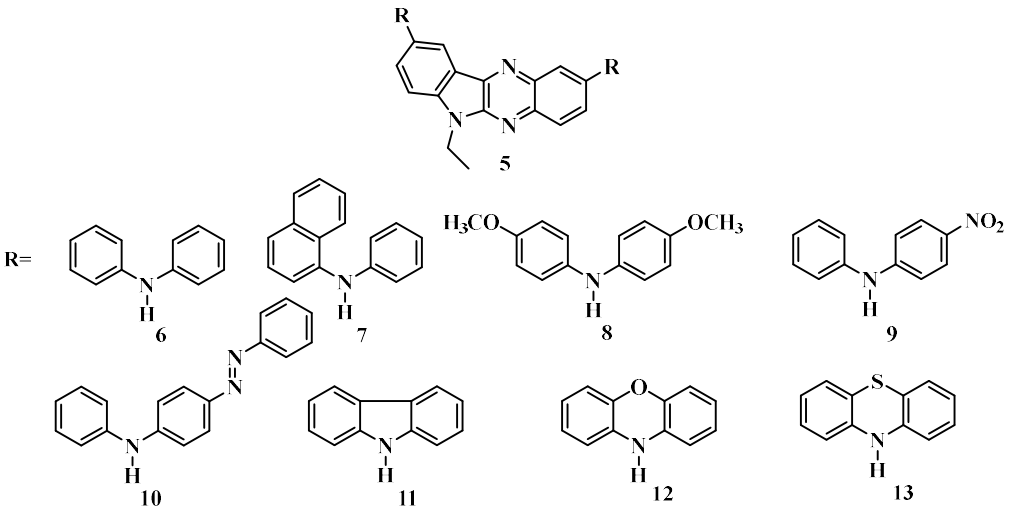

Figure 4.2 Molecular structures of indole-quinoxaline carbazole derivatives with D-A structure.

The presence of the electron donating methoxy group (–OMe) on the diarylamine segment in **8** further improved the donating capacity and showed a more significant

bathochromic shift than **6**. However, the electron withdrawing nitro (–NO_2) group and phenyldiazene (–N_2N–Ph) segment on the diarylamine unit in **9** and **10**, respectively, show strong π-accepting ability. It is observed that the oxidation potential is extremely sensitive to the nature of the corresponding donor group; the oxidation potentials of **6-13** decrease with increasing donor strength **8**>**13** >**6**>**12**>**7**>**10**>**9**>**11**.

The rigid planar structure and large steric hindrance can also affect HOMO and LUMO interaction between D and A segments and hence the HOMO-LUMO gap of D-A organic π-conjugated molecules. Liao et al designed donor-acceptor derivatives based on dibenzophenazine-dicarbonitrile-triphenylamine derivative (**14**) where two CN groups were utilized to increase the electron-accepting ability.[23]

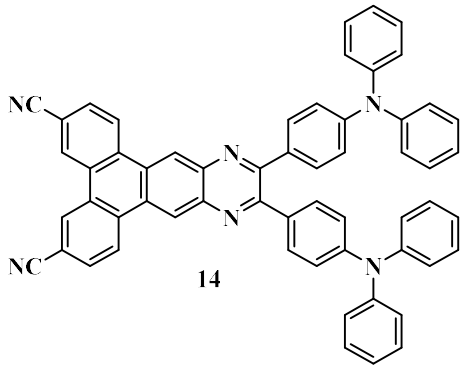

14

Figure 4.3 Molecular structure of dibenzophenazine-dicarbonitrile- triphenylamine (**14**) derivatives.

The significantly large and planar backbone to suppress the non-radiative transition and two bulky triphenylamine were employed as the D segment due to their excellent electron-donating capability. The twisted structure of caused by the steric hindrance will diminish aggregation-caused quenching (ACQ). It was an effective approach to minimize the ΔE_{ST} of conjugated molecules by adequately HOMO and LUMO. This derivative possessed a high PLQY of 97% and a sufficiently small ΔE_{ST} of 0.13 eV. Based on its properties, red, deep-red, and NIR OLED have been fabricated by utilizing different device structure strategies. The OLED in which the molecule is used as red emitter showed maximum external quantum

efficiency (EQE) of 27.4% with electroluminescence (EL) peak is at 628 nm with coordinates of (0.65, 0.35) according to the Commission Internationale de L'Eclairage (CIE). Among those reported red TADF devices, this is the best result with a peak wavelength longer than 600 nm.

Carbazole and its derivatives are commonly employed as electron donors as part of donor-acceptor systems. Carbazoles themselves are widely used compounds because they can be modified in many ways, and their properties can be controlled, including stability, tuning HOMO-LUMO levels, their ability to transport charges, etc.[24] Many compounds with carbazole units have been reported as excellent hole-transporting materials that are also highly luminescent which makes them as promising building blocks for the OLEDs.[25]

For example, Lee et al studied photophysical and electronic properties of highly efficient donor-π-acceptor-π-donor (D-π-A-π-D) derivatives where quinoxaline-(6,7)-dicarbonitrile and quinoxaline-(5,8)-dicarbonitrile as acceptor units and tertbutyl carbazole and dimethyl acridine as donor units.[26]

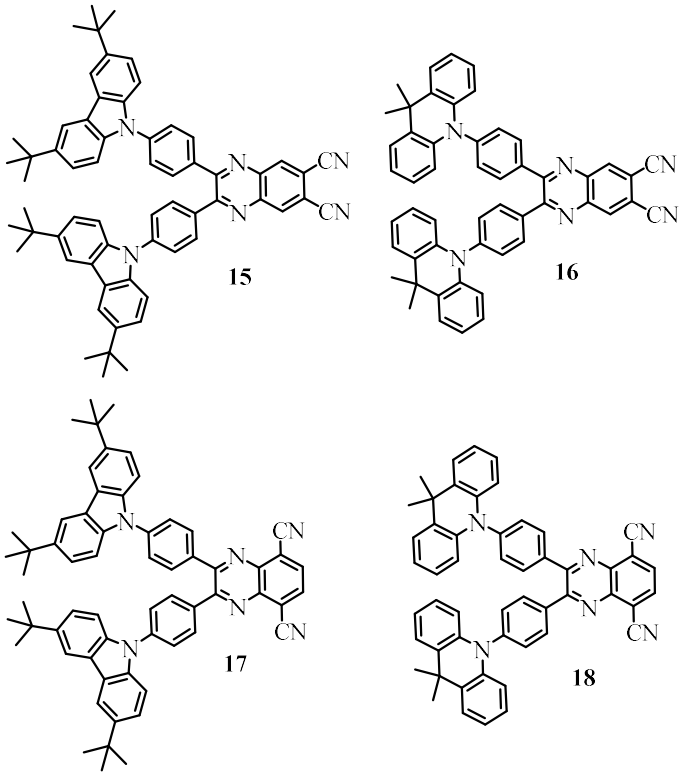

Figure 4.4 Molecular structures of quinoxaline dicarbonitrile-based D-π-A-π-D derivatives in which t-butyl carbazole and dimethyl dihydroacridine are used as donor units.

Through the introduction of the two CN units, the quinoxaline unit is able to become a stronger acceptor, and the position management of the CN substitutions (6,7 and 5, 8) is able to precisely control the electron-accepting character and molecular orbitals of the acceptor atom. To obtain high fluorescence, the phenyl ring linker between the donor and acceptor units was introduced to overlap HOMO and LUMO, and maintain a very small ΔE_{ST} through sufficient twisting between donor and acceptor. It is also observed that strong ICT absorption peaks were observed for the tertbutyl carbazole donor-based derivatives, **15** and **17,** whereas weak ICT absorption peaks were detected for the 9,9-dimethylacridine donor based derivatives **16** and **18**. This can be explained on the basis of the large HOMO−LUMO overlap and small dihedral angle of the compounds **15** and **17**, as compared to the negligible HOMO−LUMO overlap and large dihedral angle of compounds **16** and **18**. The OLED based on t-butyl carbazole substituted derivatives emitted yellow-light emission with EL maxima at 541 and 569 nm and CIE coordinates of (0.37, 0.57) and (0.47, 0.51), respectively. The TADF OLEDs based on 9,9-dimethylacridine substituted derivatives exhibited orange and red emission with EL maxima at 578 and 602 nm, and CIE coordinates of (0.49, 0.50) and (0.55, 0.44), respectively.

Ling Yu et al reported a series of new butterfly-shaped D-A-D type compounds (**19-22**) with quinoxaline as an electron acceptor a and different electron donors such carbazole, t-butyl carbazole and dimethyl dihydroacridine. Their photoluminescence (PL) spectra are successfully tuned from green to orange based on the intramolecular charge transfer effect by selecting donor units with different electron donating abilities. Moreover, through theoretical and experimental approaches, it is verified that the dihedral angles between the donor and acceptor, the value of ΔE_{ST} and the nature of T_1 play crucial roles in shaping the emissive properties. The systematic study of these quinoxaline emitters reveals a feasible strategy for designing high performance red/orange TADF emitters for OLEDs applications.

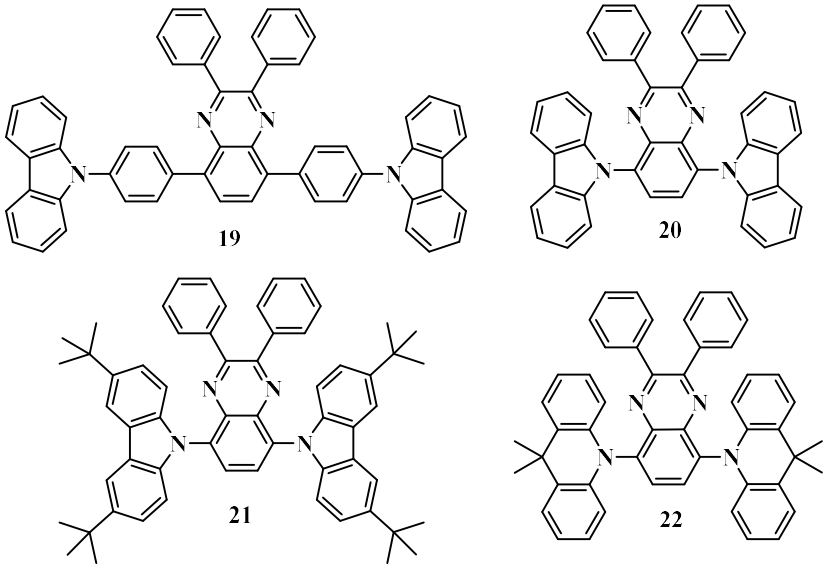

Figure 4.5 Molecular structures of quinoxaline-based D-A-D derivatives in which carbazole, t-butyl carbazole and dimethyl dihydroacridine are used as donor units.

Further, the donor-acceptor based organic fluorophores show aggregation-induced emission (AIE)[27-28], commonly observed in optoelectronics, like OLEDs. As explained by Tang et al., AIE addresses various challenges associated with aggregation concentration quenching (ACQ)[29] with the use of restricted intramolecular rotations (RIR) and conformational changes of the molecules. The AIE active derivatives have been shown to suppress the exciton annihilation in a solid-state film due to their weak intermolecular interaction and twisted conformation, which effectively prevent the π–π stacking. AIE active donor-acceptor based organic fluorophores are regarded as suitable emitters for fabricating non-doped OLEDs due to their effective solid-state emission.[30]

Hence in this chapter to understand the effect of increasing the number of donor units on photophysical and electronic properties of quinoxaline-based donor-acceptor structure, we synthesized mono substituted (**QX-1TC)** and tri substituted (**QX-3TC)** t-butyl carbazole-quinoxaile derivatives and their photophysical properties were investigated using UV-Visible spectroscopy and fluorescence spectroscopy, TCSPC and cyclovoltammetry. The nanosecond

transient absorption spectra were measured using nanosecond laser flash photolysis spectrometer. We studied also the aggregation induced emission behaviour of quinoxaline derivatives in THF water mixture. Finally, the two emitter, **QX-1TC** and **QX-3TC**, are used for the fabrication of OLEDs devices.

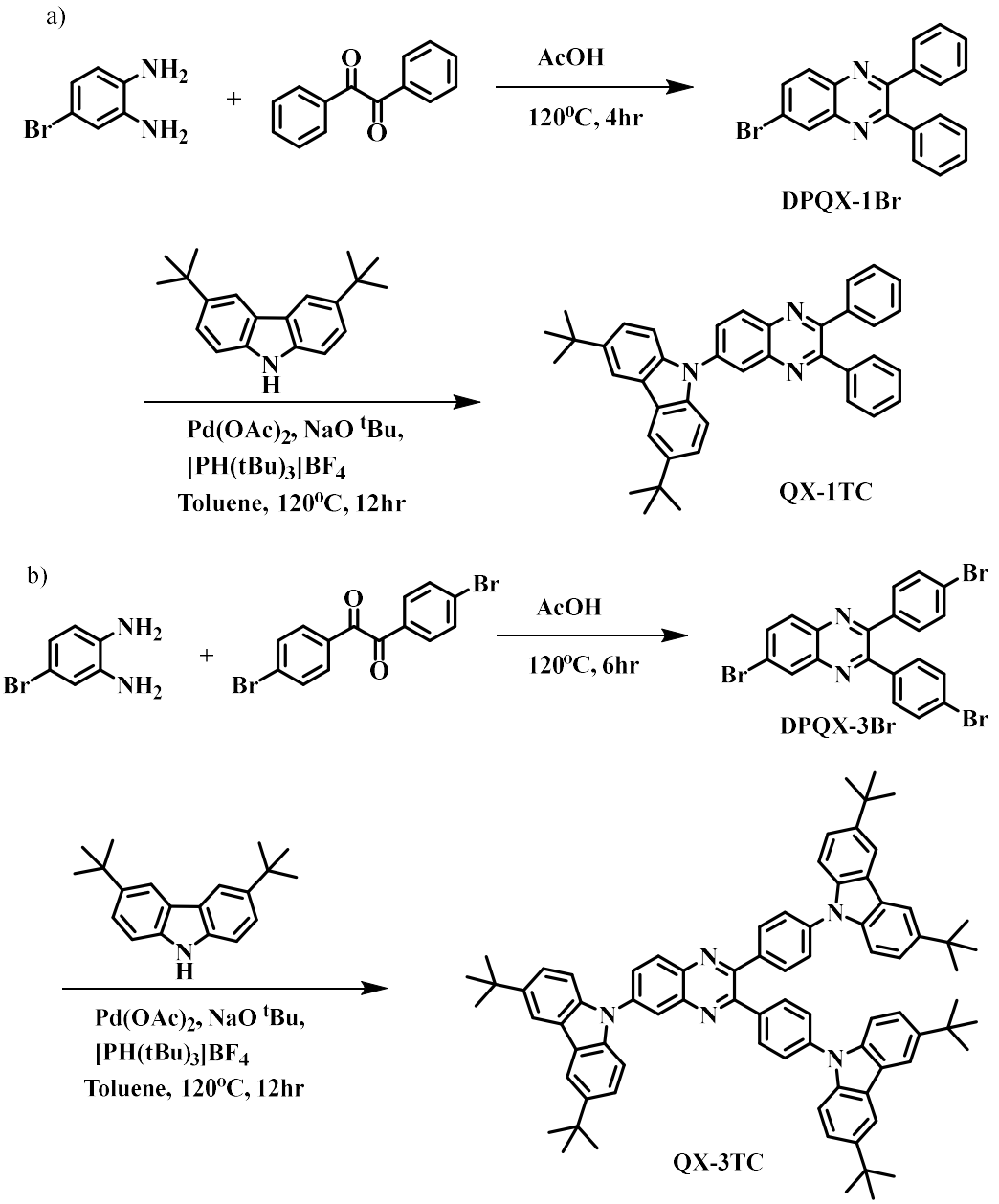

Scheme 4.1 Synthesis scheme for **QX-1TC** (a) and **QX-3TC** (b).

4.3 Results and Discussion

4.3.1 Synthesis and Characterization

The mono and tri substituted N- heterocycle quinoxaline tertbutyl carbazole derivatives, **QX-1TC** and **QX-3TC**, were synthesized according to procedure shown in **Scheme 4.1**. It involves only two step reactions. The intermediate products were synthesized by using Buchwald-Hartwig coupling reaction and final step consist of a condensation reaction. The target molecules are purified by column chromatography and the structural characterisation is done by ^{1}H NMR, ^{13}C NMR and MALDI TOF spectroscopy. The compound showed good solubility in cyclohexane, toluene, dichloromethane, chloroform, tetrahydrofuran, N,N-dimethylformamide and showed poor solubility in methanol, acetonitrile and ethanol.

4.3.2 Photophysical Properties

We studied the photophysical properties of **QX-1TC** and **QX-3TC** using UV-Visible absorption and fluorescence spectroscopy at room temperature in solvents with different polarities and the results are given in **Table 4.1**. The narrow absorption band of both derivatives at 295 nm could be due to absorption of t-butyl carbazole moiety. The absorption bands around 300-350 could be from quinoxaline acceptor core. The low energy absorption band of the derivatives at around 380-430 nm could be due to intramolecular charge transfer (ICT) arising from HOMO of tertbutyl carbazole to LUMO of quinoxaline acceptor (**Figure 4.6**). The molar extinction coefficient (ε) of **QX-3TC** (61498 $M^{-1}cm^{-1}$) is about two time higher than the **QX-1TC** (31266 $M^{-1}cm^{-1}$) in toluene, at ICT absorption band. With increase of the solvent polarity, (cyclohexane to DMF, the emission maxima of **QX-1TC** and **QX-3TC** gradually shifted from 433 nm to 570 nm and 446 to 580 nm, respectively, as shown in **Figure 4.7**.

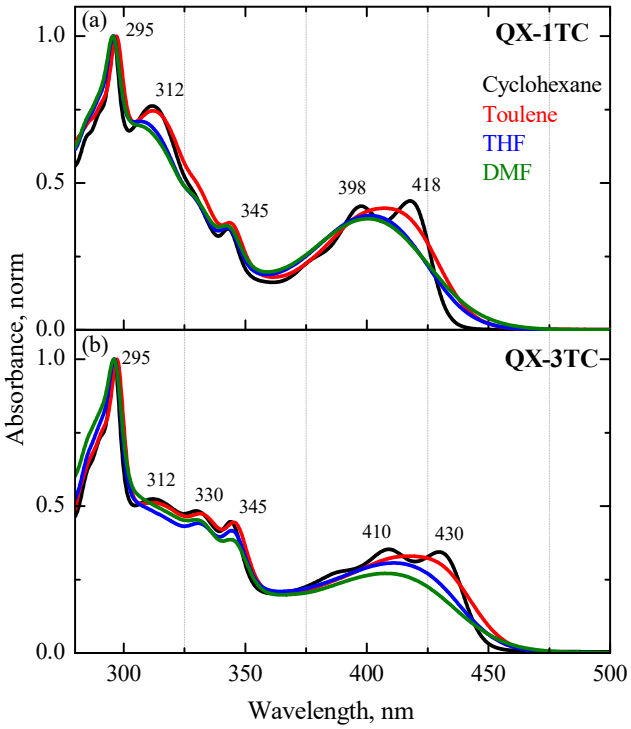

Figure 4.6 Steady state absorption spectra of **QX-1TC** (a) and **QX-3TC** (b) in different solvents.

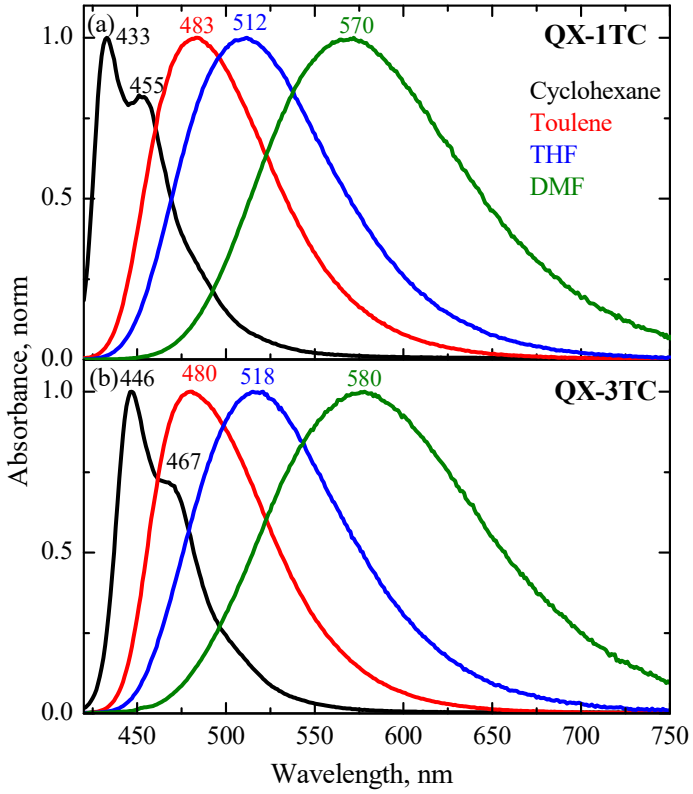

Figure 4.7 Steady state emission spectra of **QX-1TC** (a) and **QX-3TC** (b) in different solvents.

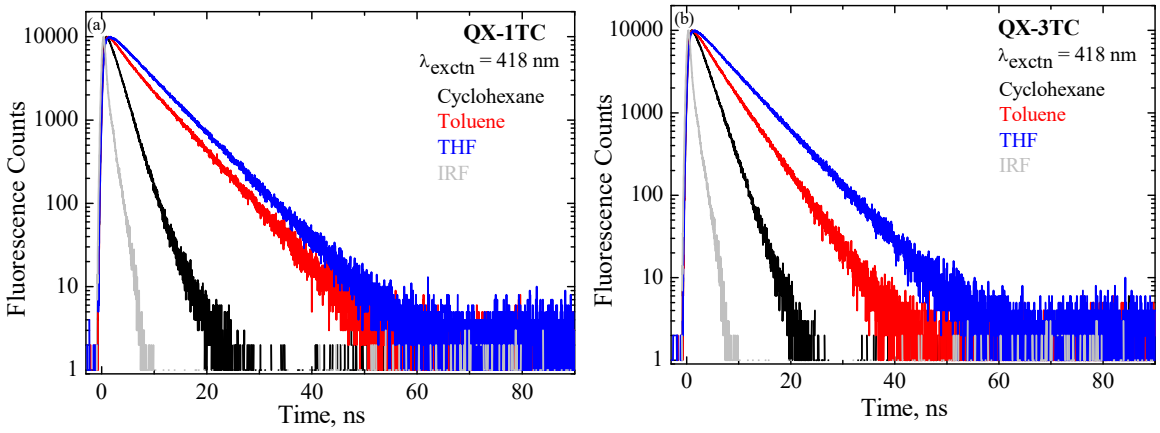

Figure 4.8 Fluorescence decay profile of **QX-1TC** (a) and **QX-3TC** (b)

The **QX-1TC** and **QX-3TC** showed large Stokes shift, 7456 and 7149 cm^{-1}respectively, in polar solvent (DMF) which indicates the presence of intramolecular charge transfer (ICT). The effect of increasing the number of donor units (tert-butyl carbazole) on ICT state is not very much profound. This can be due to orientation of HOMO orbitals of **QX-3TC** to one branch of tertbutyl carbazole unit. Therefore, the **QX-1TC** and **QX-3TC** exhibited nearly same fluorescence quantum yield and fluorescence lifetime. The fluorescence lifetime of the derivatives in various solvents were obtained from time-correlated single photon counting (TCSPC) spectrometer as shown in **Figure 4.8**. It exhibited monoexponentially decay in cyclohexane, whereas the decay showed biexponential in toluene and THF. The structured emission and monoexponentially decay profile of both chromophores in the non-polar solvent (cyclohexane) indicated that the emission could be from locally excited state (^{1}LE). On the other hand, the broad and unstructured emission and biexponential decay profiles of both chromophores in polar solvents such as THF indicating that the emission can be mainly from LE (S_1) and ICT (S_1) state. The fluorescence lifetime of both chromophores increases with increasing solvent polarity. This can be due to the stabilization of ICT state of these derivatives in polar solvents.

Table 4.1 Photophysical properties of **QX-1TC** and **QX-3TC.**

	Solvents	**Absorption max, nm (λ_{max})**	**Fluorescence max, nm (λ_{max})**	**Stokes shift, cm^{-1} ($\Delta\nu$)**	**Fluorescence quantum yield (Φ_f)**	**Fluorescence lifetime ns, (τ)**
QX-1TC	Cyclohexane	295,398, 418	433,452	1800	27%	1.91(100%)
	Toluene	295, 410	478	3470	51%	1.57 (14.49%), 6.27 (85.51%)
	THF	295, 405	510	5084	46%	0.80 (5.09%), 6.53 (94.91%)
	DMF	295, 400	570	7456	0.01	-
QX-3TC	Cyclohexane	295, 410, 430	448, 468	1888	42%	2.23 (100 %)
	Toluene	295, 420	480	2976	50%	0.38 (4.04%), 4.72 (95.96%)
	THF	295, 415	518	4791	51%	0.75 (5.17%), 6.36 (94.83%)
	DMF	295, 410	580	7149	0.01	-

4.3.3 Electrochemical Properties:

Electrochemical characterisation of both derivatives were performed in dichloromethane (DCM) using ferrocene (Fc/Fc^{+}) as standard and 0.1 M tetra-n-butylammonium-hexafluoro-phosphate (n-Bu_4NPF_6) as the electrolyte to understand the effect of increasing the number of donor on the energy level of HOMO and LUMO and optical bandgap of derivatives. The **Figure 4.9** shows the cyclic voltammogram of **QX-1TC** and **QX-3TC** in DCM. It is found that HOMO energy level of **QX-1TC** and **QX-3TC** was calculated to be -5.61 and -5.59 eV respectively, based on their oxidation potentials (1.38 and 1.34 V, respectively). At the same time, their bandgaps (Eg) estimated from the onset of absorption spectra in solutions are 2.77 and 2.68 eV respectively. Thereby, the LUMO energy levels of **QX-1TC** and **QX-3TC** were determined to be -2.84 and -2.91 eV, respectively, as summarized in **Table 4.2**. It is observed that HOMO and LUMO energy levels of **QX-1TC** and **QX-3TC** are comparable which indicating that the molecular orbital involved in electronic transition during excitation are same.

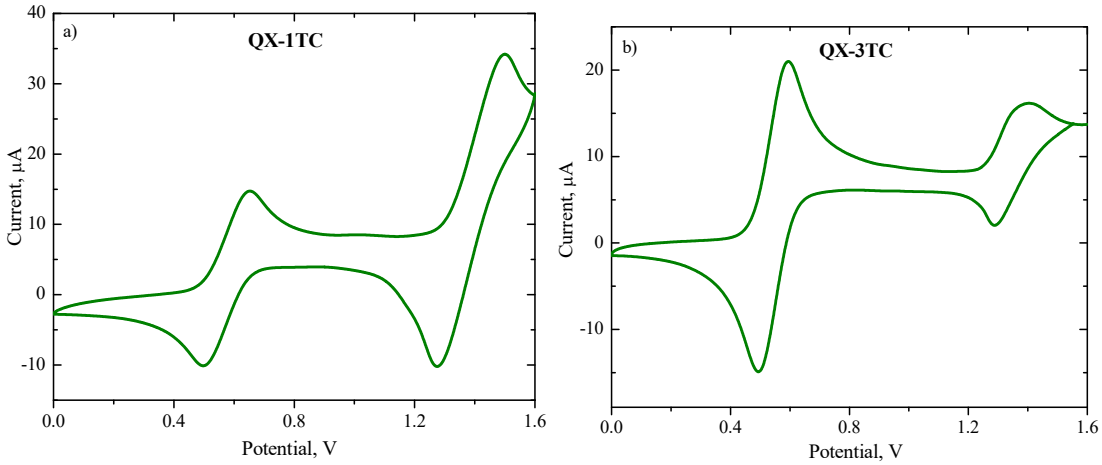

Figure 4.9 Cyclic voltammogram of **QX-1TC** (a) and **QX-3TC** (b) in DCM

Table 4.2 Electrochemical data of **QX-1TC** and **QX-3TC**

Compound	E_{oxd} (V)	E_{HOMO} (eV)	E_{LUMO} (eV)	E_g (opt) (eV)
QX-1TC	1.38	-5.61	-2.84	2.77
QX-3TC	1.34	-5.59	-2.91	2.68

4.3.4 Phosphorescence Spectra and Calculation of Singlet and Triplet Energy

The low temperature fluorescence and phosphorescence spectra of **QX-1TC** and **QX-3TC** in toluene glass matrix were measured and shown in **Figure 4.10**. The singlet and triplet energy gap (ΔE_{ST}) was also calculated. In room temperature, the quinoxaline derivatives showed broad and unstructured emission spectra upon excitation. At low temperature (77K), the emission spectra is blue shifted with emission maximum at 454 (**QX-3TC**) and 445 nm (**QX-1TC)** revealing that the emission arises from locally excited state (^{1}LE). Here, the energy level of S_1 state was found to be 2.98 (**QX-1TC**) and 3.01 eV (**QX-3TC)** from the onset of low temperature emission spectra. The broad and unstructured phosphorescence spectra indicates that the radiative decay mainly from charge transfer state (^{3}CT) with emission maximum peak of 533 (**QX-1TC**) and 545 nm (**QX-3TC)**. Consequently, the energy level of T_1 state can be calculated to be 2.48 (**QX-1TC**) and 2.48 eV (**QX-3TC)** from the onset of phosphorescence spectra. From the values of singlet and triplet state, the ΔE_{ST} values **QX-1TC** and **QX-3TC** were determined to be 0.50 and 0.58 eV for **QX-1TC** and **QX-3TC**, respectively. Interestingly, the more substitution of t-butyl carbazole group as donor did not change the energy level of triplet state and ΔE_{ST} value. This can be due to the localization of HOMO to one of tert-butyl carbazole unit of **QX-3TC**.

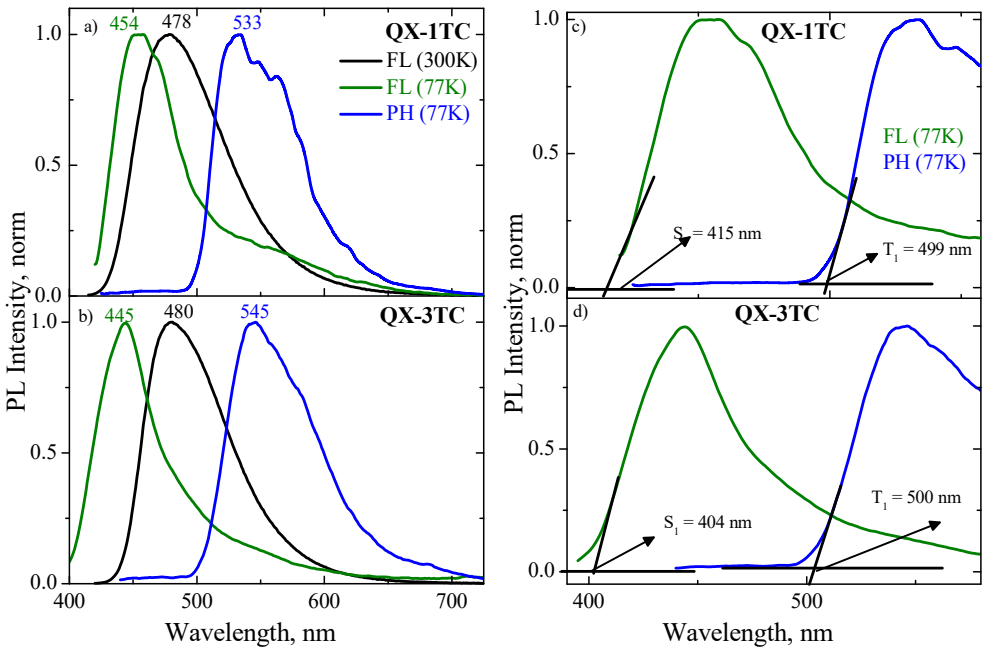

Figure 4.10 Steady state room temperature fluorescence (black) and low temperature fluorescence (77K, green) spectra and phosphorescence emission spectra of **QX-1TC** (a) and **QX-3TC** (b) in toluene. Calculation of ΔE_{ST} **QX-1TC** (c) and **QX-3TC** (d).

Table 3.2. Energy levels of singlet and triplet state.

Quinoxaline derivatives	**E $(S_1)_{onset}$ (nm)**	**E $(T_1)_{onset}$ (nm)**	**E $(S_1)_{onset}$ (eV)**	**E $(T_1)_{onset}$ (eV)**	**ΔE_{ST} (eV)**
QX-1TC	415	499	2.98	2.48	0.50
QX-3TC	404	500	3.06	2.48	0.58

4.3.5 Nanosecond Transient Absorption Studies

Nanosecond laser flash photolysis spectrophotometer is used to understand the formation of long lived components in excited states like triplet state and radical anion and cation. Nanosecond transient absorption spectra of **QX-1TC** and **QX-3TC** were measured in cyclohexane and THF as shown in the **Figure 4.11** and Figure **4.13**, respectively. The

experiments were carried out upon excitation at 355 nm in an inert atmosphere and room temperature. It is found that nanosecond transient absorption spectra of two derivatives obtained at different time interval are similar behaviour in nonpolar solvent cyclohexane and polar solvent THF. In cyclohexane, the nanosecond transient absorption spectra of **QX-1TC** and **QX-3TC** exhibited excited absorption maximum at 360 nm and a broad excited state absorption between 430 and 750 nm along with bleach absorption at 312 nm corresponds to the ground state absorption. However, in oxygen saturated cyclohexane, the peaks are effectively quenched and therefore this excited state absorption could be due to their triplet state absorption. It is found that the triplet dynamics in cyclohexane showed mono exponential relaxation processes with triplet lifetime of 1.14 and 4.52 μs for **QX-1TC** and **QX-3TC**, respectively. In THF, the nanosecond transient absorption spectra of **QX-1TC** and **QX-3TC** exhibited excited state absorption maximum at 365 nm and 490 nm and weak absorption at around 780 nm. Based on literature, the excited state absorption at 365 and 490 nm could be due to radical anion of quinoxaline and weak absorption at 780 nm is due to radical cation of carbazole suggesting the formation of charge separated state with lifetime of 1.7 μs. The similar spectral feature of nanosecond transient spectra of both derivatives reveals that the multibranching of **QX-1TC** did not significantly influence the energy of triplet state and charge separation state in excited state.

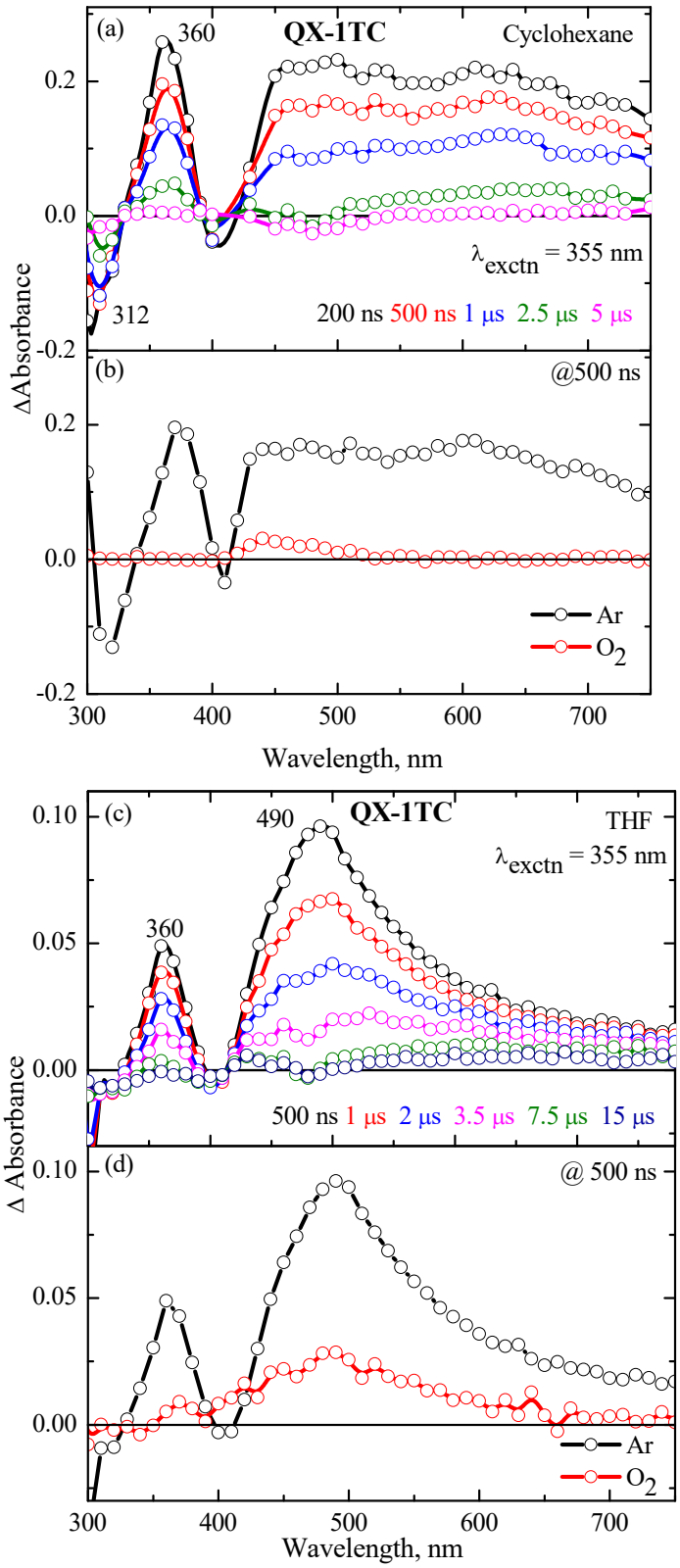

Figure 4.11 Transient absorption spectra of **QX-1TC** in (a) cyclohexane and (c) THF, respectively, obtained by exciting at 355 nm in inert atmosphere. The nanosecond transient absorption of **QX-1TC** in oxygen saturated (b) cyclohexane and (d) THF.

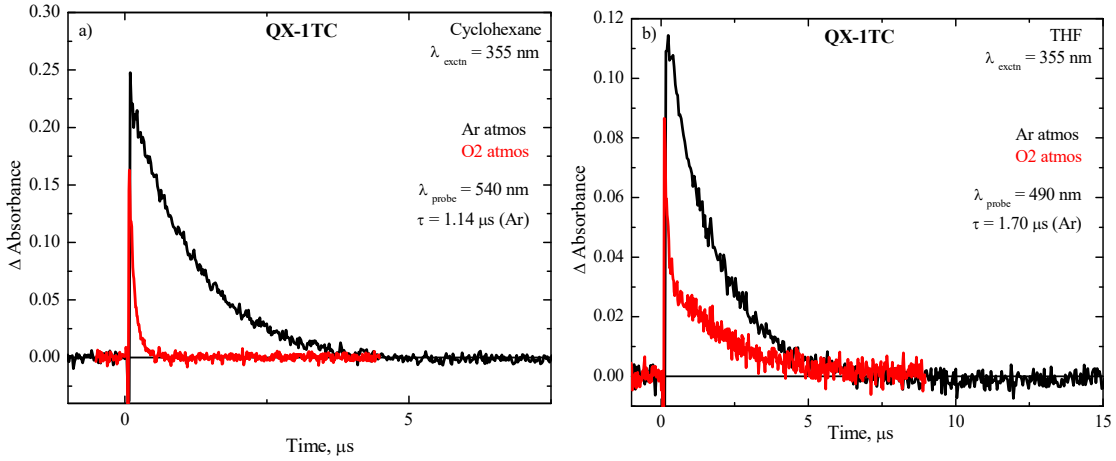

Figure 4.12 Kinetics decay profile of **QX-1TC** in argon and oxygen saturated toluene (a) and THF (b).

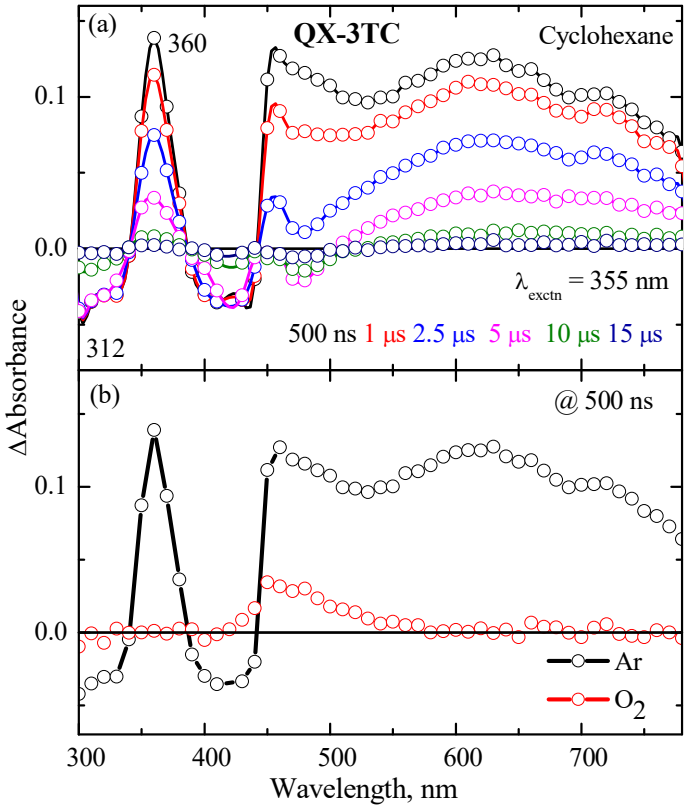

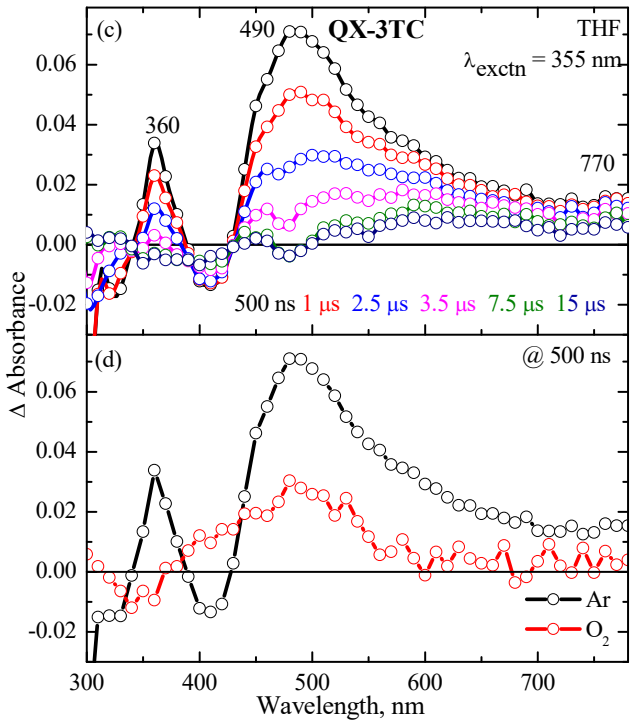

Figure 4.13 Transient absorption spectra of **QX-3TC** in (a) cyclohexane and (c) THF, respectively, obtained by exciting at 355 nm in inert atmosphere. The nanosecond transient absorption of **QX-3TC** in oxygen saturated (b) cyclohexane and (d) THF.

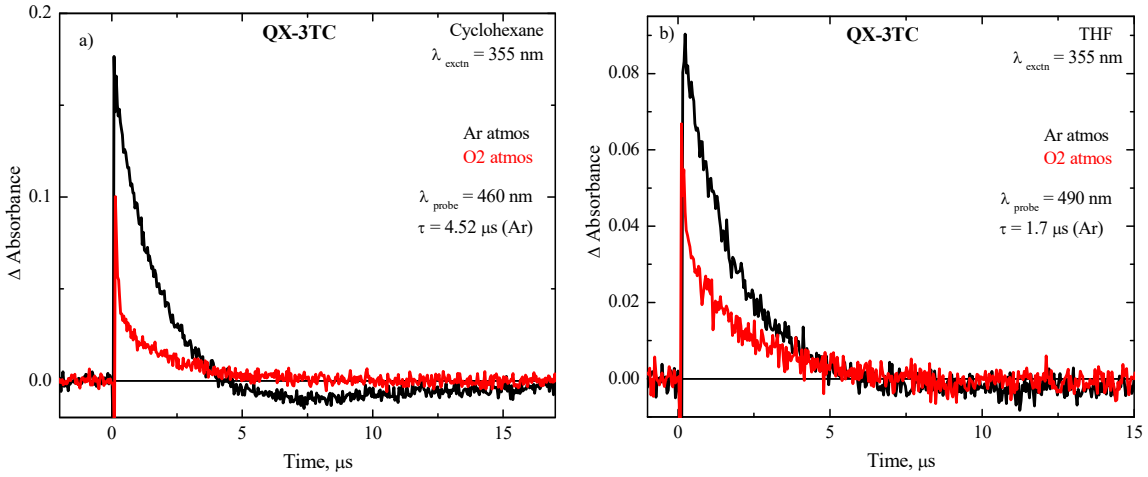

Figure 4.14 Kinetics decay profile of **QX-3TC** in argon and oxygen saturated toluene (a) and THF (b).

4.3.6 Aggregation Studies

The emission spectra of **QX-1TC** and **QX-3TC** were measured with gradual increase of the water percentage in the THF solution to investigate their AIE characteristics behaviour (**Figure 4.15**).

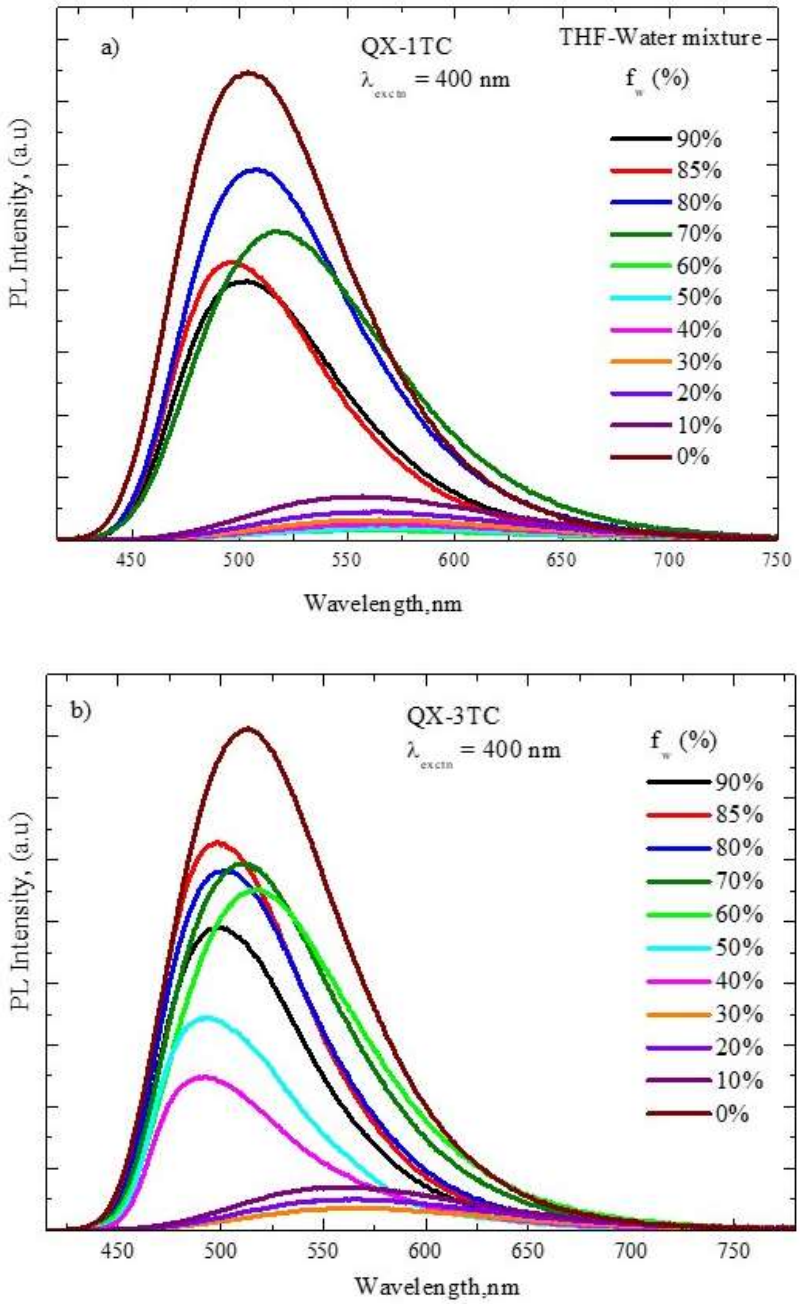

Figure 4.15 Fluorescence spectra of **QX-1TC** (a) and **QX-3TC** (b) in different THF/water mixtures obtained by exciting at 400 nm.

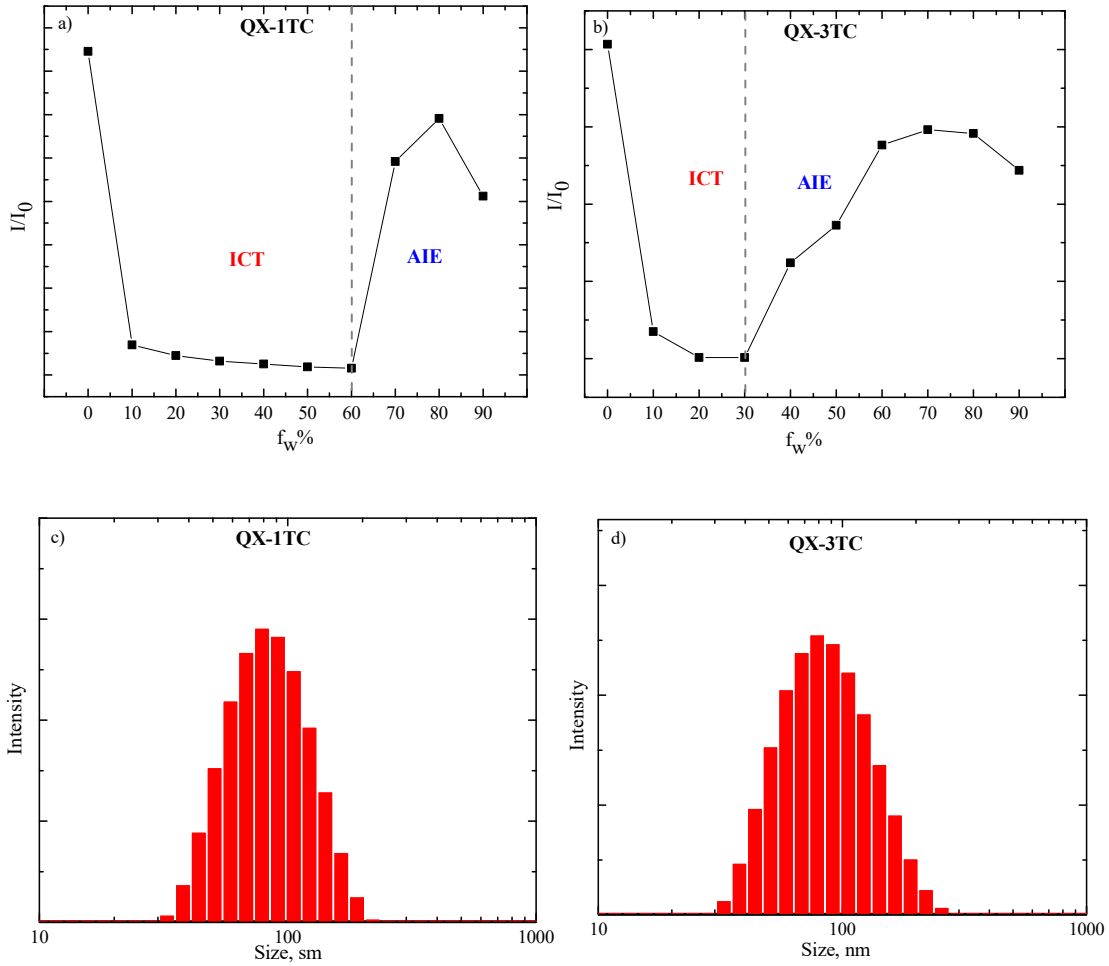

Figure 4.16 The plot of emission intensity of **QX-1TC** (a) and **QX-3TC** (b) vs % of water fraction (f_w). The size distribution of nanoaggregates of **QX-1TC** (c) and **QX-3TC** (d) in THF-Water mixture of f_w = 90%, obtained by DLS measurements.

The derivatives **QX-1TC** and **QX-3TC** are highly soluble in THF but poorly soluble in water. In the case of **QX-1TC**, as water was added to the THF solution, the fluorescence intensity was quenched and fluorescent maxima shifted to 550 nm until the f_w = 60%. This could be due to the stabilization of ICT state and effect of solvation. The fluorescent intensity was regained after f_w = 60% due to formation of aggregation. But in the case **QX-3TC**, the aggregation of molecules is started from f_w = 30% and therefore the fluorescence intensity of fluorophores was regained. This could be due to twisted conformation of derivatives which effectively avoid π-π stacking in amorphous state and therefore prevent from aggregation caused quenching (ACQ).[27] In the both cases, the

internal rotations/motions are also restricted in the aggregated state and thus the molecules become emissive in aggregated state nanoaggregates with size ranges from 100 to 550 nm (f_w = 90%) confirmed by DLS experiments (**Figure 4.16c** and **4.16d**).

4.3.7 Fabrication of OLED Devices

The non-doped multilayered OLEDs were fabricated in which the quinoxaline derivatives are used as emitting materials with the following device configuration: Device 1: ITO/ PEDOT:PSS/ 1TC (35 nm)/ TPBi (50 nm)/ LiF (1 nm)/ Al (100nm) and Device 2: ITO/ PEDOT:PSS/ 3TC (35 nm)/ TPBi (50 nm)/ LiF (1nm)/ Al (100 nm) where, PEDOT;PSS serves as a hole transporting layer, TPBi functions as a hole blocking layer, LiF is the electron injection layer. The device configuration and the energy levels are shown in the **Figure 4.17**. The electroluminescence (EL) properties of two devices are listed in **Table 4.3**.

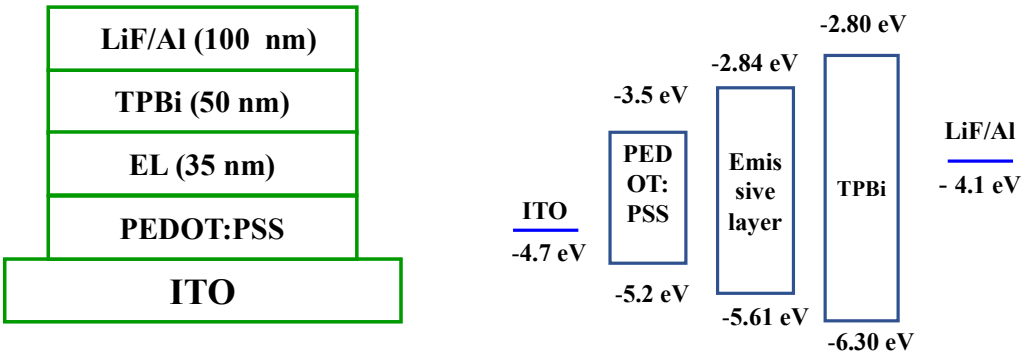

Figure 4.17 Device structure (a) and corresponding energy levels of OLED (b).

The device 1 in which **QX-1TC** is used as the emitting layer exhibiting a stable cyano coloured electroluminescence at 480 nm corresponding to CIE coordinates of 0.14, 0.28 and full width half maximum (FWHM) of 72 nm with a turn-on voltage of 9V . Similarly, the device 2 in which **QX-3TC** is used emitting layer and exhibited the same cyano coloured electroluminescence (peak at 488 nm with FWHM of 76 nm) corresponding to CIE coordinates of 0.16,0.39 with turn on voltage of 10V.

Table 4.3 Electroluminescence properties of nondoped OLEDs.

Devices	EL (nm)	Lmax (cd/m^2)	Current densinty (mA/cm^2
Device 1 (**QX-1TC**)	480	1031	334
Device 2 (**QX-3TC**)	488	1047	232

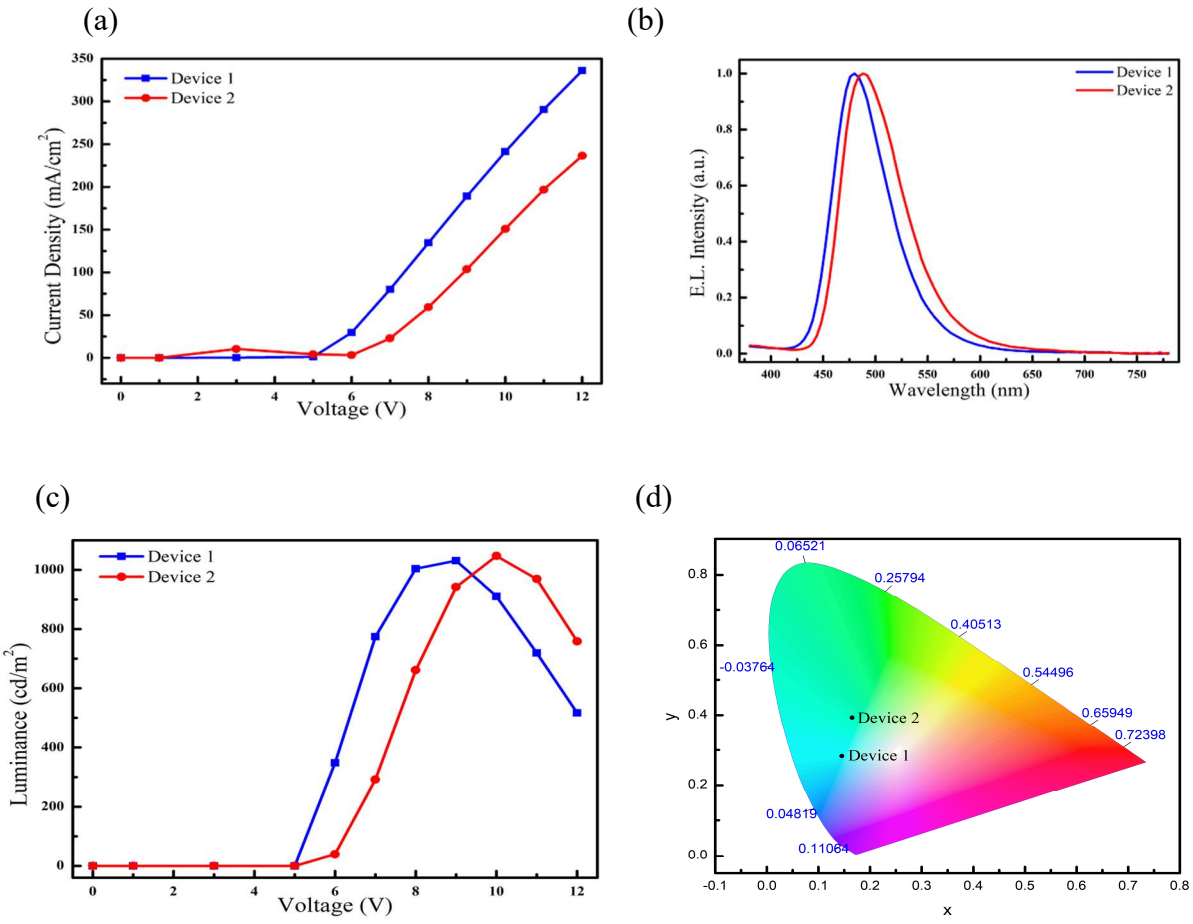

Figure 4.18 Current density-voltage plot (a), Electroluminescence spectrum of devices (b), CIE colour coordinates (c), Luminescence-voltage plot of devices(d) .

4.4 Conclusion

QX-1TC and **QX-3TC** having mono and tri substituted t-butyl carbazole derivatives were synthesized and their photophysical were characterized. The increase of tri substitution (multibranching) did not show much effect on the ICT state of these derivatives and showed comparable optoelectronic properties. These can be due to localization of HOMO to one of branches of tertbutyl carbazole donor moieties in **QX-3TC**, supported by cyclic voltammetry. The low temperature emission studies also showed that the multibranching did not influence the energy of singlet and triplet states. The nanosecond transient absorption spectra revealed that formation triplet and charge separated states in nonpolar and polar solvents respectively. Both derivatives showed the aggregation-induced emission (AIE) properties in THF- Water mixture. Both derivatives are used for non-doped OLED fabrication and devices are characterized.

4.5 Experimental Section

4.5.1 Materials and Methods

General Remarks: The chemicals, reagents and solvents for synthesis were used as received without further purification unless otherwise stated. ^{1}H-NMR and ^{13}C NMR spectra were recorded on a 500 MHz Bruker Advance II spectrometer using CDCl3 as solvent. The chemical shifts (δ) are reported in ppm and referenced to $(CH_3)_4Si$ (TMS; δ = 0 ppm) for ^{1}H or residual $CHCl_3$ (δ = 77 ppm) for ^{13}C. Mass spectral analysis was performed by using a MALDI-TOF mass spectrophotometer system.

4.5.2 Absorption and Fluorescence Spectroscopy: Solution-state UV-vis absorption spectrum was recorded on a Shimadzu UV-2600 spectrophotometer at room temperature. Fluorescent emission spectra of the solution, powder and ground samples were recorded on a HORIBA SPEX Fluorolog-3 spectrofluorometer FL-1039 equipped with a 450W Xenon

arc lamp. The powder or ground samples were sandwiched between two quartz plates placed in optical path, and spectra were recorded in front face mode. The obtained spectra were corrected using program supplied by manufacturer.

4.5.3 Fluorescence Lifetime: Time-resolved fluorescence spectra and lifetime decays were measured by using a picosecond single photon counting system (Horiba, DeltaFlex) employing 418 nm LED as excitation sources and Picosecond photon detection module (PPD-850) as a detector. The fluorescence time constants are obtained by deconvoluting with the LED profiles. The decay of the fluorescence intensity (I) with time (t) was fitted either by a mono or double-exponential function:

4.5.3 Cyclic Voltammetry: Cyclic voltammetry (CV) was performed on a CHI 604C voltammetric analyzer in DCM containing Bu_4NBF_4 (0.1 M) as a Platinum button and platinum plate were used as a working electrode and a counter electrode, respectively. All potentials were recorded versus Ag/Ag+ as a reference electrode (using ferrocene as internal standard). The scan rate was maintained at 100 mV/s.

4.5.4 Nanosecond Transient Absorption Spectra: Nanosecond transient absorption spectra were obtained by exciting the samples with the third harmonic of fundamental light (1064 nm) from a Quanta Ray Nd: YAG laser (wavelength, 355 nm, ~10 ns) and using an Applied Photophysics model LKS 60 laser kinetics spectrometer. The probing light source was a 150 W Xenon arc lamp. The light of the probe transmitted through a 1 cm quartz cuvette was dispersed by a monochromator and detected by a photomultiplier tube coupled to a digital oscilloscope (Agilent Infiniium DSO8064A, 600 MHz, 4 $GSas^{-1}$). The analyzing and laser beams were fixed at right angles to each other. The power of each laser pulse was monitored using a fast silicon photodiode.

4.5.5 Synthesis and Characterisation:

Synthesis of DK-2TC: 4.4'- dibromobenzil (914mg, 2.48 mmol), tert-butyl carbazole (1.38g, 4.96 mmol), K_2CO_3 (1.79 g, 3.02 mmol), Pd $(OAc)_2$ (48.71 mg, 0.217 mmol), $PH(^tBu)_3$ BF_4 (226.54 mg, 0.781 mmol) were transferred into a 100ml round bottom flask under argon atmosphere. The degassed toluene (50ml) was then added and resultant mixture was refluxed and stirred at 120ºC for 12 hours. After cooling to room temperature, the solvent was removed under reduced pressure. The reaction mixture is treated with DCM and water and organic layer is collected and dried. The product is purified by using column chromatography with chloroform/hexane 50:50 as eluent and subsequently evaporated and dried under reduced pressure to afford solid yellow product. Yield, 78%.^{1}H NMR (500 MHz, $CDCl_3$): δ 8.29-8.27 (d, 4H), 8.13 (s, 4H), 7.82-7.80 (d, 4H), 7.49 (s, 8H), 1.47 (s, 36H) ppm; ^{13}C NMR (125 MHz, $CDCl_3$): δ 192.95, 144.58, 144.13, 138.22, 131.90, 130.46, 126.04, 124.21, 124.02 116.52, 109.40, 34.81, 31.95 ppm.

Synthesis of DPQX-1Br: 4-bromo-1,2-diamino benzene (10g, 0.23 mol) and benzil were dissolved in 100 ml AcOH and the reaction mixture was refluxed for 4 hr. After the extraction with DCM and water, the organic layer is precipitated with ethanol. The final product is recrystallized from hot ethanol as white solid. Yield 93%. ^{1}H NMR (500 MHz, $CDCl_3$): δ 8.35-8.34 (d,1H), 8.11-8.09 (d,1H), 8.00-7.98 (m,1H), 7.58-7.56 (m, 4H), 7.45 – 7.37 (m, 6H) ppm; ^{13}C NMR (125 MHz, $CDCl_3$): δ 159.56, 159.13, 146.85, 145.09, 144.28, 144.20, 138.50, 136.46, 136.27, 135.15, 134.17, 133.24, 133.17, 128.36 ppm; HRMS (EI): m/z calcd for $C_{20}H_{13}BrN_2$: 361.0262 $[M+H]^+$; found: 361.03452.

Synthesis of DPQX-3Br (2): 4-bromo-1,2-diamino benzene (10g, .0.23 mol) and DK-2TC were dissolved in 100 ml AcOH and the reaction mixture was refluxed for 6 hr. Then workup procedure is carried out and final product is obtained by column chromatography (10: 90 chloroform: hexane). Yield 95%. ^{1}H NMR (500 MHz, $CDCl_3$) δ 8.34 (s, 1H), 8.01 (d, 1H), 7.86 (d, 1H), 7.51 (s, 4H), 7.39 (s, 4H); ^{13}C NMR (125 MHz,

$CDCl_3$): δ 152.69, 152.18, 141.72, 139.94, 137.29, 137.19, 133.96, 131.75, 131.44, 131.40, 131.34, 130.45, 124.37, 124.07, 123.97 ppm; ESI HRMS: calcd. for $C_{20}H_{11}Br_3N_2$ $[M+3]^+$: 518.8472, found: 518.8535.

Synthesis of QX-1TC: The compound DPQX-1Br (500mg, 1.38 mmol), tert-butyl carbazole (318.9mg, 1.5 mmol), NaO^tBu (800 mg, 8.304 mmol), $Pd(OAc)_2$ (30mg, 0.138 mmol), tri-tert-butylphosphonium tetrafluoroborate (144mg, 0.498 mmol) are dissolved in degassed dry toluene (50ml) and refluxed for 12 hr. The reaction mixture is cooled and solvent was removed under reduced pressure. The crude product is purified by column chromatography using hexane/chloroform (50:50) as eluent. Yield 90%; ^1H NMR (500 MHz, $CDCl_3$): δ 8.39-8.35 (m, 2H), 8.17 (s, 2H), 8.04-8.02 (d, 1H), 7.56- 7.50 (m, 8H), 7.38-7.35 (m, 6H), 1.48 (s, 18 H) ppm; ^{13}C NMR (125 MHz, $CDCl_3$): δ 152.71, 152.20, 141.75, 139.96, 137.32, 137.22, 133.98, 131.77, 131.46, 131.42, 131.36, 130.48, 124.39, 124.09, 124.00, 29.72 ppm; MALDI-TOF: m/z calcd for $C_{40}H_{37}N_3$ $[M+2H]^+$: 561.2987, found: 561.2982.

Synthesis of QX-3TC: The compound DPQX-3Br (200mg, 0.38mmol), tert-butyl carbazole (387.6mg, 1.38 mmol), NaO^tBu (656 mg, 6.8 mmol), $Pd(OAc)_2$ (25mg, 0.144 mmol), tri-tert-butylphosphonium tetrafluoroborate (199mg, 0.410 mmol) are dissolved in degassed dry toluene (50ml) and refluxed for 12 hr. The reaction mixture is cooled and solvent was removed under reduced pressure. The crude product is purified by column chromatography using hexane/chloroform (50:50) as eluent. Yield 86%. ^1H NMR (500 MHz, $CDCl_3$) δ 8.45 (s, 1H), 8.14-8.11(m, 6H), 7.93-7.91 (d, 2H), 7.86-7.84 (d, 4H), 7.67-7.66 (m, 5H), 7.49-7.43 (m, 11H), 1.46 (m, 54H) ppm; ^{13}C NMR (125 MHz, $CDCl_3$): δ 152.72, 152.21, 143.87, 143.31, 138.83, 131.52, 131.52, 131.46, 126.35, 123.98, 123.67, 116.35, 109.38, 109.27, 34.78, 32.02 ppm; HRMS (MALDI): calcd. for $C_{80}H_{83}N_5$ [M+2]: 1115.6648, found: 1115.621.

4.6 References

1. Zhao, X.; Chaudhry, S. T.; Mei, J., Chapter Five - Heterocyclic Building Blocks for Organic Semiconductors. In *Advances in Heterocyclic Chemistry*, Scriven, E. F. V.; Ramsden, C. A., Eds. Academic Press: 2017; Vol. 121, pp 133-171.

2. Ledwon, P.; Motyka, R.; Ivaniuk, K.; Pidluzhna, A.; Martyniuk, N.; Stakhira, P.; Baryshnikov, G.; Minaev, B. F.; Ågren, H., The Effect of Molecular Structure on the Properties of Quinoxaline-Based Molecules for Oled Applications. *Dyes Pigm.* **2020**, *173*, 108008.

3. Achelle, S.; Baudequin, C.; Plé, N., Luminescent Materials Incorporating Pyrazine or Quinoxaline Moieties. *Dyes Pigm.* **2013**, *98*, 575-600.

4. Xu, X.; Yu, G.; Chen, S.; Liu, Y., Synthesis and Characterization of a Quinoxaline Compound Containing Polyphenylphenyl and Strong Electron-Accepting Groups, and Its Multiple Applications in Electroluminescent Devices. *J. Mater. Chem.* **2008**, *18*, 299-305.

5. Tao, Y.; Yuan, K.; Chen, T.; Xu, P.; Li, H.; Chen, R.; Zheng, C.; Zhang, L.; Huang, W., Thermally Activated Delayed Fluorescence Materials Towards the Breakthrough of Organoelectronics. *Adv. Mater.* **2014**, *26*, 7931-7958.

6. Sarma, M.; Wong, K.-T., Exciplex: An Intermolecular Charge-Transfer Approach for Tadf. *ACS Appl. Mater. Interfaces* **2018**, *10*, 19279-19304.

7. Jo, S.; Kim, D.; Son, S.-H.; Kim, Y.; Lee, T. S., Conjugated Poly (Fluorene-Quinoxaline) for Fluorescence Imaging and Chemical Detection of Nerve Agents with Its Paper-Based Strip. *ACS Appl. Mater. Interfaces* **2014**, *6*, 1330-1336.

8. Chen, Y.; Ling, Y.; Ding, L.; Xiang, C.; Zhou, G., Quinoxaline-Based Cross-Conjugated Luminophores: Charge Transfer, Piezofluorochromic, and Sensing Properties. *J. Mater. Chem. C* **2016**, *4*, 8496-8505.

9. Wang, L.; Cui, M.; Tang, H.; Cao, D., Fluorescent Nanoaggregates of Quinoxaline Derivatives for Highly Efficient and Selective Sensing of Trace Picric Acid. *Dyes Pigm.* **2018**, *155*, 107-113.

10. Lee, J. Y.; Han, S.-Y.; Lim, B.; Nah, Y.-C., A Novel Quinoxaline-Based Donor-Acceptor Type Electrochromic Polymer. *Journal of Industrial and Engineering Chemistry* **2019**, *70*, 380-384.

11. Atar, A. B.; Jeong, J. Y.; Han, S. H.; Park, J. S., Efficient Blue-to-Transmissive Electrochromic Transitions of Alkylated Quinoxaline-Thiophene Based Donor-Acceptor Type Conjugated Polymers. *Polymer* **2018**, *153*, 95-102.

12. Wang, W.; Zhao, B.; Wu, H.; Liu, S.; Liu, H.; Guo, Z.; Wei, W.; Gao, C., Alternating Polymers Based on Alkoxy-Phenyl Substituted Indacenodithiophene and Fluorinated Quinoxaline Derivatives for Photovoltaic Cells. *Dyes and Pigments* **2017**, *145*, 345-353.

13. Zhang, J.; Cai, W.; Huang, F.; Wang, E.; Zhong, C.; Liu, S.; Wang, M.; Duan, C.; Yang, T.; Cao, Y., Synthesis of Quinoxaline-Based Donor−Acceptor Narrow-Band-Gap Polymers and Their Cyclized Derivatives for Bulk-Heterojunction Polymer Solar Cell Applications. *Macromolecules* **2011**, *44*, 894-901.

14. Peddapuram, A.; Cheema, H.; McNamara, L. E.; Zhang, Y.; Hammer, N. I.; Delcamp, J. H., Quinoxaline-Based Dual Donor, Dual Acceptor Organic Dyes for Dye-Sensitized Solar Cells. *Applied Sciences* **2018**, *8*, 1421.

15. Jung, C. Y.; Song, C. J.; Yao, W.; Park, J. M.; Hyun, I. H.; Seong, D. H.; Jaung, J. Y., Synthesis and Performance of New Quinoxaline-Based Dyes for Dye Sensitized Solar Cell. *Dyes and Pigments* **2015**, *121*, 204-210.

16. Zhao, J.; Li, H.; Li, H.; Zhao, Q.; Ling, H.; Li, J.; Lin, J.; Xie, L.; Lin, Z.; Yi, M., Synthesis, Characterization and Charge Storage Properties of Π-Biindolo [2, 3-B]

Quinoxaline for Solution-Processing Organic Transistor Memory. *Dyes and Pigments* **2019**, *167*, 255-261.

17. Jeon, J.; Jhon, H.; Kang, M.; Song, H. J.; An, T. K., Quinacridone-Quinoxaline-Based Copolymer for Organic Field-Effect Transistors and Its High-Voltage Logic Circuit Operations. *Organic Electronics* **2018**, *56*, 1-4.

18. Lindner, B. D.; Zhang, Y.; Höfle, S.; Berger, N.; Teusch, C.; Jesper, M.; Hardcastle, K. I.; Qian, X.; Lemmer, U.; Colsmann, A., N-Fused Quinoxalines and Benzoquinoxalines as Attractive Emitters for Organic Light Emitting Diodes. *Journal of Materials Chemistry C* **2013**, *1*, 5718-5724.

19. Reddy, M. R.; Han, S. H.; Lee, J. Y.; Seo, S., Synthesis and Characterization of Quinoxaline Derivative for High Performance Phosphorescent Organic Light-Emitting Diodes. *Dyes and Pigments* **2018**, *153*, 132-136.

20. Shizu, K.; Tanaka, H.; Uejima, M.; Sato, T.; Tanaka, K.; Kaji, H.; Adachi, C., Strategy for Designing Electron Donors for Thermally Activated Delayed Fluorescence Emitters. *The Journal of Physical Chemistry C* **2015**, *119*, 1291-1297.

21. Vishwakarma, V. K.; Nagar, M. R.; Lhouvum, N.; Jou, J.-H.; Ammathnadu Sudhakar, A., A New Class of Solution Processable Pyrazino[2,3-G]Quinoxaline Carbazole Derivative Based on D–a–D Architecture for Achieving High Eqe in Yellow and White Oleds. *Adv. Optical Mater.* **2022**, *10*, 2200241.

22. Singh, P. S.; Badani, P. M.; Kamble, R. M., Impact of the Donor Substituent on the Optoelectrochemical Properties of 6h-Indolo[2,3-B]Quinoxaline Amine Derivatives. *New Journal of Chemistry* **2019**, *43*, 19379-19396.

23. Zhang, Y.-L.; Ran, Q.; Wang, Q.; Liu, Y.; Hänisch, C.; Reineke, S.; Fan, J.; Liao, L.-S., High-Efficiency Red Organic Light-Emitting Diodes with External Quantum

Efficiency Close to 30% Based on a Novel Thermally Activated Delayed Fluorescence Emitter. *Advanced Materials* **2019**, *31*, 1902368.

24. Ledwon, P., Recent Advances of Donor-Acceptor Type Carbazole-Based Molecules for Light Emitting Applications. *Organic Electronics* **2019**, *75*, 105422.

25. Han, Y.-M.; Bai, L.-B.; Yin, C.-R.; Ou, C.-J.; Zhang, X.-W.; Zuo, Z.-Y.; Liu, B.; Yu, M.-N.; Lin, J.-Y.; Zhao, J.-F., Solution-Processed Diarylfluorene Derivatives for Violet-Blue Amplified Spontaneous Emission and Electroluminescence. *Journal of Materials Chemistry C* **2017**, *5*, 9903-9910.

26. Kothavale, S.; Lee, K. H.; Lee, J. Y., Isomeric Quinoxalinedicarbonitrile as Color-Managing Acceptors of Thermally Activated Delayed Fluorescent Emitters. *ACS Appl. Mater. Interfaces* **2019**, *11*, 17583-17591.

27. Hong, Y.; Lam, J. W. Y.; Tang, B. Z., Aggregation-Induced Emission: Phenomenon, Mechanism and Applications. *ChemComm* **2009**, 4332-4353.

28. He, Z.; Ke, C.; Tang, B. Z., Journey of Aggregation-Induced Emission Research. *ACS Omega* **2018**, *3*, 3267-3277.

29. v. Bünau, G., J. B. Birks: Photophysics of Aromatic Molecules. Wiley-Interscience, London 1970. 704 Seiten. Preis: 210s. *Berichte der Bunsengesellschaft für physikalische Chemie* **1970**, *74*, 1294-1295.

30. Li, Q.; Li, Z., The Strong Light-Emission Materials in the Aggregated State: What Happens from a Single Molecule to the Collective Group. *Advanced Science* **2017**, *4*, 1600484.

ABSTRACT

Name of the Student: **Mr. Hasim Fayiz P.N.** Registration No.: 10CC15A39006
Faculty of Study: Chemical Sciences Year of Submission: 2023
AcSIR academic centre/CSIR Lab: CSIR–National Institute for Interdisciplinary Science and Technology (CSIR–NIIST) Name of the Supervisor: Dr. V. Karunakaran

Title of the thesis: **Synthesis, photophysical characterization and applications of N-heterocyclic based multibranched donor-acceptor derivatives.**

The usage of N-heterocyclic compounds such as pyridine, pyrazine, triazine, quinoxaline, imidazole, oxadiazole, carbazole, phenoxazine and phenothiazine as building blocks has become increasingly important for the design of N-heterocyclic multibranched donor acceptor derivatives. These derivatives act as photofunctional material applications including organic light emitting diodes (OLED) devices, photovoltaic devices, and fluorescent sensors. The photophysical characterization of N-heterocyclic multibranched donor-acceptor derivatives will provide further insight into the development of more advanced functional molecules. The **Chapter 1** deals with a brief discussion of design principle of π-conjugated donor-acceptor derivatives, mechanism of aggregation induced emission (AIE), mechanochromic luminescence (MCL), and electroluminescence (EL) properties and application of π-conjugated donor-acceptor derivatives in the field of optoelectronic devices such as OLEDs.

In **Chapter 2**, to understand the effect of molecular geometry and strength of donor on the photophysical properties and ultrafast excited state relaxation pathways, multibranched tetraphenylpyrazine covalently linked with morpholine (weak donor and planar, **TPP-4MOP**) and phenoxazine (strong donor and twisted, **TPP-4PHO**) derivatives were synthesized and their steady state and time-resolved photophysical properties were investigated. **TPP-4MOP** showed feeble emission (~0.03) and **TPP-4PHO** exhibited strong emission (~0.18) comparatively in non-polar solvent, toluene. Whereas the emission spectra of **TPP-4PHO** in polar solvent, THF showed large Stokes shift (~9691cm^{-1}) with low fluorescence quantum yield (~0.01) due to the formation of twisted intramolecular charge transfer state (TICT). Aggregation studies of **TPP-4PHO** in THF and water mixture, reflect the elimination of TICT state by the restriction of intramolecular torsion in the aggregates leading to an increase (12 fold) of blue shifted fluorescence. The femtosecond and nanosecond transient absorption spectra of **TPP-4PHO** revealed the existence of partial TICT and TICT states in the THF leading to the triplet state. Whereas in the case of **TPP-4MOP**, the transient absorption spectra showed the formation of triplet state from the local excited state without involvement of TICT state. These studies revealed that the excited state relaxation pathways of derivatives are controlled by polarity dependent torsional motion.

The **Chapter 3** involves the investigation of effect of electron withdrawing groups on photophysical properties of two mechanochromic fluorophores with D–π–A-π–D structure, namely **QXTC-CN** and **QXTC-F**, based on quinoxaline as the acceptor unit and tertbutyl carbazole as the donor unit. Photophysical properties of these derivatives are studied in solution, aggregation and solid states. The acceptor strength of quinoxaline is tuned with the substitution of electron withdrawing groups such as cyano group (CN) and fluoride (F). The steady state absorption and emission studies show that the presence of intramolecular charge transfer state (ICT) in polar solvent. The nsTAS showed that the formation of triplet state in nonpolar solvent and occurrence of charge separation in polar solvent indicating the formation of radical anion of quinoxaline and radical cation of t-butyl carbazole. The aggregation induced emission studies showed that the fluorophores can emit in both solution and amorphous state. Both fluorophores, susceptible to external stimuli, including mechanical force (mechanochromism) and acid. Remarkably the **QXTC-CN** and **QXTC-F** showed reversible solid-state emission in response to mechanical stimuli and found that both molecules are sensitive to acid (TFA).

In **Chapter 4,** to understand the effect of increasing the number (multibranching) of donor units on acceptor, we synthesized and studied the photophysical properties of quinoxaline-based donor-acceptor derivatives having t-butyl carbazole as donor and quinoxaline as acceptor, namely **QX-1TC** (one t-butyl carabzole) and **QX-3TC** (three t-butyl carbazole). The steady-state absorption and emission spectra showed that the presence of intramolecular charge transfer transitions and emitting in the red region in polar solvents. The effect of multibranching on **QX-1TC** did not change the emission maximum, fluorescence lifetime, fluorescence quantum yield and energy of singlet and triplet state significantly (**QX-3TC**). This can be due to localization of HOMO to one of the donor units of **QX-3TC**. The nanosecond transient absorption studies showed the formation of triplets in nonpolar solvent (cyclohexane) and occurrence of charge separation in polar solvent (THF). Interestingly, aggregation-induced emission studies in THF-Water mixture showed that they are emissive in both solution and aggregated state representing good candidates for fabricating OLED devices. Device 1, in which **QX-1TC** is used as the emitting layer, exhibited an emission peak at 480 corresponding to CIE coordinates of 0.14 and 0.28 nm and full width half maximum of 72 nm with a turn-on voltage of 9V. Similarly, device 2, in which **QX-3TC** is used as an emitting layer, exhibited an emission peak at 488 nm FWHM of 76 nm, corresponding to CIE coordinates of 0.16, 0.39 with a turn-on voltage of 10V.

Details of the publications emanating from the thesis work

1. **Hasim Fayiz Pananilath**, Chinju Govind, Tessy T Devassia and Venugopal Karunakaran *, "Molecular Torsion Controls the Excited State Relaxation Pathways of Multibranched Tetraphenylpyrazines: Effect of Substitution of Morpholine Vs Phenoxazine", *Phys. Chem. Chem. Phys., **2023**, 25, DOI: 10.1039/D3CP03125J.*

2. **Hasim Fayiz Pananilath**, Karunakaran, V., "Synthesis and Characterization of Photophysical and Mechanochromic Properties of Quinoxaline Derivatives: Effect of CN and F Substitution" (To be submitted).

3. **Hasim Fayiz Pananilath**, Karunakaran, V., "Synthesis and Photophysical Properties of Quinoxaline Derived Donor-Acceptor System for OLED Application: Effect of Mono and Tri Substitution of Donor" (To be submitted).

List of posters presented in conferences

1. "Excited State Dynamics of propeller Shaped Tetraphenylpyrazine Derivatives for OLED Application", **Hasim Fayiz P.N**., Chinju Govind, Karunakaran Venugopal, 8th East Asia Symposium on Functional Dyes and Advanced Materials (EAS8), CSIR-National Institute for Interdisciplinary Science and Technology, Thiruvananthapuram, Kerala, India, December, September 20-22, **2017.**

2. "Mechano-Responsive Organic Fluorescent Materials Based on Quinoxaline Derivatives", **Hasim Fayiz P.N.**, Karunakaran Venugopal, International Conference on Energy and Environment (iCEE2k19), T.K.M. College of Arts & Science, Kollam, Kerala, India, December 12-14, **2019**.

PCCP

PAPER

Molecular torsion controls the excited state relaxation pathways of multibranched tetraphenylpyrazines: effect of substitution of morpholine *vs.* phenoxazine†

Cite this: DOI: 10.1039/d3cp03125j

Hasim Fayiz Pananilath,[ab] Chinju Govind,[ab] Tessy D. Thadathilanickal[ab] and Venugopal Karunakaran *[ab]

Received 3rd July 2023,
Accepted 8th September 2023

DOI: 10.1039/d3cp03125j

rsc.li/pccp

Multibranched donor–acceptor derivatives exhibiting desirable photophysical properties are efficiently used in optoelectronic devices, in which the excited state relaxation dynamics of the derivatives control the efficiency of the devices. Here, the effect of intramolecular torsion on the excited state relaxation dynamics of tetraphenylpyrazine (TPP) derivatives in non-polar (toluene) and polar (THF) solvents is investigated by substituting the electron donor of morpholine (**TPP-4MOP**) and phenoxazine (**TPP-4PHO**) leading to the planar and twisted configurations, respectively, using femtosecond and nanosecond transient absorption spectroscopy. In the steady state, **TPP-4MOP** showed feeble emission (Φ_F ~0.03) due to the weak donor by the delocalization of electron density supported by theoretical optimization. The **TPP-4PHO** exhibited strong emission (Φ_F ~0.18) in toluene compared to that in THF, in which it showed a large Stokes shift (~9691 cm^{-1}) with low fluorescence quantum yield (Φ_F ~0.01). The observation of large Stokes shifts, inherent nature and theoretical calculations of **TPP-4PHO** suggest the twisting of the dihedral angle between tetraphenylpyrazine and phenoxazine in the excited state leading to the twisted intramolecular charge transfer state (TICT). The femtosecond and nanosecond transient absorption and picosecond time-resolved emission spectra of **TPP-4PHO** revealed the signature of the existence of both the partial TICT and TICT states in THF leading to the triplet state. Whereas in the case of **TPP-4MOP**, the transient absorption spectra showed the formation of the triplet state from the local excited state without the involvement of the TICT state. Aggregation studies of **TPP-4PHO** in a THF and water mixture reflect the elimination of the TICT state by the restriction of intramolecular torsion in the aggregates leading to an increase of 12-fold of the fluorescence intensity along with shifting of the maximum towards the blue region. These studies revealed that the excited state relaxation pathways of the derivatives are controlled by polarity-dependent torsional motion.

I. Introduction

The enrichment of efficient fluorescence materials having donor–acceptor organic chromophores is important for their various potential applications, including organic light emitting diodes,[1–3] sensors,[4,5] lasers[6–8] and biomedical applications.[9–12] Compared to simple donor–acceptor (D–A) monomeric systems, multibranched organic derivatives consisting of donor–acceptor architectures of D_3–A or D_4–A have attracted great interest due to their desirable photophysical properties, including two photon absorption cross section, exciton coupling, excitation transfer, solvent polarity effects and non-linear optical properties by virtue of their enriched density and cooperative interaction of chromophores.[13–15] However, their excited state relaxation dynamics are complex due to their delocalization of excitation.[16,17] Indeed, their photophysical properties significantly depend on the various factors including the electronic nature of the donor and acceptor, planarity of the bridge, and nature of the ground and excited states.[16–22]

Here we selected the central moiety of pyrazine with four peripheral phenyl groups, acting as an acceptor and considered

[a] *Photosciences and Photonics Section, Chemical Sciences and Technology Division, CSIR- National Institute for Interdisciplinary Science and Technology, Thiruvananthapuram-695 019, Kerala, India. E-mail: k.venugopal@niist.res.in; Tel: 091-471-2515240*

[b] *Academy of Scientific and Innovative Research (AcSIR), Ghaziabad, 201002, India*

† Electronic supplementary information (ESI) available: Details of the steady state and time resolved experiments, synthetic procedure, structural characterization of TPP derivatives, cyclic voltammogram data, absorption, emission and fluorescence lifetime of TPP derivatives in different solvents, Lippert Mataga plots, DLS plot and fluorescent decay profile of nanoaggregates of TPP derivatives in THF-Water mixtures, kinetic decay profiles of nanosecond and femtosecond transient experiments in toluene and THF and decay-associated difference spectra of TPP derivatives in THF and toluene are provided. See DOI: **https://doi.org/10.1039/d3cp03125j**

as a potential aggregation-induced emission (AIE) core[23–26] among the AIE luminogens.[27–29] Based on the geometry of the donor, the tetraphenylpyrazine (TPP) derivatives could lead to either a planar or twisted conformation exhibiting aggregation caused fluorescence quenching by π–π interaction or aggregation induced fluorescence enhancement by restriction of intramolecular torsion, respectively, during the aggregation or in the solid state.[24,30,31] To shed more light on the intramolecular torsion, especially to understand the twisted intramolecular charge transfer (TICT) dynamics controlling the fluorescence behavior, many theoretical[32–34] and experimental[35–43] studies of the various donor–acceptor systems have been carried out.[44] The excited state relaxation dynamics of multibranched donor–acceptor derivatives have also been investigated in detail.[45–48] These studies would help to understand the inherent nature of (de)localization of excitation of these derivatives to improve the efficiency when applied to optoelectronic devices.[49–52]

Here, we investigated the steady-state and excited state relaxation dynamics of TPP derivatives by substituting the electron donor of morpholine (weak donor, **TPP-4MOP**: planar) and phenoxazine (strong donor, **TPP-4PHO**: twisted) in toluene and THF using femtosecond and nanosecond transient absorption spectroscopy to understand the effect of intramolecular torsion on the photophysical properties of multibranched donor–acceptor derivatives. The molecular structures of TPP derivatives are shown in Fig. 1. With respect to the phenyl group, it is presumed that the phenoxazine in **TPP-4PHO** is twisted due to steric constraint and morpholine in **TPP-4MOP** would be in the planar form though it can freely rotate. It is found that **TPP-4MOP** showed weak fluorescence in both solvents ($\Phi_F \sim 0.03$), whereas **TPP-4PHO** exhibited strong emission in toluene ($\Phi_F \sim 0.18$) and reduced to ~ 0.01 in THF due to the occurrence of TICT. Femtosecond transient absorption spectra supported the occurrence of partial TICT and TICT in **TPP-4PHO** in THF and excited state relaxation pathways of both the derivatives are characterized.

II. Results and discussion

Synthesis

The chemical structures and synthetic scheme of the intermediates and desired TPP derivatives are shown in Scheme 1. The TPP derivatives were synthesized from the intermediate of 2,3,5,6-tetrakis(4-bromophenyl)pyrazine by coupling with the corresponding donors (morpholine and phenoxazine) using the palladium catalyzed Buchwald–Hartwig reaction method.[1,53] The chemical structure of **TPP-4MOP** and **TPP-4PHO** was characterized by ^{1}H and ^{13}C NMR and MALDI-TOF or HRMS and spectral data are provided in the ESI.†

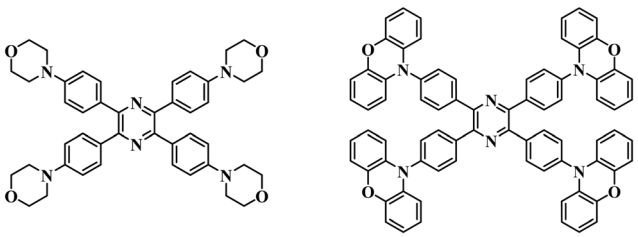

TPP-4MOP **TPP-4PHO**

Fig. 1 Molecular structure of **TPP-4MOP** and **TPP-4PHO**.

Steady-state photophysical characterization

The absorption and emission spectra of TPP derivatives were measured in solvents of various polarities and are provided in ESI† (Fig. S1 and S2). For a discussion, the absorption and emission spectra of **TPP-4MOP** and **TPP-4PHO** in toluene and THF are considered (Fig. 2). The absorption and emission spectra are converted into line shape spectra by dividing the experimental spectra measured in wavelength with the ν and ν^3, respectively, for transition dipole moment representation.[54–56] **TPP-4MOP** (**TPP-4PHO**) showed two absorption maxima at $\sim$318 (326) and 385 (395) nm. The stronger high-energy absorption maximum ($\sim$318/326, $\varepsilon \sim$ 48 785/59 360 M^{-1} cm^{-1}) is attributed to the local excited state transition originating from the individual chromophores of tetraphenylpyrazine and donors of morpholine and phenoxazine. The low energy absorption band could be due to the intramolecular charge transfer (ICT) transition of the derivatives.[24] Though the absorption spectra of **TPP-4MOP** did not show any significant changes with an increase of solvent polarity from toluene to THF, there is a shifting of the emission maximum of $\sim$3 nm to the red region with an increase of solvent polarity. In the case of **TPP-4PHO**, though there are no major changes in the absorption spectra upon changing the polarity of the solvent, there is a significant shift of the emission maximum to the red region (640 nm) in THF reflecting the variation of the permanent dipole moment of the emitting state from that of the ground state. This significant red shifted emission in the **TPP-4PHO** is consistent with more electron donating ability of phenoxazine (E_{ox}° (V) = 0.23)[57] compared to morpholine (E_{ox}° (V) = 0.86).[58] When compared to **TPP-4PHO** in toluene, there is an emission peak in the higher energy region at $\sim$470 nm in THF, which could be due to the emission arising from the local excited state of the derivative. Furthermore, to evaluate the variation of the dipole moment between the ground and excited states, the Lippert–Mataga equation[59,60] was used.

$$\upsilon_a - \upsilon_f = \frac{2(\mu_e - \mu_g)^2}{hca^3}\left[\frac{\varepsilon - 1}{2\varepsilon + 1} - \frac{n^2 - 1}{2n^2 + 1}\right] \quad (1)$$

where μ_e and μ_g are the dipole moments of the molecule in the excited and ground states, respectively, a is the effective radius of Onsager's cavity, and ε and n are the static dielectric constant and the refractive index of the solvent, respectively.

The Lippert–Mataga plot of **TPP-4MOP** (Fig. S3, ESI†) and **TPP-4PHO** (Fig. S4, ESI†) using the solvent polarity function and Stokes shift provided the change in the excited state dipole moment. For **TPP-4PHO**, it is found to be around 9.84 D and consistent with the theoretical value (9.90 D) attained by optimization. Though the solvent effect is not significant and the Lippert–Mataga plot did not appear linear for **TPP-4MOP**

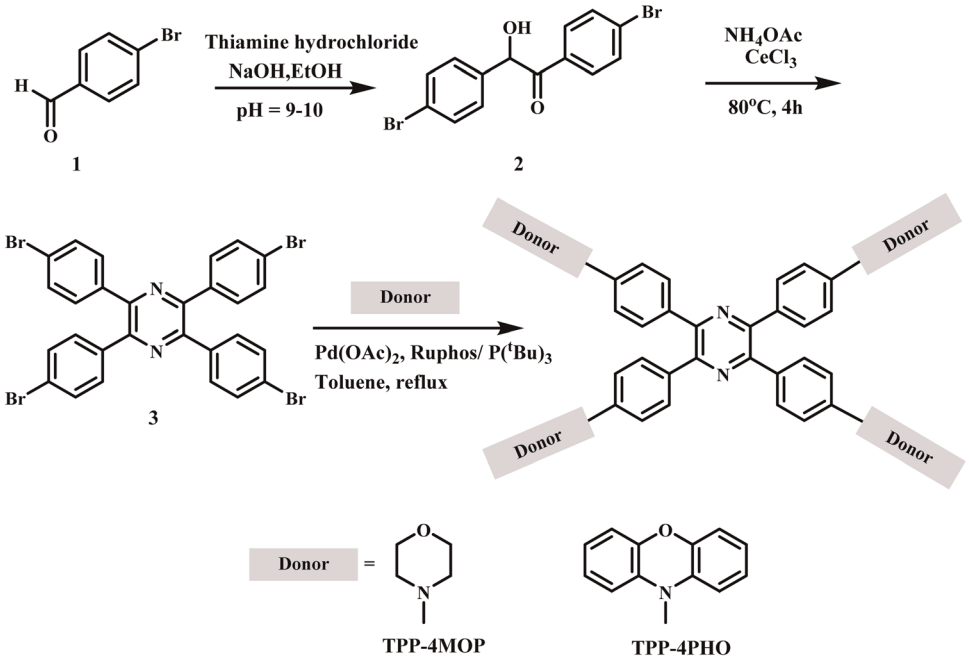

Scheme 1 Synthetic scheme of TPP derivatives.

(Fig. S3, ESI†), the calculation of change in the excited state dipole moment was attempted and found to be around 4.37 D, which deviates from the theoretical value (0.33 D). The relative fluorescence quantum yield and lifetime of TPP derivatives were measured in toluene and THF. Though there are no significant changes in the fluorescence quantum yield of **TPP-4MOP** (0.03) upon increasing the polarity of the solvent, there is a decrease in fluorescence quantum yield of **TPP-4PHO** from 0.18 (toluene) to 0.01 (THF) suggesting the involvement of a non-radiative decay pathway including a solvation process and the formation of a charge transfer state in the polar solvent. The fluorescence quantum yield in the solid-state was found to be 0.04 and 0.12 for **TPP-4MOP** and **TPP-4PHO**, respectively, matching with the values obtained in the non-polar solvent of toluene. The fluorescence lifetime of **TPP-4MOP** (0.13 ns) did not change significantly upon increasing the polarity of the solvent; however, in the case of **TPP-4PHO**, a decrease of lifetime was observed in THF (0.13 and 1.35 ns) compared to that in toluene (8.91 ns) (Fig. S5 and S6, ESI†). The radiative and non-radiative rate constants of the TPP derivatives are calculated from their fluorescence lifetime and quantum yield using the following equations.[61]

$$k_r = \frac{\Phi}{\tau_f} \quad (2)$$

$$k_{nr} = \frac{1}{\tau_f} - k_r \quad (3)$$

Upon increasing the polarity of the solvent, an increase of non-radiative constant was observed in **TPP-4PHO** which is in concurrence with the increase of the triplet quantum yield in polar solvent (*vide infra*).

Based on the literature[36,62] and the inherent nature of these derivatives, the experimental observations of the large Stokes shift, decrease of fluorescence quantum yield and lifetime could be due to the occurrence of the non-radiative conformational changes leading to the TICT. However, **TPP-4PHO** is not soluble in the highly viscous solvents to support the occurrence of intramolecular twisting.

Electrochemical characterization

The electrochemical properties of **TPP-4MOP**, **TPP-4PHO** and TPP in dichloromethane (DCM) were characterized using cyclic voltammetry (CV) with a conventional three electrode system (Fig. S7 and Table S1, ESI†). The reversible oxidation waves at +0.34 and +0.80 V and quasi-reversible reduction wave at −1.25 V were observed for **TPP-4MOP**. The reversible oxidation and quasi-reversible reduction wave of **TPP-4PHO** were observed at +0.38 and −1.25 V, respectively. The highest occupied molecular orbital (HOMO) and lowest unoccupied molecular orbital (LUMO) energy levels of **TPP-4MOP** and **TPP-4PHO** were calculated using the oxidation and reduction potential values, respectively. The values of HOMO (LUMO) were found to be −5.20 (−3.15) and −4.78 (−3.15) eV for **TPP-4MOP** and **TPP-4PHO,** respectively. The TPP showed an irreversible oxidation and reduction wave at +0.35 V and −1.25 V, respectively. It is found from the literature that the phenoxazine (PHO) and morpholine (MOP) exhibited oxidation waves at 0.23 and 0.86,[57,58] respectively.

The thermodynamic feasibility of photo-induced charge separation of TPP derivatives is examined by calculating the Gibbs free energy change (ΔG_{CS}) using the Rehm–Weller equation as follows.[63,64]

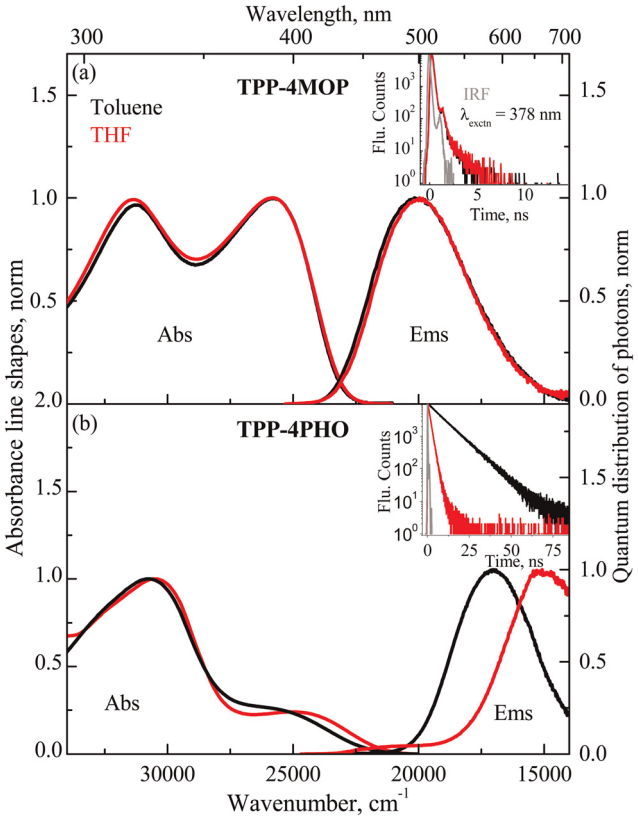

Fig. 2 Steady state absorption and emission spectra of **TPP-4MOP** (a) and **TPP-4PHO** (b) in toluene (black) and THF (red) at room temperature. The insets show the fluorescence decay profile obtained upon excitation at 378 nm.

$$\Delta G_{CS} = [E_{ox} - E_{red}] - E_{00} + \Delta G_S \quad (4)$$

$$\Delta G_S = \frac{e^2}{4\pi\varepsilon_S\varepsilon_0 R_{CC}} - \frac{e^2}{8\pi\varepsilon_0}\left(\frac{1}{R_D} + \frac{1}{R_A}\right)\left(\frac{1}{\varepsilon_{REF}} - \frac{1}{\varepsilon_S}\right) \quad (5)$$

where ΔG_S is the static Coulombic energy as defined by eqn (5), e is the electronic charge, E_{ox} and E_{red} are the oxidation and reduction potentials of the donor and acceptor moieties, respectively, and E_{00} denotes the approximated energy level with the cross point of normalized absorption and emission spectra at the singlet excited state, ε_S is the static dielectric constant of the solvent, R_{CC} is the center-to-center distance between the MOP, PHO (electron donor unit) and pyrazine (electron acceptor unit) determined by DFT optimization of the geometry, R_D and R_A are the radius of the electron donor and acceptor, respectively, ε_{REF} is the static dielectric constant of the solvent used for the electrochemical studies, and ε_0 is the permittivity of free space.

The ΔG_{CS} of the **TPP-4MOP** and **TPP-4PHO** in THF was found to be −0.98 eV and −1.24 eV respectively and the negative value of the ΔG_{CS} represents the feasibility of the intramolecular charge separation thermodynamically. The more negative value of ΔG_{CS} of the **TPP-4PHO** is consistent with the decrease of fluorescence quantum yield and the more electron donating capability of phenoxazine compared to morpholine, leading to the intramolecular charge transfer state. It is to be noted that the Rehm–Weller equation will be appropriate for individual or weakly coupled or well separated donor–acceptor derivatives rather than the multibranched donor–acceptor derivatives.

Theoretical calculations

Theoretical optimizations were carried out to understand the conformational structures of the TPP derivatives. The results of the energy gap between the HOMO and LUMO, ground state and excited state dipole moments, and S_1 and T_1 vertical excitation energies are provided in Table S3 (ESI†). Fig. 3 shows that the electron density of **TPP-4MOP** is delocalised on the entire molecule in the HOMO and LUMO. Whereas in the case of **TPP-4PHO**, the electron density is well confined on the phenoxazine and pyrazine moieties in the HOMO and in the LUMO, respectively. Such a difference of observation could be due to the stronger electron donating capability of phenoxazine compared to morpholine. The optimization of the geometries of **TPP-4PHO** in the S_1 state has been performed by using TDDFT theoretical calculations. Potential energy surface (PES) scans along the reaction coordinate involving the twisting motion of the phenoxazine group are carried out (Fig. S8, ESI†). It is found that the twisting of the phenoxazine group leads to a potential energy minimum at the twist angle of 30° and 90° in which the 90° twisting angle has the lowest energy. This is supporting our plausible mechanism of conformational relaxation involving a nonradiative partially twisted and completely twisted intramolecular charge transfer state, prior to deactivation of the S_1 state to the ground state *via* twisting of the phenoxazine group to populate the twisted structure of lower energy.

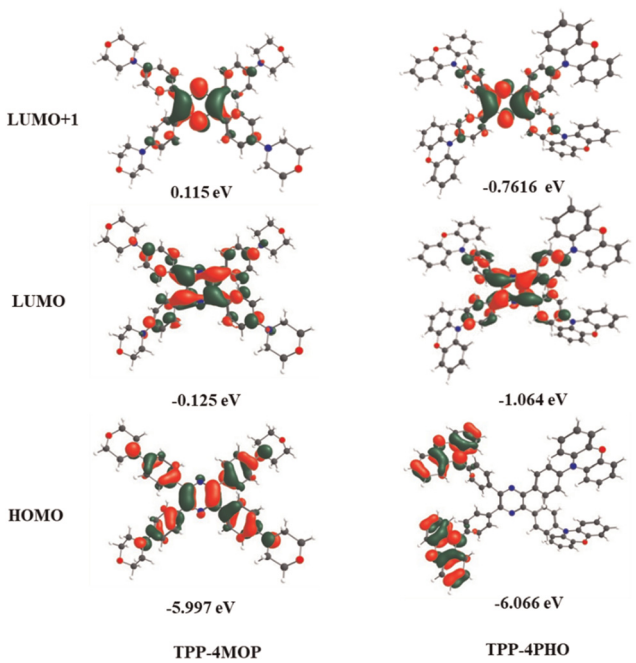

Fig. 3 Molecular orbitals of TPP derivatives with the corresponding energy levels.

Effect of aggregation

In order to examine the effect of aggregation on the emission behaviours in these derivatives, the emission spectra of **TPP-4MOP** and **TPP-4PHO** in THF upon increasing the volume fraction of water (f_w) were measured and shown in Fig. 4. With the increase of f_w until 50%, the **TPP-4MOP** showed an increase of fluorescence intensity with shifting of the maximum to the red region (~500 nm). On further increase of f_w until 80%, there was quenching of the fluorescence intensity with shifting of the maximum to the blue region (~482 nm) and an increase of fluorescence intensity was observed at f_w of 90%. In the case of **TPP-4PHO**, with increase of f_w until 40%, there was quenching of the fluorescence intensity and a peak shift towards the red region (> 700 nm). For the f_w at 50%, the fluorescence intensity increased with shifting of the maximum to the blue region (540 nm). On further increase of the water fraction to 70%, the intensity was decreased and the maximum shifted to the red region (590 nm). Upon further increase of f_w until 90%, the fluorescence intensity increased with the maximum shifted to the blue region (~560 nm). The redshift of the fluorescence maximum (>700 nm) with an increase of f_w up to 40% is due to the effect of solvation. The excursion of shifting of the emission maximum in the range of 50 to 70% of f_w could be due to the various degrees of formation of aggregates. The I/I_0 is calculated using the intensity at the fluorescence maximum of the respective solution as it is focused on understanding the overall change in fluorescence intensity by the effect of aggregation induced emission. The plot of I/I_0 *vs.* f_w in THF shown as the inset in Fig. 4 exhibits the enhancement of the fluorescence of TPP derivatives with the increase of f_w. The fluorescence enhancement of intensity of about 12 times for **TPP-4PHO** in 90% f_w was observed compared to that in neat THF, whereas **TPP-4MOP** in 90% f_w showed a very feeble increase (~1.6 times) of fluorescence intensity.

The increase of fluorescence intensity along with shifting of the maximum towards the blue region, especially in the case of **TPP-4PHO**, is attributed to the formation of nanoaggregates with size ranges from 100 to 550 nm (f_w = 90%) confirmed by DLS experiments (Fig. S9, ESI†). The enhancement of the fluorescence in the nanoaggregates could be due to the restriction of intramolecular torsion by eliminating the non-radiative TICT state leading to the increase of the radiative decay from the intramolecular charge transfer state partially twisted (pTICT) in nature. The observation of feeble fluorescence enhancement in the **TPP-4MOP** could be due to the π–π interaction in the aggregates as they are inherently planar in nature compared to **TPP-4PHO**. Since the emission maximum in a higher water fraction shifted to the blue region compared to neat solvent, the enhancement of the emission might not be due to the formation of H- and J- aggregates and needs further investigation.[65,66] The fluorescence decay profile of TPP derivatives in THF-water mixture (f_w = 90%) was measured, exhibiting a long-lived fluorescent component (~13.75 ns) due to the formation of nanoaggregates (Fig. S10, ESI†).

Thus, the formation of a twisted intramolecular charge separated state in **TPP-4PHO** is realized based on the following experimental observations. (1) There is a large Stokes shift in the emission spectra in a polar solvent (2137 cm^{-1}) compared to a non-polar solvent (175 cm^{-1}). (2) The dual emission and long lifetime of the significant red-shifted fluorescence in polar solvents are a plausible reason for the charge transfer state being of TICT character. (3) The derivative of **TPP-4PHO** is inherently twisted in nature. (4) The potential energy surface (PES) scan along the twisting of the phenoxazine group (Fig. S8, ESI†) showed the twisting of the phenoxazine group leading to a potential energy minimum at the twist angle of ~30° and 90° in which the 90° twisting angle is the lowest energy. (5) The observation of aggregation induced emission of recovering the fluorescence intensity during aggregation in **TPP-4PHO** was also perceived in BODIPY, binaphthyl and tetraphenylethene derivatives appearing non-fluorescent in polar environments due to TICT formation, but they recover their fluorescence intensity upon aggregation.[44,67–69]

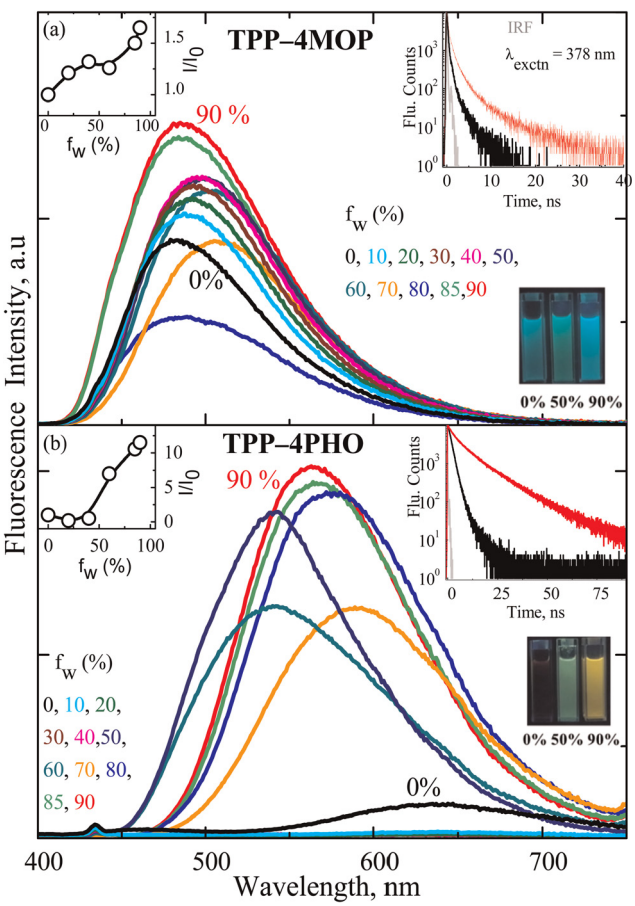

Fig. 4 Fluorescence spectra of **TPP-4MOP** (a) and **TPP-4PHO** (b) in THF/water mixtures with various volume water fractions (f_w) upon excitation at 385 nm. Left side insets show the plot of I/I_0 *vs.* f_w. Right side insets show the fluorescence decay profiles in the f_w of 0 and 90% obtained upon excitation at 378 nm. The photos of the derivatives in f_w of 0, 50 and 90% under the illumination of a UV lamp (365 nm) are also shown.

Time-resolved photophysical characterization

Femtosecond transient absorption spectra (FTAS). Femtosecond time resolved visible absorption spectroscopy is used to investigate the ultrafast components involved in the excited state relaxation pathway of **TPP-4MOP** and **TPP-4PHO** in non-polar (toluene) and polar (THF) solvents upon excitation at 385 nm.

TPP-4MOP. Fig. 5a and b shows the femtosecond transient absorption spectra of **TPP-4MOP** in toluene. At an early time scale (300 fs), it showed a positive broad excited state absorption at ~530 nm along with negative absorption at ~385 nm corresponding to ground state bleaching. With increase of the delay time of 13 ps, there was the formation of a peak at ~430 nm and a shoulder at ~620 nm. Furthermore, on increase of the delay time to ~1.5 ns, though the overall spectral intensity was decreased, the absorption maximum at 530 nm disappeared completely and the absorption maxima at ~430 and 620 nm persisted. These spectral features match with the transient absorption spectra obtained upon nanosecond laser excitation (Fig. S14, *vide infra*, ESI†). The femtosecond transient absorption spectra of **TPP-4MOP** obtained in THF are similar to that in toluene (Fig. 5c and d).

TPP-4PHO. The femtosecond transient absorption spectra of **TPP-4PHO** in toluene are shown in Fig. 6a and b. At an early time scale of 350 fs, it exhibited a broad transient absorption spectrum having a maximum at ~490 nm with a shoulder at around 525 nm. With increase of the delay time until ~31.25 ps, there was an increase in intensity of the spectra by converging the maximum at 490 nm and shoulder at 525 nm to a broad maximum at ~495 nm. The convergence of the two peaks into a broader peak might be due to the formation of a state, arising from the state absorbing at 490 nm and 525 nm, by the conformational relaxation of the chromophore during the excited state relaxation process. On further increase of the delay time to ~1.5 ns, the intensity of absorption was reduced feebly. Whereas, the femtosecond transient absorption spectra of **TPP-4PHO** in THF showed two absorption maxima at 480 and 520 nm clearly at early time scales (Fig. 6c). With increase of the delay time at ~53 ps, there is an increase of intensity by merging of these maxima into a broader maximum at ~500 nm. Interestingly, the formation of a peak at ~410 nm and a broad shoulder at ~620 nm with a weak intensity was observed during these time scales. On further increase of the delay time to ~1.5 ns (Fig. 6d), an overall decrease of the absorption intensity is observed. The excited state relaxation dynamics of **TPP-4PHO** are faster in THF when compared to toluene.

Nanosecond transient absorption spectra (NTAS). To obtain the complete dynamics of the long-lived components (*viz.*, triplet state and radical ions) observed in the femtosecond transient absorption spectra, the nanosecond transient absorption spectra of the TPP derivatives were measured in toluene and THF upon excitation at 355 nm.

TPP-4MOP. Fig. 7a shows the nanosecond transient absorption spectra of **TPP-4MOP** in toluene under an Ar atmosphere obtained at different delay times. It exhibited the two absorption bands at around 460 and 630 nm along with bleach bands

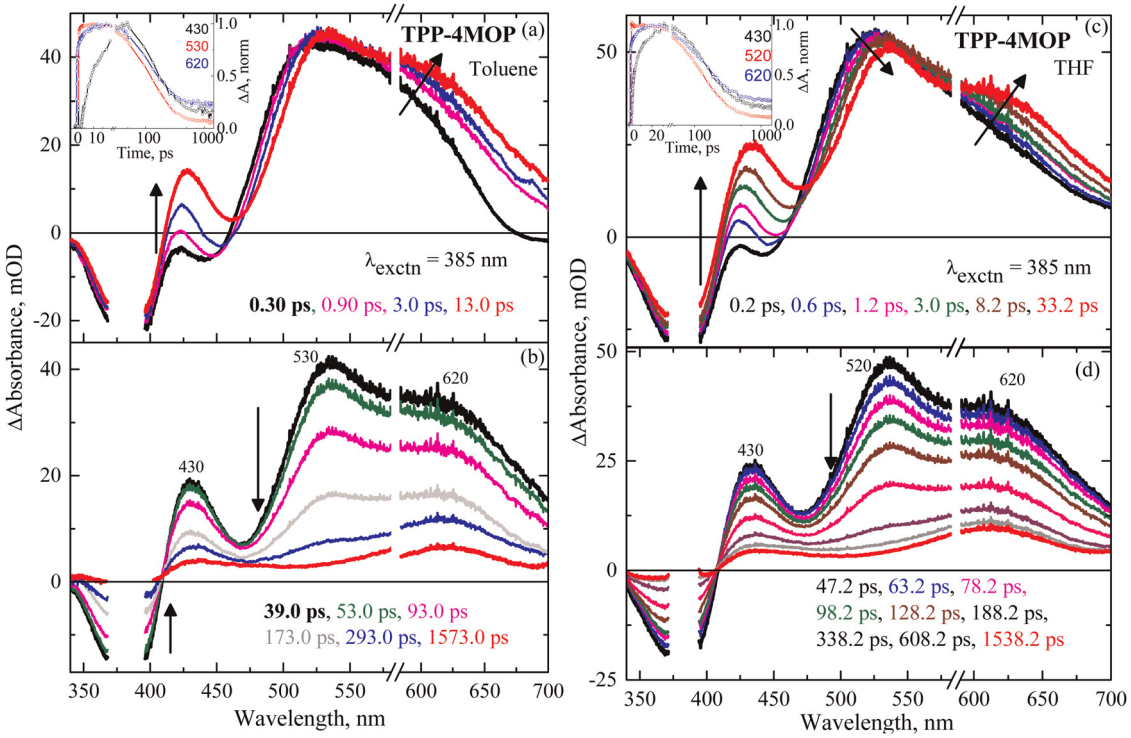

Fig. 5 Femtosecond transient absorption spectra of **TPP-4MOP** in toluene (a) and (b) and THF (c) and (d) obtained upon excitation at 385 nm at different delay times. Insets show the normalized decay of the transient absorption maximum.

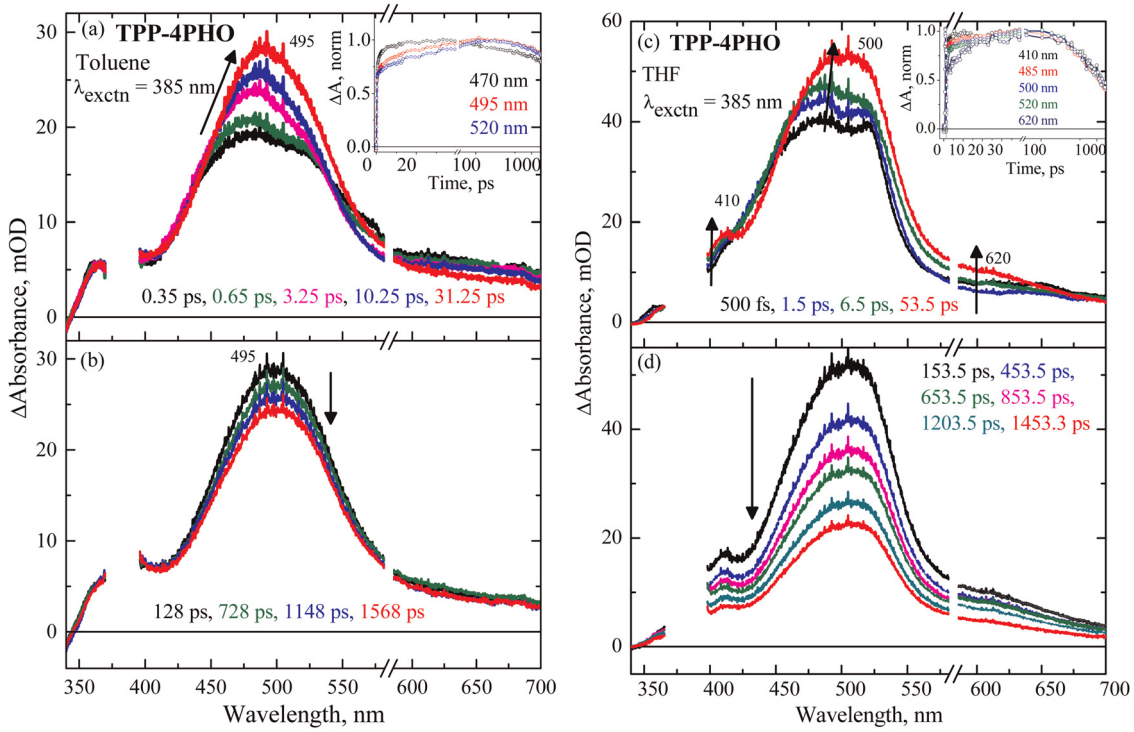

Fig. 6 Femtosecond transient absorption spectra of **TPP-4PHO** in toluene (a) and (b) and THF (c) and (d) obtained upon excitation at 385 nm at different delay times. The insets show the normalized decay of the transient absorption maximum.

at around 320 and 380 nm corresponding to the ground state (S_0) absorption maxima. The intensity of the transient absorption spectra was decreased with increase of the delay time. As in toluene, the transient absorption spectral pattern was similarly observed in THF (Fig. 7b). The transient absorption spectra were also measured under an oxygen atmosphere and quenching of the dynamics was observed (Fig. S11 and inset 7b, ESI†) in both the solvents.

TPP-4PHO. The nanosecond transient absorption spectra of **TPP-4PHO** (Fig. 8a) in toluene under an Ar atmosphere upon excitation at 355 nm showed a broad absorption maximum at 520 nm with shoulders at ~460 and 370 nm along with a bleach band at 330 nm matching to the ground state (S_0) absorption maximum. With increase of the delay time to 2.5 μs, a decrease of the shoulder at ~460 nm and persistence of absorption at ~540 and 370 nm were observed. The transient absorption spectra in an oxygen atmosphere exhibited the quenching of the dynamics (Fig. S13, ESI†). The nanosecond transient absorption spectra of **TPP-4PHO** (Fig. 8b) in THF showed similar behavior to that of toluene.

Analysis of FTAS. The femtosecond transient absorption spectra obtained in the format of a three-dimensional data set (wavelength, time, and change in absorbance) were analysed using the global analysis program, GLOTARAN[70] with a sequential model. The resulting time constants are given in Table 2 and the corresponding decay associated difference spectra (DADS) are provided in the ESI† (Fig. S18 and S19).

Time constants of TPP-4MOP. The global analysis of the femtosecond transient absorption spectra of **TPP-4MOP** in toluene (THF) gave three time constants of τ_1 = 8.92 (7.16) ps, τ_2 = ~137.96 (160.30) ps and τ_3 = 4.16 (6.36) ns. The DADS of the time constant of 8.92 (7.16) ps for **TPP-4MOP** in toluene (THF) showed negative amplitude with maxima at around 430, 530 and 620 nm consistent with FTAS representing the formation of a component after the laser excitation. The fastest component of τ_1, 8.92 ps is attributed to the decay time constant of the hot singlet state to the vibrationally relaxed local excited state of S_1. The second time constant of ~137.96 ps is consistent with the fluorescence lifetime of **TPP-MOP** obtained by TCSPC, hence it could be due to the fluorescence lifetime of the vibrationally relaxed local excited state of S_1. The third time constant might be due to the formation of the triplet state through intersystem crossing [*vide infra*]. This is supported by the fact that the transient absorption spectra at 1.5 ns and decay associated difference spectra of this time constant are exactly matching with the nanosecond transient absorption spectra (Fig. S14, ESI†). The features of the transient absorption spectra and decay associated difference spectra in THF appeared to be the same compared to those of toluene; hence, it is proposed to follow similar excited state relaxation pathways in THF as in toluene. It should be noted that the longer time constants such as 4.16 and 6.36 ns obtained by global analysis would be imprecise, since the translational delay stage in our spectrometer can reach 1.7 ns maximum limiting the capability of measuring the transient absorption spectra until 1.7 ns.

Time constants of TPP-4PHO in THF. In the case of **TPP-4PHO** in THF, there is a clear change in the spectral evolution in the femtosecond transient absorption spectra (Fig. 6c and d)

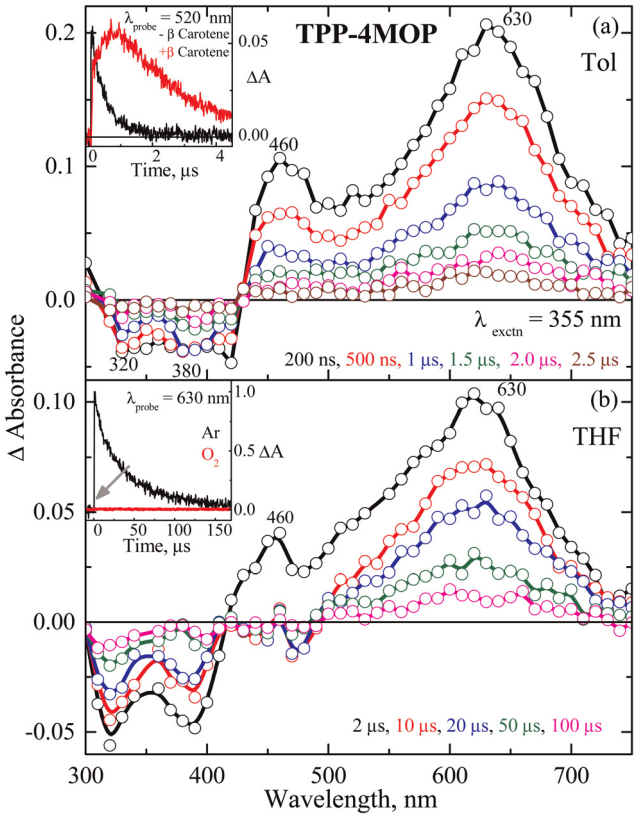

Fig. 7 Nanosecond transient absorption spectra of **TPP-4MOP** in argon saturated toluene (a) and THF (b) obtained upon excitation at 355 nm. The inset a shows the growth profile of ^{3}β-carotene formed in the mixture of **TPP-4MOP** and β-carotene at 520 nm revealing the triplet–triplet energy transfer from **TPP-4MOP** to β-carotene. The inset b shows the kinetic decay at 630 nm measured in argon and oxygen saturated THF.

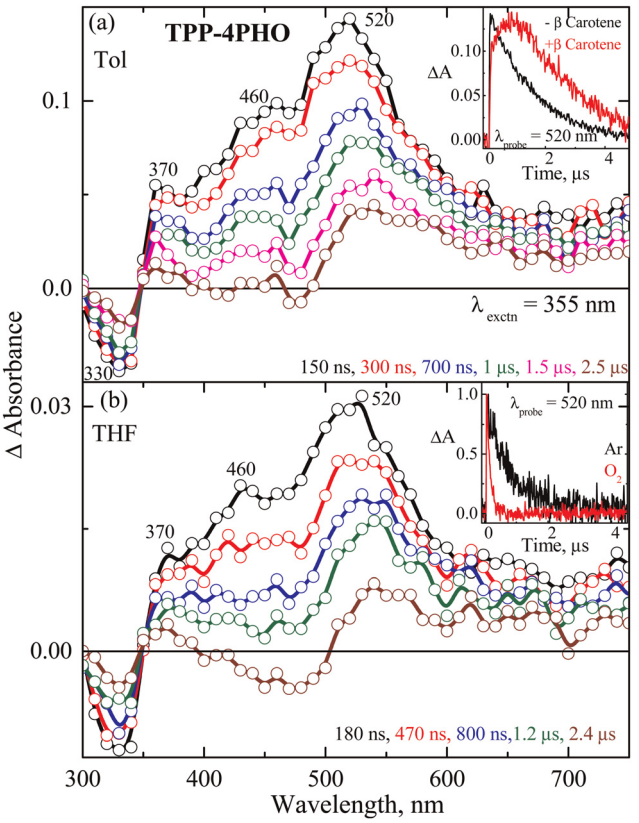

Fig. 8 Nanosecond transient absorption spectra of **TPP-4PHO** in argon saturated toluene (a) and THF (b) obtained upon excitation at 355 nm. The inset a shows the growth profile of ^{3}β-carotene formed in the mixture of **TPP-4PHO** and β-carotene at 520 nm revealing the triplet–triplet energy transfer from **TPP-4PHO** to β-carotene. The inset (b) shows the kinetic decay at 520 nm measured in argon and oxygen saturated THF.

compared to that of toluene and spectral analysis gave four (τ_1 = 526 fs, τ_2 = 24.68 ps, and τ_3 = 1.13 ns and τ_4 = 13.92 ns) time constants. All the DADS of the time constant of **TPP-4PHO** in THF except the component of 1.13 ns, showed negative amplitude due to the formation of the various species in the excited state relaxation process. The fastest time constant of ~526 fs is attributed to the relaxation of the hot singlet state to the intramolecular charge transfer state with a partially twisted nature, pTICT. Generally, the appearance of a large Stokes shift (9691 cm^{-1}) and broad fluorescence spectra in polar solvent, compared to the nonpolar solvents reflect the occurrence of a significant structural change of the derivatives upon photoexcitation in polar solvents.[36] Since the **TPP-4PHO** has an inherent nature of twisting supported by the theoretical optimization and has various degrees of freedom to rotate in polar solvent, the ICT state would initially be partially twisted in nature, pTICT.[62] However, the fastest time constant might also be due to the processes of solvation relaxation along with intramolecular vibrational relaxation, since the molecule will be vibrationally hot upon femtosecond laser excitation.[71–75] The time constant of $\tau_2 \cong$ 24.68 ps is due to the decay time constant of the pTICT state leading to the completely twisted intramolecular charge transfer state, TICT. The occurrence of the pTICT and TICT is further confirmed by the time-resolved emission spectra of **TPP-4PHO** in THF exhibiting the evolution of the shifting of the emission maximum from 600 to 640 nm corresponding to pTICT and TICT, respectively, during the delay time of 50 to 500 ps (Fig. S20, ESI†). Indeed, the decay associated spectra of 526 fs and 24.68 ps showed negative amplitude with maximum at around 485 and 520 nm, respectively, supporting the formation of components and matching with the femtosecond transient absorption spectra of **TPP-4PHO** in THF by convergence of two peaks into a single maximum as observed during the 53 ps. The fluorescence lifetimes probed at 640 nm obtained from TCSPC exhibit two components of 133 ps (4.79%) and 1.35 ns (95.21%) attributed to the fluorescence lifetime of pTICT and TICT states, respectively. Thus, the time constant of τ_3 is attributed to the fluorescence lifetime of TICT. The time constant of τ_4 ~ 13.92 ns which is beyond our experimental capability, might be due to the formation of a triplet state by charge recombination[76–78] and needs further investigation.

Time constants of TPP-4PHO in toluene. The global analysis of the femtosecond transient absorption spectra of **TPP-4PHO** in toluene gave three (τ_1 = 3.6 ps, τ_2 = 337.3 ps and τ_3 = 8.29 ns) time constants. Interestingly, the decay associated difference

Table 1 Absorption and fluorescence maxima, quantum yield and lifetime of the TPP derivatives

Compounds	Solvent	Absorption max, nm (λ_{max})	Fluorescence max, nm (λ_{max})	Stokes shift, cm^{-1}	Fluorescence quantum yield[a] (Φ_F)	Fluorescence lifetime[b], ns (τ)	Radiative constant, $10^7\ s^{-1}$ (K_r)	Non-Radiative Constant, $10^9\ s^{-1}$ (K_{nr})
TPP-4MOP	Toluene	318, 385	478	4966	0.03	0.134	22.38	7.23
	THF	318, 385	480	5141	0.03	0.136	22.05	7.13
TPP-4PHO	Toluene	326, 400	563	7554	0.18	8.91	2.02	0.09
	THF	326, 395	640	9691	0.01	0.133 (4.79%) 1.35 (95.21%)	1.06	1.05

[a] Fluorescence quantum yield in toluene and THF obtained upon excitation at 385 nm. [b] Fluorescence lifetime obtained upon excitation at 378 nm.

Table 2 Time constants for TPP derivatives in toluene and THF obtained from fsTAS

TPP derivatives	Toluene	THF
TPP-4MOP	$\tau_1 = 8.92 \pm 0.5$ ps	$\tau_1 = 7.16 \pm 0.4$ ps
	$\tau_2 = 137.96 \pm 3$ ps	$\tau_2 = 160.30 \pm 4$ ps
	$\tau_3 = 4.16 \pm 1$ ns	$\tau_3 = 6.36 \pm 1$ ns
TPP-4PHO	$\tau_1 = 3.60 \pm 0.3$ ps	$\tau_1 = 526 \pm 100$ fs
	$\tau_2 = 337.3 \pm 5$ ps	$\tau_2 = 24.68 \pm 1$ ps
	$\tau_3 = 8.29 \pm 1$ ns	$\tau_3 = 1.13 \pm 0.3$ ns
		$\tau_4 = 13.92 \pm 2$ ns

spectra of 3.6 and 337.3 ps showed negative amplitude with maximum at around 475 and 510 nm, respectively, reflecting the formation of components and consistent with the femtosecond transient absorption spectra of **TPP-4PHO** in toluene by convergence of two peaks into a single maximum as observed in the picosecond time scale. The fastest time constant of ~3.6 ps is ascribed to the formation of a partial intramolecular charge transfer state from the hot singlet excited state and consistent with its decay associated difference spectra having negative amplitude. The time constant of ~337.3 ps could be due to the formation of the time constant of the triplet state from pTICT as its DADS has negative amplitude. The third time constant, ~8.29 ns, is attributed to the fluorescence lifetime of the pTICT state of **TPP-PHO** in toluene since it is matching with the fluorescence lifetime measured by TCSPC (8.91 ns).

Analysis of NTAS

TPP-4MOP. The nanosecond transient absorption spectra of **TPP-4MOP** were measured with triplet sensitizer, β-carotene. The quenching of the dynamics at 460 and 630 nm and simultaneous growth of the peak at 520 nm due to the formation of the triplet state of β-carotene were observed (inset 7a). Thus, the transient absorption maxima at 460 and 630 nm showing similar time constants are assigned to triplet–triplet state absorption. The decay profile of the triplet absorption at 630 nm in argon saturated solution is fitted with monoexponential decay and the time constant was found to be ~0.90 and 34.07 μs for toluene and THF, respectively (Fig. S12 and inset 7b, ESI†). The triplet state quantum yield of **TPP-4MOP** was determined by energy transfer from derivatives to β-carotene in THF and compared with that from the triplet state of $Ru(bpy)_3^{2+}$ as a standard. The triplet state quantum yield was found to be 71 ± 20% in both solvents.

TPP-4PHO. The nanosecond transient absorption maximum that appeared at 520 nm having a time constant of 1.46 (1.29) μs in toluene (THF) (Fig. S13 and inset 8b, ESI†) is attributed to triplet state absorption, which is confirmed by a sensitization experiment with the triplet sensitizer, β-carotene (inset 8a) and consistent with the literature.[79] The triplet quantum yield of **TPP-4PHO** is higher in polar solvent, THF (0.41 ± 0.10), compared to that of the non-polar solvent, toluene (0.28 ± 0.10). This is consistent with the increase of K_{nr} value in polar solvent compared to that of the non-polar solvent (Table 1). Furthermore, the formation of the TICT state leading to the charge separated species is confirmed by the nanosecond

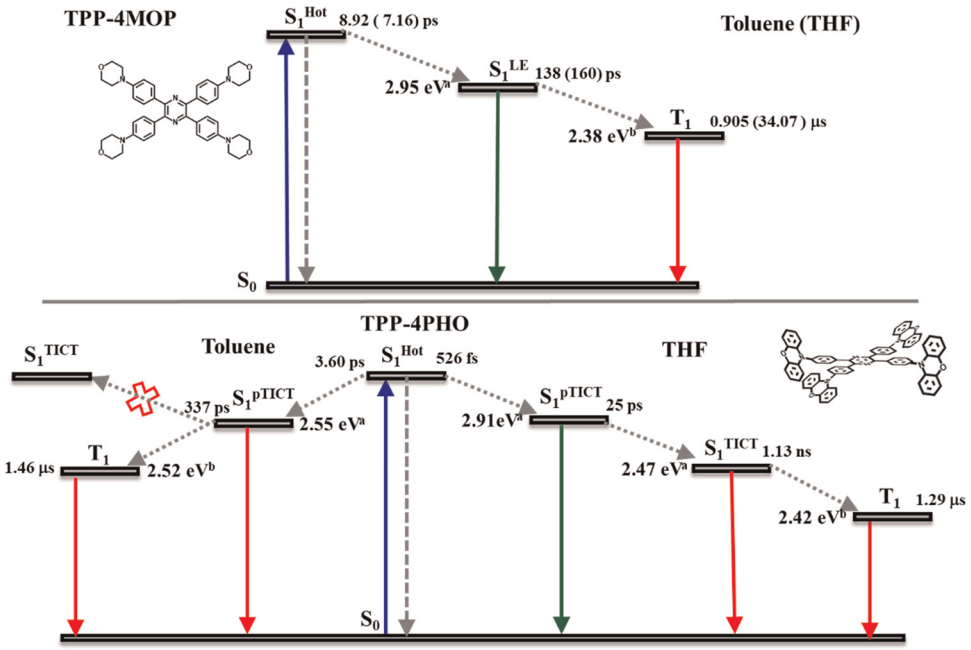

Scheme 2 Proposed excited state relaxation dynamics of **TPP-4MOP** (a) and **TPP-4PHO** (b). [a] Measured from the onset of room temperature fluorescence, [b] measured from the onset of phosphorescence spectra at low temperature (77 K).

transient absorption spectra. For example the transient absorption maximum at 370 nm quenched in the presence of oxygen, is attributed to the pyrazine radical anion and consistent with the literature.[80] The absorption peak at 540 nm having longer time constant (2.86 µs), not quenched by the presence of oxygen, is assigned to the radical cation of phenoxazine, consistent with previous reports.[77,79]

Overall, upon substitution of phenoxazine compared to morpholine in the tetraphenylpyrazines, there is an increase of molecular torsion leading to the formation of a non-radiative TICT state. This is supported by the experimental observations of the large Stokes shift, decrease of fluorescence quantum yield and lifetime and also the femtosecond and nanosecond transient absorption and picosecond time-resolved emission spectra in polar solvent. This TICT state is overcome in the aggregates by the restriction of intramolecular torsion. Thus, based on the spectral features and analysis of the dynamics from the femtosecond and nanosecond transient absorption and time-resolved emission spectra, excited state relaxation pathways of **TPP-4MOP** and **TPP-4PHO** in both solvents are proposed in Scheme 2.

III. Conclusion

Stationary and excited state relaxation dynamics of **TPP-4MOP** and **TPP-4PHO** were systematically investigated in toluene and THF to understand the effect of torsional motion on the photophysical properties of multibranched donor–acceptor derivatives. It is found that **TPP-4PHO** having a strong electron donor of phenoxazine in toluene exhibited high fluorescence quantum yield (0.18) compared to **TPP-4MOP** (0.03). However, the **TPP-4PHO** in THF exhibited a large Stokes shift (~9690 cm^{-1}) and low fluorescence quantum yield (0.01) revealing the formation of TICT. The increase of the fluorescence intensity of the aggregated form of the **TPP-4PHO** reflected the absence of the TICT state by the restriction of intramolecular torsion. The femtosecond and nanosecond transient absorption experiments of **TPP-4PHO** in THF supported the existence of TICT states decaying to the triplet state. However, the transient absorption spectra of **TPP-4MOP** exhibited the formation of a triplet state directly from the local excited state with no signature of the TICT state. These experiments revealed that the polarity dependent torsional motion plays a key role in the excited state relaxation dynamics of multibranched donor–acceptor derivatives.

Conflicts of interest

There are no conflicts of interest to declare.

Acknowledgements

H.F.P., C.G. and T.D.T thank UGC, New Delhi for their research fellowship. V.K. acknowledges the BRNS project (58/14/02/2022-BRNS/37036) and the DST-SERB Core Research Project (CRG/2022/003229), Government of India, for financial support. We thank Ms Nandana for supporting the preliminary analysis. The authors acknowledge CSIR-4PI, Bangalore, for using the computational facility.

References

1 L. Yu, Z. Wu, G. Xie, W. Zeng, D. Ma and C. Yang, Molecular Design to Regulate the Photophysical Properties of Multifunctional Tadf Emitters Towards High-Performance Tadf-Based Oleds with Eqes up to 22.4% and Small Efficiency Roll-Offs, *Chem. Sci.*, 2018, **9**, 1385–1391.

2 M. A. Baldo, D. F. O'Brien, Y. You, A. Shoustikov, S. Sibley, M. E. Thompson and S. R. Forrest, Highly Efficient Phosphorescent Emission from Organic Electroluminescent Devices, *Nature*, 1998, **395**, 151–154.

3 H.-T. Feng, X. Zheng, X. Gu, M. Chen, J. W. Y. Lam, X. Huang and B. Z. Tang, White-Light Emission of a Binary Light-Harvesting Platform Based on an Amphiphilic Organic Cage, *Chem. Mater.*, 2018, **30**, 1285–1290.

4 F. Hu, S. Xu and B. Liu, Photosensitizers with Aggregation-Induced Emission: Materials and Biomedical Applications, *Adv. Mater.*, 2018, **30**, 1801350.

5 W. Hu, *et al.*, Stimuli-Responsive Reversible Switching of Intersystem Crossing in Pure Organic Material for Smart Photodynamic Therapy, *Angew. Chem., Int. Ed.*, 2019, **58**, 11105–11111.

6 A. J. C. Kuehne and M. C. Gather, Organic Lasers: Recent Developments on Materials, Device Geometries, and Fabrication Techniques, *Chem. Rev.*, 2016, **116**(21), 12823–12864.

7 D. Okada, S. Azzini, H. Nishioka, A. Ichimura, H. Tsuji, E. Nakamura, F. Sasaki, C. Genet, T. W. Ebbesen and Y. Yamamoto, Π-Electronic Co-Crystal Microcavities with Selective Vibronic-Mode Light Amplification: Toward Förster Resonance Energy Transfer Lasing, *Nano Lett.*, 2018, **18**, 4396–4402.

8 Y. Jiang, Y.-Y. Liu, X. Liu, H. Lin, K. Gao, W.-Y. Lai and W. Huang, Organic Solid-State Lasers: A Materials View and Future Development, *Chem. Soc. Rev.*, 2020, **49**, 5885–5944.

9 D. E. J. G. J. Dolmans, D. Fukumura and R. K. Jain, Photodynamic Therapy for Cancer, *Nat. Rev. Cancer*, 2003, **3**, 380–387.

10 S. Cao, J. Shao, H. Wu, S. Song, M. T. De Martino, I. A. B. Pijpers, H. Friedrich, L. K. E. A. Abdelmohsen, D. S. Williams and J. C. M. van Hest, Photoactivated Nanomotors Via Aggregation Induced Emission for Enhanced Phototherapy, *Nat. Commun.*, 2021, **12**, 2077.

11 X. Cai and B. Liu, Aggregation-Induced Emission: Recent Advances in Materials and Biomedical Applications, *Angew. Chem., Int. Ed.*, 2020, **59**, 9868–9886.

12 C. S. Kue, S. Y. Ng, S. H. Voon, A. Kamkaew, L. Y. Chung, L. V. Kiew and H. B. Lee, Recent Strategies to Improve Boron Dipyrromethene (Bodipy) for Photodynamic Cancer Therapy: An Updated Review, *J. Photochem. Photobiol., A*, 2018, **17**, 1691–1708.

13 W. Huang, H. Wang, L. Sun, B. Li, J. Su and H. Tian, Propeller-Like D–Π–a Architectures: Bright Solid Emitters with Aiee Activity and Large Two-Photon Absorption, *J. Mater. Chem. C*, 2014, **2**, 6843–6849.

14 R. Hu, N. L. C. Leung and B. Z. Tang, Aie Macromolecules: Syntheses, Structures and Functionalities, *Chem. Soc. Rev.*, 2014, **43**, 4494–4562.

15 D. Barman, K. Narang, R. Parui, N. Zehra, M. N. Khatun, L. R. Adil and P. K. Iyer, Review on Recent Trends and Prospects in Π-Conjugated Luminescent Aggregates for Biomedical Applications, *Aggregate*, 2022, 172.

16 B. Dereka, A. Rosspeintner, R. Stężycki, C. Ruckebusch, D. T. Gryko and E. Vauthey, Excited-State Symmetry Breaking in a Quadrupolar Molecule Visualized in Time and Space, *J. Phys. Chem. Lett.*, 2017, **8**, 6029–6034.

17 E. Vauthey, Watching Excited-State Symmetry Breaking in Multibranched Push–Pull Molecules, *J. Phys. Chem. Lett.*, 2022, **13**, 2064–2071.

18 R. Ghosh and D. K. Palit, Effect of Donor–Acceptor Coupling on Tict Dynamics in the Excited States of Two Dimethylamine Substituted Chalcones, *J. Phys. Chem. A*, 2015, **119**, 11128–11137.

19 K. A. Wells, J. R. Palmer, J. E. Yarnell, S. Garakyaraghi, B. C. Pemberton, J. M. Favale, M. K. Valchar, A. Chakraborty and F. N. Castellano, Understanding the Influence of Geometric and Electronic Structure on the Excited State Dynamical and Photoredox Properties of Perinone Chromophores, *Phys. Chem. Chem. Phys.*, 2021, **23**, 24200–24210.

20 S. Paul, C. Govind and V. Karunakaran, Planarity and Length of the Bridge Control Rate and Efficiency of Intramolecular Singlet Fission in Pentacene Dimers, *J. Phys. Chem. B*, 2021, **125**, 231–239.

21 J. Kong, W. Zhang, J.-Y. Shao, D. Huo, X. Niu, Y. Wan, D. Song, Y.-W. Zhong and A. Xia, Bridge-Length- and Solvent-Dependent Charge Separation and Recombination Processes in Donor–Bridge–Acceptor Molecules, *J. Phys. Chem. B*, 2021, **125**, 13279–13290.

22 J. Kong, W. Zhang, G. Li, D. Huo, Y. Guo, X. Niu, Y. Wan, B. Tang and A. Xia, Excited-State Symmetry-Breaking Charge Separation Dynamics in Multibranched Perylene Diimide Molecules, *J. Phys. Chem. Lett.*, 2020, **11**, 10329–10339.

23 J. Guo, *et al.*, Tetraphenylpyrazine Decorated 1,3-Di(9h-Carbazol-9-Yl)Benzene (Mcp): A New Aie-Active Host with Enhanced Performance in Organic Light-Emitting Diodes, *J. Mater. Chem. C*, 2019, **7**, 11160–11166.

24 L. Pan, H. Wu, J. Liu, K. Xue, W. Luo, P. Chen, Z. Wang, A. Qin and B. Z. Tang, Tetraphenylpyrazine Based Aie Luminogens: Unique Excited State Decay and Its Application in Deep-Blue Light-Emitting Diodes, *Adv. Opt. Mater.*, 2019, **7**, 1801673.

25 M. Chen, *et al.*, Malonitrile-Functionalized Tetraphenylpyrazine: Aggregation-Induced Emission, Ratiometric Detection of Hydrogen Sulfide, and Mechanochromism, *Adv. Funct. Mater.*, 2018, **28**, 1704689.

26 M. Chen, *et al.*, Tetraphenylpyrazine-Based Aiegens: Facile Preparation and Tunable Light Emission, *Chem. Sci.*, 2015, **6**, 1932–1937.

27 G. Feng, R. T. K. Kwok, B. Z. Tang and B. Liu, Functionality and Versatility of Aggregation-Induced Emission Luminogens, *Appl. Phys. Rev.*, 2017, **4**, 021307.

28 Z. He, C. Ke and B. Z. Tang, Journey of Aggregation-Induced Emission Research, *ACS Omega*, 2018, **3**, 3267–3277.

29 J. Mei, N. L. C. Leung, R. T. K. Kwok, J. W. Y. Lam and B. Z. Tang, Aggregation-Induced Emission: Together We Shine, United We Soar!, *Chem. Rev.*, 2015, **115**, 11718–11940.

30 H. Wu, *et al.*, Novel Strategy for Constructing High Efficiency Oled Emitters with Excited State Quinone-Conformation Induced Planarization Process, *Adv. Opt. Mater.*, 2019, **7**, 1900283.

31 M. Chen, H. Nie, B. Song, L. Li, J. Z. Sun, A. Qin and B. Z. Tang, Triphenylamine-Functionalized Tetraphenylpyrazine: Facile Preparation and Multifaceted Functionalities, *J. Mater. Chem. C*, 2016, **4**, 2901–2908.

32 A. B. J. Parusel, G. Köhler and S. Grimme, Density Functional Study of Excited Charge Transfer State Formation in 4-(N,N-Dimethylamino)Benzonitrile, *J. Phys. Chem. A*, 1998, **102**, 6297–6306.

33 H.-H. G. Tsai, H.-L. S. Sun and C.-J. Tan, Td-Dft Study of the Excited-State Potential Energy Surfaces of 2-(2′-Hydroxyphenyl)Benzimidazole and Its Amino Derivatives, *J. Phys. Chem. A*, 2010, **114**, 4065–4079.

34 A. M. El-Zohry, E. A. Orabi, M. Karlsson and B. Zietz, Twisted Intramolecular Charge Transfer (Tict) Controlled by Dimerization: An Overlooked Piece of the Tict Puzzle, *J. Phys. Chem. A*, 2021, **125**, 2885–2894.

35 G. Li, D. Magana and R. B. Dyer, Direct Observation and Control of Ultrafast Photoinduced Twisted Intramolecular Charge Transfer (Tict) in Triphenyl-Methane Dyes, *J. Phys. Chem. B*, 2012, **116**, 12590–12596.

36 D. Peckus, T. Matulaitis, M. Franckevičius, V. Mimaitė, T. Tamulevičius, J. R. Simokaitienė, D. Volyniuk, V. Gulbinas, S. Tamulevičius and J. V. Gražulevičius, Twisted Intramolecular Charge Transfer States in Trinary Star-Shaped Triphenylamine-Based Compounds, *J. Phys. Chem. A*, 2018, **122**, 3218–3226.

37 S. Liu, X. Zhou, H. Zhang, H. Ou, J. W. Y. Lam, Y. Liu, L. Shi, D. Ding and B. Z. Tang, Molecular Motion in Aggregates: Manipulating Tict for Boosting Photothermal Theranostics, *J. Am. Chem. Soc.*, 2019, **141**, 5359–5368.

38 Q. Peng, L. Yang, Y. Li, Y. Zhang, T. Li, Y. Qin, Y. Song, H. Hou and K. Li, Aggregation/Viscosity-Induced Emission and Third-Order Nonlinear Optical Signal Inversion in a Tict System, *J. Phys. Chem. B*, 2020, **124**, 22684–22691.

39 N. Alarcos, B. Cohen, M. Ziółek and A. Douhal, Photochemistry and Photophysics in Silica-Based Materials: Ultrafast and Single Molecule Spectroscopy Observation, *Chem. Rev.*, 2017, **117**, 13639–13720.

40 Z. Kuang, G. He, H. Song, X. Wang, Z. Hu, H. Sun, Y. Wan, Q. Guo and A. Xia, Conformational Relaxation and Thermally Activated Delayed Fluorescence in Anthraquinone-Based Intramolecular Charge-Transfer Compound, *J. Phys. Chem. C*, 2018, **122**, 3727–3737.

41 J. Choi, D.-S. Ahn, K. Y. Oang, D. W. Cho and H. Ihee, Charge Transfer-Induced Torsional Dynamics in the Excited State of 2,6-Bis(Diphenylamino)Anthraquinone, *J. Phys. Chem. C*, 2017, **121**, 24317–24323.

42 R. Ghosh and D. K. Palit, Effect of Donor–Acceptor Coupling on Tict Dynamics in the Excited States of Two Dimethylamine Substituted Chalcones, *J. Phys. Chem. A*, 2015, **119**, 11128–11137.

43 Z. R. Grabowski, K. Rotkiewicz and W. Rettig, Structural Changes Accompanying Intramolecular Electron Transfer: Focus on Twisted Intramolecular Charge-Transfer States and Structures, *Chem. Rev.*, 2003, **103**, 3899–4032.

44 S. Sasaki, G. P. C. Drummen and G.-I. Konishi, Recent Advances in Twisted Intramolecular Charge Transfer (Tict) Fluorescence and Related Phenomena in Materials Chemistry, *J. Mater. Chem. C*, 2016, **4**, 2731–2743.

45 J. Kong, W. Zhang, G. Li, D. Huo, Y. Guo, X. Niu, Y. Wan, B. Tang and A. Xia, Excited-State Symmetry-Breaking Charge Separation Dynamics in Multibranched Perylene Diimide Molecules, *J. Phys. Chem. Lett.*, 2020, **11**, 10329–10339.

46 C. Liu, K.-C. Tang, H. Zhang, H.-A. Pan, J. Hua, B. Li and P.-T. Chou, Studies of Excited-State Properties of Multibranched Triarylamine End-Capped Triazines, *J. Phys. Chem. A*, 2012, **116**, 12339–12348.

47 N. S. Makarov, S. Mukhopadhyay, K. Yesudas, J.-L. Brédas, J. W. Perry, A. Pron, M. Kivala and K. Müllen, Impact of Electronic Coupling, Symmetry, and Planarization on One- and Two-Photon Properties of Triarylamines with One, Two, or Three Diarylboryl Acceptors, *J. Phys. Chem. A*, 2012, **116**, 3781–3793.

48 G. Ramakrishna and T. Goodson, Excited-State Deactivation of Branched Two-Photon Absorbing Chromophores: A Femtosecond Transient Absorption Investigation, *J. Phys. Chem. A*, 2007, **111**, 993–1000.

49 S. Athanasopoulos, L. Alfonso Hernandez, D. Beljonne, S. Fernandez-Alberti and S. Tretiak, Ultrafast Non-Förster Intramolecular Donor–Acceptor Excitation Energy Transfer, *J. Phys. Chem. Lett.*, 2017, **8**, 1688–1694.

50 T. Nelson, S. Fernandez-Alberti, A. E. Roitberg and S. Tretiak, Electronic Delocalization, Vibrational Dynamics, and Energy Transfer in Organic Chromophores, *J. Phys. Chem. Lett.*, 2017, **8**, 3020–3031.

51 G. Duvanel, J. Grilj and E. Vauthey, Ultrafast Long-Distance Excitation Energy Transport in Donor–Bridge–Acceptor Systems, *J. Phys. Chem. A*, 2013, **117**, 918–928.

52 R. Tautz, *et al.*, Charge Photogeneration in Donor–Acceptor Conjugated Materials: Influence of Excess Excitation Energy and Chain Length, *J. Am. Chem. Soc.*, 2013, **135**, 4282–4290.

53 M. A. Topchiy, A. F. Asachenko and M. S. Nechaev, Solvent-Free Buchwald–Hartwig Reaction of Aryl and Heteroaryl Halides with Secondary Amines, *Eur. J. Org. Chem.*, 2014, 3319–3322.

54 F. J. Avila Ferrer, J. Cerezo, E. Stendardo, R. Improta and F. Santoro, Insights for an Accurate Comparison of Computational Data to Experimental Absorption and Emission

Spectra: Beyond the Vertical Transition Approximation, *J. Chem. Theory Comput.*, 2013, **9**, 2072–2082.
55 V. Karunakaran, T. Senyushkina, G. Saroja, J. Liebscher and N. P. Ernsting, 2-Amino-7-Nitro-Fluorenes in Neat and Mixed Solventsoptical Band Shapes and Solvatochromism, *J. Phy. Chem. A*, 2007, **111**, 10944–10952.
56 G. Angulo, G. Grampp and A. Rosspeintner, Recalling the Appropriate Representation of Electronic Spectra, *Spectrochim. Acta. A. Mol. Biomol. Spectrosc.*, 2006, **65**, 727–731.
57 X. Xiao, J. Pang, A. A. Sukhanov, Y. Hou, J. Zhao, M.-D. Li and V. K. Voronkova, The Effect of One-Atom Substitution on the Photophysical Properties and Electron Spin Polarization: Intersystem Crossing of Compact Orthogonal Perylene/Phenoxazine Electron Donor/Acceptor Dyad, *J. Chem. Phys.*, 2020, **153**, 184312.
58 X.-F. Zhang and J. Wang, Morpholine-Phthalocyanine (Donor–Acceptor) Construct: Photoinduced Intramolecular Electron Transfer and Triplet Formation from Its Charge Separation State, *J. Phys. Chem. A*, 2011, **115**, 8597–8603.
59 E. Lippert, Dipolmoment Und Elektronenstruktur Von Angeregten Molekülen, *Z. Naturforsch. A*, 1955, **10**, 541–545.
60 M. Noboru, K. Yozo and K. Masao, Solvent Effects Upon Fluorescence Spectra and the Dipolemoments of Excited Molecules, *Bull. Chem. Soc. Jpn.*, 1956, **29**, 465–470.
61 C. Bin, H. Zhang, W. Luo, H. Nie, R. Hu, A. Qin, Z. Zhao and B. Z. Tang, Oxidation-Enhanced Emission: Exploring Novel Aiegens from Thieno[3,2-B]Thiophene S,S-Dioxide, *J. Mater. Chem. C*, 2017, **5**, 960–968.
62 B. Xu, J. Zhang, H. Fang, S. Ma, Q. Chen, H. Sun, C. Im and W. Tian, Aggregation Induced Enhanced Emission of Conjugated Dendrimers with a Large Intrinsic Two-Photon Absorption Cross-Section, *Polym. Chem.*, 2014, **5**, 479–488.
63 X. Zhang, A. Elmali, R. Duan, Q. Liu, W. Ji, J. Zhao, C. Li and A. Karatay, Charge Separation, Recombination and Intersystem Crossing of Directly Connected Perylenemonoimide–Carbazole Electron Donor/Acceptor Dyads, *Phys. Chem. Chem. Phys.*, 2020, **22**, 6376–6390.
64 V. Bandi, H. B. Gobeze, V. Lakshmi, M. Ravikanth and F. D'Souza, Vectorial Charge Separation and Selective Triplet-State Formation During Charge Recombination in a Pyrrolyl-Bridged Bodipy–Fullerene Dyad, *J. Phys. Chem. C*, 2015, **119**, 8095–8102.
65 F. Würthner, T. E. Kaiser and C. R. Saha-Möller, J-Aggregates: From Serendipitous Discovery to Supramolecular Engineering of Functional Dye Materials, *Angew. Chem., Int. Ed.*, 2011, **50**, 3376–3410.
66 N. J. Hestand and F. C. Spano, Expanded Theory of H- and J-Molecular Aggregates: The Effects of Vibronic Coupling and Intermolecular Charge Transfer, *Chem. Rev.*, 2018, **118**, 7069–7163.
67 R. Hu, *et al.*, Twisted Intramolecular Charge Transfer and Aggregation-Induced Emission of Bodipy Derivatives, *J. Phys. Chem. C*, 2009, **113**, 15845–15853.
68 E. Wang, J. W. Y. Lam, R. Hu, C. Zhang, Y. S. Zhao and B. Z. Tang, Twisted Intramolecular Charge Transfer, Aggregation-Induced Emission, Supramolecular Self-Assembly and the Optical Waveguide of Barbituric Acid-Functionalized Tetraphenylethene, *J. Mater. Chem. C*, 2014, **2**, 1801–1807.
69 S. Sasaki, Y. Niko, K. Igawa and G.-I. Konishi, Aggregation-Induced Emission Active D-Π-a Binaphthyl Luminophore with Dual-Mode Fluorescence, *RSC Adv.*, 2014, **4**, 33474–33477.
70 J. J. Snellenburg, S. P. Laptenok, R. Seger, K. M. Mullen and I. H. M. V. Stokkum, Glotaran: A Java-Based Graphical User Interface for the R Package Timp, *J. Stat. Softw.*, 2012, **49**, 1–22.
71 T. Gustavsson, L. Cassara, V. Gulbinas, G. Gurzadyan, J. C. Mialocq, S. Pommeret, M. Sorgius and P. van der Meulen, Femtosecond Spectroscopic Study of Relaxation Processes of Three Amino-Substituted Coumarin Dyes in Methanol and Dimethyl Sulfoxide, *J. Phy. Chem. A*, 1998, **102**, 4229–4245.
72 M. L. Horng, J. A. Gardecki, A. Papazyan and M. Maroncelli, Subpicosecond Measurements of Polar Solvation Dynamics: Coumarin 153 Revisited, *J. Phy. Chem.*, 1995, **99**, 17311–17337.
73 R. Jimenez, G. R. Fleming, P. V. Kumar and M. Maroncelli, Femtosecond Solvation Dynamics of Water, *Nature*, 1994, **369**, 471–473.
74 S. A. Kovalenko, N. P. Ernsting and J. Ruthmann, Femtosecond Stokes Shift in Styryl Dyes: Solvation or Intramolecular Relaxation?, *J. Chem. Phys.*, 1997, **106**, 3504–3511.
75 S. K. Pal, J. Peon, B. Bagchi and A. H. Zewail, Biological Water: Femtosecond Dynamics of Macromolecular Hydration, *J. Phy. Chem. B*, 2002, **106**, 12376–12395.
76 K. Chen, J. Zhao, X. Li and G. G. Gurzadyan, Anthracene–Naphthalenediimide Compact Electron Donor/Acceptor Dyads: Electronic Coupling, Electron Transfer, and Intersystem Crossing, *J. Phys. Chem. A*, 2019, **123**, 2503–2516.
77 Y. Dong, A. Elmali, J. Zhao, B. Dick and A. Karatay, Long-Lived Triplet Excited State Accessed with Spin–Orbit Charge Transfer Intersystem Crossing in Red Light-Absorbing Phenoxazine-Styryl Bodipy Electron Donor/Acceptor Dyads, *Chem. Phys. Chem.*, 2020, **21**, 1388–1401.
78 M. Imran, X. Zhang, Z. Wang, X. Chen, J. Zhao, A. Barbon and V. K. Voronkova, Electron Spin Dynamics in Excited State Photochemistry: Recent Development in the Study of Intersystem Crossing and Charge Transfer in Organic Compounds, *Phys. Chem. Chem. Phys.*, 2021, **23**, 15835–15868.
79 T. Akasaka, *et al.*, Synthesis and Photoinduced Electron-Transfer Reactions in a La2@Ih-C80–Phenoxazine Conjugate, *ChemPlusChem*, 2017, **82**, 1067–1072.
80 R. Hay and P. Pomery, Reactions of Pyrazine Radical Anions in Solution:I. Study of the Kinetics of the Dimerization of Pyrazine Radical Anions, *Aust. J. Chem.*, 1971, **24**, 2287–2292.